THE STRUCTURE OF THE CELL NUCLEUS AND CANCER CHEMORESISTANCE

by

Farzaneh Atrian Afyani

A Dissertation

Submitted to the Faculty of Purdue University

In Partial Fulfillment of the Requirements for the degree of

Doctor of Philosophy

Department of Basic Medical Sciences

West Lafayette, Indiana

May 2019

THE PURDUE UNIVERSITY GRADUATE SCHOOL
STATEMENT OF COMMITTEE APPROVAL

Dr. Sophie Lelièvre, Chair
Department of Basic Medical Sciences
Dr. Russell Main
Department of Basic Medical Sciences
Dr. Chongli Yuan
Department of Chemical Engineering
Dr. Corey Neu
Department of Mechanical Engineering

Approved by:
Laurie Jaeger
Head of the Graduate Program

Dedicated to Zahra and Mahmoud

ACKNOWLEDGMENTS

This work would never have been done without help from many co-workers, collaborators, and colleagues. My sincere thanks go foremost to my advisor, Dr. Sophie Lelièvre for the continuous support of my PhD study and related research, for her patience, motivation, and immense knowledge and to Dr. Kim McDole who very helpfully got me started in the lab.

I would like to thank my thesis committee: Dr. Russell Main, Dr. Chongli Yuan and Dr. Corey Neu for their insightful comments and encouragement. I am grateful to Dr. Laurie Jeager, Dr. Marxa Figueiredo and Dr. Elikplimi Asem, for their precious support and motivation. I thank my fellow lab mates, for the stimulating discussions, and for all the fun we have had in the last five years.

Last but not the least, I would like to thank my family: my parents, Zahra and Mahmoud, my brother, Farzad, my dearest Armin and Mehdi for supporting me spiritually throughout writing this thesis.

TABLE OF CONTENTS

ABSTRACT

Author: Atrian Afyani, Farzaneh. PhD
Institution: Purdue University
Degree Received: May 2019
Title: The Structure of The Cell Nucleus and Cancer Chemoresistance
Committee Chair: Sophie Lelièvre

Cancers have the ability to develop resistance to traditional therapies. The important role of the tumor microenvironment in transforming nonaggressive tumor cells into an aggressive and chemoresistant cancer has been abundantly addressed. Mechanical cues from the tumor environment, such as matrix stiffness and geometry, transfer to the cell nucleus via the cytoskeleton and change nuclear morphology (e. g, chromatin organization, size and shape). Such alterations are known to accompany or follow the acquisition of chemoresistance. Nuclear matrix proteins such as the Nuclear Mitotic Apparatus (NuMA) are highly involved in higher order chromatin organization and contribute to sustain the physical structure of the cell nucleus, but it is yet to be determined how such structural proteins respond to microenvironmental changes. We have shown previously that tumors cultured in curved geometry (similar to the ductal architecture of breast tissue) display significantly different drug sensitivities compared to those cultured on a flat surface, and that a major morphological difference between these two culture conditions is nuclear shape (i.e., circularity). Our hypothesis is that mechanical cues from the tumor microenvironment alter nuclear features that control the phenotypic response of cancer cells to antiproliferative drugs. Morphological analysis of the cell nucleus in the curved conformation as well as hydrogel and hanging drop systems (with amorphous geometry) showed that only nodules in the curved set-up have nuclear morphometry (shape and size) similar to that of breast tumors of the corresponding subtypes *in vivo*. In addition, we compared the sensitivity of triple negative breast tumors to cisplatin, with proven efficacy in the clinics, and SAHA, an epigenetic drug that so far failed in breast cancer treatment. Our results suggest higher sensitivity to cisplatin and lower sensitivity to SAHA of breast cancer cells cultured in duct-like geometry compared to the amorphous systems. To evaluate the importance of nuclear morphometry in drug response we altered nuclear size and shape using latrunculin. Under this condition, the number of apoptotic and growth-arrested cells increased following treatments with cisplatin and SAHA, respectively.

Nuclear morphometry was also modified by spreading cells over fibronectin-coated micropatterned surfaces. Cisplatin treatment revealed higher sensitivity of cells with bigger compared to smaller nuclear area. The nuclei with increased area had the highest number of 53BP1 foci, representing DNA double strand breaks, hence confirming a positive link between nuclear morphometry and drug sensitivity. Silencing NuMA in conventional monolayered cell cultures significantly increased nuclear size, redistributed 53BP1 within the nucleus and was linked with increased sensitivity to cisplatin and SAHA. To validate the relationship between drug sensitivity, nuclear morphometry and NuMA, in a physiologically relevant manner we cultured chemoresistant and chemosensitive breast tumors that were nonsilenced/silenced for NuMA in collagen matrix with adjustable stiffness. Nuclear morphometric analysis indicated that nuclear size and shape are unique characteristics of tumors with different phenotypes, and the impact of nuclear morphometry on drug response depended on the tumor phenotype and matrix stiffness. Moreover, high matrix stiffness reduced drug sensitivity independently of the tumor phenotype, and the influence of NuMA on nuclear size and shape and on drug sensitivity occurred in a stiffness-dependent manner. For example, low NuMA expression in high matrix rigidity was significantly associated with higher cisplatin sensitivity only in chemoresistant cells. Overall, regression analysis demonstrated that, the low NuMA expression is the major determinant of drug sensitivity in cells with different levels of chemosensitivity. Assay for Transposase Accessible Chromatin with high-throughput sequencing (ATAC-seq) revealed that NuMA might influence chromatin accessibility in a stiffness-dependent manner. Importantly, NuMA was associated with the accessibility of SP1 (a prosurvival transcription factor) DNA binding domain, regardless of matrix stiffness. These findings bring the first demonstration of a structural nuclear protein, NuMA, that influences drug response via an effect on both nuclear morphometry and chromatin accessibility.

INTRODUCTION

The goal of my thesis research was to study the impact of the physical aspect (matrix stiffness, geometry) of the tumor microenvironment (TME) on the response of cancer cells to antiproliferative drug treatment. In addition, I focused on how to incorporate physical features of the TME into the development of physiologically relevant cancer models to study tumor biology and drug screening.

Cancer is not just a mass of neoplastic cells, it is a complex accumulation of genetic mutations and altered gene expression patterns within the cells that are accompanied by a procarcinogenic environment (Wang et al., 2017) . Cancer cell survival is highly dependent on the dynamic interactions between the surrounding matrix and stromal cells. Cell-cell and cell-ECM interactions can be translated into signaling pathways, which could ultimately affect chromatin organization and cell nucleus homeostasis. In addition, emerging evidence demonstrates that environmental changes such as mechanical perturbation can regulate the epigenetic state of the cells and affect chromatin texture, gene expression and nuclear morphology (Tan et al., 2014). During carcinogenesis, increased matrix rigidity is considered the most important physical aspect of the TME that directly affects drug response and cell survival (Tan et al., 2014). In addition, the nuclear features of cancer cells such as shape, size and chromatin organization are altered upon mechanical stimulus (Madrazo, Conde, & Redondo-Munoz, 2017; Rowat, Lammerding, & Ipsen, 2006). The hypothesis that guided my thesis work is that TME signals could alter nuclear features that affect chemosensitivity, hence *in vitro* cancer models should incorporate TME features important for a realistic behavior of cancer cells in drug response. A physiologically relevant *in vitro* model in which tumor microenvironments are faithfully recapitulated is a missing concept that so far hinders the understanding of cancer cells behavior in different stages of tumorigenesis, specially chemoresistance. Due to the complexity of tumors and their surrounding environment it seems pivotal to identify phenotypic markers that could guide us when recreating tumor *in vivo* conditions.

To answer my research query, I have worked with models that integrate specific features of TME such as matrix stiffness, geometry and ECM components to identify cell nucleus behavior during drug response under physiologically relevant conditions.

The introduction of my thesis is a book chapter in which I develop information on different features of the TME and how they affect cancer cells survival and chemoresistance. In addition, I discuss how the TME affects nuclear morphology, gene expression and drug response during carcinogenesis. Finally, I propose nuclear morphology as a reliable readout in preclinical models used for designing intelligent biomaterials for cancer therapies. This introductory book chapter is followed by four first author manuscripts. The first manuscript, in the main part of the thesis, is demonstrating the role of NuMA, a nuclear matrix protein, as the major mediator of chemosensitivity, in response to TME alterations. The second manuscript in the main part of the thesis includes my contribution to the development of cell culture techniques and models to study the physical features of the TME such as matrix stiffness and geometry, on cancer phenotypes. These techniques have been used in both of my research manuscripts. In the appendix, the second research manuscript is about the optimization of the Disease on the Chip (DOC) model for high throughput drug screening. The DOC, which was previously developed in our laboratory (Vidi et al., 2014) is an *in vitro* model that mimics the geometry of the ductal structures in which adenocarcinomas develop. The last manuscript in the appendix is a special report which was published in Epigenomics in which we proposed that the lack of understanding of the tissue architecture (the specific interactions between cell-cell and cell-ECM) is the reason for the failure of epigenetic to treat solid tumors.

Overall these four manuscripts illustrate how tumor organization including the cell nucleus is mediating the impact of the TME on drug response and how incorporating TME features in drug screening models could better predict drug response.

References

Castells, M., Thibault, B., Delord, J.-P., & Couderc, B. (2012). Implication of Tumor Microenvironment in Chemoresistance: Tumor-Associated Stromal Cells Protect Tumor Cells from Cell Death. *International Journal of Molecular Sciences, 13*(8), 9545-9571. doi:10.3390/ijms13089545

Guilluy, C., & Burridge, K. (2015). Nuclear mechanotransduction: forcing the nucleus to respond. *Nucleus, 6*(1), 19-22. doi:10.1080/19491034.2014.1001705

Imbalzano, K. M., Cohet, N., Wu, Q., Underwood, J. M., Imbalzano, A. N., & Nickerson, J. A. (2013). Nuclear shape changes are induced by knockdown of the SWI/SNF ATPase BRG1 and are independent of cytoskeletal connections. *PLoS One, 8*(2), e55628. doi:10.1371/journal.pone.0055628

Madrazo, E., Conde, A. C., & Redondo-Munoz, J. (2017). Inside the Cell: Integrins as New Governors of Nuclear Alterations? *Cancers (Basel), 9*(7). doi:10.3390/cancers9070082

Merdes, A., & Cleveland, D. W. (1998). The role of NuMA in the interphase nucleus. *J Cell Sci, 111 (Pt 1)*, 71-79.

Rowat, A. C., Lammerding, J., & Ipsen, J. H. (2006). Mechanical properties of the cell nucleus and the effect of emerin deficiency. *Biophys J, 91*(12), 4649-4664. doi:10.1529/biophysj.106.086454

Senthebane, D. A., Rowe, A., Thomford, N. E., Shipanga, H., Munro, D., Mazeedi, M., . . . Dzobo, K. (2017). The Role of Tumor Microenvironment in Chemoresistance: To Survive, Keep Your Enemies Closer. *Int J Mol Sci, 18*(7). doi:10.3390/ijms18071586

Tan, Y., Tajik, A., Chen, J., Jia, Q., Chowdhury, F., Wang, L., . . . Wang, N. (2014). Matrix softness regulates plasticity of tumour-repopulating cells via H3K9 demethylation and Sox2 expression. *Nat Commun, 5*, 4619. doi:10.1038/ncomms5619

Vidi, P. A., Maleki, T., Ochoa, M., Wang, L., Clark, S. M., Leary, J. F., & Lelievre, S. A. (2014). Disease-on-a-chip: mimicry of tumor growth in mammary ducts. *Lab Chip, 14*(1), 172-177. doi:10.1039/c3lc50819f

Wang, M., Zhao, J., Zhang, L., Wei, F., Lian, Y., Wu, Y., . . . Guo, C. (2017). Role of tumor microenvironment in tumorigenesis. *J Cancer, 8*(5), 761-773. doi:10.7150/jca.17648

CHAPTER 1. PHENOTYPIC EVOLUTION OF CANCER CELLS: STRUCTURAL REQUIREMENTS FOR SURVIVAL

The following book chapter was submitted to Biomaterial for Cancer Therapeutics and is In the format required for Elsevier electronic sub**mission**

Farzaneh Atrian[1] and Sophie A. Lelièvre[1,2]

(1) Department of Basic Medical Sciences, Purdue University, West Lafayette, IN 47906-2026, USA

(2) Purdue Center for Cancer Research

1.1 Abstract

Enhancing the sensitivity of tumor cells to therapies has been a challenge. Major progress has been in the development of drugs specific to cancer types and new approaches for tumor targeting. But acquired tumor resistance is still eluding all attempts to prevent or overcome this phenomenon. We present information on physical constraints in the tumor microenvironment that have been associated with cancer progression and resistance to treatment and how these constraints might be mediated via mechanotransduction to the genome, hence influencing cell survival. The necessity of a careful knowledge of nuclear alterations linked with microenvironmental conditions and drug resistance phenotypes is emphasized in order to identify markers for the optimization of cell culture models and the measurement of the efficacy of drug treatments. The biological conditions that lead to different levels of drug sensitivity are placed in the context of drug development and delivery. Notably, *in vitro* 3D cell culture models developed with proper materials to mimic microenvironmental constraints are likely to be superior models to readily test new drugs and drug delivery methods. Moreover, we surmise that in the future, targeted drug delivery could be designed with smart materials that adapt to microenvironmental conditions for better efficacy.

Key Words: Tumor, Cell Nucleus, Mechanotransduction, Tumor Microenvironment, Chemoresistance, Extracellular Matrix

1.2 Introduction

Phenotypic overview of cancer progression

Cancer initiates as a result of changes in gene expression that are associated with a profound reorganization of the epigenome (i.e., the location and amount of epigenetic marks that control the expression of genes at any given time). Self-sufficiency in proliferation signals and insensitivity to antiproliferation signals and apoptosis pathways give rise to a population of malignant cells with indefinite replication ability; yet, the population is heterogeneous and the response to external stimuli depends on such heterogeneity. Phenotypic heterogeneity is considered an engine of cancer progression (Sophie A. Lelièvre, 2014); the cell phenotype is typically dictated by gene expression patterns and revealed or characterized by cellular morphological and functional attributes.

Cancer cells constantly modify their surrounding (e.g. via paracrine stimulation possibly leading to angiogenesis and extracellular matrix (ECM) remodeling linked to the activity of proteases and secretion of ECM molecules). These cells are detected and eliminated by the immune system in early stages of the disease because they present antigens; however, with time genetic instability and sustained division contribute to the reduction of immunogenicity (Vinay et al., 2015). In addition, most cancers are initially sensitive to radiotherapy and chemotherapy, but they often acquire resistance during chemotherapy, in part via new metabolic pathways that sustain their survival by preventing the induction of cell death pathways (Boroughs and DeBerardinis, 2015), and also as a result of the heterogeneity within the cell population (Gay, Baker, & Graham, 2016). In summary, cancer cells can be viewed as phenotypically heterogeneous, with altered gene expression controls and a high capability of adaptation (as a population) via interactions with the microenvironment.

The most obvious phenotypic alterations observed in cancers of epithelial origin is epithelial-to-mesenchymal transition (EMT). During EMT differentiated epithelial cells that usually harbor a cuboidal shape lose basoapical polarity and acquire a spindle-like shape and motility potential. The transdifferentiation characteristic of EMT occurs in almost all epithelial cancers and is required during invasiveness. The acquisition of this new phenotype involves a specialized cellular structure, including rewiring of actin microfilaments and reorganization of the cell nucleus. During EMT, reversible epigenetic alterations (such as histone de/acetylation and DNA de/methylation) lead to the conversion of euchromatin to heterochromatin and vice versa. Epigenetic alterations

are accompanied with observable changes in nuclear morphology (e.g., nucleus size and shape, chromatin texture) (Bednarz-Knoll, Alix-Panabieres, & Pantel, 2012; Chao, Wu, Acquafondata, Dhir, & Wells, 2012; Guilluy et al., 2014; Mijovic et al., 2013). These changes are such that advanced image analysis software can be used to distinguish between epithelial and EMT prostate cancer cells based on variations in nuclear appearance (Verdone et al., 2015).

Evolution of the organization of nuclei in cancer cells

For pathologists, the morphological alterations of cancer cell nuclei are of high interest because they occur during all stages of cancer and many of these alterations are already detectable by light microscopy used with routine Hematoxylin & Eosine (H&E) staining. Cancer cell nuclei undergo alterations in size, shape, envelope, chromatin pattern, and in the organization of intranuclear structures such as nucleoli and splicing factor speckles (Lelievre et al., 1998; Nandini & Subramanyam, 2011; Welkoborsky, Mann, Gluckman, & Freije, 1993). These structural alterations are considered part of the phenotypic changes of cancer cells, and alterations in chromatin are considered the intracellular drivers of these phenotypic changes. Of particular interest are also alterations in nuclear morphometry (e.g., size, shape) that appear to exquisitely respond to modifications in the microenvironment as we showed for noncancerous and cancerous breast tissues (Chittiboyina et al., 2017; Jayaraman et al., 2017).

In general, uncontrolled and accelerated cellular divisions that reflect the abnormal behavior of cancer cells result in increased nuclear area and perimeter (Friedell, Bell, Burney, Soto, & Tiltman, 1976). As shown for different types of cancers these specific morphometric parameters increase along with worsening grades of carcinomas. Moreover, nuclei can become irregular or elongated when abnormal heterochromatin aggregates adhere to the inner surface of the nuclear envelope (Nandini & Subramanyam, 2011) Nuclear budding, ring-shaped nuclei, and nuclear holes are often observed in cancer cells as well (Wani, Bhardwaj, Kumar, & Katoch, 2010). Increased nuclear to cytoplasmic ratio and the presence of additional and prominent nucleoli is usually observed in cancer cells. The number, size and irregularity of nucleoli increase with the grades of carcinoma and this phenomenon is related to the aggressiveness of the tumor (Ikeguchi et al., 1999). In fact, alterations in nuclei as observed via H&E staining are the first sign of heterogeneity in cancer cells and they are used for tumor grading. It is still unclear how tumorigenesis could affect nuclear pleomorphism (e.g., the variability in nuclear size, shape and staining). Nuclear malformations may result from genetic mutations, abnormal chromosome-chromosome interactions, aberrant

binding of chromatin to the nuclear membrane, deviant nuclear pores, irregular attachments of cytoskeletal structures to the outer nuclear envelope and disordered nuclear matrix (i.e., the structural underpinnings of nuclear organization).

Involvement of nuclear structural proteins in gene transcription

The nuclear matrix (NM) was initially defined as the three-dimensional (3D) support scaffold of the cell nucleus mainly composed of proteins and heterogenous nuclear RNA (hnRNA) (Berezney & Coffey, 1974; Nickerson & Penman, 1992). The 'scaffold' is not readily visible since it requires DNA as anchoring points and is masked by the bulk of DNA in intact cells, which has led to controversy for years regarding the existence of such NM structure. The definition of the NM is more accepted as the resulting material from biochemical extraction (i.e., what remains after removing soluble proteins and enzymatic digestion of the DNA) (Lelievre, 2009). The fact remains that the cell nucleus is highly organized through chromatin folding notably and that components of the cell nucleus determine nuclear morphology, stabilize and orient DNA during replication, and control chromatin organization and RNA synthesis. Cellular differentiation relies on higher order chromatin organization ((Abad et al., 2007) that includes the specific location of epigenetic marks characteristic of heterochromatin and euchromatin and the formation of DNA loop domains, notably at sites known as matrix attachment regions (MARs), scaffold attachment regions (SARs) and skeleton-attached sequences. These domains are supposed to be the sites of active DNA replication and to control the transcription of groups of genes (Kaiser & Semple, 2018). The onset and progression of cancer is characterized by changes in higher order chromatin (Chandramouly, Abad, Knowles, & Lelievre, 2007). and DNA looping (Aitken et al., 2018; Kaiser & Semple, 2018). Moreover, proteins found remaining after the nuclear matrix preparation and referred as nuclear matrix proteins (NMPs) are unique for each cell types, and their composition is modified in cancer progression (Getzenberg, 1994), which suggests a role for these proteins in gene expression characteristic of tissue and cancer phenotypes.

Alterations in NMP composition and function have been implicated in the pathogenesis of many cancers such as prostate, colon, breast, cervix, head & neck and bladder (Hughes & Cohen, 1999; Hughes et al., 1999). Therefore, NMPs have been proposed as potential targets for diagnosis and treatment (Li et al., 1992); Naik et al., 1996), although it seems that these cellular components might have fallen out of fashion. Interestingly, the composition of both the nuclear matrix and the intermediate filaments is qualitatively altered by the substratum on which cells are cultured

(Getzenberg, Pienta, Huang, & Coffey, 1991). Therefore, the proteins that organize the cell nucleus and mediate gene transcription are sensitive to the ECM, a tissue component drastically altered during cancer development and progression, including resistance to treatment. Classified as an NMP and a potentially interesting target for drug treatment, is the nuclear mitotic apparatus (NuMA) protein. Its organization in the cell nucleus is a marker of phenotypes, controls phenotypes, and responds to alterations in the ECM (Knowles, Sudar, Bator-Kelly, Bissell, & Lelievre, 2006; Lelievre et al., 1998; Vega et al., 2017; Vidi et al., 2012).

The ECM component of the tumor microenvironment

Tissue function is linked to tissue structure, which involves not only the internal organization of cells, but also the organization of the ECM in the microenvironment. The physiological state of the tumor microenvironment (TME) is closely connected to every step of the neoplastic disease, including development, progression and drug resistance. The TME is composed of immune and inflammatory cells, stromal cells like fibroblasts, adipose cells, vascular and lymphatic networks, and the ECM per se that is a meshwork of macromolecules such as collagen and glycoproteins, providing physical support as well as signaling to the tissue. Immune cells such as B and T cells are present at the invasive margin of tumors and are also present in the adjacent lymphoid organs. The role of immune cells in tumor progression is somewhat controversial and based on the type of cells and the type of cancer, they might be associated with poor or good prognosis. For example, T lymphocytes such as CD+8 and CD+4 are associated with good prognosis; but certain T helper 2 (TH2) cells promote tumor growth. B cell infiltration in TME is associated with good prognosis in breast and ovarian cancers, while they are protumorigenic in skin cancer (Andreu et al., 2010; de Visser, Korets, & Coussens, 2005). Cancer associated fibroblast (CAFs) or myofibroblasts are tumor-promoting via their enhancing effect on angiogenesis and their positive impact on the recruitment of immune cells. The contribution of CAFs to aggressiveness is also through secretion of ECM components and ECM remodeling enzymes (Erez, Truitt, Olson, Arron, & Hanahan, 2010). In certain types of cancers, like in intra-abdominal cancers, adipocytes promote the proliferation of tumor cells via secretion of adipokines and by providing fatty acids as fuel (Nieman et al., 2011). Tumor vascularization is often abnormal, enabling cancer cell evasion, and it is linked to hypoxic conditions via vasculature endothelial growth factor (VEGF), fibroblasts growth factor (FGF) and chemokines secreted by malignant or inflammatory cells. Importantly, the abnormal vasculature (that is leaky, with uneven branching and lumen size) causes variations in blood flow

and distribution of oxygen and nutrients, further increasing the hypoxic and inflammatory conditions of the TME (Carmeliet & Jain, 2011), and impairing the delivery and impact of anticancer drugs (Bonnans, Chou, & Werb, 2014). Stromal cells in the TME provide support for blood vessels and their depletion is associated with activation of EMT and metastasis and thus, poor prognosis (Jo et al., 2018).

The interstitial space of the TME is filled with ECM components including primarily proteoglycans (PG) and fibrous proteins. Collagen, elastin, fibronectin and laminin are the major fibrous proteins of the ECM. The hydrated gel made by the PGs fills the space in-between the fibrils. Collagen is the most abundant fibrous protein of the ECM that is responsible for cell adhesion and migration and for providing tensile strength (Rozario & DeSimone, 2010). Collagens are mainly secreted and organized by the fibroblasts. For instance, under pressure, fibroblasts organize the alignment of the collagen fibers into thicker structures (De Wever, Demetter, Mareel, & Bracke, 2008). The tropoelastins (elastin precursor molecules) made by fibroblasts are largely linked together by the lysyl oxidase (LOX) enzyme family to form the larger elastin complex. The elastic core is covered by a sheet of microfibrils composed of glycoproteins, which makes them stronger (Mithieux & Weiss, 2005). The elastin fibers are able to recoil and stretch about 1.5 times of their length. Their stretching function is regulated via their tight association with collagen. Fibronectin is a ubiquitous glycoprotein that organizes into linear and branched networks around cells and promote the bonding of neighboring cells. It is considered an extracellular mechanosensor by exposing its cryptic integrin binding sites during mechanical stress (Smith et al., 2007). During normal as well as cancer development fibronectin is required for cell migration (Hsiao et al., 2017). In addition, the assembly of other ECM proteins such as collagen depends on fibronectin incorporation into the matrix. Laminins are structural component of basement membranes, a specialized part of the ECM that is in direct contact with epithelial cells. Along with collagen type IV, laminins form a sheet-like structure that provides the specificity of the basement membranes associated with different tissue types (Yurchenco, 2011). Interestingly, in human cancers the abnormal deposition of laminin is associated with angiogenesis and metastasis (Neve, Cantatore, Maruotti, Corrado, & Ribatti, 2014), suggesting that cancer progression relies on complex changes in the ECM. Like cancer cells, the ECM has been a target of anticancer drugs, but failures have been tremendous as exemplified with the use of antimetalloproteases that led to increased cancer aggressiveness (Cathcart, Pulkoski-Gross, & Cao, 2015). The ECM is also possibly responsible for issues with drug delivery due to its heterogenous nature, which leads to

an uncontrolled diffusion of the drug to tumor and resistance to treatment (Malandrino, Mak, Kamm, & Moeendarbary, 2018; Shin et al., 2013).

Drug resistance in cancer

After several decades of research, there is still no means to effectively control chemoresistance, the main reason for death from cancer. A major cause for cross-resistance (i.e., resistance to unrelated classes of anticancer drugs) remains elusive, which constitutes a barrier to developing effective therapeutic strategies. Tumors can have intrinsic or acquired resistance to chemotherapeutic agents. Intrinsic resistance is identified by the presence of pre-existing resistance factors (such as tumor heterogeneity) within the tumor. Very often tumors acquire resistance to anticancer drugs via genetic and epigenetic alterations linked to treatment pressure. Notably, cross-resistance involves abnormal drug transportation and metabolism, alternative DNA repair pathways, deregulated apoptosis and tumor heterogeneity.

The TME plays a crucial role in the development of chemoresistance. Chemotherapeutic drugs need to access all cancer cells in a solid tumor to be effective; thus, a permissive microenvironment could affect drug sensitivity. The composition and organization of the fibrous proteins and stromal components of the ECM contribute to marked gradients in drug concentration, increased interstitial fluid pressure and abnormal metabolism, all of which affect drug responsiveness (Boroughs & DeBerardinis, 2015). The interaction between tumor cells and ECM components such as laminin and fibronectin, was shown to increase the survival rate of many tumor models *in vitro* (Pickup, Mouw, & Weaver, 2014). For example, upregulation of L1, a cell membrane glycoprotein that is involved in cell-ECM adhesion, is associated with acquired resistance to cisplatin, one of the most powerful cytotoxic drugs used in cancer treatment. Moreover, in malignant tumors, areas with less accessibility to oxygen show higher rate of cell death. The under-vascularized area induces hypoxic conditions, which can directly induce apoptosis. Therefore, TME components that are pro-angiogenic could contribute to increased tumor resistance by providing blood flow and oxygen to the hypoxic regions. Conversely, prolonged hypoxia has been associated with increased resistance as well via the acquisition of new metabolic pathways (ref). Changes in oxygenation in the vicinity of tumors and within tumors, contribute to tumor heterogeneity, and consequently, chemoresistance. It is possible that the death of cells sensitive to chemotherapy and the survival of resistant cells is a main factor for tumor progression and aggressiveness, although other, noncontradictory, theories favor cell-adhesion- or environment-mediated resistance (Cordes &

Meineke, 2003; Damiano, Cress, Hazlehurst, Shtil, & Dalton, 1999; Meads, Gatenby, & Dalton, 2009; Weaver et al., 2002). For example, ECM attachment prolonged G2 phase arrest in radiation-treated cells and reduced the number of DNA double-strand breaks and lethal chromosomal aberrations (Storch et al., 2010). Cytotoxic drug-mediated apoptosis decreased in small lung cancer cells upon adhesion to laminin, fibronectin, or collagen type IV (Sethi et al., 1999).

Despite advances to identify the factors that contribute to the survival of cancer cells, there is no effective means to overcome the challenges of resistance to treatment in patients with cancer. The lack of reconstitution of microenvironmental features of tumors in cancer research is among the leading causes of failure of therapeutic development. In the first part of this chapter, we present information on the importance of the mechanical properties of the tumor microenvironment that can be incorporated not only in preclinical models *in vitro*, but also serve as guidance for new concepts in drug release. In the second part, we discuss how phenotypic markers based on nuclear morphology could guide the recapitulation of tumor physiological conditions *in vitro*, thus enhancing the power of preclinical models to test new treatment strategies. In the last part, we envision how improved knowledge in the contribution of nuclear structure to cell survival could revolutionize the fight against treatment resistance by focusing on nuclear elements dually involved in ECM sensing and the control of phenotypes.

1.3 Part 1: Mechanical properties of the tumor microenvironment

Matrix remodeling in cancerous tissue

Excessive and uncontrolled ECM remodeling is linked with severe pathological conditions. In cancer, alterations in the mechanical properties of the cell and its environment are the focus of intense interest, since mechanics governs the induction of cancer stem cells, metastatic colonization and chemoresistance (Senthebane et al., 2017; M. Wang et al., 2017).

Desmoplasia, which corresponds to the presence of dense collagenous ECM, is a reliable marker associated with poor cancer prognosis and survival. Both noncancerous cells within the ECM and cancer cells are capable of matrix remodeling by producing and repositioning collagen, fibronectin, laminin, etc. For example, CAFs, the central modifiers of the ECM, acquire a constantly activated phenotype which results in the accumulation of fibrillar proteins (Cirri &

Chiarugi, 2011). Fibronectin is the main ECM organizer and coordinates the interaction between cancer cells and their extracellular milieu. It is upregulated in many cancers, and during EMT it is mainly present at the invasive edge of tumors. It was shown that fibronectin is a site for deposition of collagen and fibrin within the ECM (Han & Lu, 2017). Laminin contributes to ECM remodeling by activating the matrix metalloproteinase-2 (MMP-2) that cleaves ECM components. (Bonnans et al., 2014). Matrix degradation is an early step toward invasion and metastasis. The upregulated expression of the laminin receptor is associated with enhanced cell-cell and cell-ECM attachments and a metastatic phenotype of cancer cells (Givant-Horwitz, Davidson, & Reich, 2004).

Enhanced expression of certain collagen modifying enzymes such as P4H (Proline hydroxylaze), PLOD (lysine hydroxylase) and LOX by cancer cells increases the rigidity and stiffness of the cancerous tissue. Elevated matrix stiffness confers an increased risk to develop solid tumors, and it also protects cancer cells from chemotherapy-induced apoptosis (Qi & Xu, 2018). Importantly, the distribution of stromal cells within the ECM is highly heterogenous, consequently differentially affecting the distribution/production of fibrillar proteins and thus, matrix stiffness. Such heterogeneity, in turn, might differentially influence the phenotype of the tumor cells via an impact on gene transcription, which could lead to chemoresistance (Udagawa & Wood, 2010). Indeed, gene expression analysis of breast and ovarian cancer cell lines resistant to cytotoxic drugs demonstrate an upregulated status for many ECM related genes and enzymes, confirming a link between matrix remodeling and cancer resistance (Sterzynska et al., 2018). Similarly, the genes involved in ECM degradation are highly induced in *in vitro* models of EMT (Peixoto et al., 2019).

Influence of matrix stiffness and tissue geometry on cancer phenotype

Changes in the balance of forces between cells and their ECM, as it occurs upon alteration of matrix stiffness and geometry (i.e., the recognizable organization of cells within a tissue), may modify cell shape and translocate to subcellular organelles including the cell nucleus. This physical remodeling further influences gene expression. The cellular structures involved in conveying mechanical signals, such as physical tensions from the ECM to the cell nucleus, include focal adhesion sites within the cell membrane. The multiprotein complex representing focal adhesion consists of integrins, epidermal growth factor receptor (EGFR), several kinases such as focal adhesion kinase (FAK) and adaptor molecules.

The increased rigidity of the ECM promotes the activation and clustering of integrins, followed by focal adhesion assembly. The integrins are the main transmembrane receptors that connect the cytoskeleton structure to the ECM. Cytoskeleton components involving actin, microtubules and intermediate filaments reorganize upon exposure to external forces. The conversion of external mechanical forces into intracellular signals is called mechanotransduction (Figure 1). Since the cell nucleus is physically connected to the cytoskeleton via the LInker of Nucleoskeleton and Cytoskeleton (LINC) complex, it is assumed that it senses changes in microenvironmental mechanical load. Indeed, pulling integrins with fibronectin coated pipets in live cells led to severe nuclear structural changes, such as nuclear peripheral infolding and elongation of the nucleoli along the axis of the applied tension that followed the reorientation of cytoskeletal filaments (Maniotis, Chen, & Ingber, 1997). There are several examples of the phenotypic impact of mechanotransduction. For instance, integrin-mediated control of Rho (Ras homologous) GTPase in stiff tumor matrix is associated with cell proliferation and invasion (Fritz, Just, & Kaina, 1999; Provenzano, Inman, Eliceiri, Trier, & Keely, 2008; Schmitz, Govek, Bottner, & Van Aelst, 2000). The Rho GTPases constitute a family of small signaling G proteins that are mainly involved in actin regulation. Elevated Rho GTPase activity triggers the alignment of collagen fibers via actin myosin contractility, which leads to higher matrix rigidity and invasiveness (Provenzano et al., 2008). Ultimately, mechanotransduction initiated in the ECM may impact the genome that is located within a compartment under mechanical strain, like the rest of the cell (Uhler & Shivashankar, 2017b).

Epigenetic alterations such as DNA methylation and histone modifications that influence gene expression also have an impact on nuclear mechanics (i.e., the physical structures of the nucleus that define its stiffness, shape, size and chromatin organization) possibly via changes in chromatin dynamics. For example, overexpression of p300, a histone acetyltransferase, in prostate cancer alters nuclear size and shape (Debes et al., 2005). In mammary epithelial cells knockdown of the chromatin remodeling enzyme, Brahma-related gene 1 (BRG1), alters nuclear shape independently of cytoskeletal tension (Imbalzano et al., 2013). Nuclear matrix proteins such as lamin A and emerin, both at the nuclear envelope, are also known to maintain the stiffness and shape of the nucleus (Dahl et al., 2006; Lammerding et al., 2006; Lammerding et al., 2004; Scaffidi & Misteli, 2006). When applying biaxial forces to fibroblasts with knocked-down lamin A, a higher nuclear strain is observed compared to the control group, indicating reduced nuclear stiffness (Lammerding et al., 2006). In addition, loss of emerin leads to altered nuclear envelope elasticity

and increased nuclear fragility and deformation (Rowat et al., 2006). Ultimately, lower nuclear rigidity that is associated with higher nuclear deformability appears necessary for the invasive phenotype of cancer cells (Harada et al., 2014). Therefore, taking into account matrix stiffness in cancer research, including the development and use of biomaterials for therapy, is paramount. Mechanical strains in tissues are not only linked to cell-ECM interactions, the geometry of the tissue formed by the cells is also an important parameter to control cell behavior. For example, endothelial cells can sense curvature at the micron-scale via their actomyosin during migration and branching (Elliott et al., 2015; Fischer, Gardel, Ma, Adelstein, & Waterman, 2009). The formation of new tissue from osteoblasts in a scaffold made of hydroxylapatite depends on the shape of the culture surface, the osteoblasts preferably proliferating on curved channels (Rumpler, Woesz, Dunlop, van Dongen, & Fratzl, 2008). Moreover, in cells outlining a channel-like a blood vessel, the actin cytoskeleton is aligned, parallel to the fluid direction, as opposed to the random orientation observed in the absence of fluid flow (Haupt & Minc, 2018). Carcinomas might also be influenced by tissue geometry. For instance, the majority of mammary tumors arise from the terminal ductal lobular unit (TDLU) in which curvature is an essential feature of the microenvironment (Silberstein, 2001). Whether the location of these TDLUs in the breast is associated with a different matrix that would differently affect epithelial cells in their curved environment remains to be understood, but oddly, breast cancer patients with tumors located in the upper lateral quadrant of breast tissue have a better prognosis than patients with tumors in the other three quadrants of the breast (Kroman, Wohlfahrt, Mouridsen, & Melbye, 2003; Levi, Randimbison, Te, & La Vecchia, 2003).

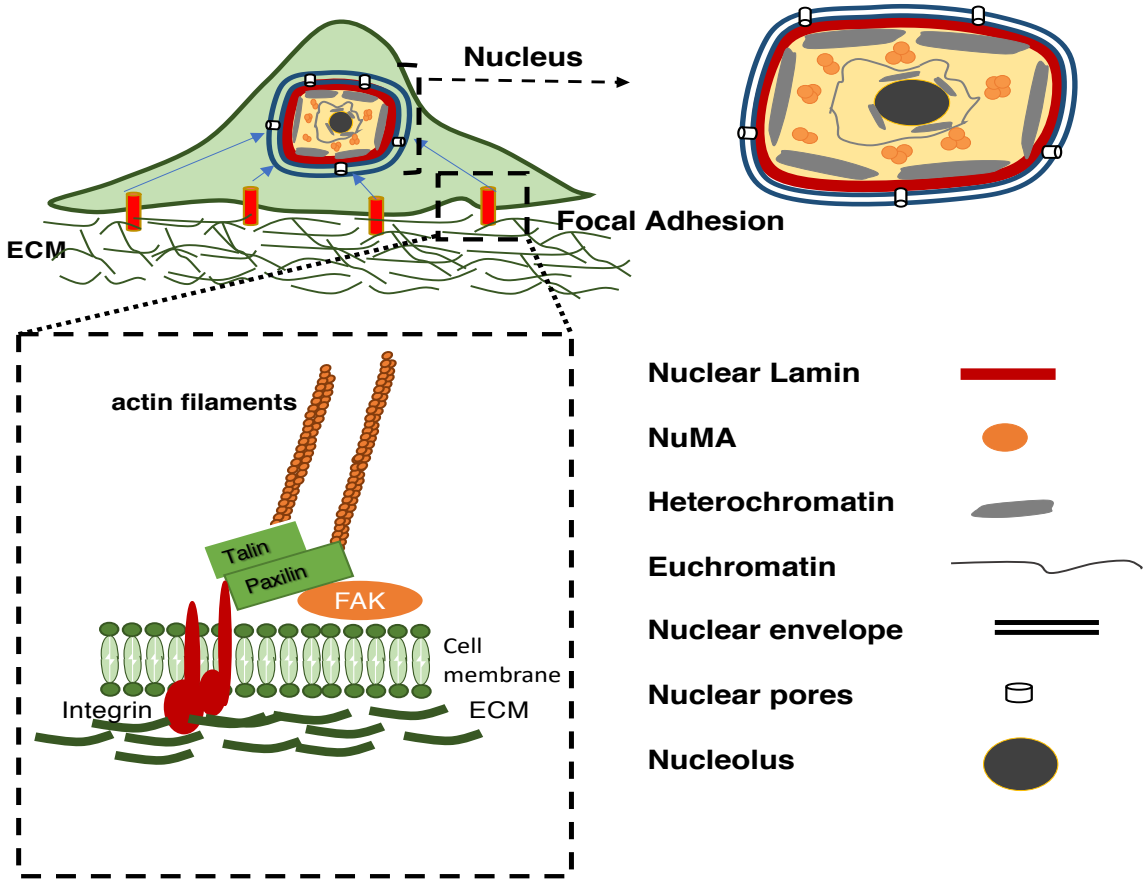

Figure 1. Mechanical forces transfer to the cell nucleus (blue arrows) via the focal adhesion complex (detailed in right bottom drawing) linked the cytoskeleton. Components of the nuclear structure transfer (nuclear envelope and pore, nuclear lamina) and/or respond (NuMA, chromatin, nucleoli) to such stimuli (shown in right drawing).

The geometrical features of the tumor and its host tissue profoundly affect tumor progression and invasion. Culture of individual tumor cells in an engineered duct lined with non-neoplastic epithelial cells revealed a higher proliferation rate for the tumor cells at the end of the duct, with high endogenous mechanical stress in the epithelial cells, compared to other locations (Boghaert et al., 2012). Whether, these geometrical features dictate the location of tumor onset by influencing the mechanical attributes of the environment remains to be understood.

Future Directions: design of 'intelligent' biomaterials that respond to microenvironmental changes

Despite molecular and biochemical advances in cancer research, major aspects of cancer onset and progression remain unsolved, which partly explains that the battle against cancer is still ongoing. One of the limits to significant progress has been attributed to the fact that cancers are seldom studied in their microenvironment, and even sophisticated *in vitro* models in 3D culture might not represent the physiological conditions that exist *in vivo* (Pampaloni, Reynaud, & Stelzer, 2007; Ravi, Paramesh, Kaviya, Anuradha, & Solomon, 2015; Schmeichel & Bissell, 2003; Yamada & Cukierman, 2007). Many aspects of the TME such as matrix stiffness, tissue geometry, spatial distribution of oxygen, metabolites and toxins, and gradients of biological molecules in general ought to be incorporated into the use of new biomaterials for *in vitro* studies. Recent advances in cell biology, microfabrication techniques and tissue engineering have led to the development of multiple technologies for cell culture. Some examples are spheroid formation techniques, organs-on-chips and 3D bioprinting; each method has its own benefits and drawbacks (Fang & Eglen, 2017; Verjans, Doijen, Luyten, Landuyt, & Schoofs, 2018). While the superiority of 3D cell culture over conventional 2D culture is a general concept, we are still far from recreating the complex tumor microenvironment *in vitro* so that it could benefit the costly procedure of clinical drug screening (Gu & Mooney, 2016). In fact, several techniques advertised for tumor making are not 3D cell culture as their merely produce cell aggregates. True 3D cell culture should induce the formation of cell assemblies with an organization reminiscent of that observed *in vivo*. Recent advances in microfabrication and biosensors with the ability to monitor physiological events in real-time made it possible to start creating cultures that readily mimic the physical parameters of tissues (Dias, Kingsley, & Corr, 2014).

For the fabrication of new 3D matrices for cell culture, injection molding could be of high interest as it could better mimic mechanical aspects of the TME. In this procedure a mixture of cells with a crosslinkable polymer (hydrogel, collagen, hyaluronic acid etc.) is injected into a mold with specific geometry (Wu, Jing, & Ding, 2006). Advanced imaging technology such as MRI and micro-CT, might help produce a highly detailed mold (Ballyns et al., 2008), enabling the recapitulation of the detailed ductal structures of glandular tissues, even in specific regions of these tissues. The major pitfall of design by molding is the loss of organ context (with the absence of spatial organization of epithelial cells and of cellular components of the ECM such as fibroblasts). Other techniques, such as layer-by-layer printing allowing multilayer constructs of different

polymers (possibly with desired stiffness) and cell contents would probably extend the possibilities to recreate an appropriate microenvironment (Gruene et al., 2011). With such TME the design and testing of new drug delivery system will be more reliable. For example, hyaluronic acid-based nanocarriers are biocompatible, biodegradable and nonimmunogenic. They can specifically bind to cancer cells with highly expressed CD44 (a cell surface adhesion receptor) and by conjugating proteins, antibodies and drugs with these nanoparticles, targeted intracellular delivery would be possible (Choi, Saravanakumar, Park, & Park, 2012). But, to achieve intracellular delivery the nanoparticles need to reach and enter the tumor cells and thus, they should be tested under different matrix stiffness conditions and with tumor cultured in different geometrical patterns (Wong et al., 2011).

Advances in high-resolution imaging and analytical technologies have provided methods to visualize and quantify the dynamic interactions between the cancer cells and their environment. This approach is necessary to measure forces at the cell–ECM interface in real time (Liu, Chaudhuri, & Parekh, 2017), especially since signaling pathways (e.g., FAK) and biproducts of cancer cell metabolism (e.g., reactive oxygen species) are able to change the rigidity of the ECM. Matrix rigidity has emerged as a key parameter for controlling diverse functions in cancer cells (such as cell motility,-adhesion, invasion and drug resistance). Therefore, the successful future design of *in vitro* models is likely to incorporate real time biosensors for matrix stiffness and natural polymeric materials so that these models are best fitted for developing and testing nanoparticles for targeted delivery. In addition, the delivery of drugs via targeting nanoparticles or gels for slow release (Paulsson & Edsman, 2002) would benefit from integrating matrix stiffness information by designing systems that either utilize mechanical conditions around tumors or are capable of modifying mechanical conditions to improve delivery.

1.4 Part 2: Nuclear structure as a mediator of information

Physical properties of the cell nucleus

The physical properties of the cell nucleus reflect important nuclear functions such as chromatin organization and gene expression. The nucleus is limited by a nuclear envelope (NE) and communicates with the cytoplasm via embedded nuclear pore complexes. It is structurally supported by an underlying scaffold. The outer nuclear membrane is in continuity with the endoplasmic reticulum and the inner membrane is associated with the nuclear lamina, which

provides support to the whole nucleus. The LINC complexes located within the NE serve as mechanical connection between the cell membrane/cytoplasm compartments and the nucleus compartment. All of the cytoskeletal components including actin microfilaments, intermediate filaments and microtubules are anchored to the nucleus via binding to specific LINC proteins. The LINC complex is very dynamic and can form multiple connection sites depending on their composition and purpose. For example, in migrating cells, the formation of transmembrane actin-associated nuclear (TAN) lines via the LINC complex rearranges the actin filaments perpendicular to the cell direction. A LINC complex such as Sad1/ UNC-84 (SUN)2 and nesprin2G forms linear arrays and is coupled with actin cables for nuclear movements and force transmission (Luxton, Gomes, Folker, Vintinner, & Gundersen, 2010). The Sad1/ UNC-84 (SUN) domain of the LINC complex is an adhesion protein that is essential for the correct assembly and positioning of the Nuclear Pore Complexes (NPCs). These nuclear structures fuse the inner and outer nuclear membranes and provide portals for the exchange of macromolecules between nucleus and cytoplasm (Lee & Burke, 2018; Strambio-De-Castillia, Niepel, & Rout, 2010). The NPCs are also connected to the genome and nuclear intermediate filament proteins that participate in the nuclear matrix.

The intermediate filament proteins of the cell nucleus are collectively involved in DNA replication, epigenetic regulation and genome organization. Among these proteins, the network of lamins has received the highest attention notably because mutations in their genes are associated with multiple diseases involved in premature aging such as Hutchinson Gilford Progeria Syndrome (refs). Lamins are located close to the inner nuclear membrane and expand into the nucleoplasm, except in the nucleolus (Dittmer & Misteli, 2011; Zwerger et al., 2015). Abnormal lamin expression in cancers is associated with miRNA-31 upregulation which is involved with cell proliferation (Malhas, Saunders, & Vaux, 2010). In addition, Lamin A depletion is associated with changes in nuclear shape and an increase in nuclear membrane tension (Dahl, Kahn, Wilson, & Discher, 2004). In contrast to lamins, the coiled coil structural protein, NuMA is present throughout the nucleus (Harborth, Wang, Gueth-Hallonet, Weber, & Osborn, 1999) and in the nucleolus where it controls the transcription of rDNA (Jayaraman et al., 2017). With 10^6 copies per nucleus NuMA is almost as abundant as the lamins and considered a major nuclear matrix component (Radulescu & Cleveland, 2010). NuMA controls the organization of heterochromatin and euchromatin into epigenetic regions during mammary epithelial differentiation (Abad et al., 2007). These findings supports an earlier report of NuMA binding to the AT rich domains of

MARs (Luderus, den Blaauwen, de Smit, Compton, & van Driel, 1994), implicating this protein in higher order chromatin organization. The overexpression of NuMA truncated at its C-terminus relocated the DNA, histone 1 and nucleoli to the nuclear envelope (Gueth-Hallonet, Wang, Harborth, Weber, & Osborn, 1998). Overall, the structural proteins of the nucleus appear to maintain the physical structure of this organelle and provide a supporting/organizing matrix for the DNA.

The presence of perinuclear actin cap above and around the interphase nucleus suggests how cell shape could regulate nuclear shape. Cell culture based experiments have revealed that the assembly and contractility of the actin filaments along the main axis of the cell pull the nucleus down and prevent it to bulge from the cell surface (S. B. Khatau et al., 2009). The actin cap is connected to the nuclear membrane via LINC complexes, and the lamin network is essential for its formation (S. B. Khatau et al., 2009). An increase in nuclear volume occurs when disrupting actin filaments using latrunculin (Rowat et al., 2006), which indicates that actin integrity is necessary for the maintenance of nuclear structure. In addition to its perinuclear presence, actin also localizes and functions within the nucleus. Nuclear actin is found in two forms. There are actin polymers without an obvious filamentous structure, and actin polymers that resemble cytoplasmic actin but are distinct enough not to stain with phalloidin. Nuclear actin is involved in many important nuclear functions such as transcription and chromatin remodeling, but it also participates in maintaining the physical structure of the nucleus. For example, the formation of transient actin filaments is essential for nuclear expansion and chromatin decondensation during exit from mitosis in mammalian cells (Baarlink et al., 2017). Actin dynamics is highly regulated in a cell cycle dependent manner; for example, the occurrence of nuclear protrusion during the G1 phase of mitosis (which is the time at which chromatin starts to decondense) is due to the polymerization of actin filaments beneath the nuclear membrane. It is still unclear how nuclear F-actin actually functions during chromatin decondensation and nuclear expansion. Also, whether actin dynamics within the nucleus is coordinated with other nucleoskeleton components is still unknown. Although the lamin network is the major regulator of actin dynamics at the nuclear envelope, its depletion does not affect actin organization (S. B. Khatau et al., 2009; Lammerding & Wolf, 2016).

Nuclear proteins involved in mechanosensing

Mechanosensing describes the ability of the cell to sense the mechanical cues from its microenvironment. Force sensitive structures within the cells transduce mechanical stimuli into gene transcription signals, thus enabling cells to adapt to their physical environment. The nucleus is the stiffest organelle in the cells. It is mechanically linked to the rest of the cell content through complex structures in the nuclear envelope described earlier, hence allowing for cytoskeleton and external forces to be sensed. Mechanostimuli might lead to nuclear changes either via their integration by the cell nucleus or as a form of resistance from the nucleus. Nuclear mechanosensing describes a range of molecular events from changes of nuclear protein conformation and transcription factor localization to chromosome rearrangement and nuclear morphological deformation, all of which alter gene expression (Guilluy & Burridge, 2015). Nuclear deformation is an early stage of cancer cell metastasis, the role of which is poorly understood. Notably, it is not known how physical alterations are received and interpreted into gene transcriptional signals. It is anticipated that ECM mechanical impact is involved in the initiation of the process.

Several nuclear proteins and complexes have been identified as mechanosensors. LINC is the main complex within the nuclear envelope that transfers mechanical forces from the cytoskeleton to the nucleus. The cytoplasmic members (Nesprin proteins) of the LINC are connected to the cytoskeletal components and outer nuclear membrane via the klarsicht, ANC-1, syne homology (KASH) domain. The SUN domains span through the perinuclear space and transfer the physical forces to the network of lamins (Figure 2). Studies performed on isolated nuclei showed that in response to physical forces, lamin A is recruited to the LINC complex via Nesprin 1, which would further strengthen the nuclear membrane (Guilluy et al., 2014). Lamins are also associated with heterochromatin and a wide range of transcription factors and therefore, they might be good candidates to regulate gene expression during mechanosensing. Indeed, lamin A proteins are responsive to tissue stiffness (Swift et al., 2013). Lamin expression and phosphorylation levels are elevated in a stiff matrix, which leads to a morephysically stable nucleus. In addition, in tissues with high physical stress such as muscle, Bone and heart lamin A expression is practically 30-fold higher than in softer tissues like the brain. Such elevation of lamins was shown to protect nuclear integrity, chromosome territories and lamin-chromatin interaction, which is important for epigenetic regulation and the occurrence of DNA breaks (Heald & McKeon, 1990; Meuleman et al., 2013; Zullo et al., 2012).

There is speculation regarding the role of NPCs in nuclear mechanosensing because they are associated with both cytoskeleton and genome contents (directly and through lamins) with an active role during transcription and mRNA transport (Akhtar & Gasser, 2007; Griffis, Craige, Dimaano, Ullman, & Powers, 2004). Following nucleus expansion due to mechanical forces, it is possible for the nuclear pores to be more permissive to structural proteins (e.g. actin~40 kDa) that are then transferred inside the nucleus (Fedorchak, Kaminski, & Lammerding, 2014). An open question is whether mechanical forces are transferring only via the LINC or through the entire NE. Also, the existence of mechanosensors residing amidst the genome, inside the nucleus, is not known. It is assumed that mechanosensing involves cytoplasmic resident proteins traveling from the cytoplasm to the cell nucleus, although nuclear resident proteins that have the ability to shuttle between nucleus and cytoplasm, hence communicating with the cytoskeleton upon physical perturbation, might also be an option. Overall, the continuity of the interaction from the ECM to the cell nucleus, with a potential impact on gene expression outlines the possibility that drug delivery might also encounter physical obstacles to reach the nuclear compartment (if the drug needed there), and even more, certain regions within the genome, the compaction of which might depend on mechanical conditions in the ECM.

Future Directions: Identification of internal nuclear features that have the ability to link microenvironmental changes and chromatin

The important role of chromatin reorganization and epigenetic reprograming in transforming nonaggressive tumor cells into an aggressive and chemoresistant cell populations has been abundantly addressed. For the longest time, cancer progression has been characterized by pathologists as the acquisition of heterogeneous alterations in nuclear morphology (e.g., chromatin appearance, nucleus size and shape). For example, in ovarian cancer, DNA hypomethylation and increased nuclear area correlate with greater cell proliferation rates, aneuploidy, and reduced survival probability (Zeimet et al., 2011).

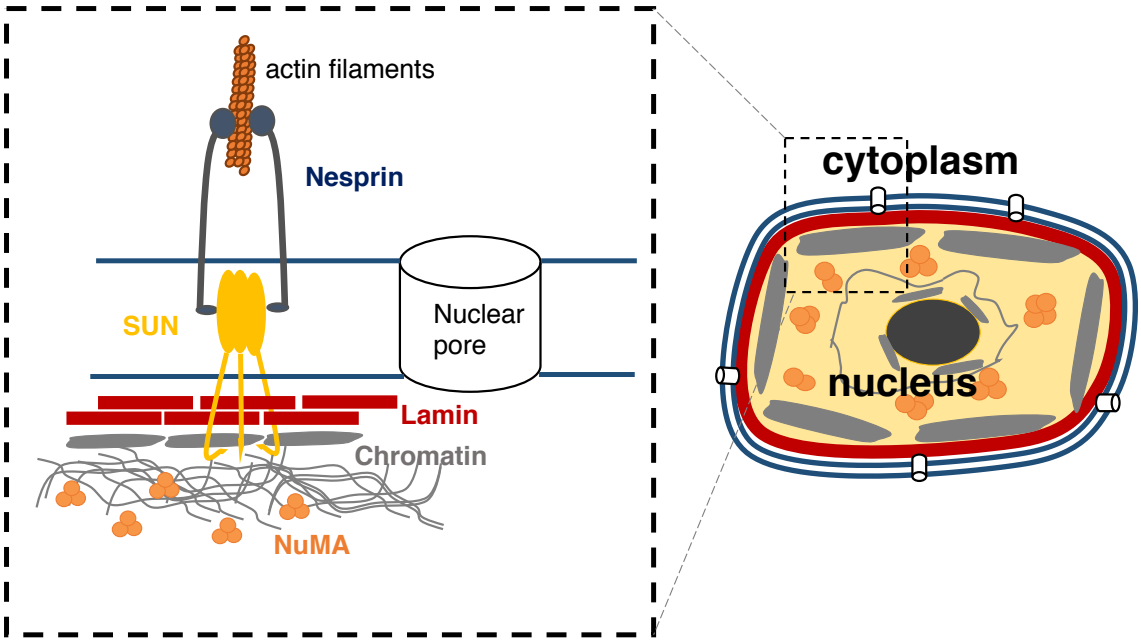

Figure 2. Linker of nucleoskeleton and cytoskeleton (LINC) complex is associated with both inner and outer membranes of the nucleus. The Nesprin proteins are connected to cytoskeleton components such as actin. The SUN-domains are associated with both nuclear lamins and chromatin and span through the inner nuclear membrane.

In addition, in lung cancer inactivation of p53 is associated with nuclear enlargement, irregular nuclear envelope and chromatin density ((Yang, Maciejowski, & de Lange, 2017). Specifically, alterations in the TME are associated with changes in nuclear morphology (Uhler & Shivashankar, 2017b); yet, the link between the latter and chromatin rearrangement remains to be identified.

Close interactions of nuclear scaffold components, such as lamins and NuMA, with chromatin specify the distinct spatial organization of the cell nucleus and are thought to facilitate the hierarchical packaging of chromatin (Getzenberg, Pienta, Ward, & Coffey, 1991). Therefore, it seems logical to consider the interfilamentous proteins of the nuclear scaffold or nucleoskeleton as the mediators of external forces and chromatin organization. Lamin A/C was the focus of many mechanosensing studies in which morphological changes in cancer cell nuclei were linked to lamin expression, but different types of mechanosensors might exist and be independently activated.

Indeed, lamins are mainly associated with heterochromatin, the part of genome with repressive signals. A protein like NuMA is likely to also respond to mechanical stress. It shares conformational characteristics with lamin (both are interfilamentous proteins). It was shown that RNAs anchor NuMA to the lamin scaffold, which maintains lamin expansion through the nuclear matrix, and RNAse digestion of the complete nuclear matrix induces an extensive depletion of NuMA while the nuclear matrix loses its integrity and turns into large aggregates (Barboro et al., 2002). In contrast to lamins, NuMA interacts open chromatin regions and chromatin remodeling proteins such as SNF2h/SMARCA5; it also facilitates the hierarchical packaging of chromatin (Vidi et al., 2012).

Mechanosensors in the cell nucleus might be an interesting series of proteins to integrate in studies focusing on the physical impact of the microenvironment on cancer phenotype, and notably resistance to treatment. Moreover, drugs or drug delivery systems that would make use of physical properties important to control cell behavior would benefit from the better knowledge of nuclear mechanosensors, since these molecules could become part of the readout for the successful design of new therapies.

1.5 Part 3: Nuclear dynamics in anticancer drug resistance and cell survival

Drug resistance and survival in cancer cell populations

For many years chemoresistance studies in cancer were focusing only on cancer cells. The impact of tumor interactions with the surrounding environment has received a well-deserved attention over the last decade to better understand the mechanisms that allow tumors to thrive and overcome cytotoxic treatments. Tumor cell survival is enhanced via cell-cell and cell-ECM interactions. Cells communicate with each other by transferring peptides through their gap junctions, exchanging membrane proteins and interacting via ligand receptors, which contributes to the acquisition of a complex, heterogeneous tumor phenotype. The cellular interactions leading to an exchange of membrane patches, called trogocytosis, is a characteristic of immune cells, but this phenomenon also exists between cancer and stromal cells. In the latter case, it is associated with the acquisition of a mesenchymal phenotype by tumor cells and with chemoresistance, as shown with ovarian and breast cancers (Lis et al., 2010; Rafii et al., 2008). This phenomenon might explain how stromal cells found near cancer cell populations play a supportive role. It was shown that the coculture of cancer cells and CAFs induces cytokine-mediated chemoresistance. Cytokines

such as interleukin-6 protect cancer cells from therapy-induced DNA damage, oxidative stress and apoptosis by triggering repair mechanisms and anti-apoptotic pathways. Moreover, by providing integrin-binding ligands, such as ECM components, stromal cells contribute to integrin signaling that are responsible for the activation of anti-apoptotic pathways in cancer cells. Signaling becomes enhanced due to an increase in the expression of integrins that subsequently increases the number of binding sites to ECM proteins (specially fibronectin and collagen) (Aoudjit & Vuori, 2012; Damiano, 2002). The resulting promotion of cell survival and chemoresistance occurs via the regulation of multiple signaling pathways (e.g. PI3K-AKT, ERK and NF-κB).

Increased matrix stiffness is an important physical aspect of the TME that directly affects drug response. The prosurvival effect of the TME occurs first by reducing drug diffusion because of the heterogenous distribution of ECM proteins and the presence of the tumor mass that affect the interstitial fluid pressure (Balkwill, Capasso, & Hagemann, 2012). Moreover, the abnormal accumulation of collagen I is linked to the invasive phenotype of EMT, an important factor for the acquisition of chemoresistance in cancer cells (Cramer, Jones, El-Hamidi, & Celli, 2017) (Figure 3). For instance, invasive populations (i.e., populations that contain cells with migration capabilities at the edge of the tumor nodule) of pancreatic ductal adenocarcinoma cultured within collagen I showed resistance upon oxaliplatin chemotherapy, while the primary cells of the nodules showed higher sensitivity to the drug (Cramer et al., 2017). Chemoresistance of triple negative breast cancer cells (MDA-MB-231) to doxorubicin that occurs in a stiff matrix is three times higher than in a softer matrix. Interestingly, the luminal breast cancer MCF-7 cells did not respond to doxorubicin in a stiffness-dependent manner. These two cell types possess a different ability to sense alterations in ECM stiffness as shown by the translocation of mechanotransducer YAP only in MDA-MB-231 cells (Joyce et al., 2018), which directly links mechanotransduction with chemoresistance. Importantly, matrix stiffness influences H3K9 methylation at the nuclear periphery, just under the nuclear envelope. This effect is replicated by applying stress via magnetic beads on the cell surface, suggesting that stiff matrix-induced H3K9 methylation may be (at least) in part due to the elevation of physical stress within the cell (Tan et al., 2014).

Overall, complex mechanisms of cell-ECM interactions preside to the acquisition of chemoresistance in cancer cells, indicating that *in vitro* studies need to represent the dynamic interactions of tumors with their environment. Cell-ECM interactions can be translated into signaling pathways which could ultimately affect chromatin organization and cell nucleus homeostasis. Therefore, we propose that alterations in the structure of the cell nucleus constitute a

reliable marker based on which the cancer model can be optimized (Chittiboyina et al., 2017; Lelièvre & Chittiboyina, 2018). From early changes in nuclear morphometric values and visibly detectable nucleolar and chromatin reorganization at the onset of cancer development, to an extensive deformation and epigenetic reshufflings during migration and chemoresistance, the nucleus is a constant reporter of cancer cell phenotypes. Therefore, monitoring nuclear behavior could help engineers in their design of biomaterials that better mimic *in vivo* condition.

Nuclear dynamics and alterations in genome functions

Chemoresistance is a leading cause of death in cancer patients. There are urgent and unmet needs for improved targeting agents and reversal of treatment resistance. Major features of nuclear dynamics, chromatin reorganization and epigenetic reprograming are emerging as essential to transform nonaggressive tumors into aggressive and chemoresistant cancers. The epigenetic rearrangement leading to chemoresistance is thought to accompany or follow the acquisition of an invasive disease stage (Housman et al., 2014). Since the advent of pathological analysis, cancer progression has been characterized as the acquisition of heterogeneous alterations in nuclear morphology (e.g., chromatin appearance, nucleus size and shape).

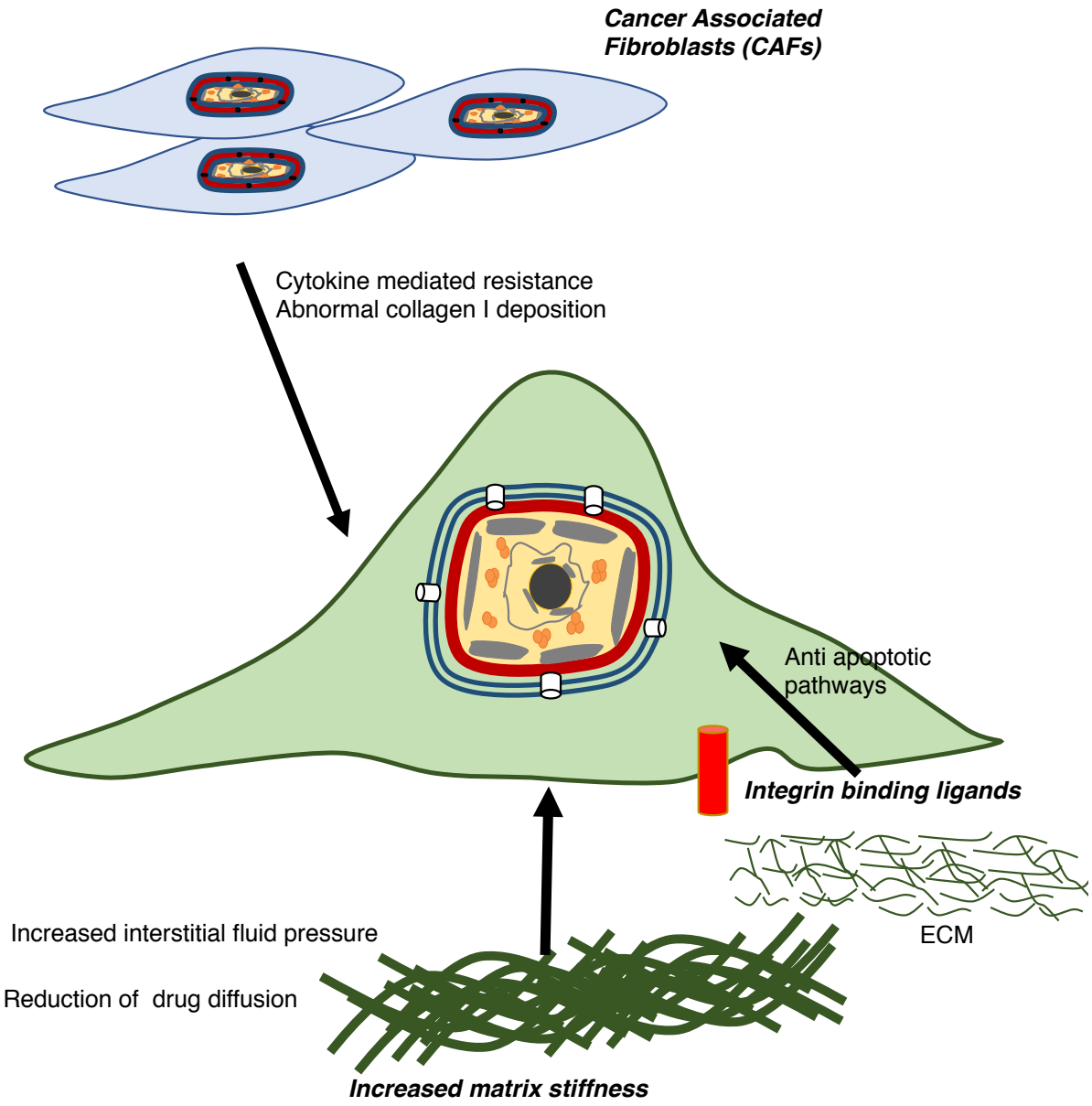

Figure 3. Features of the tumor microenvironment that are involved in the survival of cancer cells. *Cancer Associated Fibroblasts* (CAFs) secrete cytokines and deposit collagen I that mediate resistance to induced cell death. Varied expression of ECM components such as fibronectin, laminin and collagen I, provide *integrin binding ligands,* which similarly to CAFs activate anti apoptotic and cell proliferation signals.

Increased matrix stiffness is associated with increased interstitial fluid pressure and reduction of drug diffusion. Interestingly, epigenetic modifications and global changes in the chromatin of

individual cells are associated with alterations in nuclear morphology and could predict chemotherapy outcome (Kurdistani, 2014). Hence, texture analysis of chromatin and nuclear size is an approach that may be used in the development and refinement of diagnoses as well as in the prognosis and the follow-up of cancer. Reversible DNA methylation and histone modifications (acetylation and deacetylation) are major epigenetic mechanisms of gene expression control. DNA methylation usually occurs at CpG islands within genes promoters. While histone acetylation can occur more generally throughout the genome and it alters chromatin conformation. Simply, histone acetylation opens the chromatin and deacetylation closes it. These mechanisms are out of control in chemoresistance. For instance, demethylation of *MDR1 (*multidrug resistance protein 1) promoter in cancer cell lines was found to be strongly associated with the acquisition of a multidrug resistant phenotype (Kantharidis et al., 1997). In another study, an inverse relationship was found between tamoxifen resistance in breast cancer and methylation of the *ERβ* (Estrogen receptors beta) gene. In general, tamoxifen-resistant tumors showed higher *ERβ* gene methylation than control tumors (Chang et al., 2005). These results imply that nuclear dynamics and alterations in chromatin texture, mainly because of epigenetic reprograming, could change gene expression.

Emerging evidence demonstrate that mechanical factors along with transcriptional and biochemical factors, can regulate the epigenetic state of the cells and dictate phenotypic changes. For example, when culturing fibroblasts on microfabricated surfaces with different geometry, increased cellular area and elevated levels of H3 acetylation were observed concomitantly with increased nuclear volume (Jain, Iyer, Kumar, & Shivashankar, 2013). In addition, culturing primary fibroblast cells on microgroove topography coated with cell-adhesive substrates, induced pronounced changes in histone acetylation and methylation patterns; the latter were specifically dependent on cell morphological changes and actin–myosin tension (Downing et al., 2013). In Summary, mechanical alterations from the environment seem to impose gene regulation via the modification of the epigenome.

Future Directions: Platforms and biomaterials to integrate nuclear reorganization and cell survival in tumors

A considerable portion of the current knowledge in cancer biology has been acquired using traditional cell culture (i.e., two-dimensional (2D) culture) in which environmental factors of cancer development have been overlooked. Consequently, the design and test of molecules and tools for cancer treatment has been greatly delayed and even impaired. Cell culture that fails to recapitulate cell-cell and cell-ECM interactions as they exist *in vivo* lacks features essential for cancer cells vitality. It is now recognized that the lack of compliance with tumor organization is in part responsible for the observed differences in drug efficacy and toxicity tests in 2D culture of cancer cells compared to *in vivo*. With inappropriate cell culture, clinically effective candidates might be easily missed, while compounds with low or no clinical success move on to animal testing (in which specific human TME might not be reproducible) and even clinical trials, making drug development a costly and time-consuming process. Therefore, it is necessary to develop *in vitro* models of drug screening that provide higher fidelity to the *in vivo* situation including, as we discussed above, physical constraints since they influence cells all the way to the genome that controls phenotypes and drug sensitivity.

The 3D cell culture models, that promote the organization of cells into recognizable patterns observed *in vivo*, are often categorized into nonmatrix and matrix-based cultures. An example of the nonmatrix method is the hanging drop used to create tumor spheroids via self-aggregation of cancer cells. Here the spheroid size depends on the initial number of cells. However, these spheroids are devoid of cell-ECM interactions and the cell-cell interactions are possibly at the lowest level due to the aggregation of single cells instead of cell division. Matrix-based cultures encompass any nodule formation using ECM-based or synthetic hydrogel scaffolds. If appropriate for the purpose of the work, the matrix would allow cell proliferation, nodule formation and even cell migration. The physiological relevance of these models is particularly high when using hydrogel scaffolds of biological origin, as long as the ECM is of the type necessary to promote cancer phenotype. NonECM-based hydrogel might also be relevant if the cells are capable of secreting matrix components. However, regardless of the conditions, important features of the tissue architecture such as geometry, stiffness and stromal cells component might be necessary depending on the type of cancer.

The engineered design of intelligent matrix to reveal *in vivo*-like tumor cell responses in models *in vitro* used for drug design and testing, including new delivery methods, will require precise and simultaneous control over toxins, oxygen and nutrients distribution, as well as matrix structural porosity and mechanical properties. Since the acquisition of chemoresistance is concurrent with aggressiveness and invasion, we propose that *in vitro* cancer models should recapitulate the corresponding matrix features with nuclear features as the readout. Cancer cells *in vivo* migrate by gradually degrading their surrounding ECM and find their way through vasculature and secondary tissues by following leader cancer cells and associated stromal cells that provide a supportive migrating niche (Paul, Mistriotis, & Konstantopoulos, 2017). Specifically, stromal cells such as CAFs and macrophages are capable of opening up migration paths via the secretion of proteinases and collagen crosslinking enzymes, hence potentially influencing drug diffusion depending on the delivery method. In addition, the fibrillar scaffold of collagen *in vivo* is very heterogenous (the presence of low to high fibrillar density within the same tissue) with pore sizes varying from 1 μm to 20 μm in diameter and collagen free spaces ranges of 10-1000 μm^2 (Gritsenko, Ilina, & Friedl, 2012). The cell nucleus undergoes dramatic deformation (e.g., the nuclear envelop ruptures and the associated DNA is damaged) when tumor cells pass through the pores and fiber-like channels within the ECM. As, mentioned earlier these invasive cells are also the most resistant to the anticancer drugs. Therefore, to faithfully mimic the ECM necessary to develop treatment against cells resistant to therapy, the biomaterials used for the 3D model of drug assessment should not simply allow the formation of a homogenous networks of collagen fibrils (with either high or low stiffness) with similar pore size; instead, a dynamic and heterogenous texture with varying pore sizes is required. In addition, the presence of stromal cells such as CAFs, epithelial and endothelial cells as well as a defined geometry of the tissue could further improve the design of the model. One example of model with specific geometry, the Disease-on the Chip (DOC), has been developed to culture cancer nodules in curved surfaces, hence mimicking the environment of tumors developing in glandular tissues like that of the breast, prostate or pancreas (Vidi et al., 2014). It will be important to compare drug efficacy assessments on the DOC to that of other models with low fidelity to the original tissue.

The second aspect of intelligent materials design pertains to its use with drugs for *in vivo* delivery. New methods make use of targeted delivery with homing devices, which should not be affected by the TME. But these methods increasingly rely also on the slow release of drugs locally (Weiser & Saltzman, 2014) or on nanoparticles to deliver the cytotoxic agent to specific locations

within the cells (Kwon, Lee, Han, & Park, 2012). As we discussed in previous sections, the microenvironmental context of the tumor is particularly important to consider since it might directly impair the function of hydrogels or could affect the compartmentalization of the drugs if the internal cell organization, notably in the nucleus has been modified by the TME. New intelligent materials might be able to detect stiffness and other TME conditions and modify them to ensure proper drug delivery and activity.

1.6 Conclusion

Recent statistical reports indicate that cancer is still a leading cause of death worldwide, with an estimated burden of 12 million deaths for 2030, a number that is above that of the population of certain countries. The lack of a thorough understanding of cancer cell survival mechanisms and of understanding of the role of the TME in cancer chemoresistance are essential and costly gaps in knowledge. The development of new biomaterials and cell culture methods to reproduce the TME has been on a rising slope, but we are still far from the culture models that could faithfully predict patients' response to chemotherapy and provide optimal testbeds for new therapies. Delays in the development of improved therapies are in part due to the complexity of the prosurvival surroundings of cancers and the lack of biomarkers to guide scientists through the recapitulation, *in vitro*, of tumor phenotypes as *in vivo*.

We have given examples of the plasticity of nuclear morphology and global chromatin organization in tumor cells that exists throughout tumor stages. We propose that nuclear features that mirror phenotypes, usually because they control phenotype, could act as valuable sources for determining the reliability of the cancer models to be used for development and testing of therapies. Indeed, certain nuclear features have been used to predict chemotherapy outcome in cancer patients (Zeimet, Fiegl et al. 2011; Yang, Maciejowski et al. 2017). Importantly, nuclear morphology responds to TME changes such as matrix rigidity and toxins level (Uhler et al., 2017; Chittiboyina et al., 2018). The use of nuclear features in cancer in not new since pathologists have relied on nuclear analyses for diagnosis for decades. However, the application of nucleus-based knowledge to improve the design of preclinical models is a novel development (Lelièvre and Chittiboyina, 2018).

We have also given information on the importance of the TME in influencing cancer progression and resistance to treatment that should alert the scientific community to the importance of enabling

the next generation of intelligent biomaterials with capabilities to monitor and modify the TME, including rigidity, oxygen, nutrients and toxins distribution in real time. These capabilities would ensure that therapy delivery methods are effective locally and with certain designs, like slow release of medications, the effectiveness is adaptive to local conditions and sustained.

1.7 References

Abad, P. C., Lewis, J., Mian, I. S., Knowles, D. W., Sturgis, J., Badve, S., . . . Lelievre, S. A. (2007). NuMA influences higher order chromatin organization in human mammary epithelium. *Mol Biol Cell, 18*(2), 348-361. doi:10.1091/mbc.E06-06-0551

Aitken, S. J., Ibarra-Soria, X., Kentepozidou, E., Flicek, P., Feig, C., Marioni, J. C., & Odom, D. T. (2018). CTCF maintains regulatory homeostasis of cancer pathways. *Genome Biol, 19*(1), 106. doi:10.1186/s13059-018-1484-3

Akhtar, A., & Gasser, S. M. (2007). The nuclear envelope and transcriptional control. *Nat Rev Genet, 8*(7), 507-517. doi:10.1038/nrg2122

Andreu, P., Johansson, M., Affara, N. I., Pucci, F., Tan, T., Junankar, S., . . . Coussens, L. M. (2010). FcRgamma activation regulates inflammation-associated squamous carcinogenesis. *Cancer Cell, 17*(2), 121-134. doi:10.1016/j.ccr.2009.12.019

Aoudjit, F., & Vuori, K. (2012). Integrin signaling in cancer cell survival and chemoresistance. *Chemother Res Pract, 2012*, 283181. doi:10.1155/2012/283181

Baarlink, C., Plessner, M., Sherrard, A., Morita, K., Misu, S., Virant, D., . . . Grosse, R. (2017). A transient pool of nuclear F-actin at mitotic exit controls chromatin organization. *Nature Cell Biology, 19*(12), 1389-1399. doi:10.1038/ncb3641

Balkwill, F. R., Capasso, M., & Hagemann, T. (2012). The tumor microenvironment at a glance. *J Cell Sci, 125*(Pt 23), 5591-5596. doi:10.1242/jcs.116392

Ballyns, J. J., Gleghorn, J. P., Niebrzydowski, V., Rawlinson, J. J., Potter, H. G., Maher, S. A., . . . Bonassar, L. J. (2008). Image-guided tissue engineering of anatomically shaped implants via MRI and micro-CT using injection molding. *Tissue Eng Part A, 14*(7), 1195-1202. doi:10.1089/ten.tea.2007.0186

Barboro, P., D'Arrigo, C., Diaspro, A., Mormino, M., Alberti, I., Parodi, S., . . . Balbi, C. (2002). Unraveling the organization of the internal nuclear matrix: RNA-dependent anchoring of NuMA to a lamin scaffold. *Exp Cell Res, 279*(2), 202-218.

Bednarz-Knoll, N., Alix-Panabieres, C., & Pantel, K. (2012). Plasticity of disseminating cancer cells in patients with epithelial malignancies. *Cancer Metastasis Rev, 31*(3-4), 673-687. doi:10.1007/s10555-012-9370-z

Berezney, R., & Coffey, D. S. (1974). Identification of a nuclear protein matrix. *Biochem Biophys Res Commun, 60*(4), 1410-1417.

Boghaert, E., Gleghorn, J. P., Lee, K., Gjorevski, N., Radisky, D. C., & Nelson, C. M. (2012). Host epithelial geometry regulates breast cancer cell invasiveness. *Proc Natl Acad Sci U S A, 109*(48), 19632-19637. doi:10.1073/pnas.1118872109

Bonnans, C., Chou, J., & Werb, Z. (2014). Remodelling the extracellular matrix in development and disease. *Nat Rev Mol Cell Biol, 15*(12), 786-801. doi:10.1038/nrm3904

Boroughs, L. K., & DeBerardinis, R. J. (2015). Metabolic pathways promoting cancer cell survival and growth. *Nat Cell Biol, 17*(4), 351-359. doi:10.1038/ncb3124

Carmeliet, P., & Jain, R. K. (2011). Molecular mechanisms and clinical applications of angiogenesis. *Nature, 473*(7347), 298-307. doi:10.1038/nature10144

Cathcart, J., Pulkoski-Gross, A., & Cao, J. (2015). Targeting Matrix Metalloproteinases in Cancer: Bringing New Life to Old Ideas. *Genes Dis, 2*(`1), 26-34. doi:10.1016/j.gendis.2014.12.002

Chandramouly, G., Abad, P. C., Knowles, D. W., & Lelievre, S. A. (2007). The control of tissue architecture over nuclear organization is crucial for epithelial cell fate. *J Cell Sci, 120*(Pt 9), 1596-1606. doi:10.1242/jcs.03439

Chang, H. G., Kim, S. J., Chung, K. W., Noh, D. Y., Kwon, Y., Lee, E. S., & Kang, H. S. (2005). Tamoxifen-resistant breast cancers show less frequent methylation of the estrogen receptor beta but not the estrogen receptor alpha gene. *J Mol Med (Berl), 83*(2), 132-139. doi:10.1007/s00109-004-0596-2

Chao, Y., Wu, Q., Acquafondata, M., Dhir, R., & Wells, A. (2012). Partial mesenchymal to epithelial reverting transition in breast and prostate cancer metastases. *Cancer Microenviron, 5*(1), 19-28. doi:10.1007/s12307-011-0085-4

Chittiboyina, S., Rahimi, R., Atrian, F., Ochoa, M., Ziaie, B., & Lelièvre, S. A. (2017). Gradient-on-a-Chip with Reactive Oxygen Species Reveals Thresholds in the Nucleus Response of Cancer Cells Depending on the Matrix Environment. *ACS Biomaterials Science & Engineering, 4*(2), 432-445. doi:10.1021/acsbiomaterials.7b00087

Choi, K. Y., Saravanakumar, G., Park, J. H., & Park, K. (2012). Hyaluronic acid-based nanocarriers for intracellular targeting: interfacial interactions with proteins in cancer. *Colloids Surf B Biointerfaces, 99*, 82-94. doi:10.1016/j.colsurfb.2011.10.029

Cirri, P., & Chiarugi, P. (2011). Cancer associated fibroblasts: the dark side of the coin. *Am J Cancer Res, 1*(4), 482-497.

Cordes, N., & Meineke, V. (2003). Cell adhesion-mediated radioresistance (CAM-RR). Extracellular matrix-dependent improvement of cell survival in human tumor and normal cells in vitro. *Strahlenther Onkol, 179*(5), 337-344. doi:10.1007/s00066-003-1074-4

Cramer, G. M., Jones, D. P., El-Hamidi, H., & Celli, J. P. (2017). ECM Composition and Rheology Regulate Growth, Motility, and Response to Photodynamic Therapy in 3D Models of Pancreatic Ductal Adenocarcinoma. *Mol Cancer Res, 15*(1), 15-25. doi:10.1158/1541-7786.MCR-16-0260

Dahl, K. N., Kahn, S. M., Wilson, K. L., & Discher, D. E. (2004). The nuclear envelope lamina network has elasticity and a compressibility limit suggestive of a molecular shock absorber. *J Cell Sci, 117*(Pt 20), 4779-4786. doi:10.1242/jcs.01357

Dahl, K. N., Scaffidi, P., Islam, M. F., Yodh, A. G., Wilson, K. L., & Misteli, T. (2006). Distinct structural and mechanical properties of the nuclear lamina in Hutchinson-Gilford progeria syndrome. *Proc Natl Acad Sci U S A, 103*(27), 10271-10276. doi:10.1073/pnas.0601058103

Damiano, J. S. (2002). Integrins as novel drug targets for overcoming innate drug resistance. *Curr Cancer Drug Targets, 2*(1), 37-43.

Damiano, J. S., Cress, A. E., Hazlehurst, L. A., Shtil, A. A., & Dalton, W. S. (1999). Cell adhesion mediated drug resistance (CAM-DR): role of integrins and resistance to apoptosis in human myeloma cell lines. *Blood, 93*(5), 1658-1667.

de Visser, K. E., Korets, L. V., & Coussens, L. M. (2005). De novo carcinogenesis promoted by chronic inflammation is B lymphocyte dependent. *Cancer Cell, 7*(5), 411-423. doi:10.1016/j.ccr.2005.04.014

De Wever, O., Demetter, P., Mareel, M., & Bracke, M. (2008). Stromal myofibroblasts are drivers of invasive cancer growth. *Int J Cancer, 123*(10), 2229-2238. doi:10.1002/ijc.23925

Debes, J. D., Sebo, T. J., Heemers, H. V., Kipp, B. R., Haugen, D. L., Lohse, C. M., & Tindall, D. J. (2005). p300 modulates nuclear morphology in prostate cancer. *Cancer Res, 65*(3), 708-712.

Dias, A. D., Kingsley, D. M., & Corr, D. T. (2014). Recent advances in bioprinting and applications for biosensing. *Biosensors (Basel), 4*(2), 111-136. doi:10.3390/bios4020111

Dittmer, T. A., & Misteli, T. (2011). The lamin protein family. *Genome Biol, 12*(5), 222. doi:10.1186/gb-2011-12-5-222

Downing, T. L., Soto, J., Morez, C., Houssin, T., Fritz, A., Yuan, F., . . . Li, S. (2013). Biophysical regulation of epigenetic state and cell reprogramming. *Nature Materials, 12*(12), 1154-1162. doi:10.1038/nmat3777

Elliott, H., Fischer, R. S., Myers, K. A., Desai, R. A., Gao, L., Chen, C. S., . . . Danuser, G. (2015). Myosin II controls cellular branching morphogenesis and migration in three dimensions by minimizing cell-surface curvature. *Nat Cell Biol, 17*(2), 137-147. doi:10.1038/ncb3092

Erez, N., Truitt, M., Olson, P., Arron, S. T., & Hanahan, D. (2010). Cancer-Associated Fibroblasts Are Activated in Incipient Neoplasia to Orchestrate Tumor-Promoting Inflammation in an NF-kappaB-Dependent Manner. *Cancer Cell, 17*(2), 135-147. doi:10.1016/j.ccr.2009.12.041

Fang, Y., & Eglen, R. M. (2017). Three-Dimensional Cell Cultures in Drug Discovery and Development. *SLAS Discov, 22*(5), 456-472. doi:10.1177/1087057117696795

Fedorchak, G. R., Kaminski, A., & Lammerding, J. (2014). Cellular mechanosensing: getting to the nucleus of it all. *Prog Biophys Mol Biol, 115*(2-3), 76-92. doi:10.1016/j.pbiomolbio.2014.06.009

Fischer, R. S., Gardel, M., Ma, X., Adelstein, R. S., & Waterman, C. M. (2009). Local cortical tension by myosin II guides 3D endothelial cell branching. *Curr Biol, 19*(3), 260-265. doi:10.1016/j.cub.2008.12.045

Friedell, G. H., Bell, J. R., Burney, S. W., Soto, E. A., & Tiltman, A. J. (1976). Histopathology and classification of urinary bladder carcinoma. *Urol Clin North Am, 3*(1), 53-70.

Fritz, G., Just, I., & Kaina, B. (1999). Rho GTPases are over-expressed in human tumors. *Int J Cancer, 81*(5), 682-687.

Gay, L., Baker, A.-M., & Graham, T. A. (2016). Tumour Cell Heterogeneity. *F1000Research, 5*. doi:10.12688/f1000research.7210.1

Getzenberg, R. H. (1994). Nuclear matrix and the regulation of gene expression: tissue specificity. *J Cell Biochem, 55*(1), 22-31. doi:10.1002/jcb.240550105

Getzenberg, R. H., Pienta, K. J., Huang, E. Y., & Coffey, D. S. (1991). Identification of nuclear matrix proteins in the cancer and normal rat prostate. *Cancer Res, 51*(24), 6514-6520.

Getzenberg, R. H., Pienta, K. J., Ward, W. S., & Coffey, D. S. (1991). Nuclear structure and the three-dimensional organization of DNA. *J Cell Biochem, 47*(4), 289-299. doi:10.1002/jcb.240470402

Givant-Horwitz, V., Davidson, B., & Reich, R. (2004). Laminin-induced signaling in tumor cells: the role of the M(r) 67,000 laminin receptor. *Cancer Res, 64*(10), 3572-3579. doi:10.1158/0008-5472.CAN-03-3424

Griffis, E. R., Craige, B., Dimaano, C., Ullman, K. S., & Powers, M. A. (2004). Distinct functional domains within nucleoporins Nup153 and Nup98 mediate transcription-dependent mobility. *Mol Biol Cell, 15*(4), 1991-2002. doi:10.1091/mbc.e03-10-0743

Gritsenko, P. G., Ilina, O., & Friedl, P. (2012). Interstitial guidance of cancer invasion. *J Pathol, 226*(2), 185-199. doi:10.1002/path.3031

Gruene, M., Pflaum, M., Hess, C., Diamantouros, S., Schlie, S., Deiwick, A., . . . Chichkov, B. (2011). Laser printing of three-dimensional multicellular arrays for studies of cell-cell and cell-environment interactions. *Tissue Eng Part C Methods, 17*(10), 973-982. doi:10.1089/ten.TEC.2011.0185

Gu, L., & Mooney, D. J. (2016). Biomaterials and emerging anticancer therapeutics: engineering the microenvironment. *Nat Rev Cancer, 16*(1), 56-66. doi:10.1038/nrc.2015.3

Gueth-Hallonet, C., Wang, J., Harborth, J., Weber, K., & Osborn, M. (1998). Induction of a regular nuclear lattice by overexpression of NuMA. *Exp Cell Res, 243*(2), 434-452. doi:10.1006/excr.1998.4178

Guilluy, C., & Burridge, K. (2015). Nuclear mechanotransduction: forcing the nucleus to respond. *Nucleus, 6*(1), 19-22. doi:10.1080/19491034.2014.1001705

Guilluy, C., Osborne, L. D., Van Landeghem, L., Sharek, L., Superfine, R., Garcia-Mata, R., & Burridge, K. (2014). Isolated nuclei adapt to force and reveal a mechanotransduction pathway in the nucleus. *Nat Cell Biol, 16*(4), 376-381. doi:10.1038/ncb2927

Han, Z., & Lu, Z. R. (2017). Targeting Fibronectin for Cancer Imaging and Therapy. *J Mater Chem B, 5*(4), 639-654. doi:10.1039/C6TB02008A

Harada, T., Swift, J., Irianto, J., Shin, J. W., Spinler, K. R., Athirasala, A., . . . Discher, D. E. (2014). Nuclear lamin stiffness is a barrier to 3D migration, but softness can limit survival. *J Cell Biol, 204*(5), 669-682. doi:10.1083/jcb.201308029

Harborth, J., Wang, J., Gueth-Hallonet, C., Weber, K., & Osborn, M. (1999). Self assembly of NuMA: multiarm oligomers as structural units of a nuclear lattice. *EMBO J, 18*(6), 1689-1700. doi:10.1093/emboj/18.6.1689

Haupt, A., & Minc, N. (2018). How cells sense their own shape – mechanisms to probe cell geometry and their implications in cellular organization and function. *Journal of Cell Science, 131*(6). doi:10.1242/jcs.214015

Heald, R., & McKeon, F. (1990). Mutations of phosphorylation sites in lamin A that prevent nuclear lamina disassembly in mitosis. *Cell, 61*(4), 579-589.

Housman, G., Byler, S., Heerboth, S., Lapinska, K., Longacre, M., Snyder, N., & Sarkar, S. (2014). Drug resistance in cancer: an overview. *Cancers (Basel), 6*(3), 1769-1792. doi:10.3390/cancers6031769

Hsiao, C. T., Cheng, H. W., Huang, C. M., Li, H. R., Ou, M. H., Huang, J. R., . . . Kuo, J. C. (2017). Fibronectin in cell adhesion and migration via N-glycosylation. *Oncotarget, 8*(41), 70653-70668. doi:10.18632/oncotarget.19969

Hughes, J. H., & Cohen, M. B. (1999). Nuclear matrix proteins and their potential applications to diagnostic pathology. *Am J Clin Pathol, 111*(2), 267-274.

Hughes, J. H., Katz, R. L., Rodriguez-Villanueva, J., Kidd, L., Dinney, C., Grossman, H. B., & Fritsche, H. A., Jr. (1999). Urinary nuclear matrix protein 22 (NMP22): a diagnostic adjunct to urine cytologic examination for the detection of recurrent transitional-cell carcinoma of the bladder. *Diagn Cytopathol, 20*(5), 285-290.

Ikeguchi, M., Oka, S., Saito, H., Kondo, A., Tsujitani, S., Maeta, M., & Kaibara, N. (1999). Computerized nuclear morphometry: a new morphologic assessment for advanced gastric adenocarcinoma. *Ann Surg, 229*(1), 55-61.

Imbalzano, K. M., Cohet, N., Wu, Q., Underwood, J. M., Imbalzano, A. N., & Nickerson, J. A. (2013). Nuclear shape changes are induced by knockdown of the SWI/SNF ATPase BRG1 and are independent of cytoskeletal connections. *PLoS One, 8*(2), e55628. doi:10.1371/journal.pone.0055628

Jain, N., Iyer, K. V., Kumar, A., & Shivashankar, G. V. (2013). Cell geometric constraints induce modular gene-expression patterns via redistribution of HDAC3 regulated by actomyosin contractility. *Proceedings of the National Academy of Sciences, 110*(28), 11349-11354. doi:10.1073/pnas.1300801110

Jayaraman, S., Chittiboyina, S., Bai, Y., Abad, P. C., Vidi, P. A., Stauffacher, C. V., & Lelievre, S. A. (2017). The nuclear mitotic apparatus protein NuMA controls rDNA transcription and mediates the nucleolar stress response in a p53-independent manner. *Nucleic Acids Res, 45*(20), 11725-11742. doi:10.1093/nar/gkx782

Jo, Y., Choi, N., Kim, K., Koo, H. J., Choi, J., & Kim, H. N. (2018). Chemoresistance of Cancer Cells: Requirements of Tumor Microenvironment-mimicking In Vitro Models in Anti-Cancer Drug Development. *Theranostics, 8*(19), 5259-5275. doi:10.7150/thno.29098

Joyce, M. H., Lu, C., James, E. R., Hegab, R., Allen, S. C., Suggs, L. J., & Brock, A. (2018). Phenotypic Basis for Matrix Stiffness-Dependent Chemoresistance of Breast Cancer Cells to Doxorubicin. *Front Oncol, 8*, 337. doi:10.3389/fonc.2018.00337

Kaiser, V. B., & Semple, C. A. (2018). Chromatin loop anchors are associated with genome instability in cancer and recombination hotspots in the germline. *Genome Biol, 19*(1), 101. doi:10.1186/s13059-018-1483-4

Kantharidis, P., El-Osta, A., deSilva, M., Wall, D. M., Hu, X. F., Slater, A., . . . Zalcberg, J. R. (1997). Altered methylation of the human MDR1 promoter is associated with acquired multidrug resistance. *Clin Cancer Res, 3*(11), 2025-2032.

Khatau, S. B., Hale, C. M., Stewart-Hutchinson, P. J., Patel, M. S., Stewart, C. L., Searson, P. C., . . . Wirtz, D. (2009). A perinuclear actin cap regulates nuclear shape. *Proc Natl Acad Sci U S A, 106*(45), 19017-19022. doi:10.1073/pnas.0908686106

Knowles, D. W., Sudar, D., Bator-Kelly, C., Bissell, M. J., & Lelievre, S. A. (2006). Automated local bright feature image analysis of nuclear protein distribution identifies changes in tissue phenotype. *Proc Natl Acad Sci U S A, 103*(12), 4445-4450. doi:10.1073/pnas.0509944102

Kroman, N., Wohlfahrt, J., Mouridsen, H. T., & Melbye, M. (2003). Influence of tumor location on breast cancer prognosis. *Int J Cancer, 105*(4), 542-545. doi:10.1002/ijc.11116

Kurdistani, S. K. (2014). Chromatin: a capacitor of acetate for integrated regulation of gene expression and cell physiology. *Curr Opin Genet Dev, 26*, 53-58. doi:10.1016/j.gde.2014.06.002

Kwon, I. K., Lee, S. C., Han, B., & Park, K. (2012). Analysis on the current status of targeted drug delivery to tumors. *J Control Release, 164*(2), 108-114. doi:10.1016/j.jconrel.2012.07.010

Lammerding, J., Fong, L. G., Ji, J. Y., Reue, K., Stewart, C. L., Young, S. G., & Lee, R. T. (2006). Lamins A and C but not lamin B1 regulate nuclear mechanics. *J Biol Chem, 281*(35), 25768-25780. doi:10.1074/jbc.M513511200

Lammerding, J., Schulze, P. C., Takahashi, T., Kozlov, S., Sullivan, T., Kamm, R. D., . . . Lee, R. T. (2004). Lamin A/C deficiency causes defective nuclear mechanics and mechanotransduction. *J Clin Invest, 113*(3), 370-378. doi:10.1172/JCI19670

Lammerding, J., & Wolf, K. (2016). Nuclear envelope rupture: Actin fibers are putting the squeeze on the nucleus. *J Cell Biol, 215*(1), 5-8. doi:10.1083/jcb.201609102

Lee, Y. L., & Burke, B. (2018). LINC complexes and nuclear positioning. *Semin Cell Dev Biol, 82*, 67-76. doi:10.1016/j.semcdb.2017.11.008

Lelievre, S. A. (2009). Contributions of extracellular matrix signaling and tissue architecture to nuclear mechanisms and spatial organization of gene expression control. *Biochim Biophys Acta, 1790*(9), 925-935. doi:10.1016/j.bbagen.2009.03.013

Lelièvre, S. A., & Chittiboyina, S. (2018). Microphysiological systems to study microenvironment-cell nucleus interaction: importance of tissue geometry and heterogeneity. *Microphysiological Systems, 2*, 12-12. doi:10.21037/mps.2018.11.02

Lelievre, S. A., Weaver, V. M., Nickerson, J. A., Larabell, C. A., Bhaumik, A., Petersen, O. W., & Bissell, M. J. (1998). Tissue phenotype depends on reciprocal interactions between the extracellular matrix and the structural organization of the nucleus. *Proc Natl Acad Sci U S A, 95*(25), 14711-14716.

Levi, F., Randimbison, L., Te, V. C., & La Vecchia, C. (2003). Influence of tumor location on breast cancer prognosis. *Int J Cancer, 107*(4), 683-684. doi:10.1002/ijc.11418

Li, L. H., DeKoning, T. F., Kelly, R. C., Krueger, W. C., McGovren, J. P., Padbury, G. E., . . . et al. (1992). Cytotoxicity and antitumor activity of carzelesin, a prodrug cyclopropylpyrroloindole analogue. *Cancer Res, 52*(18), 4904-4913.

Lis, R., Capdet, J., Mirshahi, P., Lacroix-Triki, M., Dagonnet, F., Klein, C., . . . Poupot, M. (2010). Oncologic trogocytosis with Hospicells induces the expression of N-cadherin by breast cancer cells. *Int J Oncol, 37*(6), 1453-1461.

Liu, A. P., Chaudhuri, O., & Parekh, S. H. (2017). New advances in probing cell-extracellular matrix interactions. *Integr Biol (Camb), 9*(5), 383-405. doi:10.1039/c6ib00251j

Luderus, M. E., den Blaauwen, J. L., de Smit, O. J., Compton, D. A., & van Driel, R. (1994). Binding of matrix attachment regions to lamin polymers involves single-stranded regions and the minor groove. *Mol Cell Biol, 14*(9), 6297-6305.

Luxton, G. W., Gomes, E. R., Folker, E. S., Vintinner, E., & Gundersen, G. G. (2010). Linear arrays of nuclear envelope proteins harness retrograde actin flow for nuclear movement. *Science, 329*(5994), 956-959. doi:10.1126/science.1189072

Malandrino, A., Mak, M., Kamm, R. D., & Moeendarbary, E. (2018). Complex mechanics of the heterogeneous extracellular matrix in cancer. *Extreme Mech Lett, 21*, 25-34. doi:10.1016/j.eml.2018.02.003

Malhas, A., Saunders, N. J., & Vaux, D. J. (2010). The nuclear envelope can control gene expression and cell cycle progression via miRNA regulation. *Cell Cycle, 9*(3), 531-539. doi:10.4161/cc.9.3.10511

Maniotis, A. J., Chen, C. S., & Ingber, D. E. (1997). Demonstration of mechanical connections between integrins, cytoskeletal filaments, and nucleoplasm that stabilize nuclear structure. *Proc Natl Acad Sci U S A, 94*(3), 849-854.

Meads, M. B., Gatenby, R. A., & Dalton, W. S. (2009). Environment-mediated drug resistance: a major contributor to minimal residual disease. *Nat Rev Cancer, 9*(9), 665-674. doi:10.1038/nrc2714

Meuleman, W., Peric-Hupkes, D., Kind, J., Beaudry, J. B., Pagie, L., Kellis, M., . . . van Steensel, B. (2013). Constitutive nuclear lamina-genome interactions are highly conserved and associated with A/T-rich sequence. *Genome Res, 23*(2), 270-280. doi:10.1101/gr.141028.112

Mijovic, Z., Kostov, M., Mihailovic, D., Zivkovic, N., Stojanovic, M., & Zdravkovic, M. (2013). Correlation of nuclear morphometry of primary melanoma of the skin with clinicopathological parameters and expression of tumor suppressor proteins (p53 and p16(INK4a)) and bcl-2 oncoprotein. *J BUON, 18*(2), 471-476.

Mithieux, S. M., & Weiss, A. S. (2005). Elastin. *Adv Protein Chem, 70*, 437-461. doi:10.1016/S0065-3233(05)70013-9

Nandini, D. B., & Subramanyam, R. V. (2011). Nuclear features in oral squamous cell carcinoma: A computer-assisted microscopic study. *J Oral Maxillofac Pathol, 15*(2), 177-181. doi:10.4103/0973-029X.84488

Neve, A., Cantatore, F. P., Maruotti, N., Corrado, A., & Ribatti, D. (2014). Extracellular matrix modulates angiogenesis in physiological and pathological conditions. *Biomed Res Int, 2014*, 756078. doi:10.1155/2014/756078

Nickerson, J. A., & Penman, S. (1992). Localization of nuclear matrix core filament proteins at interphase and mitosis. *Cell Biol Int Rep, 16*(8), 811-826.

Nieman, K. M., Kenny, H. A., Penicka, C. V., Ladanyi, A., Buell-Gutbrod, R., Zillhardt, M. R., . . . Lengyel, E. (2011). Adipocytes promote ovarian cancer metastasis and provide energy for rapid tumor growth. *Nat Med, 17*(11), 1498-1503. doi:10.1038/nm.2492

Pampaloni, F., Reynaud, E. G., & Stelzer, E. H. (2007). The third dimension bridges the gap between cell culture and live tissue. *Nat Rev Mol Cell Biol, 8*(10), 839-845. doi:10.1038/nrm2236

Paul, C. D., Mistriotis, P., & Konstantopoulos, K. (2017). Cancer cell motility: lessons from migration in confined spaces. *Nat Rev Cancer, 17*(2), 131-140. doi:10.1038/nrc.2016.123

Paulsson, M., & Edsman, K. (2002). Controlled drug release from gels using lipophilic interactions of charged substances with surfactants and polymers. *J Colloid Interface Sci, 248*(1), 194-200. doi:10.1006/jcis.2001.8182

Peixoto, P., Etcheverry, A., Aubry, M., Missey, A., Lachat, C., Perrard, J., . . . Hervouet, E. (2019). EMT is associated with an epigenetic signature of ECM remodeling genes. *Cell Death Dis, 10*(3), 205. doi:10.1038/s41419-019-1397-4

Pickup, M. W., Mouw, J. K., & Weaver, V. M. (2014). The extracellular matrix modulates the hallmarks of cancer. *EMBO Rep, 15*(12), 1243-1253. doi:10.15252/embr.201439246

Provenzano, P. P., Inman, D. R., Eliceiri, K. W., Trier, S. M., & Keely, P. J. (2008). Contact guidance mediated three-dimensional cell migration is regulated by Rho/ROCK-dependent matrix reorganization. *Biophys J, 95*(11), 5374-5384. doi:10.1529/biophysj.108.133116

Qi, Y., & Xu, R. (2018). Roles of PLODs in Collagen Synthesis and Cancer Progression. *Front Cell Dev Biol, 6*, 66. doi:10.3389/fcell.2018.00066

Radulescu, A. E., & Cleveland, D. W. (2010). NuMA after 30 years: the matrix revisited. *Trends Cell Biol, 20*(4), 214-222. doi:10.1016/j.tcb.2010.01.003

Rafii, A., Mirshahi, P., Poupot, M., Faussat, A. M., Simon, A., Ducros, E., . . . Mirshahi, M. (2008). Oncologic trogocytosis of an original stromal cells induces chemoresistance of ovarian tumours. *PLoS One, 3*(12), e3894. doi:10.1371/journal.pone.0003894

Ravi, M., Paramesh, V., Kaviya, S. R., Anuradha, E., & Solomon, F. D. (2015). 3D cell culture systems: advantages and applications. *J Cell Physiol, 230*(1), 16-26. doi:10.1002/jcp.24683

Rowat, A. C., Lammerding, J., & Ipsen, J. H. (2006). Mechanical properties of the cell nucleus and the effect of emerin deficiency. *Biophys J, 91*(12), 4649-4664. doi:10.1529/biophysj.106.086454

Rozario, T., & DeSimone, D. W. (2010). The extracellular matrix in development and morphogenesis: a dynamic view. *Dev Biol, 341*(1), 126-140. doi:10.1016/j.ydbio.2009.10.026

Rumpler, M., Woesz, A., Dunlop, J. W., van Dongen, J. T., & Fratzl, P. (2008). The effect of geometry on three-dimensional tissue growth. *J R Soc Interface, 5*(27), 1173-1180. doi:10.1098/rsif.2008.0064

Scaffidi, P., & Misteli, T. (2006). Lamin A-dependent nuclear defects in human aging. *Science, 312*(5776), 1059-1063. doi:10.1126/science.1127168

Schmeichel, K. L., & Bissell, M. J. (2003). Modeling tissue-specific signaling and organ function in three dimensions. *J Cell Sci, 116*(Pt 12), 2377-2388. doi:10.1242/jcs.00503

Schmitz, A. A., Govek, E. E., Bottner, B., & Van Aelst, L. (2000). Rho GTPases: signaling, migration, and invasion. *Exp Cell Res, 261*(1), 1-12. doi:10.1006/excr.2000.5049

Senthebane, D. A., Rowe, A., Thomford, N. E., Shipanga, H., Munro, D., Mazeedi, M., . . . Dzobo, K. (2017). The Role of Tumor Microenvironment in Chemoresistance: To Survive, Keep Your Enemies Closer. *Int J Mol Sci, 18*(7). doi:10.3390/ijms18071586

Sethi, T., Rintoul, R. C., Moore, S. M., MacKinnon, A. C., Salter, D., Choo, C., . . . Haslett, C. (1999). Extracellular matrix proteins protect small cell lung cancer cells against apoptosis: a mechanism for small cell lung cancer growth and drug resistance in vivo. *Nat Med, 5*(6), 662-668. doi:10.1038/9511

Shin, Y., Kim, H., Han, S., Won, J., Jeong, H. E., Lee, E. S., . . . Chung, S. (2013). Extracellular matrix heterogeneity regulates three-dimensional morphologies of breast adenocarcinoma cell invasion. *Adv Healthc Mater, 2*(6), 790-794. doi:10.1002/adhm.201200320

Silberstein, G. B. (2001). Tumour-stromal interactions. Role of the stroma in mammary development. *Breast Cancer Res, 3*(4), 218-223.

Smith, M. L., Gourdon, D., Little, W. C., Kubow, K. E., Eguiluz, R. A., Luna-Morris, S., & Vogel, V. (2007). Force-induced unfolding of fibronectin in the extracellular matrix of living cells. *PLoS Biol, 5*(10), e268. doi:10.1371/journal.pbio.0050268

Sophie A. Lelièvre, K. B. H., Pierre-Alexandre Vidi. (2014). Application of Theranostics to Measure and Treat Cell Heterogeneity in Cancer *Cancer Theranostics* (pp. 493-516).

Sterzynska, K., Klejewski, A., Wojtowicz, K., Swierczewska, M., Andrzejewska, M., Rusek, D., . . . Januchowski, R. (2018). The Role of Matrix Gla Protein (MGP) Expression in Paclitaxel and Topotecan Resistant Ovarian Cancer Cell Lines. *Int J Mol Sci, 19*(10). doi:10.3390/ijms19102901

Storch, K., Eke, I., Borgmann, K., Krause, M., Richter, C., Becker, K., . . . Cordes, N. (2010). Three-dimensional cell growth confers radioresistance by chromatin density modification. *Cancer Res, 70*(10), 3925-3934. doi:10.1158/0008-5472.CAN-09-3848

Strambio-De-Castillia, C., Niepel, M., & Rout, M. P. (2010). The nuclear pore complex: bridging nuclear transport and gene regulation. *Nat Rev Mol Cell Biol, 11*(7), 490-501. doi:10.1038/nrm2928

Swift, J., Ivanovska, I. L., Buxboim, A., Harada, T., Dingal, P. C., Pinter, J., . . . Discher, D. E. (2013). Nuclear lamin-A scales with tissue stiffness and enhances matrix-directed differentiation. *Science, 341*(6149), 1240104. doi:10.1126/science.1240104

Tan, Y., Tajik, A., Chen, J., Jia, Q., Chowdhury, F., Wang, L., . . . Wang, N. (2014). Matrix softness regulates plasticity of tumour-repopulating cells via H3K9 demethylation and Sox2 expression. *Nat Commun, 5*, 4619. doi:10.1038/ncomms5619

Udagawa, T., & Wood, M. (2010). Tumor-stromal cell interactions and opportunities for therapeutic intervention. *Curr Opin Pharmacol, 10*(4), 369-374. doi:10.1016/j.coph.2010.06.010

Uhler, C., & Shivashankar, G. V. (2017). Regulation of genome organization and gene expression by nuclear mechanotransduction. *Nat Rev Mol Cell Biol, 18*(12), 717-727. doi:10.1038/nrm.2017.101

Vega, S. L., Liu, E., Arvind, V., Bushman, J., Sung, H. J., Becker, M. L., . . . Moghe, P. V. (2017). High-content image informatics of the structural nuclear protein NuMA parses trajectories for stem/progenitor cell lineages and oncogenic transformation. *Exp Cell Res, 351*(1), 11-23. doi:10.1016/j.yexcr.2016.12.018

Verjans, E. T., Doijen, J., Luyten, W., Landuyt, B., & Schoofs, L. (2018). Three-dimensional cell culture models for anticancer drug screening: Worth the effort? *J Cell Physiol, 233*(4), 2993-3003. doi:10.1002/jcp.26052

Vidi, P. A., Chandramouly, G., Gray, M., Wang, L., Liu, E., Kim, J. J., . . . Lelievre, S. A. (2012). Interconnected contribution of tissue morphogenesis and the nuclear protein NuMA to the DNA damage response. *J Cell Sci, 125*(Pt 2), 350-361. doi:10.1242/jcs.089177

Vidi, P. A., Maleki, T., Ochoa, M., Wang, L., Clark, S. M., Leary, J. F., & Lelievre, S. A. (2014). Disease-on-a-chip: mimicry of tumor growth in mammary ducts. *Lab Chip, 14*(1), 172-177. doi:10.1039/c3lc50819f

Wang, M., Zhao, J., Zhang, L., Wei, F., Lian, Y., Wu, Y., . . . Guo, C. (2017). Role of tumor microenvironment in tumorigenesis. *J Cancer, 8*(5), 761-773. doi:10.7150/jca.17648

Wani, F. A., Bhardwaj, S., Kumar, D., & Katoch, P. (2010). Cytological grading of breast cancers and comparative evaluation of two grading systems. *J Cytol, 27*(2), 55-58. doi:10.4103/0970-9371.70738

Weaver, V. M., Lelievre, S., Lakins, J. N., Chrenek, M. A., Jones, J. C., Giancotti, F., . . . Bissell, M. J. (2002). beta4 integrin-dependent formation of polarized three-dimensional architecture confers resistance to apoptosis in normal and malignant mammary epithelium. *Cancer Cell, 2*(3), 205-216.

Weiser, J. R., & Saltzman, W. M. (2014). Controlled release for local delivery of drugs: barriers and models. *J Control Release, 190*, 664-673. doi:10.1016/j.jconrel.2014.04.048

Welkoborsky, H. J., Mann, W. J., Gluckman, J. L., & Freije, J. E. (1993). Comparison of quantitative DNA measurements and cytomorphology in squamous cell carcinomas of the upper aerodigestive tract with and without lymph node metastases. *Ann Otol Rhinol Laryngol, 102*(1 Pt 1), 52-57. doi:10.1177/000348949310200110

Wong, C., Stylianopoulos, T., Cui, J., Martin, J., Chauhan, V. P., Jiang, W., . . . Fukumura, D. (2011). Multistage nanoparticle delivery system for deep penetration into tumor tissue. *Proc Natl Acad Sci U S A, 108*(6), 2426-2431. doi:10.1073/pnas.1018382108

Wu, L., Jing, D., & Ding, J. (2006). A "room-temperature" injection molding/particulate leaching approach for fabrication of biodegradable three-dimensional porous scaffolds. *Biomaterials, 27*(2), 185-191. doi:10.1016/j.biomaterials.2005.05.105

Yamada, K. M., & Cukierman, E. (2007). Modeling tissue morphogenesis and cancer in 3D. *Cell, 130*(4), 601-610. doi:10.1016/j.cell.2007.08.006

Yang, Z., Maciejowski, J., & de Lange, T. (2017). Nuclear Envelope Rupture Is Enhanced by Loss of p53 or Rb. *Mol Cancer Res, 15*(11), 1579-1586. doi:10.1158/1541-7786.MCR-17-0084

Yurchenco, P. D. (2011). Basement membranes: cell scaffoldings and signaling platforms. *Cold Spring Harb Perspect Biol, 3*(2). doi:10.1101/cshperspect.a004911

Zeimet, A. G., Fiegl, H., Goebel, G., Kopp, F., Allasia, C., Reimer, D., . . . Marth, C. (2011). DNA ploidy, nuclear size, proliferation index and DNA-hypomethylation in ovarian cancer. *Gynecol Oncol, 121*(1), 24-31. doi:10.1016/j.ygyno.2010.12.332

Zullo, J. M., Demarco, I. A., Pique-Regi, R., Gaffney, D. J., Epstein, C. B., Spooner, C. J., . . . Singh, H. (2012). DNA sequence-dependent compartmentalization and silencing of chromatin at the nuclear lamina. *Cell, 149*(7), 1474-1487. doi:10.1016/j.cell.2012.04.035

Zwerger, M., Roschitzki-Voser, H., Zbinden, R., Denais, C., Herrmann, H., Lammerding, J., . . . Medalia, O. (2015). Altering lamina assembly reveals lamina-dependent and -independent functions for A-type lamins. *J Cell Sci, 128*(19), 3607-3620. doi:10.1242/jcs.171843

CHAPTER 2. THE NUCLEAR MITOTIC APPARATUS (NUMA) PROTEIN CONTROLS DRUG RESISTANCE IN CANCER VIA AN IMPACT ON NUCLEAR ORGANIZATION

The following manuscript is going to be submitted to Cancer Discovery and is in the format required for t**he journal**

Farzaneh Atrian[1], Weijian Gong[1], Christopher Schor[1], Luopin Wang[2], Rahim Rahimi[3], Kurt Hodges[4], Majid Kazemian[2,5] and Sophie A. Lelièvre[1,5]

(1) Department of Basic Medical Sciences, Purdue University, West Lafayette, IN, USA

(2) Department of Computer Science, Purdue University, West Lafayette, IN, USA

(3) Department of Materials Engineering, Purdue University, West Lafayette, IN, USA

(4) Department of Pathology, University of Cincinnati, OH, USA

(5) Purdue University Center for Cancer Research

Corresponding author: Professor Sophie A. Lelièvre

625 Harrison Street, Lynn Hall, Purdue University, IN 47907-2023, USA

Phone: (765) 46 7793

Fax: (765) 494 9781

Email: lelievre@purdue.edu

2.1 Introduction

Resistance to chemotherapy has plagued cancer management since the first use of antiproliferative drugs more than 60 years ago. Progress in research tools have now identified chemoresistance, especially resistance to multiple classes of drugs or cross-resistance, has the

result of changes in gene expression profiles hat alter mechanisms, such as DNA repair, cell proliferation and differentiation (Housman et al., 2014). Beyond changes in gene expression, little is known regarding the behavior of the cell nucleus related to chemoresistance. Alterations in nuclear morphology are a hallmark of cancer cells, as shown by changes in nucleus shape and size, the in the organization of nonchromatin and chromatin elements(Bednarz-Knoll et al., 2012; Chao et al., 2012; Guilluy et al., 2014; Mijovic et al., 2013). Many of these changes have been associated with survival and aggressiveness of cancer cells. For example, increased nucleus size and lower nuclear stiffness are directly linked with cell proliferation and malignancy. Alterations in chromatin texture (mainly the distribution of euchromatin and heterochromatin) can be traced to the response to chemotherapeutic drugs. (Nandini & Subramanyam, 2011).

The tumor microenvironment (TME) has been recognized as a major inducer of resistance to chemotherapy (Uhler & Shivashankar, 2017a). As physical (e.g., nuclear size and shape) and biochemical (e.g., gene organization) features of the nucleus responds to microenvironmental changes (Chittiboyina et al., 2017; Jayaraman et al., 2017; Uhler & Shivashankar, 2017a) we anticipate that the organization of the cell nucleus might be a mediator of TME-induced behavioral changes in tumors. Specifically, alterations in matrix stiffness are associated with chemoresistance in breast cancer (Joyce et al., 2018) and we have shown that an increased matrix stiffness further alters nuclear morphometry towards signs of increased aggressiveness (Chittiboyina et al., 2017).

Here we demonstrate that nuclear morphometry participates to some extent in the determination of drug sensitivity and responds to changes in matrix stiffness depending on the degree of tumor sensitivity to treatment. The nuclear structural protein NuMA is identified as a protein that influences not only nuclear morphometry, but also chromatin compaction in response to increased extracellular constraints, with notably an impact on SP1 motifs involved in cellular homeostasis, including cell survival control.

2.2 Results

Nuclear morphometry influences sensitivity to antiproliferative drugs

To investigate the impact of the physical environment on nuclear morphometric parameters and a potential relation with drug sensitivity, we used chemotherapy sensitive triple negative breast cancer HMT3522 T4-2 cells (Supplementary Figure 1. A) (Briand, Petersen, & Van Deurs, 1987; Vidi et al., 2014; Weaver et al., 2002). Tumors were formed using three methods, the disease-on-the-Chip (DOC) in which tumors grow within the

constraint of a curved geometry (Vidi et al., 2014), hanging drops in which tumor cells aggregate to form large spheroids with constraints linked to the high density of cells within the small volume of culture medium, and a soft nonbiological gel (99.5% water) with minimal physical constraints. The smallest nuclear area and circularity were measured in the DOC, the system with highest physical constraints among the three 3D culture methods (Figure 1. A, B; Table 1). Incubation with cytotoxic drug cisplatin, the standard of treatment for triple negative breast cancer (Silver et al., 2010), revealed that tumor cells displaying the largest average area and highest average nuclear circularity, had the highest sensitivity at 50 μM based on apoptosis marker caspase 3 (Figure 1. C). A similar conclusion could be made for SAHA, a drug to which triple negative breast cancer are normally insensitive (Eckschlager, Plch, Stiborova, & Hrabeta, 2017) based on proliferation marker Ki-67 (Figure 1 D; Supplementary Figure 1. B). Yet, the responses did not follow the difference in area and circularity when comparing DOC and hanging drop, which warranted further assessment of the relationship between nuclear morphometry and drug sensitivity.

Figure 1. Increased nuclear area is associated with higher sensitivity to chemotherapeutic drugs. T4-2 cells were culture for **two-three** days in the disease-on-a-chip (DOC), **2-4** days in hanging drop (HD) and **2-4** days **in** hydrogel (HG) before treatment with either SAHA (10 μM) or cisplatin (50 μM) for 24 hours. Shown are the graphs of average nuclear area (A), average nuclear circularity (B), apoptotic response (caspase 3 staining) to cisplatin (C) and proliferation response (Ki67 staining) to SAHA (D). T4-2cells were also cultured in 2D in the presence or absence of Latrunculin (0.6 μM) for 24 hours with or without cisplatin (50 μM). Shown are the graphs of average nuclear area and average nuclear circularity (E), apoptotic response (caspase 3 staining) to cisplatin (F), average number of 53BP1 foci (green) **from all nuclei** with accompanying representative fluorescence images (G). The arrowheads point to examples of nuclei with foci among the population of nuclei that for the great majority displays 53BP1 foci following latrunculin treatment. Nuclei are stained with DAPI (blue). N = 3, with **100** nuclei analyzed per replicate; **P*<0.05. Scale bar, **1**0 μm

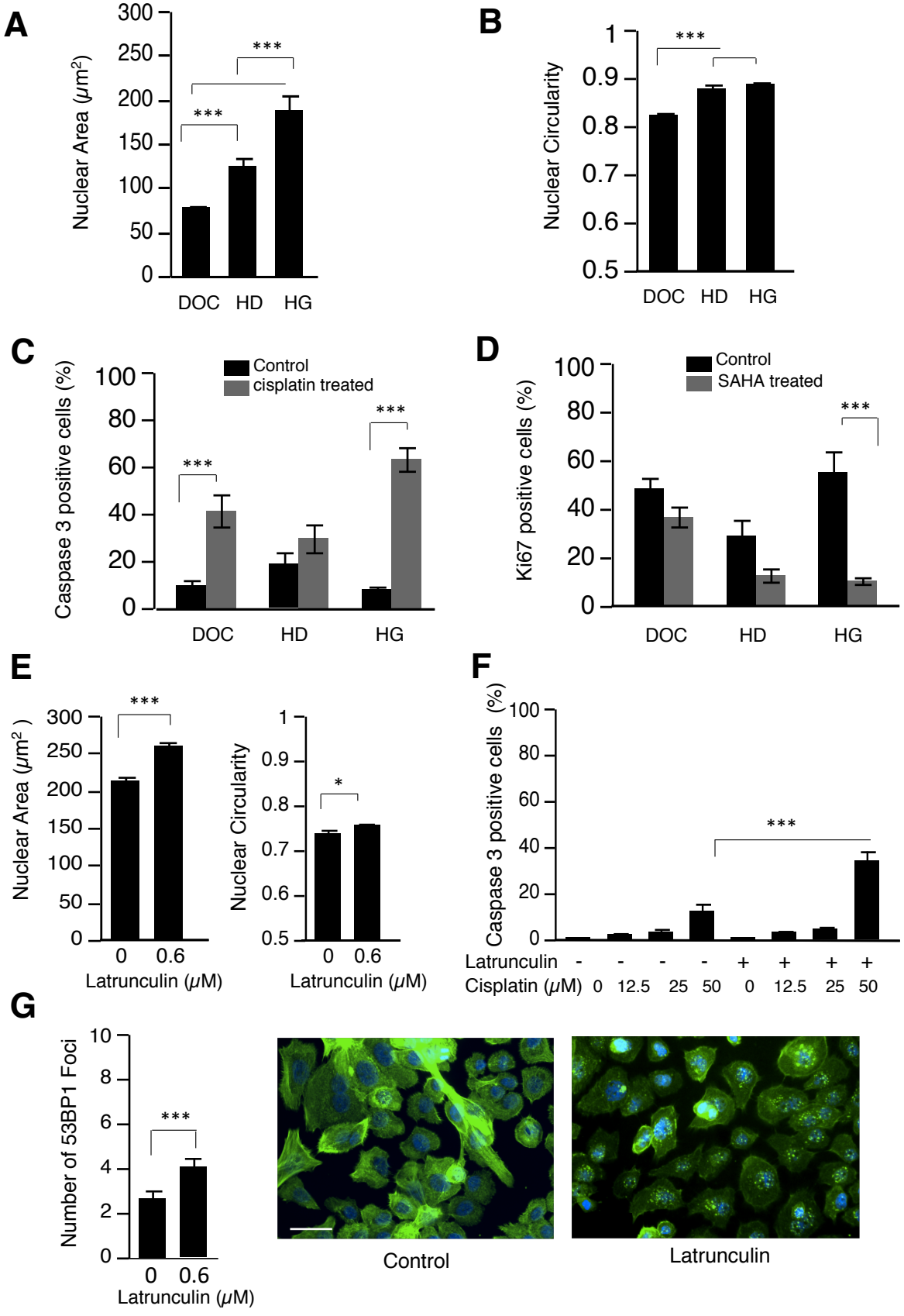
A
Nuclear Area (μm²)
300
250
200
150
100
50
0
***
***
DOC HD HG
B
Nuclear Circularity
1
0.9
0.8
0.7
0.6
0.5
***
DOC HD HG
C
Caspase 3 positive cells (%)
Control
cisplatin treated
100
80
60
40
20
0
***
***
DOC HD HG
D
Ki67 positive cells (%)
Control
SAHA treated
100
80
60
40
20
0
***
DOC HD HG
E
Nuclear Area (μm²)
300
250
200
150
100
50
0
***
0 0.6
Latrunculin (μM)
Nuclear Circularity
1
0.9
0.8
0.7
0.6
0.5
*
0 0.6
Latrunculin (μM)
F
Caspase 3 positive cells (%)
100
80
60
40
20
0
***
Latrunculin - - - - + + + +
Cisplatin (μM) 0 12.5 25 50 0 12.5 25 50
G
Number of 53BP1 Foci
10
8
6
4
2
0
***
0 0.6
Latrunculin (μM)
Control
Latrunculin

Actin depolymerizing drug, latrunculin, was used to experimentally increase nuclear area and circularity (Versaevel, Grevesse, & Gabriele, 2012) at a noncytotoxic concentration of 0.6 μM for 24 hours in standard 2D culture (Figure 1. E; Supplementary Figure 1. C; Table 1). Cotreatment of T4-2 cells with latrunculin and a series of cisplatin concentrations for 24 hours increased the percentage of apoptotic cells (by ~50% for the highest concentration of cisplatin considered effective in these cells), compared to the cells treated only with cisplatin (Figure 1 F). To identify an alteration in nuclear homeostasis that might lead to increased sensitivity for cisplatin, we stained for 53 binding protein 1 (53BP1), a protein that marks fragilized DNA regions (Panier & Boulton, 2014). Indeed, there was a significant increase in the number of 53BP1 foci (but not in total amount as shown by Western blot) in latrunculin treated cells compared to control (Figure 1G; supplementary Figure 1 D). A similar tendency for increased sensitivity was observed in the presence of latrunculin compared to cells treated only with SAHA, without reaching statistical significance. The impact of nuclear morphometry on cell nucleus homeostasis was further investigated using only external physical influence. Cancer cells were seeded on fibronectin coated micropatterned surfaces of different sizes with circular (800 μm^2), square (800 μm^2), oval (1,600 μm^2) and rectangular (1,600 μm^2) shapes (Figure 2 A). In the larger surfaces in which cells extended without resistance to fill the allotted space, an augmentation in nuclear area was accompanied with a significant increase in the number of 53BP1 foci), even if circularity was decreasing. Small microwells with square and circular shapes displayed the smallest areas, but the highest circularity for the cell nuclei, with no significant differences between these two cellular shapes for these parameters; yet, these cells displayed the two highest numbers of 53BP1 foci on average per cell among the four microwell conditions (Figure 2 B, C; Table 1). These results suggest a functional response within the cell nucleus to changes in nuclear area as well as nuclear circularity, that might depend on the degree of physical constraint of cells.

Table 1. Nuclear Morphometry values for different culture models and conditions

Culture models/Conditions	Nuclear Area (μm^2)	Nuclear Circularity
DOC	77	0.822
Hanging Drop	124	0.878
Hydrogel	187	0.887
0 μM of latrunculin	213	0.737
0.6 μM of latrunculin	259	0.755
Oval microwell	260	0.83
Rectangular microwell	326	0.778
Square microwell	129	0.896
Circle microwell	104	0.89

Cell Line	Matrix Stiffness	Nuclear Area (μm^2)	Nuclear Circularity
T4-2	900	235	0.856
T4-2	2020	219	0.852
MDA-MB-231	900	139	0.807
MDA-MB-231	2020	166	0.786

Figure 2. Extracellular constraints modify nuclear morphometry and the response to cisplatin. T4-2 cells were cultured for 2-3 days within laser-cut microwells of various sizes and shape (A-C) or in 3D embedded in collagen I with low (900 Pa) or high (2020 Pa) stiffness levels (D-F). Shown are representative images of individual cells stained for actin microfilaments (red) and DNA (DAPI, blue) in the different types of wells (Round and Square of 800 μm^2; oval and rectangular of 1600 μm^2) (A), the average nuclear area and circularity for the different types of microwells (B) and the average number of fluorescent foci of 53BP1 per nucleus for the different types of microwells (C). For 3D cell culture, shown are the graphs of average nuclear area and circularity (D), representative images of the compaction of tumor nodules (E) stained for their nuclei with DAPI (blue), and the percentage of apoptotic cells (Caspase 3 staining) in response to treatment with cisplatin (50 μM) for 24 hours (F). N = 3; 100 nuclei analyzed per replicate; *$P<0.05$. Scale bar, 100 μm (A), 100 μm (C), 10 μm (E).

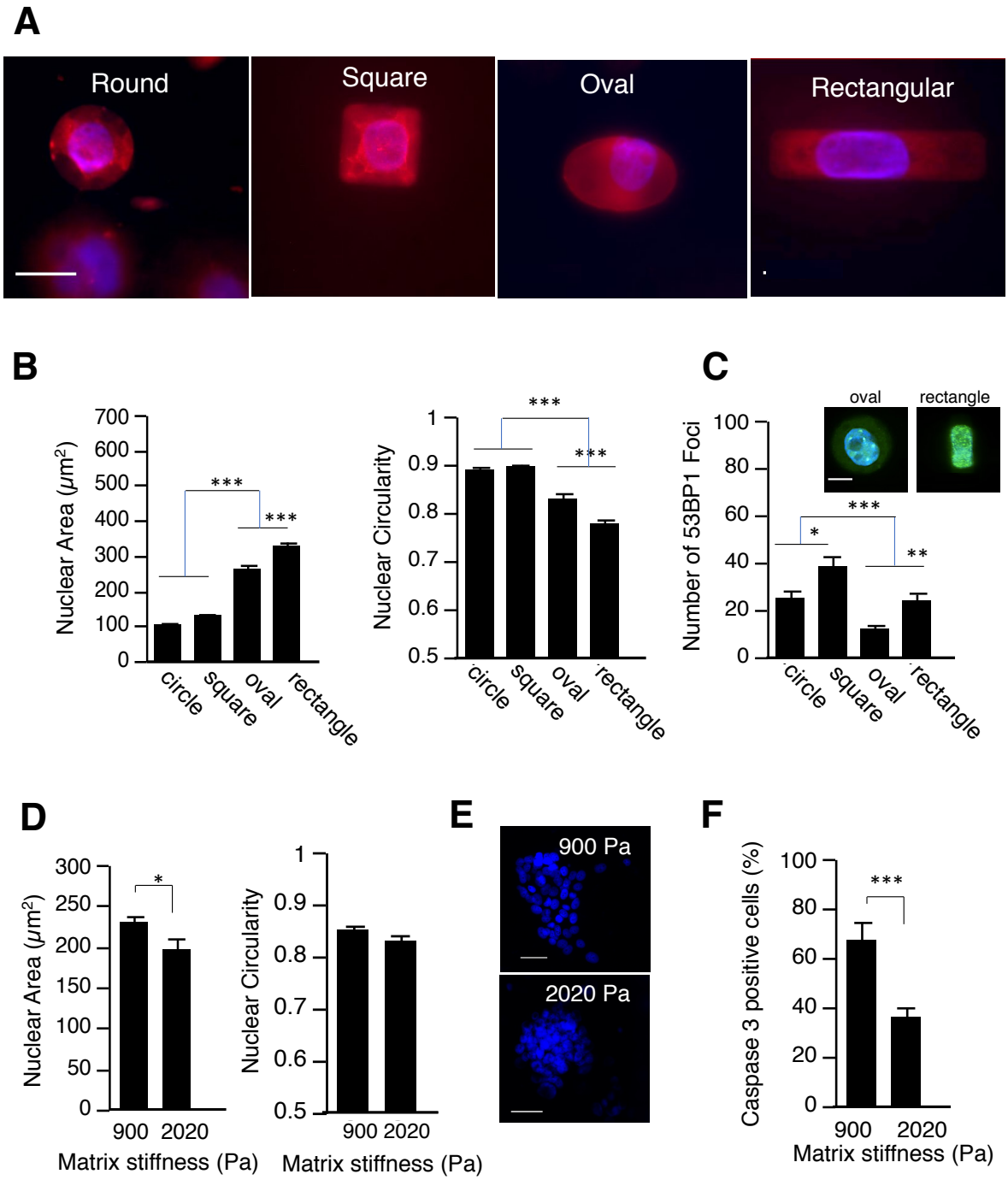
A
Round
Square
Oval
Rectangular
B
Nuclear Area (μm²)
700
600
500
400
300
200
100
0
***
***
circle
square
oval
rectangle
Nuclear Circularity
1
0.9
0.8
0.7
0.6
0.5
***
***
circle
square
oval
rectangle
C
oval
rectangle
Number of 53BP1 Foci
100
80
60
40
20
0
***
*
**
circle
square
oval
rectangle
D
Nuclear Area (μm²)
300
250
200
150
100
50
0
*
900 2020
Matrix stiffness (Pa)
Nuclear Circularity
1
0.9
0.8
0.7
0.6
0.5
900 2020
Matrix stiffness (Pa)
E
900 Pa
2020 Pa
F
Caspase 3 positive cells (%)
100
80
60
40
20
0
***
900 2020
Matrix stiffness (Pa)

The importance of mechanical constraints to influence the cell nucleus with an impact on anticancer drug response was further investigated in 3D cell culture under microenvironmental stiffness present in invasive breast cancer. Nuclear morphometric analysis indicated that high collagen I matrix stiffness (Young's modulus of 2020 Pa, a rigidity experienced by human breast tumors; (Samani & Plewes, 2004) was accompanied with decreased nuclear area and circularity in T4-2 cells, although for the latter the decrease was not significant, compared to normal matrix stiffness (Young's modulus of 900 Pa). The constraint due to increased stiffness was also evidenced by the more compact appearance of tumors in 2020 Pa matrix stiffness (Figure 2. D, E; Table 1). The percentage of apoptotic cells induced by 50 μM of cisplatin was significantly lower in 2020 Pa compared to 900 Pa stiffness (Figure 2. F), confirming a link between mechanical constraint, nuclear size and drug sensitivity in these cells.

Figure 3. Silencing NuMA in cells sensitive to chemotherapeutic drugs alters nuclear area and sensitivity to cisplatin depending on microenvironmental constraints. T4-2 cells were culture in 2D, transfected with nonspecific siRNAs or with siNuMA and cultured for another **three** days in 2D (A-C) or cultured for another 24 hours before being seeded in collagen I of 900 Pa or 2020 Pa and cultured for **2-3** days to allow the formation of tumor nodules (D-H). For the experiments in 2D culture, shown are the average nuclear area and circularity for cell populations transfected with nonspecific (NS) siRNA (+) or siNuMA (-) (A), the average number of 53BP1 foci **all nuclei** in NS siRNA (+) and siNuMA (-) populations (B), and the apoptotic response (caspase 3 staining) to 24 hours of treatment with cisplatin (50 μM) in NS siRNA (+) and siNuMA (-) populations (C). For the experiments done in collagen I embedded culture with tumor nodules, shown are the average nuclear area (D) and circularity (E) for (NS) siRNA (+) or siNuMA (-) depending on matrix stiffness, the densitometry results for the expression of NuMA in (NS) siRNA (+) or siNuMA (-) populations with a representative western blot (Lamin B is used as loading control) (F), the apoptotic response (caspase 3 staining) following treatment with cisplatin (50 μM) in NS siRNA (+) and siNuMA (-) populations depending on matrix stiffness (G) and the densitometry results for the expression of NuMA depending on matrix density (H). N = 3; **150** nuclei analyzed per replicate; **P*<0.05.

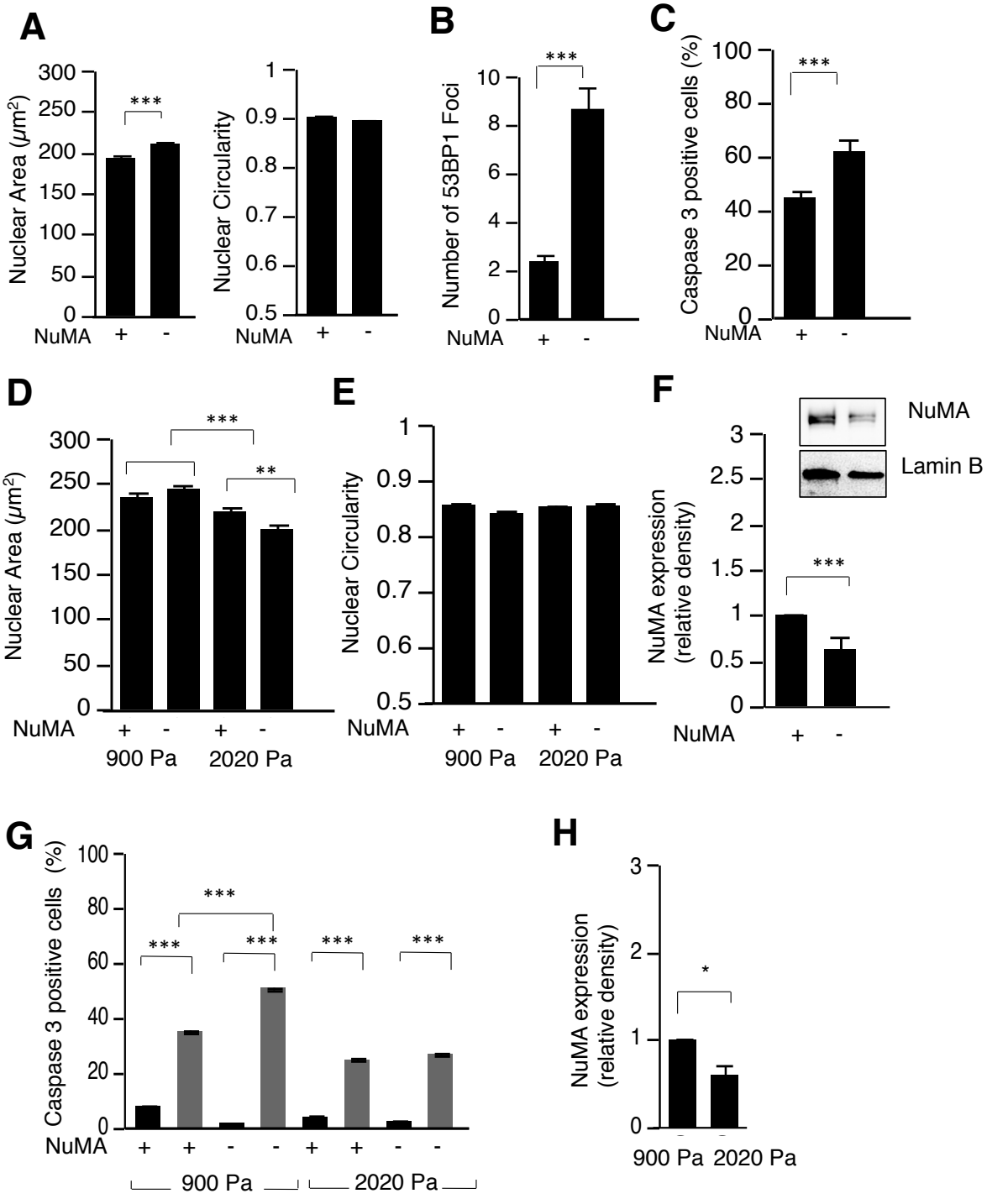
A
Nuclear Area (μm²)
300
250
200
150
100
50
0
***
NuMA + -
Nuclear Circularity
1
0.9
0.8
0.7
0.6
0.5
NuMA + -
B
Number of 53BP1 Foci
10
8
6
4
2
0
***
NuMA + -
C
Caspase 3 positive cells (%)
100
80
60
40
20
0
***
NuMA + -
D
Nuclear Area (μm²)
300
250
200
150
100
50
0
***
**
NuMA + - + -
900 Pa 2020 Pa
E
Nuclear Circularity
1
0.9
0.8
0.7
0.6
0.5
NuMA + - + -
900 Pa 2020 Pa
F
NuMA
Lamin B
NuMA expression (relative density)
3
2.5
2
1.5
1
0.5
0
***
NuMA + -
G
Caspase 3 positive cells (%)
100
80
60
40
20
0
***
***
***
***
***
NuMA + + - - + + - -
900 Pa
2020 Pa
H
NuMA expression (relative density)
3
2
1
0
*
900 Pa 2020 Pa

The structural protein NuMA influences nuclear morphometry.

The nuclear mitotic apparatus (NuMA) protein is a marker of early alterations in the nucleus associated with apoptosis (Weaver et al., 1996); it is part of the internal nuclear structural network proposed to maintain the organization of the nucleus (Lelievre et al., 1998) and controls the DNA damage response, including 53BP1 (Salvador Moreno et al., 2019). To determine whether the presence of NuMA might influence nuclear morphometry, the protein expression was reduced in T4-2 cells in 2D culture using siRNA (Supplementary Figure 2A). The decrease in NuMA protein level was accompanied with a significant increase in nuclear area, and a tendency for lower circularity (although the latter was not significant). Accordingly, the number of 53BP1 foci increased as did the sensitivity to cisplatin (Figure 3 A, B, C). The absence of NuMA was shown to release 53BP1 from nucleoplasmic storage (Salvador Moreno et al., 2019); thus, we measured NuMA levels in latrunculin-treated cells in which 53BP1 was found to be increased (see supplementary Figure 2 E). Indeed, NuMA expression was significantly lower under these conditions. A similar scenario occurred with cytochalasin treatment also known to change nuclear morphometry by disrupting actin (Chen, Co, & Ho, 2015) which was associated with an increase in cisplatin sensitivity, although nuclear area and circularity was significantly decreased (Supplementary Figure 2 B, C, D). Intriguingly, NuMA silencing was accompanied with the disruption of the actin organization in the cytoplasm, suggesting and interplay between NuMA and actin organization (Supplementary Figure 1 E, F). Sensitivity for SAHA was also enhanced. Hence, the level of NuMA appears to supersede the effect of nuclear morphometry.

Figure 4. Silencing NuMA in cells resistant to chemotherapeutic drugs increases sensitivity to cisplatin in a stiff matrix. MDA-MB-231 cells were cultured in 2D, transfected with nonspecific (NS) siRNAs or with siNuMA and cultured for another 24 hours before being seeded in collagen I of 900 Pa or 2020 Pa and cultured for 2-3 days to allow the formation of tumor nodules. Shown are the average nuclear area (A) and circularity (B), and the apoptotic response (caspase 3 staining) to 24 hours of treatment with cisplatin (50 μM, C; 75 μM, D) in NS siRNA (+) and siNuMA (-) populations depending on matrix stiffness. (E) Densitometry analysis for NuMA expression depending on matrix stiffness. N = 3; 150 nuclei analyzed per replicate; **P*<0.05.

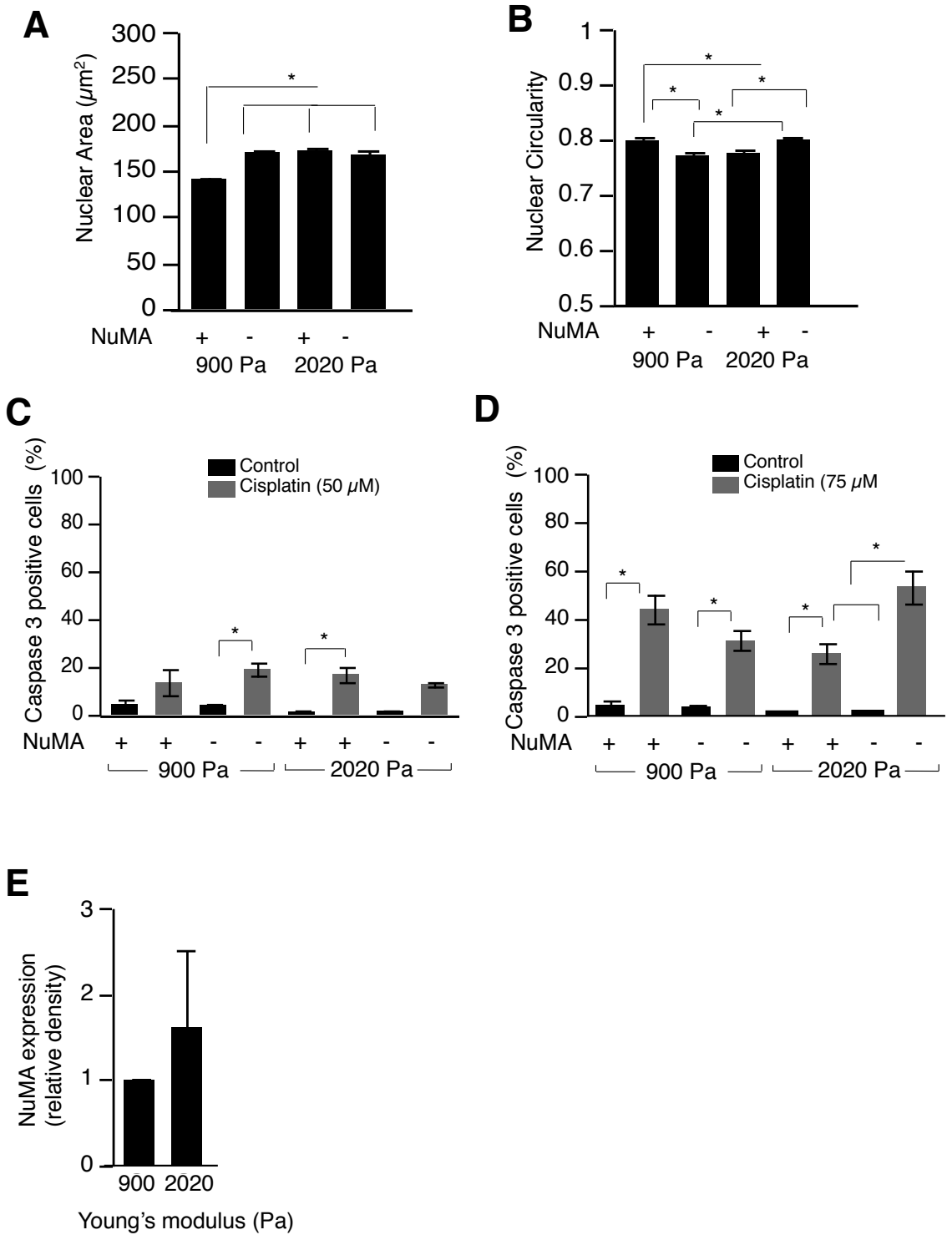
A
Nuclear Area (μm²)
300
250
200
150
100
50
0
*
*
NuMA + - + -
900 Pa 2020 Pa
B
Nuclear Circularity
1
0.9
0.8
0.7
0.6
0.5
*
*
*
*
NuMA + - + -
900 Pa 2020 Pa
C
Caspase 3 positive cells (%)
Control
Cisplatin (50 μM)
100
80
60
40
20
0
*
*
NuMA + + - - + + - -
900 Pa
2020 Pa
D
Caspase 3 positive cells (%)
Control
Cisplatin (75 μM
100
80
60
40
20
0
*
*
*
*
NuMA + + - - + + - -
900 Pa
2020 Pa
E
NuMA expression (relative density)
3
2
1
0
900 2020
Young's modulus (Pa)

When T4-2 cells treated with siNuMA were placed in soft collagen stiffness (900 Pa) sensitivity to Cisplatin was reduced although there were no significant changes in nuclear area and circularity (Figure 3 D, E, F, G; Supplementary Figure 3 A). Noticeably, the increase in cisplatin sensitivity was not due to an increase in the percentage of cells in the cell cycle, as shown by Ki-67 staining (Supplementary Figure 3 B). When tumors were grown in a stiffer matrix (2020 Pa), and thus, reacted to the mechanical stimulus as shown by YAP translocation to the cell nucleus (Supplementary Figure 3 C), the nuclei were smaller on average and, in this case, the decrease in NuMA expression in siRNA NuMA-treated cells further led to a decrease in nuclear area; whereas nuclear circularity remained unaffected (Figure 3 D, E). The tumors with silenced NuMA in a stiffer matrix did not show a difference in cisplatin sensitivity compared to tumors with nonsilenced NuMA (Figure 3 G). Thus, losing NuMA enables nuclear shrinkage in the presence of high stiffness. Interestingly, although NuMA expression was lower at high stiffness degree (Figure 3 H), it was insufficient to increase significantly the response to cisplatin in the presence of small nuclei. Similar results were obtained with cytotoxic drug doxorubicine (Supplementary Figure 3 D).

In contrast to T4-2 cells, TNBC MDA-MB-231 cells are considered resistant to chemotherapy, with an LC50 of 75 μM for cisplatin based on 2D culture. When measuring nuclear morphometry in MDA-MB-231 cells, both nuclear area and circularity were significantly lower than in T4-2 cells (Supplementary Figure 4 A; Table 1), either in 900 Pa or in 2020 Pa collagen I. Like for T4-2 cells, silencing NuMA in the softer matrix increased nuclear area and cisplatin sensitivity in the MDA-MB-231 cells (Figure 4 A, B, C). However, MDA-MB-231 cells behave very differently compared to T4-2 cells when cultured in stiffer collagen I (2020 Pa).

Figure 5. A decreasing level of NuMA is significantly associated with increased sensitivity to cisplatin in both resistant and sensitive breast cancer cells. Fit model analysis was used for linear regression analysis in which the drug sensitivity was considered the independent factor (constant) and other variables such as NuMA expression (A), nuclear area (B) and nuclear circularity (C) were considered as dependent factors (variables). 12 biological replicates were included in the analysis for T4-2 cells and MDA-MB-231 cells**.**

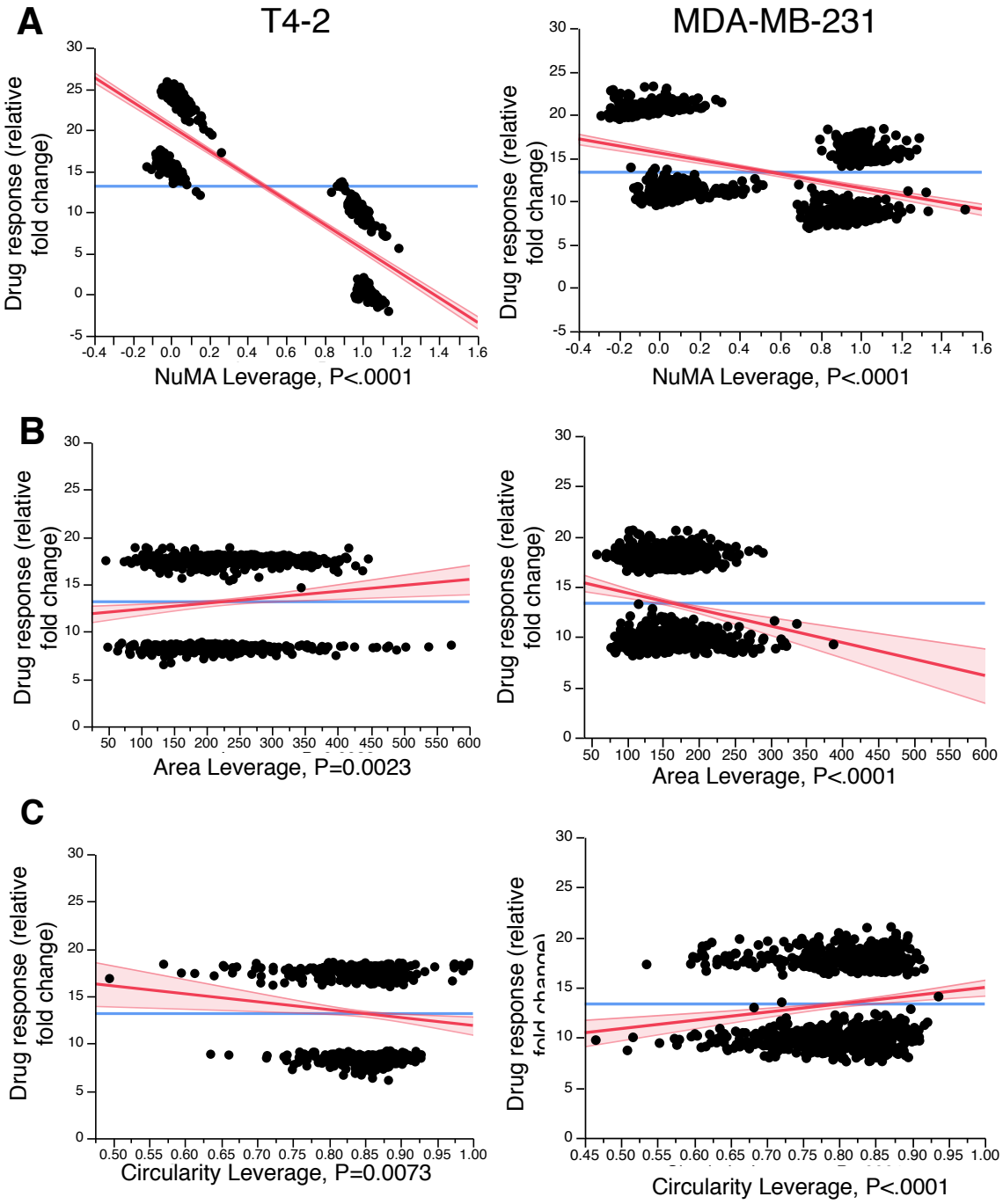
A
T4-2
MDA-MB-231
Drug response (relative fold change)
NuMA Leverage, P<.0001
NuMA Leverage, P<.0001
B
Area Leverage, P=0.0023
Area Leverage, P<.0001
C
Circularity Leverage, P=0.0073
Circularity Leverage, P<.0001

The cell nucleus area did not shrink compared to 900 Pa conditions, instead it increased significantly, and silencing NuMA did not lead to nuclear shrinkage. Instead, nuclear circularity significantly increased upon silencing NuMA (Figure 4 A, B, C, E). According to nuclear area increase in 2020 Pa compared to 900 Pa, cisplatin sensitivity was higher in 2020 Pa at 50 μM cisplatin, with no further change when NuMA was silenced. Surprisingly, at 75 μM cisplatin MDA-MB-231 cells sensitivity was lower at 2020 Pa compared to 900 Pa, and lower upon silencing NuMA in 900 Pa conditions, but it became significantly higher compared to any other condition when silencing NuMA in 2020 Pa matrix (Figure 4 D). Intriguingly, these changes in sensitivity were associated with alterations in circularity instead of alterations in nuclear area. Like for T4-2 cells, changes in cisplatin sensitivity could not be linked to the percentage of cells in the cell cycle (Supplementary Figure 4 C). When we analyzed NuMA level in MDA-MB-231 cells it was at least 50% higher than in T4-2 cells at 900 Pa and 2020 Pa (Supplementary Figure 4 D) and, in contrast to T4-2 cells, NuMA did not significantly respond to mechanical load at 2020 Pa (Figure 4 E). To further decipher the possible link between NuMA, nuclear morphometry and drug sensitivity, regression analyses were performed on all experiments (n=12) run with T4-2 cells and MDA-MB-231 cells. Tumors nodules formed by both cell types had a significantly increased sensitivity to cisplatin when NuMA expression was low (Figure 5 A). However, the relationship to nuclear morphometry was opposite between the two phenotypes. T4-2 cells displayed an increased sensitivity to cisplatin with increased nuclear area and a low circularity; whereas MDA-MB-231 cells displayed an increased sensitivity with small nuclear areas and high values for circularity (Figure 5 B, C). Hence, cells resistant to chemotherapy appear ‘wired’ differently in the nucleus compared to cells sensitive to chemotherapy.

NuMA controls chromatin accessibility via SP1 DNA regions

Changes in nuclear morphometry have been reported to influence global chromatin organization (Chao et al., 2012; Mijovic et al., 2013). We have shown previously that higher order chromatin organization in breast epithelial cells is under the control of NuMA (Abad et al., 2007). To identify whether NuMA controls the accessibility of genes associated with drug response we performed an Assay for Transposase-Accessible Chromatin using sequencing (ATAC-seq). Indeed T4-2 cells had more open DNA regions after silencing NuMA compared to controls in both 900 and 2020 Pa conditions (Figure 6 A, C). For both conditions, NuMA was mostly associated with the motif accessibility of SP1 (specificity protein 1) transcription factor that

binds to GC-rich sequences in the promoters of genes involved in cellular homeostasis, notably the control of cell survival (Figure 6 B, D) and in the presence of NuMA, SP1 motifs were significantly more accessible than in the silenced NuMA conditions. When NuMA was silenced SP1 expression was lower as shown in 2D culture and in cytochalasin-treated T4-2 cells (Figure 6 E), reinforcing the possibility that in the absence of NuMA, SP1-mediated gene regulation is down.

Figure 6. NuMA controls chromatin compaction, especially at SP1 motifs. T4-2 cells were culture in 2D, transfected with nonspecific siRNAs or with siNuMA and cultured for another 24 hours before being seeded in collagen I of 900 Pa or 2020 Pa and cultured for 2-3 days to allow the formation of tumor nodules. Chromatin was prepared for ATAC-seq analysis. (A) Density plots for merged open regions (right panel) and relative position profile (left panel) in 900 Pa with cell nonsilenced (900 N) and silenced (900S) for NuMA. Chromatin is slightly more open in 900 S. (B) Top transcription factors with motifs that are more prevalent in 900 N than 900 S samples. (C) Density plots for merged open regions (right panel) and relative position profile (left panel) in 2020 Pa for cells nonsilenced (2020 N) and silenced (2020 S) for NuMA. Chromatin is slightly more open in 2020 S. (D) Top transcription factors with motifs that are more prevalent in 2020 N than 2020 S samples. (E) densitometry analysis of SP1 expression (n=1) and accompanying western blot image, in T4-2 cells culture in 2D and treated with 0.5 μM of cytochalasin D (cyto-D) for 24 hours or silenced for NuMA (siNuMA; extracts were prepared three days after transfection).

A

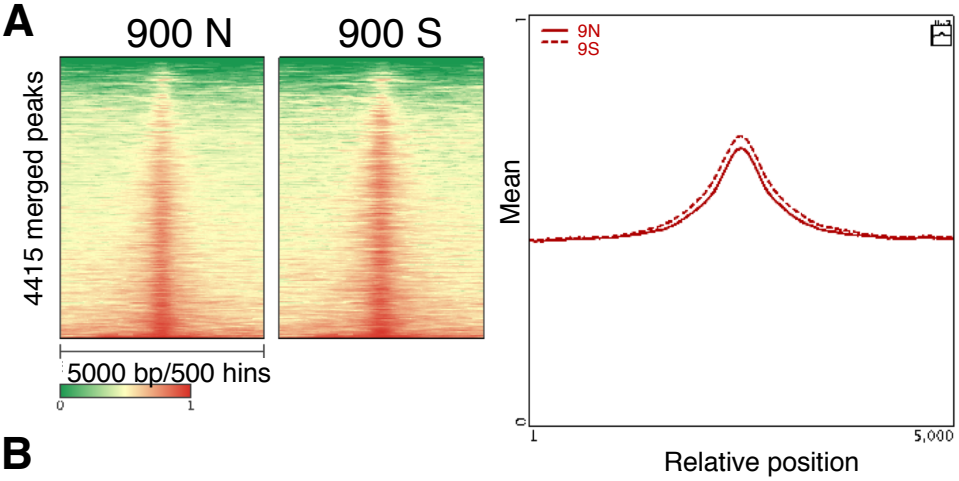

B

Transcription factor	% of open regions in motifs	P-Value
SP1	9.04	1e-34
KLF3	10.07	1e-22
SP5	17.89	1e-19
ATF1	5.25	1e-15

C

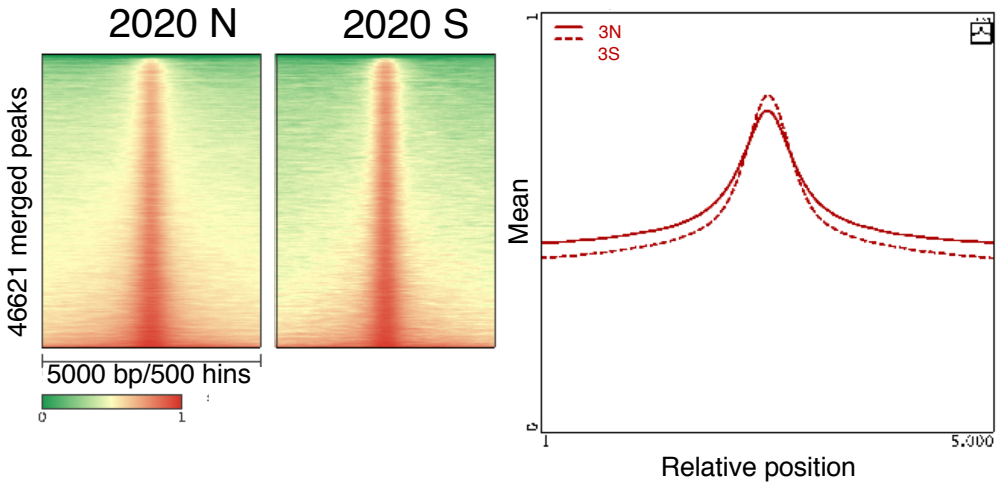

D

Transcription factor	% of open regions in motifs	P-Value
BATF	23.11	1e-2367
SP1	13.10	1e-795
ETS	5.28	1e-471
NRF	3.24	1e-412

E

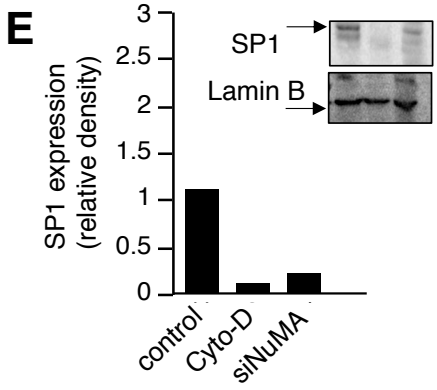

2.3 Discussion

Pathological situations including cancer (Zink, Fischer, & Nickerson, 2004) alter the size and shape of the nucleus. The organization of the nucleus was shown to exert a significant influence on cell proliferation, gene expression (Jain et al., 2013) and protein synthesis (Thomas, Collier, Sfeir, & Healy, 2002). Our results show that nuclear morphometry changes in response to the geometry of the cell culture surface and the level of matrix stiffness. Nuclear morphometry is also specific to the level of drug response in cancer cells. Silencing NuMA leads to a significant increase in nuclear size in T4-2 cells as shown in 2D culture. The lower level of NuMA expression in these cells was accompanied with a significant decrease in actin expression. Moreover, in the latrunculin treated cells that have disrupted actin network and display a higher nuclear area, NuMA expression is significantly lower compared to the control. These results imply that there might be an interplay between NuMA and actin in controlling nuclear size. In contrast, although nuclear lamin is a major regulator of actin dynamics at the nuclear envelope, its depletion does not affect actin organization in the cytoplasm (Shyam B. Khatau et al., 2009; Lammerding & Wolf, 2016). Further investigations are necessary to elucidate the nature of NuMA-actin interactions and how this relationship controls nuclear morphometry.

In contrast to 2D culture, when culturing T4-2 and MDA-MB-231 cells in collagen matrix the relationship between nuclear morphometry and drug sensitivity becomes more complex. Silencing NuMA increases nuclear area in low matrix stiffness for both cell types but it has no effect on nuclear area in the rigid matrix. Thus, the impact of NuMA on nuclear morphometry is limited by the extracellular conditions. Paradoxically higher nuclear area is not necessarily associated with higher sensitivity to chemotherapeutic drugs. However, lower NuMA expression is significantly associated with higher cisplatin sensitivity regardless of the cell type, suggesting that it is at the center of the control of cell survival. This possibility is strengthened by NuMA controls chromatin compaction and access to specific DNA motifs. These results corroborate our previous demonstration that NuMA plays a role in higher order chromatin organization in non-neoplastic mammary epithelial cells (Abad et al., 2007). At that time, we did not observe a drastic impact of altering NuMA in T4-2 phenotype (Chandramouly et al., 2007), but we only focused on proliferation and these experiments did not take into account matrix stiffness. The fact that the impact of NuMA on tumor phenotype is best observed in relation to extracellular matrix stiffness highlights the importance of tissue context in models *in vitro*.

An intriguing observation is the different relationship between drug sensitivity and nuclear morphometry and the different response of NuMA (notably its expression) to increasing stiffness when comparing tumors resistant and tumors sensitive to chemotherapeutic drugs. These differences might be linked to the cells ability to sense or react to extracellular stiffness. For example, sensitivity of MDA-MB-231 to doxorubicin was shown to be three times higher in a stiff matrix compared to a softer matrix. Whereas, the luminal breast cancer cells, MCF-7 did not respond to doxorubicin in a stiffness dependent manner (Joyce et al., 2018). Whether mechanotransduction in resistant and sensitive cancer cells is involving a different pathway or alterations in mechanosensors would be an important query to answer for the exploration of new therapeutic solutions for cancers resistant to treatment.

The fact that silencing NuMA in chemotherapy-sensitive and -resistant cells leads to different responses regarding changes in drug sensitivity suggests that NuMA might organize the chromatin differently in these cells. Indeed, the distribution of NuMA is highly linked to cell phenotypes (Vega et al., 2017) and it is probably a mirror of the protein's interaction with different areas in the genome. This possibility is supported by our observation that the top ranked open DNA regions identified with ATAC-seq varied greatly depending on matrix stiffness, itself linked to differences in levels of drug sensitivity. Unraveling the mechanisms by which microenvironmental mechanical constraints control chromatin organization is among the fundamental steps to follow in order to further the knowledge on the biology of the cell nucleus.

2.4 Materials and Methods

Cell culture

Non-neoplastic S1 HMT-3522 breast epithelial cells (Briand et al., 1987) were seeded at 2.4×10^4 cells/cm^2 and cultured between passages 52 and 60 in H14 medium [Dulbecco's modified Eagle's medium (DMEM)/F12 (Invitrogen), supplemented with 30.3 IU/ml prolactin (Sigma-Aldrich), 2 mg/ml insulin (Sigma-Aldrich), 2.6 μg/ml sodium selenite (BD Biosciences), 8 mg/ml β-estradiol (Sigma-Aldrich), 5 mg/ml hydrocortisone (Sigma-Aldrich), 20 mg/ml transferrin (Sigma-Aldrich) and 20 mg/ml Epidermal Growth Factor (EGF) (BD Biosciences)] as previously described. S1-derived malignant T4–2 HMT-3522 cells (cultured between passages 28 + 4 and 28 + 10) (Briand et al., 1987) and MDA-MB-23-1 cells were seeded at 1.16×10^4 cells/cm^2 in H14 medium without

EGF. Malignant cells were routinely used after four to six days in 2D culture and after two to four days in 3D cultures (Matrigel, DOC, hydrogel, hanging drop and collagen). For coculture with S1 cells on the DOC, T4-2 cells were first seeded on a thin layer of EHS-derived hydrogel (Matrigel, BD Biosciences) in H14 that was supplemented with 5% Matrigel drip, as described previously (Plachot et al., 2009) and were released from Matrigel^{TM} after three days. Tumor nodules were added on top of the S1 cells following the steps described previously (Vidi et al., 2014) The culture of T4-2 cells in hydrogel (PuraMatrix) was performed based on a previously described protocol (Abu-Yousif, Rizvi, Evans, Celli, & Hasan, 2009)The nodule formation of T4-2 cells in hanging drop was achieved after cells were placed in suspension at final concentrations of 8000 cells/20 µl of H14 for two days. Collagen I of desired stiffness (Young's modulus 900 and 2020 Pa) was prepared according to manufacturer's guidelines (Advanced Biomatrix, 5201-1KIT). Cell culture vessels were first coated with a thin layer of collagen gel at 12 µl/ cm^2. Following trypsin treatment and centrifugation, the pellet of cells was dissolved in 20 µl of DMEM/F12 medium and mixed with the collagen gel to obtain a density of 1.73×10^4 cells/55 µl of collagen per 1 cm^2. Treatment with cytotoxic drugs cisplatin (Sigma-Aldrich, St Louis, MO) and doxorubicin (Sigma-Aldrich, St Louis, MO) was done for 24 hours. Treatment with cytostatic drug SAHA (Sigma-Aldrich, St Louis, MO) was performed for 24 hours followed by one day of rest (no drug added to the cell culture medium). Treatment with actin depolymerizing agents, latrunculin (ENZO life Science, Farmingdale, NY) and cytochalasin D (Sigma-Aldrich, St Louis, MO) was performed for 24 hours.

Antibodies

Monoclonal antibodies were used to detect Lamin B (1/10 000 dilution; ab16048 Abcam), Caspase-3 (Cell Signaling Technologies, Boston, MA 1/300 dilution), NuMA (1/2, clone B_1C_{11}, a kind gift from Dr Jeffrey Nickerson, University of Massachusetts, Worcester, MA, USA), p53 binding protein 1 (53BP1) (1 µg/ml, ab36823, Abcam), Ki67 (1:1000 dilution,VP-K451,Vector Laboratories, INC.).

Immunofluorescence staining of cell in cultures

Cells cultured on either flat surface in 2D or embedded within collagen I. Immunofluorescence labelling was performed as described previously (Plachot & Lelievre, 2004) Incubation with

primary antibodies was performed at 4°C overnight. Secondary antibodies included either 12.5 µg/ml fluorescein isothiocyanate (FITC)-conjugated donkey anti-rabbit IgG (Jackson Immunoresearch, West Grove, PA) or 6.7 µg/ml Alexa-Fluor 568-conjugated goat anti-mouse IgG (InVitrogen Corporation). Actin microfilaments were stained using Alexa Fluor® 594/ Alexa Fluor® 488 Phalloidin (Thermo Fisher Scientific) for 30 minutes at room temperature. Nuclei were counterstained for DNA with 0.5 µg/ml DAPI (4′,6-diamidino-2-phenylindole)

. After removal of excess DAPI, samples were mounted with ProLong® Diamond antifade reagent (Fisher Scientific, Pittsburgh, PA).

Preparation of total cell extracts and western blot analysis

Cells from 2D culture were scraped off and centrifuged at 800 g for 15 minutes in PBS buffer mixed with protease inhibitors, pefabloc (1 mg/ml; Sigma-Aldrich), NaF (250 µM; Sigma-Aldrich), aprotinin (1 µg/ml; Sigma-Aldrich). Cells from 3D culture with collagen were released from the gel by using 100 µl /cm^2 Collagenase 1 (1mg/ml Advanced Biomatrix, 5030) upon incubation for 30 min at 37°C. Protein samples were prepared as previously described (Abad et al., 2007) and protein concentrations were measured using a Bio-Rad Protein Assay kit (Bio-Rad laboratories, Hercules, CA). The samples (30 µg proteins) were run in 10% SDS polyacrylamide gel at 55 mA current on a Bio-Rad gel apparatus (Bio-rad laboratories). Proteins were transferred onto a nitrocellulose membrane (Bio-rad laboratories) at 25 volts for 50 minutes using Trans-Blot® SD Semi-Dry Electrophoretic Transfer Cell. Secondary antibodies were horseradish peroxidase conjugated (GE Healthcare, Pittsburgh,PA; 1:10000 dilution). Immunoreactive protein bands were detected using ECL WesternSuper plus (Thermofisher). Images of the protein bands were analyzed using GeneSys Image Acquisition Software version 3.9.1 (Syngene, Frederick, MD) and normalized to lamin B or beta actin. All densitometric analyses were performed with Image J (https://**imagej**.nih.gov/ij).

siRNA transfection

Cell cultures at 20–30% confluency were transfected with 25 nM NuMA siRNA and non-targeting siRNA (GE Dharmacon) using Lipofectamine transfection reagent (ThermoFisher Scientific) for 24 h. Cells were maintained in culture post-transfection either for an additional three days in 2D culture or kept for 24 hours in 2D culture before trypsinization and seeding in collagen I.

Image acquisition and analysis

Immunofluorescence images were captured using Q-capture image acquisition software linked to a IX70 inverted fluorescence microscope (Olympus, Waltham, MA), with 20 x objective (NA =0.5) and the images were processed using the image **analysis** *ImageJ*.

ATAC-seq analysis

Samples were prepared in collagen matrix as explained before. The DNA extracted from fresh samples and library preparation performed followed the steps in Buenrostro et al., 2015 (Buenrostro, Wu, Chang, & Greenleaf, 2015). Two runs of size selection were performed before the samples were submitted to the sequencing center.

Image acquisition and analysis

Immunofluorescence images were captured using Q-capture image acquisition software linked to a IX70 inverted fluorescence microscope (Olympus, Waltham, MA), with 20 x objective (NA =0.5) and the images were processed using the image **analysis** *ImageJ*.

Statistical analysis

Statistical analysis was performed using JMP® 13.2.0 software. Data are presented as means ± s.e.m. We used unpaired Student's *t*-test for comparison of two samples, and analysis of variance (ANOVA) with Tukey's HSD (Honest Significant Difference) test for comparison of more than two samples. The fit model analysis was used for linear regression analysis in which the drug sensitivity was considered the independent factor (constant) and other variables such as NuMA expression, nuclear area and nuclear circularity were considered as dependent factors (variables). *P*-value levels are indicated in the figure legends. $P < 0.05$ was considered significant.

2.5 References

Abad, P. C., Lewis, J., Mian, I. S., Knowles, D. W., Sturgis, J., Badve, S., . . . Lelievre, S. A. (2007). NuMA influences higher order chromatin organization in human mammary epithelium. *Mol Biol Cell, 18*(2), 348-361. doi:10.1091/mbc.E06-06-0551

Abu-Yousif, A. O., Rizvi, I., Evans, C. L., Celli, J. P., & Hasan, T. (2009). PuraMatrix encapsulation of cancer cells. *J Vis Exp*(34). doi:10.3791/1692

Bednarz-Knoll, N., Alix-Panabieres, C., & Pantel, K. (2012). Plasticity of disseminating cancer cells in patients with epithelial malignancies. *Cancer Metastasis Rev, 31*(3-4), 673-687. doi:10.1007/s10555-012-9370-z

Briand, P., Petersen, O. W., & Van Deurs, B. (1987). A new diploid nontumorigenic human breast epithelial cell line isolated and propagated in chemically defined medium. *In Vitro Cell Dev Biol, 23*(3), 181-188.

Buenrostro, J. D., Wu, B., Chang, H. Y., & Greenleaf, W. J. (2015). ATAC-seq: A Method for Assaying Chromatin Accessibility Genome-Wide. *Curr Protoc Mol Biol, 109*, 21 29 21-29. doi:10.1002/0471142727.mb2129s109

Chandramouly, G., Abad, P. C., Knowles, D. W., & Lelievre, S. A. (2007). The control of tissue architecture over nuclear organization is crucial for epithelial cell fate. *J Cell Sci, 120*(Pt 9), 1596-1606. doi:10.1242/jcs.03439

Chao, Y., Wu, Q., Acquafondata, M., Dhir, R., & Wells, A. (2012). Partial mesenchymal to epithelial reverting transition in breast and prostate cancer metastases. *Cancer Microenviron, 5*(1), 19-28. doi:10.1007/s12307-011-0085-4

Chen, B., Co, C., & Ho, C. C. (2015). Cell shape dependent regulation of nuclear morphology. *Biomaterials, 67*, 129-136. doi:10.1016/j.biomaterials.2015.07.017

Chittiboyina, S., Rahimi, R., Atrian, F., Ochoa, M., Ziaie, B., & Lelièvre, S. A. (2017). Gradient-on-a-Chip with Reactive Oxygen Species Reveals Thresholds in the Nucleus Response of Cancer Cells Depending on the Matrix Environment. *ACS Biomaterials Science & Engineering, 4*(2), 432-445. doi:10.1021/acsbiomaterials.7b00087

Eckschlager, T., Plch, J., Stiborova, M., & Hrabeta, J. (2017). Histone Deacetylase Inhibitors as Anticancer Drugs. *Int J Mol Sci, 18*(7). doi:10.3390/ijms18071414

Guilluy, C., Osborne, L. D., Van Landeghem, L., Sharek, L., Superfine, R., Garcia-Mata, R., & Burridge, K. (2014). Isolated nuclei adapt to force and reveal a mechanotransduction pathway in the nucleus. *Nat Cell Biol, 16*(4), 376-381. doi:10.1038/ncb2927

Housman, G., Byler, S., Heerboth, S., Lapinska, K., Longacre, M., Snyder, N., & Sarkar, S. (2014). Drug resistance in cancer: an overview. *Cancers (Basel), 6*(3), 1769-1792. doi:10.3390/cancers6031769

Jain, N., Iyer, K. V., Kumar, A., & Shivashankar, G. V. (2013). Cell geometric constraints induce modular gene-expression patterns via redistribution of HDAC3 regulated by actomyosin contractility. *Proceedings of the National Academy of Sciences, 110*(28), 11349-11354. doi:10.1073/pnas.1300801110

Jayaraman, S., Chittiboyina, S., Bai, Y., Abad, P. C., Vidi, P. A., Stauffacher, C. V., & Lelievre, S. A. (2017). The nuclear mitotic apparatus protein NuMA controls rDNA transcription and mediates the nucleolar stress response in a p53-independent manner. *Nucleic Acids Res, 45*(20), 11725-11742. doi:10.1093/nar/gkx782

Joyce, M. H., Lu, C., James, E. R., Hegab, R., Allen, S. C., Suggs, L. J., & Brock, A. (2018). Phenotypic Basis for Matrix Stiffness-Dependent Chemoresistance of Breast Cancer Cells to Doxorubicin. *Front Oncol, 8*, 337. doi:10.3389/fonc.2018.00337

Khatau, S. B., Hale, C. M., Stewart-Hutchinson, P. J., Patel, M. S., Stewart, C. L., Searson, P. C., . . . Wirtz, D. (2009). A perinuclear actin cap regulates nuclear shape. *Proceedings of the National Academy of Sciences, 106*(45), 19017-19022. doi:10.1073/pnas.0908686106

Lammerding, J., & Wolf, K. (2016). Nuclear envelope rupture: Actin fibers are putting the squeeze on the nucleus. *J Cell Biol, 215*(1), 5-8. doi:10.1083/jcb.201609102

Lelievre, S. A., Weaver, V. M., Nickerson, J. A., Larabell, C. A., Bhaumik, A., Petersen, O. W., & Bissell, M. J. (1998). Tissue phenotype depends on reciprocal interactions between the extracellular matrix and the structural organization of the nucleus. *Proc Natl Acad Sci U S A, 95*(25), 14711-14716.

Mijovic, Z., Kostov, M., Mihailovic, D., Zivkovic, N., Stojanovic, M., & Zdravkovic, M. (2013). Correlation of nuclear morphometry of primary melanoma of the skin with clinicopathological parameters and expression of tumor suppressor proteins (p53 and p16(INK4a)) and bcl-2 oncoprotein. *J BUON, 18*(2), 471-476.

Nandini, D. B., & Subramanyam, R. V. (2011). Nuclear features in oral squamous cell carcinoma: A computer-assisted microscopic study. *J Oral Maxillofac Pathol, 15*(2), 177-181. doi:10.4103/0973-029X.84488

Panier, S., & Boulton, S. J. (2014). Double-strand break repair: 53BP1 comes into focus. *Nat Rev Mol Cell Biol, 15*(1), 7-18. doi:10.1038/nrm3719

Plachot, C., Chaboub, L. S., Adissu, H. A., Wang, L., Urazaev, A., Sturgis, J., . . . Lelievre, S. A. (2009). Factors necessary to produce basoapical polarity in human glandular epithelium formed in conventional and high-throughput three-dimensional culture: example of the breast epithelium. *BMC Biol, 7*, 77. doi:10.1186/1741-7007-7-77

Plachot, C., & Lelievre, S. A. (2004). DNA methylation control of tissue polarity and cellular differentiation in the mammary epithelium. *Exp Cell Res, 298*(1), 122-132. doi:10.1016/j.yexcr.2004.04.024

Salvador Moreno, N., Liu, J., Haas, K. M., Parker, L. L., Chakraborty, C., Kron, S. J., . . . Vidi, P. A. (2019). The nuclear structural protein NuMA is a negative regulator of 53BP1 in DNA double-strand break repair. *Nucleic Acids Res*. doi:10.1093/nar/gkz138

Samani, A., & Plewes, D. (2004). A method to measure the hyperelastic parameters of ex vivo breast tissue samples. *Phys Med Biol, 49*(18), 4395-4405.

Silver, D. P., Richardson, A. L., Eklund, A. C., Wang, Z. C., Szallasi, Z., Li, Q., . . . Garber, J. E. (2010). Efficacy of neoadjuvant Cisplatin in triple-negative breast cancer. *J Clin Oncol, 28*(7), 1145-1153. doi:10.1200/JCO.2009.22.4725

Thomas, C. H., Collier, J. H., Sfeir, C. S., & Healy, K. E. (2002). Engineering gene expression and protein synthesis by modulation of nuclear shape. *Proc Natl Acad Sci U S A, 99*(4), 1972-1977. doi:10.1073/pnas.032668799

Uhler, C., & Shivashankar, G. V. (2017). Chromosome Intermingling: Mechanical Hotspots for Genome Regulation. *Trends Cell Biol, 27*(11), 810-819. doi:10.1016/j.tcb.2017.06.005

Vega, S. L., Liu, E., Arvind, V., Bushman, J., Sung, H. J., Becker, M. L., . . . Moghe, P. V. (2017). High-content image informatics of the structural nuclear protein NuMA parses trajectories for stem/progenitor cell lineages and oncogenic transformation. *Exp Cell Res, 351*(1), 11-23. doi:10.1016/j.yexcr.2016.12.018

Versaevel, M., Grevesse, T., & Gabriele, S. (2012). Spatial coordination between cell and nuclear shape within micropatterned endothelial cells. *Nat Commun, 3*, 671. doi:10.1038/ncomms1668

Vidi, P. A., Maleki, T., Ochoa, M., Wang, L., Clark, S. M., Leary, J. F., & Lelievre, S. A. (2014). Disease-on-a-chip: mimicry of tumor growth in mammary ducts. *Lab Chip, 14*(1), 172-177. doi:10.1039/c3lc50819f

Weaver, V. M., Carson, C. E., Walker, P. R., Chaly, N., Lach, B., Raymond, Y., . . . Sikorska, M. (1996). Degradation of nuclear matrix and DNA cleavage in apoptotic thymocytes. *J Cell Sci, 109 (Pt 1)*, 45-56.

Weaver, V. M., Lelievre, S., Lakins, J. N., Chrenek, M. A., Jones, J. C., Giancotti, F., . . . Bissell, M. J. (2002). beta4 integrin-dependent formation of polarized three-dimensional architecture confers resistance to apoptosis in normal and malignant mammary epithelium. *Cancer Cell, 2*(3), 205-216.

Zink, D., Fischer, A. H., & Nickerson, J. A. (2004). Nuclear structure in cancer cells. *Nat Rev Cancer, 4*(9), 677-687. doi:10.1038/nrc1430

Supplementary Figure 1. **A.** Sigmoid graphs for percentage of cell death in T4-2 population treated with 0, 12.5, 25 and 50 μM of cisplatin for 24 hours in 2D and 3D cultures. **B.** Sigmoid graphs for percentage of proliferative T4-2 cells treated with 0, 1.25, 2.5 and 10 μM of SAHA (24 hours and rest for the next 24 hours) in 2D and 3D cultures **C.** Percentage of T4-2 cells positive for caspase 3 after receiving 0 (control) or 0.6 μM of latrunculin for 24 hr. **D.** Bar graph of densitometry analysis of 53BP1 expression, based on western blots, in T4-2 cells treated with nonspecific siRNA (NuMA +) or siNuMA (NuMA -), with treatment (+) or not (-) with 0.6 μM Latrunculin for 24 hours on day two of 2D culture. **E**. T4-2 were treated as in D and nuclear area was analyzed with imageJ based on DAPI staining. The bottom panel shows representative images of cells stained with phalloidin to reveal the organization of actin microfilaments. **F**. Bar graph of densitometry results for beta actin under treatment conditions as in D. N = 3, with 100 nuclei analyzed per replicate. Scale bar 10 μm *P<0.5

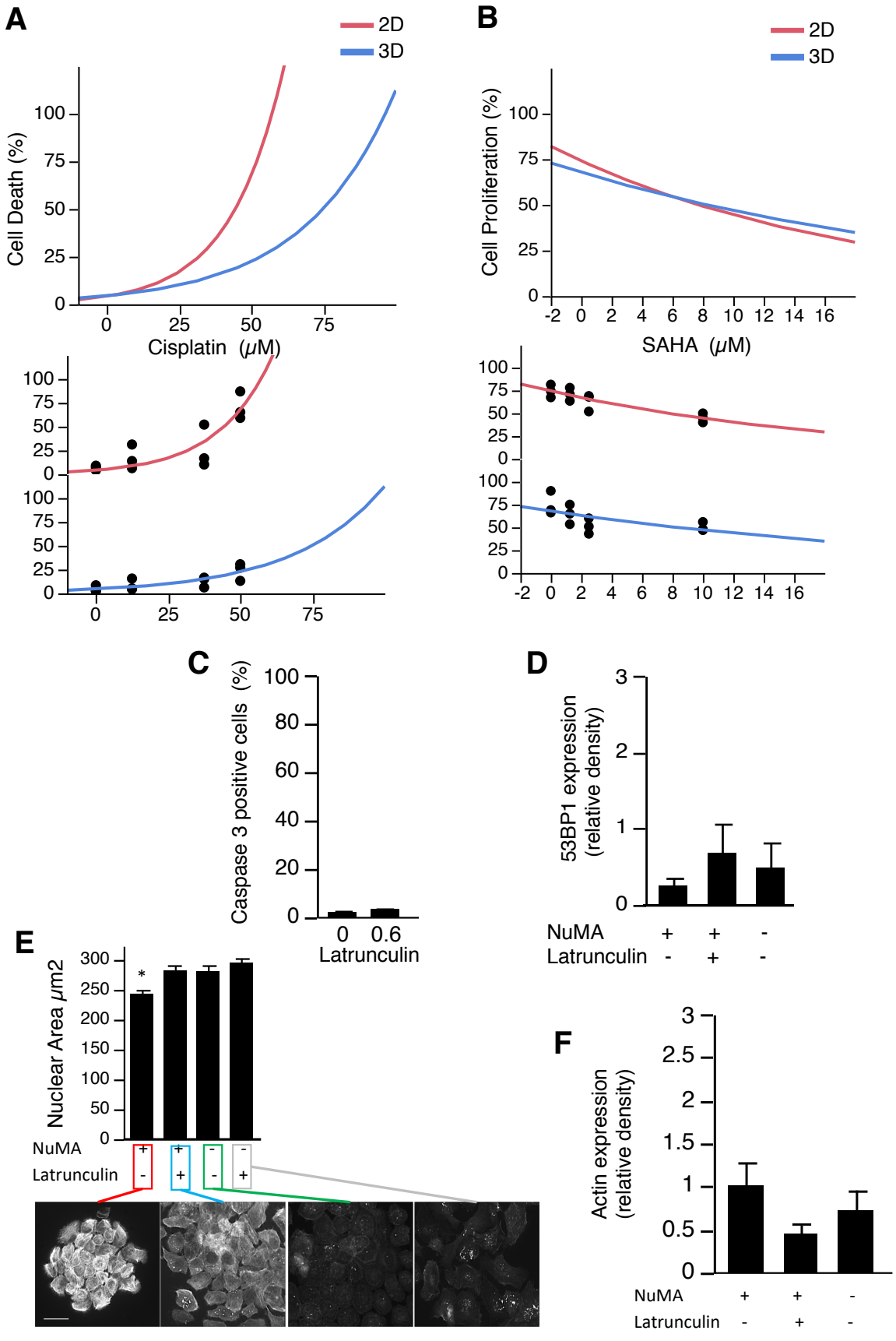
A
2D
3D
Cell Death (%)
Cisplatin (μM)
B
2D
3D
Cell Proliferation (%)
SAHA (μM)
C
Caspase 3 positive cells (%)
0 0.6
Latrunculin
D
53BP1 expression (relative density)
NuMA + + -
Latrunculin - + -
E
Nuclear Area μm2
NuMA
Latrunculin
F
Actin expression (relative density)
NuMA + + -
Latrunculin - + -

Supplementary Figure 2. A. T4-2 cells were treated with nontarget siRNA (NT) and NuMA siRNA (siNuMA) in monolayer culture (2D) for 24 hours followed by four days of culture. Representative images of immunostaining for NuMA (red) and counterstaining of nuclei with DAPI (blue). **B.** Graphs of the percentages of apoptotic cells (caspase 3 staining; left) or proliferating cells (Ki67 staining, right) in T4-2 populations treated with cisplatin (50 μM) or with SAHA (10 μM) and/or cytochalasin D (0.5 μM) or both for 24 hours on day two of 2D culture. **C.** Bar graphs of average nuclear area and circularity in T4-2 cells treated or not with cytochalasin D (0.5 μM) for 24 hours on day two of 2D culture. **D**. Graph of densitometry analysis for NuMA under latrunculin treatment or siRNA (siNuMA) treatment with representative western blot. **E**. Graph of densitometry analysis for NuMA under cytochalasin treatment or siRNA (siNuMA) treatment with representative western blot. Lamin B was used as loading control. N = 3 for (except for E, N=1), with **100** nuclei analyzed per replicate. **P*<0.05, ***P*<0.01, ****P*<0.001. Scale bar, 10 μm

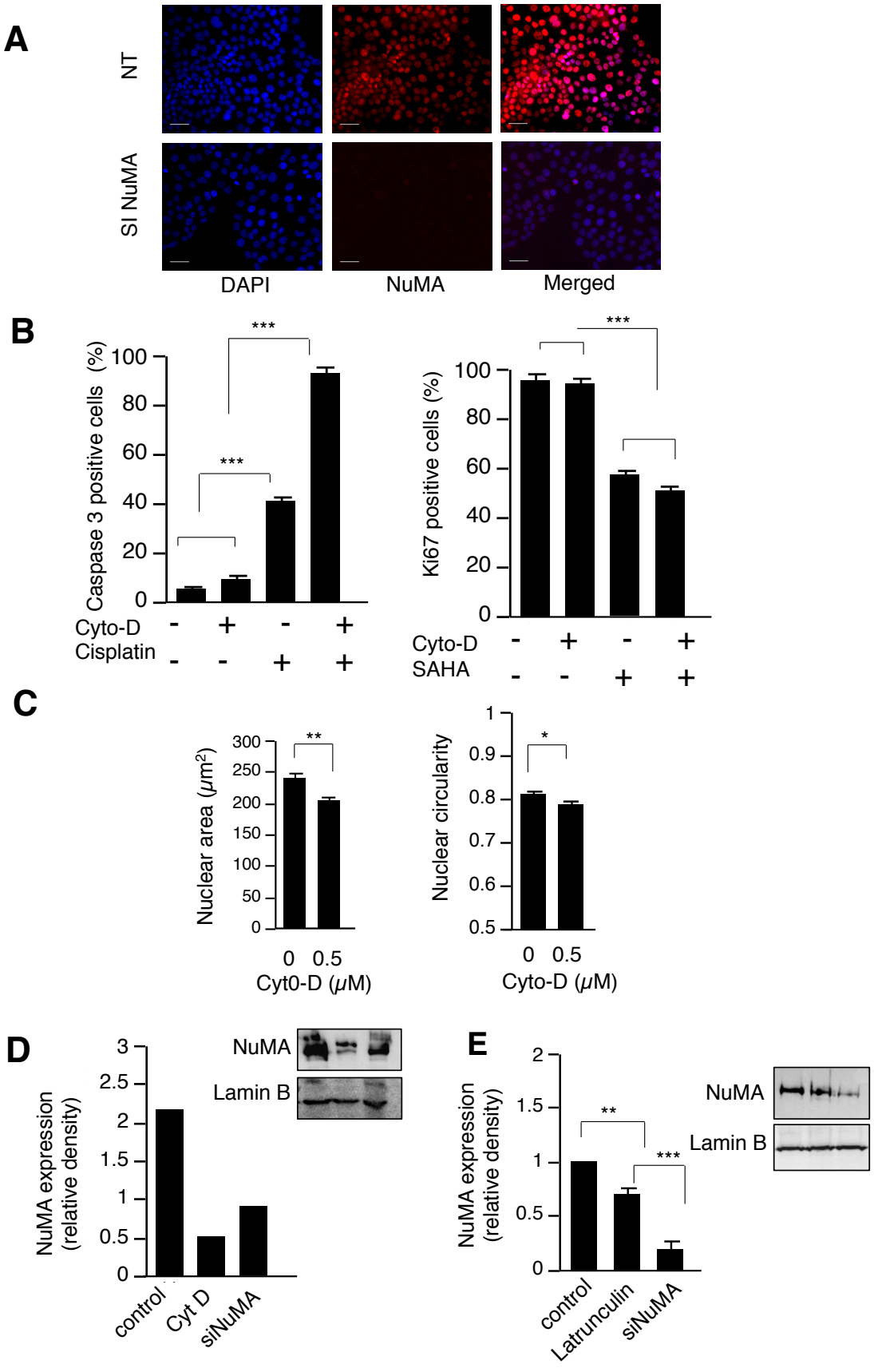
A
NT
SI NuMA
DAPI
NuMA
Merged
B
Caspase 3 positive cells (%)
Cyto-D
Cisplatin
Ki67 positive cells (%)
Cyto-D
SAHA
C
Nuclear area (μm²)
Cyt0-D (μM)
Nuclear circularity
Cyto-D (μM)
D
NuMA expression (relative density)
NuMA
Lamin B
control
Cyt D
siNuMA
E
NuMA expression (relative density)
NuMA
Lamin B
control
Latrunculin
siNuMA

Supplementary Figure 3. T4-2 cells were treated with nontargeting (NT) siRNA and siRNA for NuMA (siNuMA) for 24 hours in 2D culture before seeding in collagen I of 900 Pa or of 2020 Pa and culture for another 3 days. **A**. Fluorescence images of NuMA immunostaining (red) and counterstaining of cell nucleus with DAPI (blue). **B**. Bar graph of percentages of proliferating cells (Ki67 staining). **C**. Immunostaining for mechanosensor YAP (green) with its presence in the cell nuclei at 2020 Pa. **D**. Percentages of apoptotic cells (caspase 3 staining) following treatment with 10 μM of doxorubicin (DOX) for 24 hours on day third of 3D culture. N =3 (B, D) with 100 nuclei analyzed per replicate; **P*<0.05. Scale bar, 10 μm

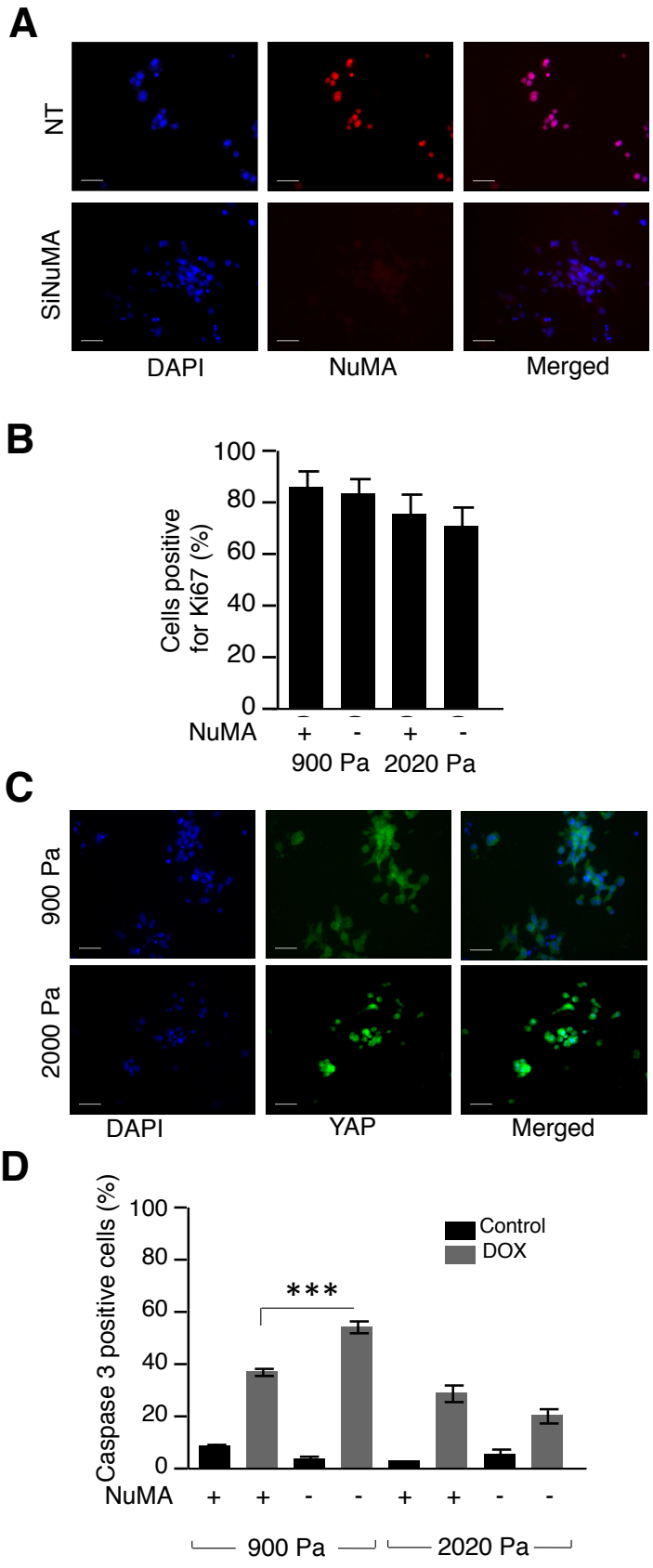
A
NT
SiNuMA
DAPI
NuMA
Merged
B
Cells positive for Ki67 (%)
100
80
60
40
20
0
NuMA + - + -
900 Pa 2020 Pa
C
900 Pa
2000 Pa
DAPI
YAP
Merged
D
Caspase 3 positive cells (%)
100
80
60
40
20
0
Control
DOX
***
NuMA + + - - + + - -
900 Pa
2020 Pa

Supplementary Figure 4. T4-2 cells and MDA-MB-231 cells were cultured in collagen I of 900 Pa or 2020 Pa for three days. **A.** Average nuclear area based on DAPI staining and imageJ analysis **B.** nuclear circularity based on DAPI staining and imageJ analysis. **C.** Percentage of MDA-MB-231 cells positive for proliferative (Ki67) marker in cells treated with nontargeting siRNA (+) or siRNA for NuMA (-) for 24 hours in 2D culture before embedding in the collagen matrix and culture for 3 days. **D.** Graph of densitometry analysis of NuMA expression levels measured on western blots. Cells were cultured in collage I of 900 Pa or 2020 Pa for 72 hours before protein extraction. N =3 (for **D,** N=2) with 100 nuclei analyzed per replicate; **P*<0.05, ***P*<0.01, ****P*<0.001.

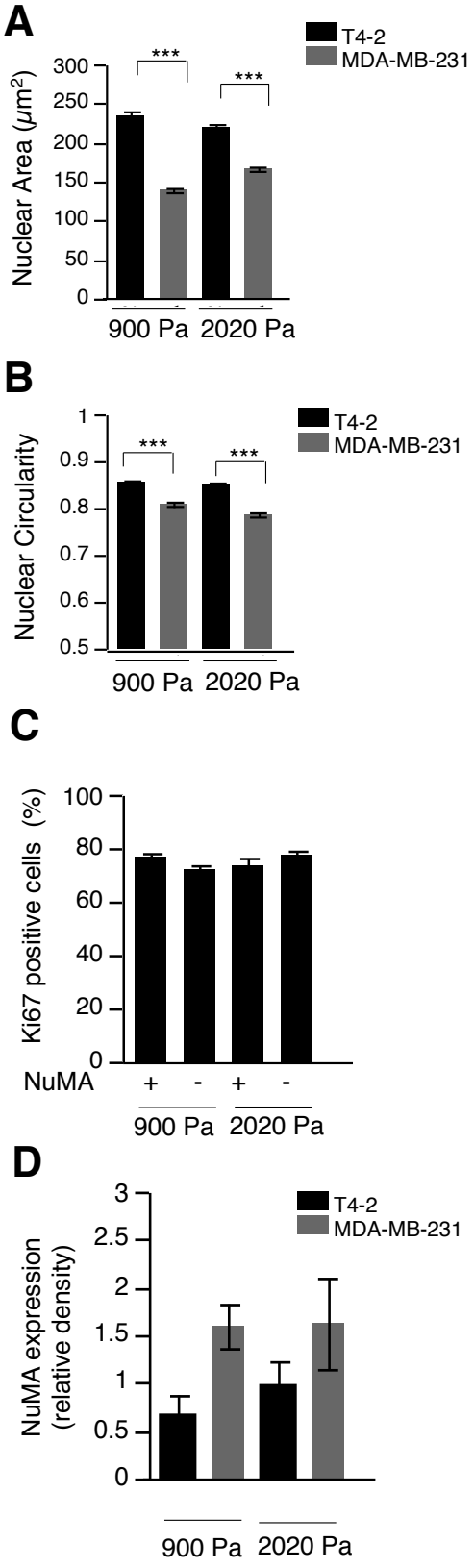
A
T4-2
MDA-MB-231
Nuclear Area (μm²)
300
250
200
150
100
50
0
***
***
900 Pa
2020 Pa
B
T4-2
MDA-MB-231
Nuclear Circularity
1
0.9
0.8
0.7
0.6
0.5
***
***
900 Pa
2020 Pa
C
Ki67 positive cells (%)
100
80
60
40
20
0
NuMA
+
-
+
-
900 Pa
2020 Pa
D
T4-2
MDA-MB-231
NuMA expression (relative density)
3
2.5
2
1.5
1
0.5
0
900 Pa
2020 Pa

CHAPTER 3. CELL CULTURE AND COCULTURE FOR ONCOLOGICAL RESEARCH IN APPROPRIATE MICROENVIRONMENTS

The following manuscript was submitted to Current Protocols in Chemical Biology and is in the format required for the journal

Running title: **Extracellular Matrix-based Culture of Cancer Models**

Apekshya Chhetri*[1], Shirisha Chittiboyina*[1,2], Farzaneh Atrian*[1], Yunfeng Bai*[1], Davide A. Delisi[1], Rahim Rahimi[3], John Garner[4], Yuri Efremov[5,6], Kinam Park[4,7], Rabih Talhouk[8], Sophie A. Lelièvre[1,2,9†]

[1] Department of Basic Medical Sciences, Purdue University College of Veterinary Medicine, West Lafayette, Indiana, West Lafayette, Indiana. United States of America

[2] 3D Cell Culture Core (3D3C) Facility, Birck Nanotechnology Center, Purdue University Discovery Park

[3] Department of Materials Engineering, Purdue University

[4] Akina, Inc. 3495 Kent Avenue, West Lafayette, IN 47906

[5] Birck Nanotechnology Center, Purdue University Discovery Park

[6] **School of Mechanical Engineering, Purdue University**

[7] Weldon School of Biomedical Engineering, Purdue University

[8] Department of Biology, American University of Beirut, Beirut, Lebanon

[9] Purdue University Center for Cancer Research

* first coauthors

†Corresponding author: Department of Basic Medical Sciences, 625 Harrison Street, Lynn Hall, Purdue University, West Lafayette, Indiana, 47907-2026, United States of America

Phone: 765 496 7793

Fax: 765 494 0781

email: lelievre@purdue.edu

Significance statement

The goal of 3-Dimensional (3D) cell culture techniques is to ensure that the cells are studied under physiologically relevant conditions, such that the impact of the extracellular matrix (ECM), including its biomechanical properties are translated to the cells as *in vivo*. The effects of the ECM on cancer development and progression, from a non-neoplastic stage to aggressive phenotypes have been highlighted by research covering several decades. Replicating microenvironmental conditions through 3D culture provides a more realistic assessment of the response of cancer cells to risk factors for progression and for drug treatment compared to the traditional 2-dimensional culture. It is anticipated that appropriate 3D cell culture techniques will be invaluable to not only identify molecular mechanisms of cancer cell behavior, but also translate successful research on targeted cancer therapy for clinical applications.

3.1 Abstract

With the increase in knowledge on the importance of the tumor microenvironment, cell culture models of cancers can be adapted to better recapitulate physiologically relevant situations. Three main microenvironmental factors influence tumor phenotype, the biochemical components that stimulate cells, the fibrous molecules that influence the stiffness of the extracellular matrix, and noncancerous cells like epithelial cells, fibroblasts, endothelial cells and immune cells. Here we present methods for the culture of carcinomas by considering the stiffness of the matrix, and for the coculture of tumors and fibroblasts as well as epithelial cells in the presence of matrix. Information is provided to help with choices and assessment of the matrix support and to work with serum free medium. Using an example of tissue-chip recapitulating the environmental geometry of carcinomas we also highlight the development of engineered platforms that provide exquisite control of cell culture parameters necessary in research and development.

Keywords: Cancer, tumor, extracellular matrix, collagen I, fibroblast, epithelium

3.2 Introduction

Several decades of research have clearly established that the extracellular matrix (ECM) i.e., a water-rich meshwork of proteins and polysaccharides, is not simply supporting cells. Rather, it provides a dynamic microenvironment, owing to the presence of various signaling molecules and to the specific strength of its network of fibers that feed biochemical and mechanotransduction pathways within cells. There are two major types of ECM, (i) the interstitial matrix that surrounds

cells and tissues and (ii) the basement membrane, a specialized form of ECM that separates epithelial cells from the surrounding stroma (Bonnans, 2014; Theocharis, 2016). Amongst the interstitial fibrous proteins, collagen I is the most abundant and its density and cross-linking greatly contributes to microenvironmental stiffness (Lin, 2015).

Even though the basic components of natural matrices are the same, differences exist depending on the type of tissue or organ and these differences participate in dictating the specific phenotype and function of cells. Importantly, as proposed in the early 80s (Bissell, 1982), a body of literature has confirmed the existance of a bidirectional influence between the cells (all the way to the cell nucleus) and the ECM that participates in tissue development and the progression of diseases like cancers. Therefore, studying, *in vitro*, cell and tissue phenotypes, regardless of normal or diseased stages, is best served by a physiologically relevant microenvironment in cell cultures. At minimum, ECM molecules should be provided as inducers for cells to secrete and organize a complete matrix, hence leading to tissues with an architecture that resembles the situation *in vivo*. When cell culture promotes *in vivo*-like tissue architecture it is called three-dimensional (3D) cell culture.

Differences between tumors and normal tissues encompass not only cell phenotypes, but also the microenvironment. The tumor microenvironment constitutes an active field of research considering its importance to readily control the behavior of tumor cells (Spill, 2016). The remodeling of the ECM that contributes to increased matrix stiffness is a phenomenon that was revealed more than a decade ago (Paszek, 2005) and has now been commonly observed in tumors (Fullár, 2015; Leight, 2017). Incorporating a defined ECM stiffness in models of cancer reproduced *in vitro* has become an important goal of 3D cell culture. In addition to an increased density of fibrous ECM molecules via secretion by cells, a major mechanism that participates in local remodeling of the tumor microenvironment is through degradation of collagen by metalloproteinases (Conlon, 2018). Collagenase is one such enzyme essential for the degradation of collagen *in vivo*; but it is also used *in vitro* to release tumor nodules from cell culture.

The tumor microenvironment is also comprised of cells contributing to tumor behavior, like stromal cells or fibroblasts, specifically known as Cancer Associated fibroblasts (CAFs) that participate in ECM remodeling, and immune cells (Cohen , 2017). A standard method to study the interaction of cells in the microenvironment with tumors *in vitro* is to conduct cocultures (i.e., cultures of different cell types in the same culture vessel), enabling paracrine exchange and

alterations in matrix stiffness as appropriate. Differences in phenotype for stromal as well as tumor cells have been shown in cocultures compared to monocultures, illustrating the mutual influence of these cells to promote cancer progression (Northey, 2017).

In this article, we present two sets of basic protocols related to the study of epithelial glandular cancers (or carcinomas) that represent the bulk of the global cancer burden. The first set of protocols discusses the importance of the choice of the ECM and its stiffness for the culture of tumors cells. The second set of protocols presents examples of cultures pertaining to integrated studies with cells known to control cancer behavior, including fibroblasts and non-neoplastic epithelial cells that are located near carcinomas. The cells of the tumor microenvironment influence the progression of most cancers of epithelial origin.

3.3 Basic Protocol 1

Culture of cancer cells in matrices of specific stiffness level

The purpose of this method is to place cancer cells in a microenvironmental context that provides an optimal level of constraints for them to display their phenotype. For instance, cancer cells have different degrees of invasive capabilities, and a matrix too stiff or not stiff enough would influence such capabilities. A similar issue might occur with proliferation capabilities. Most cancer cells make their own ECM components, but carcinomas (the frequent cancers of glandular epithelial origin) grow within the interstitial matrix that normally delineates tissues in an organ; the basis for such matrix is collagen. There are many types of collagens depending on the organ (Kular, 2014). The protocol detailed below is focused on collagen type-I (collagen I), the major constituent of the microenvironment of carcinomas. We will use examples of breast carcinomas that recapitulate ductal carcinoma in situ (DCIS), a noninvasive form of cancer, and invasive ductal carcinomas (IDC) with low and high aggressiveness based on their invasive and metastatic potentials. The steps included in the Protocol are the management of cells prior to culture within collagen, the preparation of collagen and embedding of cells (to provide a layer thin enough for direct immunostaining), the observation of cells within collagen and the release of cells from collagen for further desired analyses.

Materials

1.1 Reagents and solutions

1.1.1. Cell Culture Medium and ECM

In the examples chosen for this protocol we will use cell lines from the HMT-3522 cancer progression series, notably DCIS S2 and IDC T4-2 cells. This series was developed in serum free medium (Briand, 1987; Briand,1996), and we have adapted all other cell lines used in the laboratory to similar culture with known additives.

Four additives are considered core additives necessary for all cell types as they provide necessary support for survival (via the regulation of uptake of extracellular molecules by the cells, inhibition of apoptosis, support of the function of antioxidant enzymes) and proliferation. These additives are Transferrin, Hydrocortisone, Insulin and sodium Selenite [THIS].

1. Dulbecco's Modified Eagle's Medium (DMEM/F12, Life Technologies™)

2. Prolactin (Sigma-Aldrich®, Catalog #L-6520); final concentration, 5 µg/ml

3. Insulin (Sigma-Aldrich® Catalog #I-4011): final concentration, 250 ng/ml

4. Hydrocortisone (Sigma-Aldrich® Catalog #H-0888); final concentration, 1.4 µM

5. β-Estradiol (Sigma-Aldrich® Catalog #E-2758); final concentration, 0.1 nM

6. Sodium selenite (BD Biosciences Catalog #354201); final concentration, 2.6 ng/ml

7. Transferrin (Sigma-Aldrich® Catalog #T-2252); final concentration, 10 µg/ml

8. Epidermal growth factor (Corning Life Sciences (previously sold through BD Biosciences Catalog #354001); final concentration, 5 ng/ml

Additives are added from their working stock solution into the cell culture medium in order to reach the final concentration necessary for each additive. Details regarding these additives are included in the REAGENTS and SOLUTIONS section and in Table 1.

*Note that with serum free medium, Soybean trypsin inhibitor needs to be added to the cell suspension collected after using trypsin to detach cells from the cell culture flask (*Vidi, 2013*).*

9. Collagen matrix: In this protocol we are using PhotoCol® (Catalog No #5201-1KIT) from Advanced Biomatrix as tunable collagen I.

1.1.2 Cell detachment

- Trypsin-EDTA (0.25% 1 mM EDTA-4Na) (Gibco, REF: 25200-056)
- Soybean trypsin inhibitor (SBTI) T-6522 type I-S (BD Biosciences #354201) (stock concentration 10 mg/ml prepared in milli-Q water; final concentration, 0.18 mg/ml)

- Collagenase (Advanced Biomatrix, Catalog #5030-50 mg bottle) (stock concentration 5 mg/ml prepared in PBS; final concentration, 1 mg/ml in PBS for our range of Young's modulus [up to 2000 Pa]; note: *up to 5 mg/ml can be used in case of a denser matrix)*

1.2 Materials

- Ice bucket
- Pipettor with 1, 5, 10 ml pipets
- Micropipettor with 10-20, 200, 1 ml tips
- Eppendorf tubes
- Cell culture compatible plastic tubes (15 and 50 ml depending on the volume of medium necessary)
- 4-well chambered slides (used for direct immunostaining of cultures)
- Petri dishes to contain the chambered slides

Protocol steps

1.3 Management of cells prior to culture within collagen I

It is very important to perform standard cell cultures very carefully, with always the same number of cells seeded in flask for each passage and always the same confluence chosen to split the cell population for propagation (Plachot, 2009; Vidi, 2013); otherwise the phenotype drifts (e.g., cells modify their aggressiveness) over weeks. This drift is usually only seen in 3D culture and by the time the drift in phenotype is observed, it is impossible to recover the original phenotype. We also recommend keeping all experiments always within the same window of passages (that usually spans no more than 10 passages) and to acquire cells from a trusted source.

Prior to using the cells for 3D culture, it must be ensured (using a microscope) that the expected cell population confluence in the flask to be used for cell seeding in the experiment has been reached (e.g., no more than 70-80% for cancer cells) and that the cells look fine, in terms of shape notably.

1.4 Collagen I-based cell culture

An ice-bucket filled with ice should be placed inside the laminar flow hood when working with collagen. (The bucket must be wiped with ethanol before taking it inside the laminar flow hood).

Collagen I with appropriate matrix stiffness is prepared according to the protocol explained in ***SUPPORT PROTOCOL 1***).

1.4.1. The following steps must be performed at least 30 minutes before the start of the cell culture:

The best results in 3D cell culture are obtained with cells cultured in serum-free medium. A medium with serum does not prevent using 3D culture, but there might be issues with reproducibility due to the change in batch of serum (that contains many unknown components with variable concentrations) and interference of serum components with the reagents used for the treatment of cells depending on the experiment. Protocols to wean cells off serum and choose and prepare additives for serum-free culture are available online; nevertheless, we have included information on the preparation of the additives that we use for the cells presented in these protocols and our serum weaning procedure in sections "REAGENTS and SOLUTIONS" and ***SUPPORT PROTOCOL 4****. Here we are using serum-free culture for breast cancers (see 1.1 reagents and solutions).*

- The laminar flow hood is sterilized with UV for at least 30 minutes prior to use. *Note that we do not use antibiotics for cell culture. The use of antibiotics is not recommended for cell culture as it might lead to the survival of resistant bacteria that could devastate cultures in the long run. It is better to use sterile cell culture elements (containers, pipettes, etc.), thoroughly clean every piece of equipment before placing it in the hood and clean the hood before and after use (and make use of UV as appropriate).*
- Fresh DMEM medium is prepared using additives to create the DMEM/F12 cell culture medium for breast cancer cells [5 µg/ml (or 0.15 IU/ml) prolactin, 250 ng/ml insulin, 1.4 µM hydrocortisone, 0.1 nM β-estradiol, 2.6 ng/ml sodium selenite, 10 µg/ml transferrin, 5 ng/ml EGF].
  Note that this cocktail works well for the T4-2 and MDA-MB-231 cell lines that we will use as examples of breast IDC in this protocol, but for the S2 cells used as example of DCIS in ***ALTERNATIVE PROTOCOL 1****, we do not add EGF, otherwise these cells would not thrive (regardless of the culture conditions).*
- When using additives, it is essential to indicate the preparation dates for the stocks and replace additives based on these dates (no use beyond expiration should be attempted, otherwise the cells might not proliferate, or their phenotype might drift). When the cells are removed from their culture vessels trypsin is used like for other cells, but since there is

no serum in the culture, Soybean Trypsin Inhibitor (SBTI) needs to be added to cancel the effect of trypsin after the few minutes incubation necessary to detach the cells. Once stored in the fridge, this SBTI should be no older than two weeks to be used and sodium Selenite and EGF should be no older than one week; the other additives should not be kept longer than one month (Table 1).

1.4.2 Removal of cells from their 2D culture device in preparation for embedding in collagen

- T-75 flasks and/or T-25 flasks in which the cells were cultured are taken out of the incubator, checked for the expected confluence (70-80% for cancer cells) with a microscope and brought inside the laminar flow hood.
- The medium is discarded from the flasks.
- 750 µl (for T-75) or 250 µl (for T-25) of Trypsin are added and spread evenly on the cell layer.
- The Trypsin is discarded.
- One ml or 330 µl of trypsin is added to the T-75 or T-25 flask, respectively, spread like above briefly and the flask is incubated at 37°C for no more than 5-10 minutes.
  (Start the timer "ON" once the flask is placed inside the incubator). After 4-5 minutes the flask is taken out, tapped on the sides and checked for floating cells with a microscope. Within 10 minutes the trypsin should have detached most of the cells.
- After the incubation period is over, 3 ml (T-25) or 9 ml (T-75) of DMEM+SBTI solution are added into the culture flask (SBTI working concentration is 0.18 mg/ml) to inhibit trypsin. The solution is mixed with the pipettor two or three times, washing the entire surface where the cells were cultured. Proper suspension of all cells in the flask is essential.
- Around 100 µl of suspension is added into a prelabeled Eppendorf tube for cell counting. Based on the number of cells counted, the necessary volume of suspension can be calculated for cell seeding purposes.
- The necessary amounts of cells and corresponding volumes to take from the trypsin-treated flasks are calculated (Table 2); the cells are spun down for five minutes at 3000 g and the cell pellet is resuspended in only 5 µl of medium (e.g., for cells to be placed in one well of a chambered slide), so there is no significant dilution effect in the collagen I preparation to

be used in the next step. (This volume usually corresponds to no more than 10 % of the total volume in which the cells are embedded in the next step).

1.4.3 Embedding of cells in collagen I (thin layer)

- An ice bucket dedicated to the "cell culture" laboratory is filled with ice and the collagen-containing tube is transferred from 4°C (refrigerator) to the ice bucket inside the laminar flow hood. (*Note that the collagen I with appropriate stiffness was prepared prior to cell culture*; see ***SUPPORT PROTOCOL 1***).
- The tissue culture devices to be used depend on the experiment. Here we are working on a protocol for immunostaining with a thin layer of collagen I, and we typically use 4-well chambered slides. These devices are labelled inside the laminar flow hood, with indication of the content for each well as appropriate and the date.
- The surface of each well is first coated with an ultrathin layer of collagen-I (14 µl/cm^2) and incubated at 37°C for five minutes until the gel becomes opaque.

Add a few drops of the calculated volume of solution so that they cover all the surface of the well. Use the tip of the pipettor to mix the drops together by gently moving the tip back and forth between the drops. If you keep the tip attached to the micropipettor, ensure that the plunger is pushed down to the first notch all the time and avoid taking back the solution into the tip. Some people keep a small volume of solution in the tip (then the plunger is not pushed all the way down to the first notch) so that they can add it in the final step all around the surface of the well. In that case the remaining collagen solution is slowly released to prevent bubble formation (as usual stop pushing on the plunger when you reach the second notch to avoid making bubbles).

- The resuspended cells (in the small volume of medium mentioned at the end of section 1.4.2) are mixed with the collagen I suspension (55 µl/cm^2) by gentle mixing inside a pipette tip (once or twice), and the mixture is immediately added as per the note below on top of the ultrathin coat of collagen.

Briefly, take 10 µl of collagen and add this volume into the ~5 µl of cell suspension (see last bullet point of 1.4.2), mixing up-and-down with the plunger only once. This step will allow

the cells to get accustomed to the collagen environment. Then, add the necessary volume of collagen (you may subtract the initial 10 µl volume that was just added). As the collagen solution is viscous, you will have to push the plunger of the micropipettor down and stop at the second notch, then release the plunger just a little and wait for a few seconds for the solution to go up the tip, then release the plunger a little more, etc., until the whole volume is taken. Carefully release the collagen solution into the cell suspension, use slow release by maintaining pressure on the plunger of the pipette. Do not add the last drop of the solution as it creates bubbles. Now mix the solution up and down with the plunger only once. Take the entire volume of collagen solution containing the cells and slowly release the solution on top of the well that is precoated with collagen. Add two drops next to each other in the well (and mix the drops together by moving the tip of the micropipettor across the drops if necessary, with no more than one or two back and forth tip movement to avoid disturbing the cells). You should do this step very gently to drag the gel solution also to the sides or towards the edges of the well.

- The chambered slides are incubated at 37°C for 25 minutes.
- After incubation, 500 µl of H-14 culture medium are added carefully by bringing the pipette tip close to the side of culture vessel, without disturbing the gel.
- The 3D cultures are placed in the cell culture incubator and the medium is replaced every two to three days unless the experiment necessitates changing the medium every 24 hours (depending on the type of reagent used for certain treatments for instance).

1.5 Release of cells from collagen I

The cells that have been cultured in collagen either isolated (e.g., fibroblasts) or to form nodules (e.g., tumors) may be removed from the gel using collagenase.

- Aspirate the medium gently without touching the surface of the gel. It is desirable to ensure that all the medium has been removed from the gel by tilting the chambered slide at an angle to facilitate medium aspiration.
- Collagen requires the use of a dislodging enzyme, collagenase (Advanced Biomatrix, working concentration 1 mg/ml], that breaks the gel. The desired volume (78 µl/cm^2) of collagenase is calculated based on the surface area of the culture vessel and added drop by drop directly on top of the cell culture, covering the entire surface of the culture vessel.

- The culture vessel is then incubated at 37°C for 45 minutes. After the incubation period, the solution is observed with a microscope to ensure that the cells or the multicellular nodules are floating. The cell culture vessel can be further incubated with collagenase for 15 minutes if necessary.
- The floating nodules are then removed from the culture vessel (avoid taking the gel; it is recommended to not aspirate the solution into the 1 ml pipet tip from the bottom of the dish as most cells or nodules are floating on the surface).
- The collected cells or nodules are placed into an Eppendorf tube and centrifuged at 3000 g for five minutes.
- The supernatant is removed carefully using a small pipette tip connected to the vacuum pipe, ensuring that the pellet remains at the bottom of the tube.
- The pellet is then washed three times with cell culture medium, each wash consisting of a centrifugation at 3000 g for five minutes. Importantly, after each centrifugation, the pellet is 'washed' without being resuspended or dislodged (do not move the solution up and down in the pipet tip; it will prevent the pellet from being stuck to the wall of the pipet tip). The washing step is important to remove as much of the collagenase solution as possible.
- After the 3rd wash, the 4th wash can be performed with Phosphate Buffered Saline (PBS) if the cells are to be lysed for analysis or with medium again before proceeding with trypsinization and cell reseeding based on the planned experiment.

1.6 Choice of matrix depending on the type of cancer

A characteristic of the DCIS type of carcinomas that grow within the breast ducts without invading into the interstitium, is an intact basement membrane, as shown by immunostaining, and an increased stiffness of the collagen in the interstitium (~2-fold; Lopez, 2011). Culturing these cells usually works well with Matrigel™ that provides the initial signaling for the cells to display basal polarity (see ***ALTERNATIVE PROTOCOL 1***). Basal polarity is measured by the presence of a continuous staining for β4- or α6-integrin and basement membrane components collagen IV or laminin 5 at the outer side of the tumor nodule (Plachot, 2009; Fig. 1). However, Matrigel™ typically has a stiffness close to the normal breast stroma (i.e., Young's modulus of 700-800 Pa as measured by indentation of unconstrained matrix; see ***SUPPORT PROTOCOL 2***). To reach a stiffness around 1,400 Pa and maintain basal polarity, we mix basement membrane component

laminin 111 (76 µg/ml) with the collagen of appropriate stiffness prior to embedding the cells (Chittiboyina, 2018). An example of DCIS cells is the HMT-3522 S2 line (Rizki, 2008) that were selected after omitting EGF from the culture medium at passage 118 of non-neoplastic S1 cells spontaneously immortalized in cell culture (Briand, 1987). The initial sample of epithelial cells to derive the HMT-3522 series was from a non-neoplastic fibrocystic breast tissue.

The characteristics of IDC types of carcinomas are invasiveness and a stiffer matrix (at least 2000 Pa if measured on unconstrained samples; Lopez, 2011). For instance, the T4-2 cells were established when after 238 passages the S2 cells became tumorigenic in mice; the tumorigenic status was confirmed via subculture *in vitro* of the cells from the tumor developed *in vivo*, and re-inoculation of these cells into mice that led to another tumor formation from which the cell line was ultimately derived (Briand, 1996). The T4-2 cells are considered mildly invasive and a triple negative subtype of breast cancer (Estrogen Receptor (ER), Progesterone Receptor (PR) and Human Epidermal Growth Factor 2 (HER2) negative). The formation of tumors and the invasive phenotype of these cells greatly depend on the collagen I matrix stiffness (Fig. 2A). In contrast to T4-2 cells, triple negative MDA-MB-231 cells are highly aggressive (which is also characterized by resistance to treatment; Amaro, 2016). This aggressiveness is easily visible when comparing T4-2 and MDA-MB-231 cells for the same matrix stiffness of 2,000 Pa (Fig. 2B).

For each type of cancer, it is important to identify the matrix stiffness that should be used. If this information is not available in the literature, measurement from real tumors is feasible with the appropriate knowledge and equipment. Measurement of stiffness in cell culture for validation of the stiffness reached or to check the impact of added factors on matrix stiffness is also feasible with a similar equipment, as shown in ***SUPPORT PROTOCOL 2***.

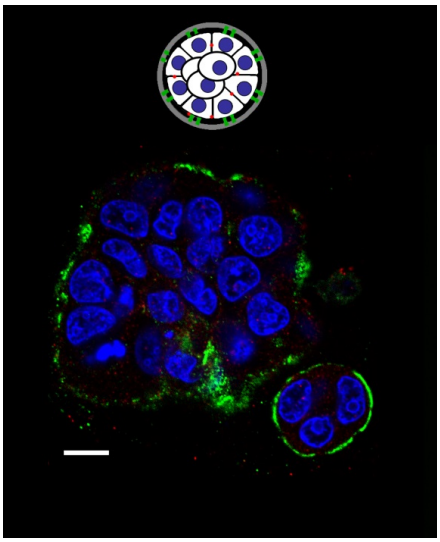

Fig 1. Basal polarity in a DCIS model. HMT-3522 S2 cells were cultured with the EHS-gel drip method for 10 days, and immunostained for basal polarity marker α6-integrin (green). Two nodules are shown, revealing the heterogeneity in nodule appearance (size) in this population of cells. Nuclei are stained with DAPI (blue). The drawing illustrates the organization of cells within these nodules. Size bar, 10 μm

ALTERNATIVE PROTOCOL 1

EHS-gel drip culture

If using a basement type of ECM is the option chosen depending on the tumors of interest, there is an abundant literature regarding this type of culture with reconstituted basement membrane or Engelbreth-Holm-Swarm (EHS)-derived gel (e.g., Matrigel^{TM}); we have published protocols (Vidi, 2013) and we have made aspects of the technique available online (see Internet Resources). The drip method possible with EHS-derived matrix is popular due to the low amount of material needed and easy recording of immunofluorescence images.

- The EHS-derived gel is initially stored at -20°C in one ml aliquots; once an aliquot is thawed on ice in the fridge overnight, the thawing date should be indicated, and the tube should be kept continuously on ice in the fridge. It can be used for up to one month.
- An ice-bucket filled with ice should be placed inside the laminar flow hood when working with EHS-derived gel.

While holding the EHS-gel bottle, care should be given to not touch the bottom part as the solution can solidify quickly at higher than ice-cold temperature.

The expiration date on the EHS gel lot is important to consider, since beyond this date cells might not properly differentiate anymore if the product starts to degrade.

- The steps to prepare the hood and detach and count the cells prior to performing the drip culture are the same as for ***BASIC PROTOCOL 1***.
- When using a drip method the cells can be pooled for several wells or culture vessels (since there is no embedding) using the N+1 approach (i.e., calculate the number of cells needed for the "number of vessels of the same surface + 1 vessel" so that you do not run short of volume needed for the last vessel--- indeed, the slight miscalibration of micropipettors and loss of microdrops on the surface of the tips lead to loss of liquid amount in the main solution).
- The surface of each culture vessel is coated with a thin layer of EHS-derived gel (42 µl/cm^2) using a pipette tip (see Internet Resources) and incubated at 37°C for 15-30 minutes until the gel is formed. (The volume of EHS-derived gel for different culture vessels is indicated in Table 2).
- The calculated volume of cells (N+1 for the same vessel types) is centrifuged and cells are resuspended in half of the total volume of medium that will be required for the culture.
- The solution must be mixed (up-and-down in the pipette tip) several times to resuspend the cell pellet completely in the culture medium.
- Then, the volume of cell suspension necessary for each vessel is added drop by drop all over the surface of the coated gel using a micropipettor. The stock cell suspension is mixed a couple of times up-and-down in the tip or pipette in-between the seeding of each culture vessel.

- The cells that have been seeded are kept in the hood for 5-10 minutes so that they settle to the bottom of the well or dish.
- In the meantime, a solution containing 10% of EHS-derived gel in cell culture medium is prepared utilizing the remaining half of the medium (Table 2). The solution should be mixed gently (only once), to avoid bubbles as far as possible.
- The 10% EHS-derived solution is added drop by drop over the entire surface of the culture vessel, on top of the seeded cells such that it covers both the center and the periphery of the culture area (see Internet Resources). The cell culture medium is changed regularly (every 2-3 days), but the EHS-derived gel drip is not added anymore.

To add volumes of solution into small culture vessels, it is important that the pipettor is held correctly and placed properly without disturbing the gel or spilling the medium out of the culture dish. Another hand could be used to support the pipettor and keep the hand holding the pipettor steady. If there are any bubbles formed when adding the medium into the gel, especially when adding the last drop, the bubbles can usually be removed using the pipette tip. However, if a bubble is difficult to remove, it is better to leave it so that the distribution of cells is not disturbed.

ALTERNATIVE PROTOCOL 2

Culture on top of nonbiological gel

There have been several nonbiological gels designed as scaffolds for the culture of tumors (Rijal, 2017). There is a wide disparity among the gels regarding their appropriateness for cell culture; once again, the stiffness degree will be paramount to best mimic tumor phenotypes. The use of nonbiological gels is possible, without additional reagents, with tumors capable of making their own matrix. For each type of gel, the manufacturer's recommendations will dictate how to use the gel. Here we give an example of the A3DH gel that we tested with T4-2 IDC cells for possible use in high throughput drug screening.

- The gel is prepared by adding 5 ml of DMEM/F12 cell culture medium to 0.25 g of A3DH (Akina, Inc.) to have a final concentration of 5% (w/v). Then, the hydrogel is kept under refrigerated conditions (approximately 2-8^{o}C) for ~48 hours to reach a state of dissolution.

The A3DH material is a stearate-modified methyl cellulose. This polymer dissolves readily at cold temperatures and forms into a gel at biological temperatures (37°C) providing for a

thermogelling material that has appropriate biocompatibility and physicomechanical properties for the formation of spheroids with tumors cells.

- 26.3 µl are added per cm^2 in a way similar to that described for EHS gell culture (see ***ALTERNATIVE PROTOCOL 1***).
- Culture vessels are placed in the cell culture incubator at 37°C for 90 minutes.
- Cells are added to the culture vessel, on top of the gel, drop by drop in the volume of liquid necessary for cell culture on the surface of that vessel.

Here the cancer cells are cultured on top of the gel without the need for a drip or embedding (Fig. 3). This method might be particularly useful for high throughput cell culture required for drug screening as long as the tumors recapitulate a phenotype like in vivo. This technique might not be an option to study invasiveness since tumor nodules are formed on top of the nonbiological gel and the necessary attractants for invasion are not present in the gel.

SUPPORT PROTOCOL 1

Collagen Preparation

Here we report the method used with tunable collagen I from Advanced Biomatrix. Other types of collagen I matrix are available, like the Collymers (Geniphys Inc.) that we used for stiffness measurement in the ***SUPPORT PROTOCOL 2***. The gels vary depending on the origin of the collagen I and the level of purification. Collagen obtained from both companies are polymerized at acidic pH and room temperature leading to the formation of a gel. Polymerization via the kits purchased provide an appropriate ECM of a determined stiffness. The Advanced Biomatrix Collagen is derived from Bovine tissues while Geniphys collagen is derived from porcine dermis. The Geniphys collymer kit contains 0.01M hydrochloric acid as a diluent to adjust Oligomer concentration along with three other solutions; namely, 10X Polymerization Buffer PLUS, 0.1M sodium hydroxide, and a Polymerization Supplement used to induce step-wise Oligomer polymerization (Geniphys, Oligomer-PD, Catalogue No: CM1001). The Advanced Biomatrix kit (PhotoCol®, Catalogue No #5201-1KIT (formerly #5201-1EA)), includes Pure Collagen I, 20 mM acetic acid, and a neutralizing solution.

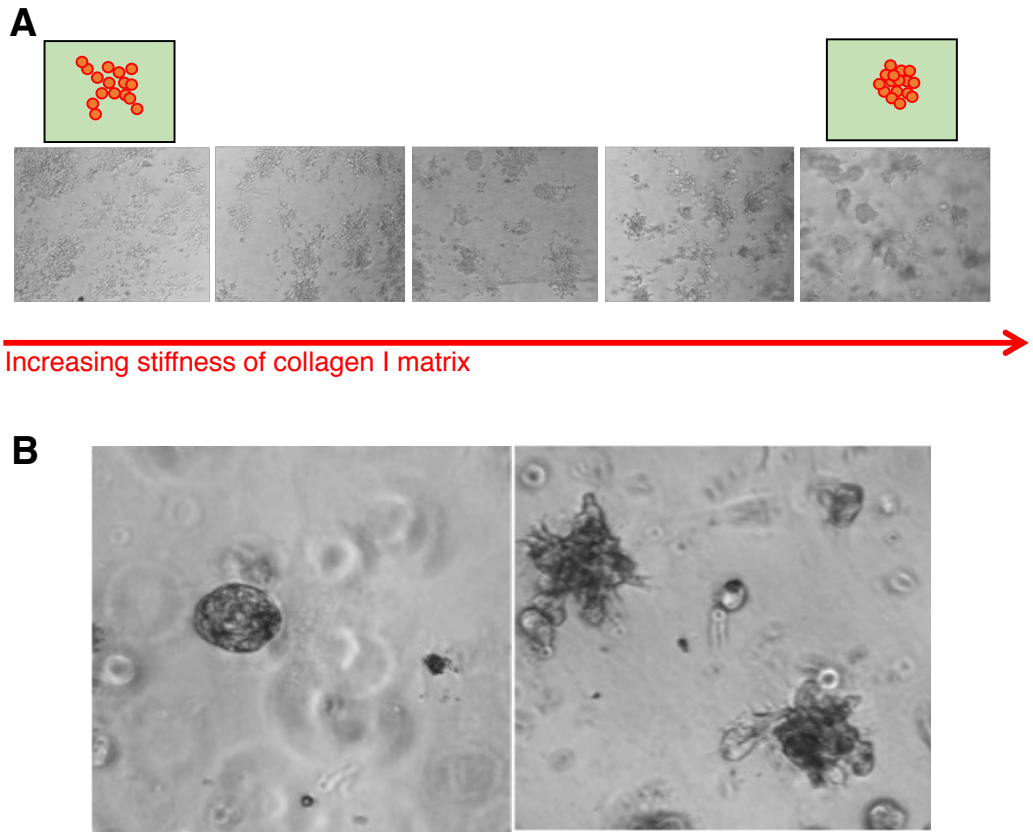

Fig 2. Influence of matrix stiffness on cancer cells. (**A**) T4-2 cells were seeded in collagen I with a range of stiffness degrees (100 to 1,500 Pa). Bright field images at day 6 of culture show increasing cohesion of cancer cells with increasing matrix stiffness. Drawings display the cellular organization at low and high stiffness degrees. Size bar, 100 µm. (**B**) T4-2 cells (poorly invasive) and MDA MB-231 (highly invasive) cells were seeded within the collagen 1 matrix with stiffness adjusted to 2,000 Pa to mimic *in vivo* tumor environment. Bright field images are shown for day 6 of culture. Arrows indicate invasive arms formed by the nodules from MDA MB-231 cells. Scale bar, 25 µm

Materials and reagents

1. Acetic acid, 20 mM (Advanced Biomatrix, Catalogue Number: 5079-50ML)
2. Neutralizing Solution (Advanced Biomatrix, Catalogue Number: 5205-10ML)
3. Pure Collagen I (PhotoCol^{R}, Advanced Biomatrix, Catalogue Number: 5198-100MG)

Different stiffness degrees can be obtained by mixing different concentrations of collagen I, acetic acid and neutralizing solution. A photoinitiator component is used when photo cross-linking is desired to reach certain degrees of stiffness as per the manufacturer's instructions. Here we present a protocol that does not make use of the photoinitiator.

Protocol Steps

An ice bucket filled with ice is necessary to keep the collagen solution cold. *Note: While holding the collagen bottle, care should be given to not touch the bottom part as the solution can solidify quickly at higher than ice-cold temperature.*

- Based on the desired matrix stiffness and the entire surface of culture needed for the experiment, the calculated volume of pure collagen I is placed into a prelabelled Eppendorf tube. The removal of the solution needed should be performed carefully and gently since collagen is a viscous polymer, avoiding the formation of bubbles along the process. Place the Eppendorf tube on ice when not handled. During handling make sure that the bottom of the tube is not touched to avoid raising the temperature of the solution.

To take the volume of collagen I solution needed, bring the pipette tip inside the collagen stock bottle, making sure not to touch the neck of the bottle with the end of the tip. The collagen is viscous, thus take the pipette tip sufficiently inside the bottle (although not too deep). When you 'aspirate' the needed volume, wait a few seconds with the pipette tip plunged inside the solution for the needed volume to come up into the tip, then carefully remove it from the bottle. Take an Eppendorf tube and slowly release the content of the pipette tip at the very bottom of the tube without touching that part of the tube with your hand in order not to raise the temperature too quickly. Make sure not to release all the collagen from the pipette tip. As you are nearing the last drop of the polymer in the pipette tip, stop its release (in order words, do no push through the second notch with the pipette plunger). Acting this way will prevent the formation of bubbles. Place the Eppendorf tube immediately on ice.

- The collagen I solution is taken immediately back to the refrigerator after the desired volume has been taken, and the 20 mM of acetic acid stock solution is brought into the laminar flow hood from 4°C and placed on ice.
- The required volume of acetic acid, depending on the stiffness chosen, is added into the Eppendorf tube containing the collagen I and the tube is kept on ice.

Take the necessary volume of acetic acid from its storage bottle. Carefully and slowly release the acetic acid into the collagen solution of the Eppendorf tube. Make sure that you are releasing the content to the side wall towards the bottom of the tube (not directly within the gel at the very

bottom of the tube, otherwise a bubble will form). Do not release the last drop (second notch when pushing on the plunger), to avoid bubble formation.

- The acetic acid is also stored in the refrigerator after use.
- The neutralizing solution is stored at room temperature. The required volume is added carefully into the Eppendorf tube containing the mixture of collagen I and acetic acid, in a similar manner as the one used to add the acetic acid.

The neutralizing solution is used to reach a final pH of 7.0 to 7.4. In the mixing steps with acetic acid and neutralizing solution, mixing up-and-down with the pipettor should only be done once to ovoid bubble formation.

- This final solution is kept on ice or in the fridge until used for the experiment; however, if coating will be delayed by more than 30 minutes compared to the preparation of the solution, we usually wait to add the neutralizing solution so that there is no gel formation with time in the tube. We only add the neutralizing solution when we know that we will coat the gel within 30 minutes of preparation.

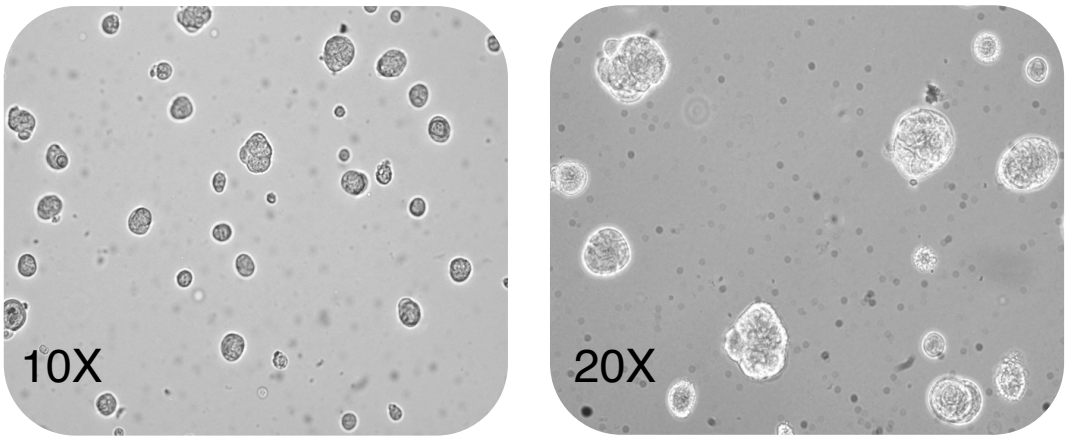

Fig 3. T4-2 cells cultured on the A3DH gel form tumor nodules. Each well of a 12 well plate was coated with 100 µl of the A3DH solution and incubated at 37°C for 90 minutes. Cancer cells were seeded on the gel (79,000 cells per well) and cultured for 48 hours. Shown are bright field microscope images taken with 10X and 20X objectives.

SUPPORT PROTOCOL 2

Measurement of Matrix Stiffness *in vitro*

The stiffness of collagen I gel is linked to the density of fibers. It is the reason why increased stiffness is achieved in part by increasing the concentration of collagen I in the solution. This increased density can be seen with atomic force microscopy (AFM) (Fig. 4A). The latter can also be used to measure stiffness (Young's modulus); however, measurement by microindentation requires many sampling points to get an average information and it is not convenient to determine the global stiffness of a gel. One of the most common characterization methods for determining the overall mechanical properties of a material is by studying its behavior under stretch until the material ruptures, while continuously recording both the applied stress and strain. Depending on the tested specimen, the material type, and the targeted application, the mechanical solicitation can be applied through tension or through compression. Although tensile mechanical tests are widely used for characterization of different metal- and polymer-based biomedical materials, the samples for this type of tests need to be prepared in a certain dumbbell or ring shape geometry with some level of integrity to be clamped between the two holders of the tensile machine. This sample preparation is very challenging for low strength collagen-based hydrogels, the liquid content of which is above 99%. As an alternative, unconfined compression test is one of the most popular mechanical testing configurations that may be used for measuring mechanical properties of soft materials. In this process, the sample (in the form of a disc), is compressed at a constant rate between two flat plates while allowed to freely expand in the radial direction. The deformation speed can range from 0.1 to 10 mm/min and the applied force is constantly recorded. The stiffness is determined by the extrapolated slope from the normalized stress vs. strain curve.

Materials and reagents

- Universal testing system (eXpert 4000 micro test system, ADMET, Inc) with custom designed sample compression stage made of acrylic that was designed for characterizing mechanical properties of soft materials (e.g., tissue, hydrogel).
- Collagen I gel prepared to obtain a certain stiffness degree

Protocol steps

The measurement of the Young's modulus of the gel is based on data recorded throughout the whole process that begins with the contact of the probe with the surface of the gel and stops at the contact of the probe with the surface of the container at the bottom of the gel. In our experience, the depth (ordia thickness) of 0.5 cm for the gel provides measurements of increased reliability compared to thinner gels.

- Multi-well (4-well) plates (ThermoFisher Scientific, 176740) are used as the vessel to contain the gel initially. Three replicates are prepared side by side.
- 800 μl of collagen I-based gel are prepared at the desired stiffness for each well following the instruction provided by the manufacturer of the gel system.
- The solution is incubated at 37°C for 20 minutes to form a gel.

- Cell culture medium is added on the top of the gel to mimic the conditions of cell culture until the day of measurement (in the example shown here, we did measurements on day 8, to mimic the length of time for the cell culture experiment of interest in that particular case).
- The day of the measurement, all tests are conducted in standard ambient conditions. The cell culture medium is removed before the measurement that lasts less than one minute.
- The compression tests are performed with disk collagen samples of 16 mm diameter and 5 mm height, after transfer on a base plate.
- In this setup the based plate is stationary while the other plate is attached to the load and moved at a constant rate of 6 mm/min.

Compression measurements that are done directly on the gel inside a constraining container (e.g., a well) might result in incorrect measurements (i.e., with higher Young's modulus). This effect can be explained by the mechanical constraints that are induced from the wall of the culture well while applying force onto the gel. Indeed, when measuring stiffness of the Collymers (collagen I gel) we found that results from the unconstrained samples were comparable to the reference (e.g., the proposed stiffness achieved based on the gel preparation according to the manufacturer's instructions).

- The recorded stress/strain data are used to extract the elastic modulus of each sample (Fig. 4B, C).

Fig 4. Assessment of collagen I organization. (**A**) Collymers gel blocks were prepared in a 4-well chambered slide at 500 and 1,500 Pa according to the manufacturer's instruction. Gel blocks were incubated with H14 medium for three days before removal from the wells. The blocks were then transferred into a clean container, washed thrice with PBS, and dried out at 37°C before being subjected to imaging via scanning of the gel surface with an MFP-3D-BIO atomic force microscope (Asylum Research, Oxford Instruments, USA). Topography images are presented with vertical scale shown as the colorbar. (**B**) Constrained agarose gel sample (sample is not released from the container, orange line) compared to free agarose gel sample (released from the container, blue line) shows one order of magnitude difference for the recorded stress or stiffness (Pa) under increasing strain with the universal testing system. (**C**) Example of stiffness measurement on unconstrained collagen I gel prepared to achieve a stiffness of 1,000 Pa, measured at 0.999 kPa or 999 Pa (= average slope of stress vs. strain); R^2 (*R-Squar* in the table) shows how linear the data points are (close to 1 is ideally linear), indicating that the Young's modulus measured is within the elastic region of the material (i.e., there is no destruction).

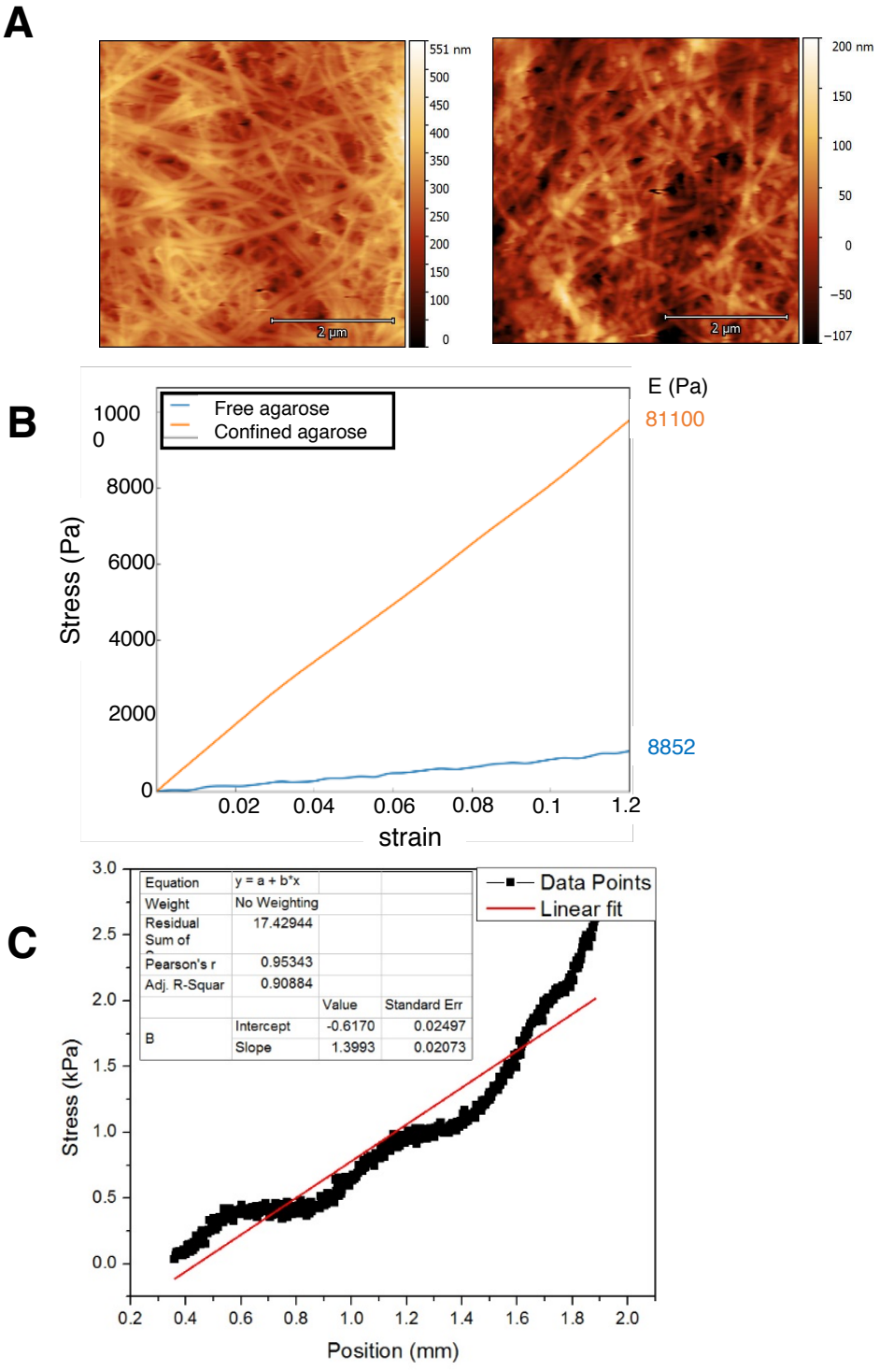
A
551 nm
500
450
400
350
300
250
200
150
100
0
2 µm
200 nm
150
100
50
0
−50
−107
2 µm
B
Free agarose
Confined agarose
E (Pa)
81100
8852
Stress (Pa)
10000
8000
6000
4000
2000
0
0.02
0.04
0.06
0.08
0.1
1.2
strain
C
Equation
y = a + b*x
Weight
No Weighting
Residual Sum of
17.42944
Pearson's r
0.95343
Adj. R-Squar
0.90884
Value
Standard Err
B
Intercept
-0.6170
0.02497
Slope
1.3993
0.02073
Data Points
Linear fit
Stress (kPa)
3.0
2.5
2.0
1.5
1.0
0.5
0.0
0.2
0.4
0.6
0.8
1.0
1.2
1.4
1.6
1.8
2.0
Position (mm)

3.4 Basic Protocol 2

Coculture of cancer cells with noncancer cells to create a more complex microenvironment

The purpose of the coculture section is to familiarize scientists with the questions and tasks related to setting up the culture of cancer cells with other cells from their surroundings. As described in the introduction different cell types have been shown to influence carcinomas, such as non-neoplastic epithelial cells, resident stromal cells or immune cells. The mode of coculture depends on the scientific query since coculture can be done within the same matrix or in separate chambers. Coculture in separate chambers is reported in many publications either using an insert in a cell culture well or using microfluidics to connect distinct cell culture chambers with fluid that can be exchanged from one chamber to another (Goers, 2014; Mi, 2016; Lee, 2018). However, matrix stiffness being important for the behavior of all cell types, many projects will also require coculturing cells in the same physical microenvironment (which of course could be replicated in separate chambers as well), enabling cells to be near each other and even make contact as they would *in vivo*. The first basic protocol detailed below provides information on coculture of tumors with fibroblasts within a collagen I matrix. The second protocol presents the coculture, on a tissue-chip, of tumors with differentiated non-neoplastic cells lining the ducts where carcinomas usually grow.

2.1 Coculture of tumors in the presence of fibroblasts

In the examples chosen for this protocol we will use a cell line from the HMT-3522 cancer progression series, the IDC T4-2 cells, and human fibroblasts, HMS-32.

Materials

2.1.1 Reagents and solutions

- For the cancer cells the medium and additives depend on the cell type and are described in section 1.1.1

For the fibroblasts we use:

1. Dulbecco's Modified Eagle's Medium (DMEM/F12, Life Technologies™), stored at 4°C.

2. Insulin (Sigma-Aldrich® Catalog #I-4011): final concentration, 250 ng/ml

3. Hydrocortisone (Sigma-Aldrich® Catalog #H-0888); final concentration, 1.4 µM

4. Sodium selenite (BD Biosciences Catalog #354201); final concentration, 2.6 ng/ml

5. Transferrin (Sigma-Aldrich® Catalog #T-2252); final concentration, 10 µg/ml

6. Epidermal growth factor (Corning Life Sciences (previously sold through BD Biosciences Catalog #354001); final concentration, 5 ng/ml

7. Fibroblast growth factor (FGF, ThermoFisher); final concentration, 2.5 ng/ml

8. Transforming Growth Factor (TGF, ThermoFisher); final concentration, 7.5 pg/ml

9. Collagen matrix: here we are using PhotoCol® (Catalog No #5201-1KIT) from Advanced Biomatrix as tunable collagen I.

2.1.2 Cell detachment

- Trypsin-EDTA (0.25% 1 mM EDTA-4Na) (Gibco, REF: 25200-056)
- Soybean trypsin inhibitor T-6522 type I-S (BD Biosciences #354201; final concentration of 0.18 mg/ml)

Note that with serum free medium, Soybean trypsin inhibitor needs to be added to the cell suspension collected after using trypsin to detach cells from the cell culture flask.

2.1.2 Materials

- Ice bucket
- Pipettor with 1, 5, 10 ml pipets
- Micropipettor with 10-20, 200, 1 ml tips
- Eppendorf tubes
- Cell culture compatible plastic tubes (15 and 50 ml depending on volume of medium necessary)
- 4-well chambered slides (used for direct immunostaining of cultures)
- Petri dishes to contain the chambered slides

Protocol steps

2.1.3 Management of fibroblasts prior to coculture with tumor nodules within collagen I

Fibroblasts (either primary cells or a cell line) have their own set of additives including the basic [THIS] additives with also Transforming growth factor beta 1 (TGFβ) and Fibroblast growth factor (FGF) (see section 2.1.1; Table 1).

Here we are using a cell line of human mammary fibroblasts (HMS-32) that was obtained from normal breast (Human-TERT immortalized human mammary stromal cell line from a reduction of mammoplasty patient #32; a kind gift from Brittney-Shay Herbert, IU Simon Cancer Center; Shay, 1993; Shay, 1995; Subbaramajah, 2016). This type of cells can be used to study the activation of these fibroblasts depending on the tumor microenvironment and the tumor themselves, as well as the effect of fibroblasts from a noncancerous tissue on tumors (as we show in the example of coculture here). For other types of experiments, the direct use of carcinoma associated fibroblasts (CAFs) derived from cancers might be better suited.

Cells are cultured in flasks for passages and always used in the same window of 10 passages so that we can compare among experiments and maintain the phenotype. HMS-32 cells are seeded in flask at 5,000 cells/cm^2, and the medium with additives is changed every two to three days. Cell propagation for the new passage is done when confluence has reached ~80% (usually after six days of culture). The culture method in collagen I that will be used for the coculture (2.1.5) was first set up as a monoculture to recapitulate the behavior of resting fibroblasts. The HMS-32 cell line was also weaned off serum (see ***SUPPORT PROTOCOL 4***).

2.1.4 Management of tumor cells prior to coculture with fibroblasts within collagen I

In this protocol we will start coculture directly with preformed tumors. Therefore, in preparation for this experiment, cancer cells are first cultured in collagen I as per ***BASIC PROCOTOL 1*** for five days (which leads to tumors of 150 microns in diameter on average). The culture device used should be commensurate to the number of nodules needed for the experiment (typically with the T4-2 cells we obtain 700 nodules per cm^2 when seeded at the usual concentration for collagen I embedded culture).

Note that the density of tumors obtained from monoculture should be measured for each cell line or primary cells of interest to prepare for the coculture that will require the proper cell-tumor cell ratio.

Once the tumors are ready for coculture, they are released from collagen I as per ***BASIC PROTOCOL 1*** and immediately counted to be mixed with the fibroblasts in the appropriate ratio.

2.1.5 Collagen I-based coculture

In this protocol we are mixing tumors and fibroblasts for embedding in collagen I matrix. Once fibroblasts are detached from their cell culture flask and counted, and tumors are removed from collagen I and counted, the two cell types are mixed to mimic approximately the cell-to-cell ratio that is observed *in vivo*. For triple negative breast tumors, the ratio has been estimated as one fibroblast for five cancer cells. Therefore, to use this ratio with preformed tumors, it is essential to first estimate the number of tumors cells per tumor nodules. The calculation of this number is reported in ***SUPPORT PROTOCOL 3***.

- Before detaching cells (fibroblasts) or nodules (cancer cells) from their containers, both seed cultures should be observed via microscopy to make sure that the fibroblasts and tumor nodules are in good shape. There is no point in pursuing the experiment if one of the cell types is not behaving as expected normally.
- Both cell culture media can be mixed (i.e., all necessary additives for both cell types are included in DMEM/F12 medium). The medium is prepared by adding the additives from the working stocks to reach the necessary final concentrations for each additive, and it is kept in the water bath at 37ºC until use.
- Place a clean ice bucket containing ice inside the hood for the preparation and handling of the collagen solution; follow ***SUPPORT PROTOCOL 1*** for the preparation of the collagen at the needed Young's modulus (or stiffness degree).
- The detachment of tumor nodules from the collagen I culture should be done first since it takes up to 45-60 minutes of incubation at 37ºC.
    - Before adding collagenase, aspirate the cell culture medium, then briefly wash with PBS (pre-warmed at 37°C) to remove excess salt, minerals, etc., as these components might interfere with collagenase activity.
    - After incubating with collagenase at 37°C for one hour, there is usually no gel left; Nodules should be washed three times with 0.6-1 ml of culture medium to get rid of the solution (collagen + collagenase) with five

minutes of centrifugation at 1000 g after each wash. (The volume for the washes depends on the size of the pellet; e.g., for a pellet of cells from a 35 mm dish we use 0.6 ml; for a pellet of cells from a 60 mm dish, we use 1 ml).

Once floating nodules are observed (using a microscope), they can be collected with a 1 ml pipette; however, care should be given to not include any gel that might be left (although not frequent) along with the nodules (avoid taking the nodules from the bottom of the culture vessel in that case).

- Finally, tumor nodules should be resuspended in one ml of medium with additives and an aliquot of 50 µl should be used to count the number of nodules with the hemocytometer. This count should be done during the incubation time of the fibroblasts with trypsin (see next step).
- Just before counting the nodules, the fibroblasts in the 25 cm^2 cell culture flask should be treated for detachment with 300 µl Trypsin-EDTA as per ***BASIC PROTOCOL 1***.
- There should be enough time during the 10 minutes of trypsin treatment to not only count the tumor nodules, but also coat the surface of the culture vessel to be used for the coculture with the thin coat of collagen I (14 µl/cm^2; see step 1.4.3). The culture vessels should then be placed in the cell culture incubator until use (at least 5-10 minutes).
- After 10 minutes of incubation with trypsin, if the fibroblasts are detached completely from the surface of the flask, they are mixed immediately in 3 ml of the freshly prepared medium with the addition of 60 µl of Soybean Trypsin Inhibitor-1 (SBT1) from the working stock concentration 10 mg/ml, before centrifuging for five minutes at 2000 g. The supernatant is removed carefully with vacuum, and one ml of freshly prepared cell culture medium is added to resuspend the cell pellet. It should be done carefully and by mixing up-and-down only a few times to avoid the risk of losing cells via their sticking to the tip of the pipette.
- An aliquot of 50 µl should be used to count the number of cells with the hemocytometer.
- Then, the necessary volumes of fibroblasts and tumor nodules are spun down separately, and each pellet is put in suspension in 20 µl of medium before being mixed together and embedded in collagen I as per step 1.4.3.

Note that we use a higher volume than usual (5 to 10 µl) to dissociate the pellets because we need 50,000 fibroblasts per well of a chambered slide (so close to seven folds the amount used for monoculture) in order to have the fibroblast/tumor cell ratio of 1/5 (see ***SUPPORT PROTOCOL 3****) and we are starting from tumor nodules (instead of single cells). This increase in volume for cell/tumor suspension is necessary due to the size of the pellets.*

Here we show cocultures with fibroblasts seeded with IDC cells from day 1 and with IDC tumors preformed in collagen I for three days prior to coculture. The fibroblasts are from a noncancerous ECM environment and seem to repress the development of the tumor nodules compared to the control monoculture (see fibroblasts-cancer cells coculture compared to monoculture of cancer cells for representative images) (Fig. 5).

The cells may be distinguished with a vital dye by staining one of the two cell types prior to embedding (each dye needs to be tested in 3D culture for a specific cell type to make sure that it is not cytotoxic) or cells expressing fluorescent molecules (e.g., GFP) may be used.

2.2. Coculture of tumors with non-neoplastic epithelial cells

We are presenting a protocol used for drug screening in our laboratory in which non-neoplastic HMT-3522 S1 cells (Briand, 1987) are seeded on hemichannels made of acrylic called disease-on-a-chip (DOC) and coated with ECM molecule, laminin 111. Preformed tumors are added into the channels as per a previous publication (Vidi, 2014). This system is useful for rapid seeding of cells in a tissue geometry that matters for drug sensitivity. It is not used for measuring invasive potential as tumor cells cannot go through the acrylic support. Other options to maintain the possibility of observing an invasive phenotype are being developed in our laboratory.

Materials and reagents

2.2.1 Culture medium and ECM

- Non-neoplastic cells are cultured in the same medium as T4-2 cells (see step 1.1.1) with the addition of epidermal growth factor (EGF) (Corning Life Sciences, Catalog: #354001, final concentration 5 ng/ml
- Laminin 111 (Corning Life Sciences, Catalog: #354239; final concentration, 133 µg/ml)

2.2.2 Hemichannels

Acrylic is used to prepare hemichannels of 100 µm in width to mimic the diameter of the terminal ducts in the breast (where tumors arise normally). The in-house preparation of these channels has been described previously (Vidi, 2014). These chips are sterilized by ethylene oxide exposure in an Anprolene Sterilizer model AN74i (Andersen Products Inc.). Sterilization is performed in accordance with the manufacturer's instructions for a 24-hour sterilization cycle and ETO exposure confirmed by observing color-change on enclosed Anpro Dosimeter (Andersen Products Inc.). The sterilized products are aseptically handled and packaged in sterilized materials in a UV laminar flow hood (Labconco Purifier Class II biosafety cabinet, Model 36204-00) wiped down with 70% ethanol (Decon Laboratories) solution.

Protocol steps

2.2.3 culture of S1 cells to form a layer of polarized epithelium

laminin-111 is diluted in DMEM/F12 to 133 µg/ml. For one chip (2.3 X 2 cm), 100 µl of laminin solution are added (8.3 µl laminin of stock 1 mg/ml in 91.7 µl DMEM/F12). This laminin solution is spread drop-by-drop over the DOC gently but rapidly, ensuring that the entire surface is covered.

To spread the laminin, move the tip back and forth in different directions.

- The chips are then dried in a mini oven overnight at 37°C.
- The chips are sterilized again the following day for 30 minutes under UV irradiation in the laminar flow hood.
- Each chip is placed in a the well of a 6-well plate (surface per well is 9.08 cm^2).
- S1 cells are detached from their cell culture flask, treated with SBTI and counted as per step 1.4.2. For the DOC we add a higher concentration of cells compared to usual 2D culture (23,300 cells /cm2), which for the surface of the chip (2.3 X 2 cm) corresponds to 318,000 cells (~3 fold the usual concentration).
- The cell pellet is suspended in one ml of medium (times the number of chips + 1, if more than one chip is used), and one ml is gently added drop-by-drop over the hemichannels. Cells are left to settle down in the laminar flow hood for 10 minutes. Then, 2 ml of cell culture medium are added around the DOC gently, to let the medium progressively rise and submerge the chip.

To add the cells onto the DOC, gently release this solution on top of the laminin coated hemichannels from one end to another following a 'zig zag' pattern to cover all the channels.

- Cells are cultured for eight days and the medium is changed every two days by adding it next to the DOC so that it gently covers the chip.
- After eight days the cells should be basoapically polarized and out of the cell cycle. This complete differentiation can be confirmed with immunostaining for proliferation marker Ki67, basal polarity marker β4-integrin and apical polarity marker ZO-1 (Vidi, 2014).

Note that the proper imaging of basoapical polarity requires confocal microscopy and stacking of optical sections to display the orthogonal view (xz).

2.2.4 Culture of tumor cells

- The T4-2 cells are cultured in collagen as per ***BASIC PROTOCOL 1*** for three days to initiate tumor formation.
- Nodules are dislodged from the collagen I gel with collagenase and washed as per step 1.5.
- To know how many tumors to seed, we take 50 µl of the solution with nodules and mix with 50 µl of trypsin, then incubate at 37°C for a few minutes to separate cells. The cell concentration is determined with the hemocytometer. Then, we calculate the volume to use so that we have 16,600 cells/ml of medium in the chosen culture vessel (thus, the desired amount of cancer cells is 50,000 cells per chip in 3 ml of medium to give enough nodules for one DOC device).

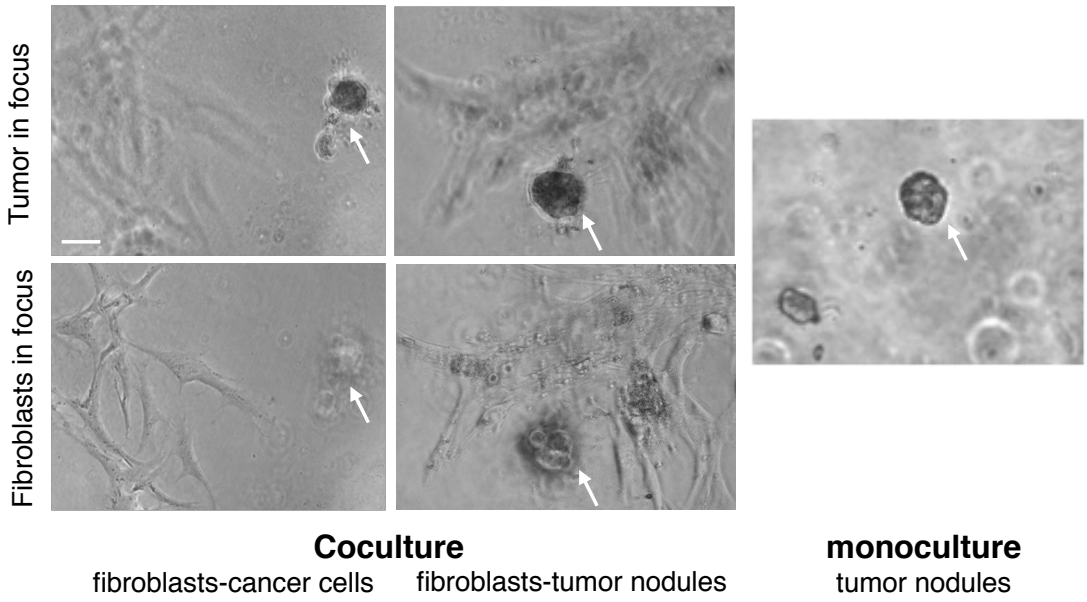

Fig 5. Coculture of IDC cells and fibroblasts. Coculture: Bright field images of HMS-32 cells with T4-2 nodules with either cells mixed from day 1 of culture and kept for six days in collagen I (2,000 pa) [fibroblasts-cancer cells], or fibroblasts mixed with tumor nodules (collected on day 3 of monoculture in a collagen I matrix) and cocultured for three days in collagen I (2,000 Pa) [fibroblasts-tumor nodules]. The arrows point to tumor nodules. Images are shown with either the tumor in focus or the fibroblasts in focus. Monoculture: Bright field image of T4-2 cells cultured alone in collagen I (2,000) for six days to match the cell culture length of the T4-2 cells used for the cocultures. Scale bar, 25 μm

Note: It seems that for consistency between chips for an experiment, it is better to count cells rather than nodules as it gives a more accurate idea of the number of cancer cells present on the chip, even if they are distributed in many nodules.

if individual tumor cells were added directly onto the S1 cell layer, no tumor would grow as it seems that the non-neoplastic cells in that culture condition prevent the proliferation of tumor cells.

2.2.5 coculture of the epithelium and the tumor nodules

- After the volume needed to have 16,600 cells/ml (for 3 ml) is calculated, it is spun down and the pellet is gently resuspended in 500 µl of complete cell culture medium and added onto the entire DOC surface drop-by-drop.
- The nodules are left to settle down within the DOC hemichannels for five minutes.
- The rest of the culture medium (2.5 ml) is added slowly to the side of the DOC so that it rises to submerge the chip.

If the DOC is floating in the culture well, try to push it down to the bottom using a pipette tip.

To distinguish the two cell types, cells transfected with a fluorescent molecule (e.g., EGFP, dsRED, etc.) might be used. Alternatively, tumor nodules can be stained with diI (ThermoFisher Scientific, Cat #D-282; stock solution 1 mg/ml), a vital dye that is not toxic for the HMT3522 cells in 3D culture (Fig. 6). Briefly, the number of nodules necessary for the experiment (following counting) are incubated in 1-2 ml of DiI solution at final concentration 1 µg/ml (from stock concentration 1 mg/ml) in the cell culture medium [the volume depends on the quantity of cells; e.g., 1 ml if cells are from a 35 mm dish, 2 ml if cells are from a 60 mm dish] for each culture vessel, in a 15 ml falcon tube for 30 minutes in the cell culture incubator at 37°C. Then, the cell pellets are washed three times with DMEM before adding the nodules drop by drop and the remaining volume of medium as explained above.

SUPPORT PROTOCOL 3

Cell density calculation for coculture of Tumors and fibroblasts in collagen I

According to pathologist Kurt Hodges (personal communication), the ratio of triple negative IDC cells to fibroblasts should be 5:1.

Cancer cell diameter = 20 µm

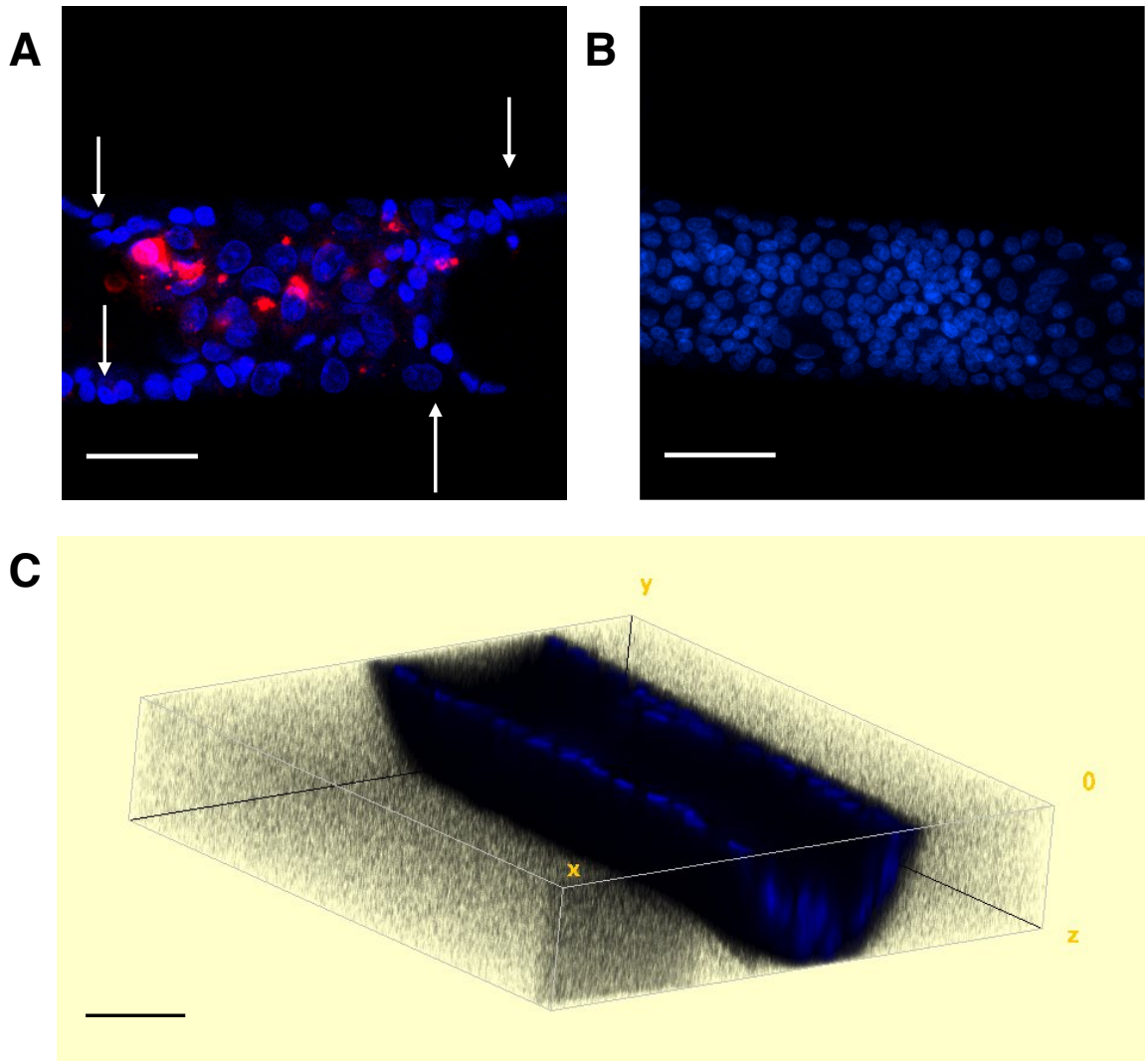

Fig 6. Coculture of non-neoplastic epithelial cells and cancer cells in the DOC. (**A**) Immunofluorescence image resulting from the staining of T4-2 tumors with dil prior to their seeding in the hemichannel. Non-neoplastic S1 cells were cultured on acrylic hemichannels covered with laminin 111 for 10 days to sustain their proliferation and differentiation. Tumor nodules (three days old, prepared in 3D culture) were stained with dil (red) and seeded in the hemichannels for the coculture with S1 cells. Cell nuclei were stained with DAPI (blue). Arrows point to areas with S1 cells only, (this image is focused on the top of the hemichannel). (**B**) Image focused on the bottom portion of a hemichannel of the DOC containing only the monolayer of S1 cells. (**C**) Reconstituted hemichannel with 3D view based on the stacking of optical sections of the layer of S1 cells (shown using the 3D viewer of imageJ; only the cells delineating the limits of the hemichannel in this image are shown). Size bar, 50 µm

Average tumor size measured after five days of culture in collagen I (2,000 Pa) = 125 µm

Volume of tumor= 4/3 x (3.14 X $(125/2)^3$) = 1,022135 μm^3

Volume of a cell = 4/3 x (3.14 X $(10)^3$ = 4,182 μm^3

Volume of Tumor nodules/ Volume of cells = 1,022135 / 4,182 = 244

Thus, number of cancer cells per nodule = 244

There are on average 1000 nodules per chambered slide well of T4-2 in collagen I culture (2,000 Pa) after five days. Thus, there are 244 X 1000 = 244,000 cancer cells/well

This number is almost four times the number of T4-2 cells usually seeded per well (62,100).

[T4-2: 43,150 cells/cm^2; number of cells per well of a chambered slide = 43,150 X 1.44 cm^2 = ~62,100 cells / well / 100 µl of collagen spread [14 µl/cm^2 thin coat of collagen + 55 µl/cm2 of collagen for embedding] (note that 20% (so 20 µl) of that volume is a thin coat done prior to adding the cells to 80% of the volume, so 80 µl)]

Since the tumor nodules/fibroblasts ratio is 5:1, the number of fibroblasts required for the coculture is 50,000 per well of a 4-well chambered slide if we put 1,000 nodules per chamber as compared to the usual 7,200 fibroblast per well (since seeding is usually 5,000 cells/cm^2).

SUPPORT PROTOCOL 4

Culture of fibroblasts of the interstitium to mimic normal conditions

The culture of fibroblasts requires to obtain the proper density, shape and orientation as *in vivo*. Indeed, high density of cells might lead to lack of proliferation arrest (fibroblasts are normally resting cells unless they are stimulated) and high density of collagen I might induce an orientation of fibroblasts parallel to each other, similar to what is observed in fibrosis. Hence, the density of cells at seeding is an important parameter to consider for each cell line or source of primary fibroblasts. The density of cells is assessed via observation with bright field microscopy as shown with the example of NIH-3T3 cells that are fibroblasts of murine origin (Fig. 7A). Another important parameter for cell culture is the medium. Weaning HMS-32 breast fibroblasts off serum was an important step for the coculture with tumors (*see protocol for weaning cells of serum in the culture medium below*). These cells were not drastically affected by the switch in medium as shown by the same ratio of cells with different shapes and nuclear morphometric analysis (Fig. 7B-D). Indeed, the shape of fibroblasts (spindle-like, dendritic-like and flat) is an indication of their phenotype and the average morphometry of the cell nucleus reflects the global phenotype of

the population under a given condition (Chittiboyina, 2018; Lelièvre, 2018). In 3D culture in normal collagen I stiffness, cells are resting and predominantly adopt a an elongated or spindle-like shape under normal matrix stiffness (770 Pa), whereas an increase in the percentage of cells with a flattened phenotype is often an indication of stress-activated fibroblasts (Sampson, 2011).

Materials

See step 2.1.1 for the culture medium

Protocol Steps

For embedding in collagen I the method is similar to that presented in ***BASIC PROTOCOL 1***.

The weaning off serum method is briefly explained below:

Weaning off serum for cell line(s) previously cultured in 10% Fetal Bovine Serum (FBS) in medium can be usually accomplished in two continuous cell passages through a sequential FBS reduction process, although depending on the cell lines it might take longer. We have weaned off serum several breast cell lines (e.g., MDA-MB-231, MCF10A) and fibroblasts (HMS-32); the only cell line that we could not accustom to a serum-free medium is the MCF7 (these cells have been cultured for long times without a standard protocol and it seems that there are now many strains depending on the laboratories according to experts with these cells).

- When the process of weaning off serum is initiated, cells after seeding should be cultured in 75% FBS-supplemented medium combined with 25% of chemically defined serum-free medium (i.e., 25% of the normal concentration of each necessary additive).
- Cells should be fed every two days after initial cell seeding and the medium should contain sequentially reduced FBS and gradually increased defined chemicals at each feeding step, i.e. the medium for first time feeding should contain 50% FBS-supplemented medium and 50% chemically defined serum-free medium. Likewise, the medium for the second time feeding should contain 25% FBS-supplemented medium and 75% chemically-defined medium.
- Cells should be detached from the flask after they reach the usual confluence for propagation (e.g., it usually takes six days of culture for fibroblasts to reach 70-80% confluence), and a new generation of cells should be seeded in 10% FBS-supplemented medium and 90% chemically-defined medium to avoid potential crisis in FBS free

medium. (It might be advisable to start the new flask with 25/75 ratio of FBS and chemically defined medium and then, go to 10/90 at the next feeding stage).

- After the cells are fed twice with the same medium (so after seeding in a new flask and one feeding step), the cells should be fed with 100% of chemically-defined medium for the third feeding and thereafter.
- A successful serum weaning off procedure should not change cell morphology drastically.

Note: If the cells appear to suffer during the weaning off procedure, they should be placed back in the last FBS/chemically defined medium ratio that showed a healthy cell culture until the cells recover. Then, reducing FBS content should be continued with smaller decreases in percentages (hence, more intermediate steps). If the cells look good but simply do not proliferate as fast as before, it might be normal (as long as they still proliferate), or if they are stalled, a similar process "with stepping back" as explained in the text above can be adopted.

Fig 7. Influence of culture conditions on the phenotype of fibroblasts. (**A**) NIH3T3 cells were embedded in Collymers prepared at different stiffness degrees (100, 770, 1500 Pa) with a seeding density of 1,250 cells/cm^2 and cultured in DMEM/F12 medium supplemented with 10% FBS. Note the differences in cell density in the plane of focus and in orientation of the cells in the matrix depending on matrix stiffness. Images were taken with an Olympus IX70 microscope (objective 10x) on day 5 of culture. (**B-D**). HMS-32 cells were cultured in collagen I matrix of stiffness 770 Pa for six days at seeding density of 5,000 cells/cm^2. Bar graphs show the analysis of nuclear circularity and size with and without serum (**B**) and the phenotypic distribution of mammary stromal fibroblasts (**C**). Fluorescence images representing three phenotypes of HMS-32 cells (spindle-like, dendritic and flat) are shown with nuclei stained with DAPI (blue) and the actin cytoskeleton stained with phalloidin (green) (**D**)**.** n = 3 with 150 cells analyzed per group. Scale bar, 5 μm

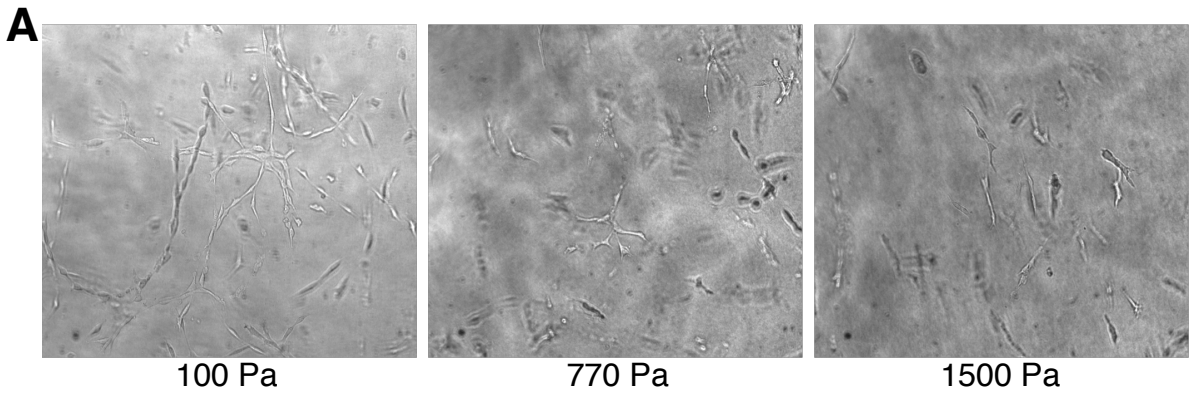
A
100 Pa
770 Pa
1500 Pa

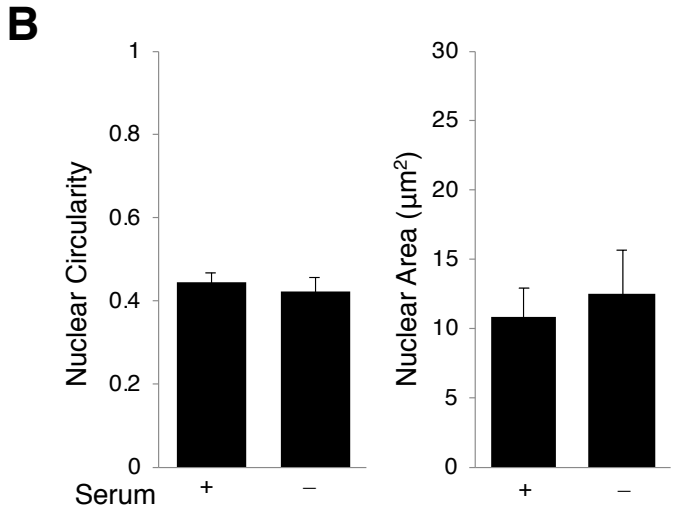
B
Nuclear Circularity
1
0.8
0.6
0.4
0.2
0
Serum
+
–
Nuclear Area (μm²)
30
25
20
15
10
5
0
+
–

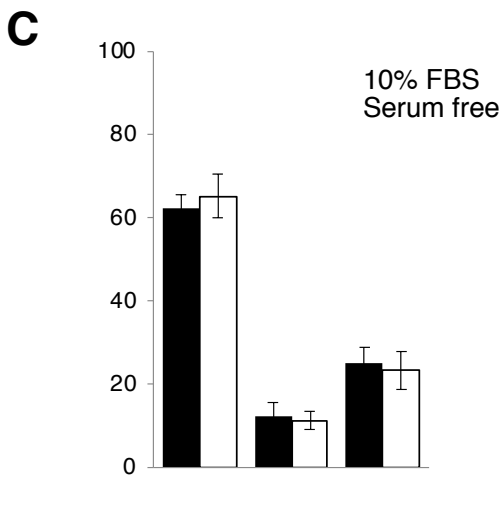
C
10% FBS
Serum free
100
80
60
40
20
0

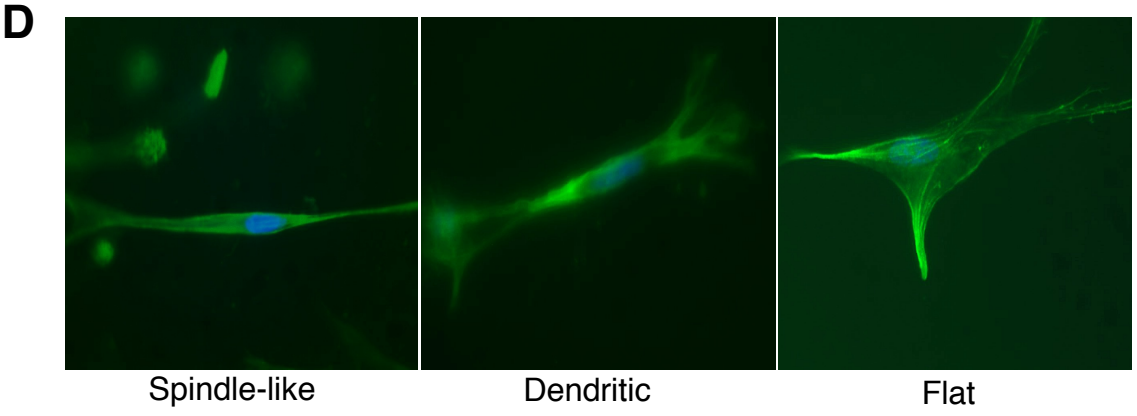
D
Spindle-like
Dendritic
Flat

3.5 Reagents and Solutions

In this section we thought it would be helpful to give a detailed description of the preparation of the additives mentioned for used with serum free cell culture in the protocols as well as the preparation of SBTI.

β-estradiol

Sigma catalog #E-2758

Preparation Procedure:

- Weigh 10 mg of β-estradiol in a 20 ml sterile beaker. Cover the beaker immediately with aluminum foil (the one used to sterilize the beaker). This step can be performed under non-sterile conditions.
- From here onwards, work must be performed under the laminar flow hood and with the light OFF[1]. Disinfect the beaker and any other material (e.g. Ice-bucket) appropriately by wiping with a tissue paper sprayed with 70% ethanol, before introducing in the hood. Also, carefully follow all other rules for working inside the cell culture room.
- Before beginning, it is better to prepare the dark glass vials needed for aliquoting. We usually UV sterilize the autoclaved glass vials used for this purpose overnight, by opening the lids/caps of the bottles and placing the lid facing upward such that the all the surfaces of the bottle including its neck and lids are properly sterilized. You can prepare the labels on the vials before they are UV sterilized; label as many vials as you will need, from a stock of sterile vials only used for preparing additives. The proper labelling should include the additive's code, concentration, expiration date and the initials of the person who prepared the additive.
- Add 1.25 ml of cold 95% (190 proof) ethanol[2], to make an 8 mg/ml solution. When completely dissolved, place the beaker on ice, and transfer the solution to a labeled sterile dark glass vial, placed on ice. Do not filter.
- Serially dilute the 8 mg/ml stock in the following manner, using a sterile labeled dark glass vial each time:

- Take 50 µl of the 8 mg/ml stock and add 1.45 ml of 95% (190 proof) ethanol to make 1.5 ml of 10^{-3}M or $2.67x10^{-1}$ mg/ml stock.
- Take 20 µl of the 10^{-3}M and add 1.98 ml of 95% (190 proof) ethanol to make 2 ml of 10^{-5}M or $2.67x10^{-3}$ mg/ml stock.
- Take 20 µl of the 10^{-5}M and add 1.98 ml of 95% (190 proof) ethanol to make 2 ml of 10^{-7}M or $2.67x10^{-3}$ mg/ml working stock.
- Do not filter any of the stocks; place all vials on ice right after use.

- Make 500 µl aliquots of the 10^{-7} M or $2.67x10^{-3}$ mg/ml working stock using sterile dark glass vials. Prepare each aliquot separately. Use a new tip for each aliquot and avoid touching the walls of the glass vials[3]. Place each aliquot on ice, immediately after preparation.
- Transfer to the appropriate freezer. Since β-estradiol does not freeze, due to the presence of ethanol, there is no need to place the aliquots on dry ice[4].
- Note the number of aliquots made, concentration, expiration date etc. in the usage log for β-estradiol.

Storage and Usage:

- The 8 mg/ml (stable for one year), 10^{-3} M (stable for one year) and 10^{-5} M (stable for six months) concentrated stocks are always kept at -80°C. Some aliquots of the 10^{-7} M working stock (stable for six months) are kept at -20°C for ready availability. The rest of the working stock is kept at -80°C and transferred to -20°C when the -20°C stock runs out.
- To avoid confusions, in the -80°C freezer, it is useful to keep the working stock separated from the concentrated stock.
- Aliquots are removed from -20°C when needed for cell culture and kept at 4°C for a period of up to one month.
- Write down on the glass vial the date when an aliquot is thawed, for reference for determining the expiration date at 4°C.

Note:

The 8 mg/ml, 10^{-3} M and 10^{-5} M stocks can be used later to prepare more diluted stocks (follow the expiration dates). Remove vials from the freezer and place on ice immediately. All tubes are kept on ice; transfer the tubes to the corresponding freezer once the preparation is done.

[1] β-estradiol is light sensitive. For this reason, only dark glass vials must be used for its preparation.

[2]Ethanol 95% (190 proof) should be from a commercially available source and ready for use.

[3] Should you touch the wall or neck of a container; the tip should be discarded. If a vial containing an aliquot might have become accidentally contaminated (e.g., if there is any doubt that the tip used was not properly handled), it should be discarded. The bottom line is, under suspicion of risk of contamination, better discard than regret!!

[4]Spray dry ice with 70% ethanol (to decrease the temperature of the ice) before placing the aliquots in dry ice.

Epidermal growth factor

(previously sold by BD Biosciences), Currently sold by Corning Life Sciences catalog # 354001

Preparation Procedure:

- Work must be performed under the laminar flow hood. Disinfect EGF (100 µg) bottle and any other material (e.g. ice-bucket) appropriately by wiping with a tissue paper sprayed with 70% ethanol, before introducing in the hood. Also, carefully follow all other rules for working inside the cell culture room. Place the 100 µg EGF bottle on ice as soon as it is introduced in the hood.
- Before beginning, it is better to prepare the Eppendorf tubes needed for aliquoting. We usually UV sterilize the autoclaved 1.5 ml Eppendorf tubes used for this purpose overnight, by opening their caps, facing upward such that the all the content of the tube is properly sterilized. You can prepare the labels on the Eppendorf tubes before they are UV sterilized and label as many tubes as you will need, from a stock of sterile Eppendorf tubes only used for preparing additives. The proper labelling should include the additive's code, concentration, expiration date and the initials of the person who prepared the additive.

- Filter 7 ml of sterile deionized Milli-Q water[1] using a 10 ml syringe and a 0.22 μm pore size filter; transfer to an ice-cold 15 ml falcon tube. Place the tube on ice.
- Disinfect the bottle of EGF thoroughly, especially the neck and top of the bottle. Do this by wiping it with a 70% ethanol-sprayed tissue paper, before and after removing the metal cap (there is a rubber stopper underneath). Avoid spraying the bottle directly. Leave rubber stopper lose and keep the bottle on ice.
- Dissolve the 100 μg of EGF, contained in the bottle, in 5 ml of prefiltered sterile water. When completely dissolved (swirl the bottle) and place on ice. If it is easier to handle, transfer the solution to an ice-cold 15 ml falcon tube and keep on ice. Do not filter
- Keeping the bottle/tube on ice, make 50 μl and 100 μl aliquots. Prepare each aliquot separately. Use a new tip for each aliquot and avoid touching the walls of the Eppendorf tube[2]. Place each aliquot on ice, immediately after preparation.
- Fast freeze all aliquots by placing them on dry ice[3] for about 5-10 minutes. When completely frozen (solution is completely white) transfer to the appropriate freezer.

Storage and Usage:

- Some aliquots of the working stock are kept at -20°C for ready availability. The rest of the stock is kept at -80 °C and transferred to -20°C when the -20°C stock runs out. Storage at both temperatures is fine for up to three months.
- Aliquots are thawed from -20°C, when needed and kept at 4°C for a period of up to one week.

Note:

[1]The stock bottle of sterile deionized Mili-Q water used for the preparation of additives must NOT be used for any other purpose.

[2] Should you touch the wall or neck of a container; the tip should be discarded. If a vial containing an aliquot might have become accidentally contaminated (e.g., if there is any doubt that the tip used was not properly handled), it should be discarded. The bottom line is, under suspicion of risk of contamination, better discard than regret!!

[3]Spray dry ice with 70% ethanol (to decrease the temperature of the ice) before placing the aliquots.

Fibroblast growth factor

Thermo-Fisher, catalog #PHG0264

- Before beginning, it is better to prepare the Eppendorf tubes needed for aliquoting. We usually UV sterilize the autoclaved 1.5 ml Eppendorf tubes used for this purpose overnight, by opening their caps, facing upward such that the surface of the tube is properly sterilized. You can prepare the labels on the Eppendorf tubes before they are UV sterilized and label as many tubes as you will need, from a stock of sterile Eppendorf tubes only used for preparing additives. The proper labelling should include the additive's code, concentration, expiration date and the initials of the person preparing the additive.
- The bottle of FGF should be briefly centrifuged prior to opening. DO NOT VORTEX!
- Weigh 2 mg of BSA in a sterile 20 ml beaker used only for cell culture. Immediately close the lid of the beaker with aluminum foil as soon as you have added the BSA.
- Work must be performed in the laminar flow hood. Disinfect the FGF (10 µg) bottle and any other material including the beaker and ice-bucket appropriately by wiping with a tissue paper sprayed with 70% ethanol, before introducing in the hood. Also, carefully follow all other rules for working inside the cell culture room. Place the 10 µg TGF-β bottle on ice as soon as it is introduced in the hood.
- Dissolve weighed BSA in 2 ml of 1X PBS[2] to prepare a 0.1 % w/v solution and transfer it to a 10 ml falcon tube. Filter the solution using a 0.2 µm pore size filter.
- Add 100 µl of sterile Milli-Q[1] water to the FGF bottle to make a concentration of 100 µg/ml (intermediate solution).
- Add all intermediate solution (100 µl) into 900 µl 0.1% BSA in PBS to make a concentration of 10 µg/ml (working stock solution).
- Aliquot 50 µl from the working stock solution in each Eppendorf tube and store them at -20°C (freezer in cell culture room). Prepare each aliquot separately. Use a new tip for each aliquot and avoid touching the walls of the Eppendorf tube[2]. Place each aliquot on ice, immediately after preparation.
- Fast freeze all aliquots by placing them on dry ice[3] for about 5-10 minutes. When completely frozen (solution is completely white) transfer to the appropriate freezer.

Storage and Usage:

- Some aliquots of the working stock concentration are kept at -20°C for ready availability. The rest of the stock is kept at -80°C and transferred to -20°C when the -20°C stock runs out.
- Aliquots are thawed once from -20ºC, when needed and kept at 4ºC for a period of up to one week.

Note:

[1]The stock bottle of sterile deionized Mili-Q water used for the preparation of additives must NOT be used for any other purpose.

[2]The bottle of sterile PBS used for the preparation of additives must NOT be used for any other purpose.

[3]*Should you touch the wall or neck of a container; the tip should be discarded. If a vial containing an aliquot might have become accidentally contaminated (e.g., if there is any doubt that the tip used was not properly handled), it should be discarded. The bottom line is, under suspicion of risk of contamination, better discard than regret!!*

Hydrocortisone

Sigma, catalog #H-0888

- Weigh 50 mg of Hydrocortisone in a 20 ml sterile beaker. Cover the beaker immediately with the aluminum foil (the one used to sterilize the beaker). This step can be performed under nonsterile conditions.
- From here onwards, work must be performed in the laminar flow hood. Disinfect the beaker and any other material (e.g., ice-bucket) appropriately by wiping with a tissue paper sprayed with 70% ethanol, before introducing it in the hood. Also, carefully follow all other rules for working inside the cell culture room.
- Before beginning, it is better to prepare the Eppendorf tubes needed for aliquoting. We usually UV sterilize the autoclaved 1.5 ml Eppendorf tubes used for this purpose overnight, by opening their caps, facing upward such that the surface of the tube is properly sterilized.

You can prepare the labels on the Eppendorf tubes before they are UV sterilized and label as many tubes as you will need, from a stock of sterile Eppendorf tubes only used for preparing additives. The proper labelling should include the additive's code, concentration, expiration date and the initials of the person who prepared the additive.

- Dissolve Hydrocortisone in 10 ml of cold 95% (190 proof) ethanol[1], to make $1.4x10^{-2}$ M (5 mg/ml) concentrated stock. When completely dissolved, place the beaker on ice. The solution can be transferred to an ice-cold, properly labelled 15 ml falcon tube if it is easier to handle. Do not filter.
- Keep the beaker (covered when not in use) or falcon tube on ice, make 500 µl aliquots. Prepare each aliquot separately. Use a new tip for each aliquot and avoid touching the walls of the beaker or Eppendorf[2]. Place each aliquot on ice[3], immediately after preparation.
- Dilute 0.5 ml of $1.4x10^{-2}$ M (5 mg/ml) solution in 4.5 ml of cold 95% (190 proof) ethanol in a 15 ml falcon tube, to make $1.4x10^{-3}$ M (0.5 mg/ml) working stock. The falcon tube containing 95% (190 proof) ethanol can be placed on ice before adding 0.5 ml of $1.4x10^{-2}$ M (5 mg/ml) solution. Do not filter.
- Keep the falcon tube on ice to make 500 µl aliquots in the manner described in step 4.
- Transfer to the appropriate freezer. Since hydrocortisone does not freeze, due to the presence of ethanol, there is no need to place the aliquots on dry ice. Note the number of aliquots made, concentration, expiration date etc. in the usage log for Hydrocortisone.

Storage and Usage:

- The concentrated stock (5 mg/ml) is always kept at -80°C. Some aliquots of the 10^{-3} M working stock are kept at -20°C for ready availability. The rest of the working stock is kept at -80°C and transferred to -20°C when the -20°C stock runs out.
- To avoid confusions, in the -80°C freezer, it is useful to keep the working stock separated from the concentrated stock.
- Aliquots are removed from -20°C when needed and kept at 4°C for a period of up to one month.

The 5 mg/ml stock can be used later to prepare more diluted stocks, but the initial expiration date should be considered. Remove from the freezer and place on ice immediately. Keep on ice and transfer tubes to the corresponding freezer once the dilution is done.

[1]Ethanol 95% (190 proof) should be ready for use, from a commercially available source.

[2] Should you touch the wall or neck of a container; the tip should be discarded. If a vial containing an aliquot might have become accidentally contaminated (e.g., if there is any doubt that the tip used was not properly handled), it should be discarded. The bottom line is, under suspicion of risk of contamination, better discard than regret!!

[3]Spray dry ice with 70% ethanol (to decrease the temperature of the ice) before placing the aliquots.

Insulin

Sigma, Catalog #I-4011

- Weigh 25 mg of Insulin in a 40 ml sterile beaker. Cover the beaker immediately with aluminum foil. This step can be performed under nonsterile conditions.
- From here onwards work must be performed in the laminar flow hood. Disinfect the beaker and any other material (e.g, ice-bucket) appropriately by wiping with a tissue paper sprayed with 70% ethanol, before introducing in the hood. Also, carefully follow all other rules for working inside the cell culture room. Place the beaker on ice as soon as it is introduced in the hood.
- Before beginning, it is better to prepare the Eppendorf tubes needed for aliquoting. We usually UV sterilize the autoclaved 1.5 ml Eppendorf tubes used for this purpose overnight, by opening their caps, facing upward such that the surface of the tube is properly sterilized. You can prepare the labels on the Eppendorf tubes before they are UV sterilized and label as many tubes as you will need, from a stock of sterile Eppendorf tubes only used for preparing additives. The proper labelling should include the additive's code, concentration, expiration date and the initials of the person who prepared the additive.
- Add 12.5 ml of 5 mM HCl[1] to the Insulin, to make a 2 mg/ml concentrated stock. When completely dissolved, transfer to an ice-cold, labelled 15 ml falcon tube. Filter and transfer to another ice-cold 15 ml falcon tube, using a 20 ml syringe and a 0.22 µm syringe-filter.
- Keep the falcon tube on ice, transfer 1.5 ml of the 2 mg/ml concentrated stock to an ice-cold, labeled 50 ml falcon tube for later dilution (See step 7). Place the tube on ice.

- Make 1.5 ml aliquots with the remaining 2 mg/ml stock. Prepare each aliquot separately. Use a new tip for each aliquot and avoid touching the walls of the Eppendorf tube[2]. Place each aliquot on ice, immediately after preparation.
- Add 28.5 ml of cold, sterile deionized Mili-Q water[3] to the 2 mg/ml concentrated stock solution contained in the 50 ml falcon tube (See step 5), to make a 100 µg/ml working stock. Filter and transfer to another ice-cold 50 ml falcon tube, using a 60 ml syringe and a 0.22 µm pore size filter.
- Make 1 ml aliquots of the 100 µg/ml working stock, as in step 6.
- Fast freeze all aliquots by placing them on dry ice for about 5-10 minutes. When completely frozen (solution is completely white) transfer to the appropriate freezer.

Storage and Usage:

- The 2 mg/ml concentrated stock is always kept at -80°C. Some aliquots of the 100 µg/ml working stock are kept at -20°C for ready availability. The rest of the working stock is kept at -80°C and transferred to -20°C when the -20°C stock runs out.
- To avoid confusions in the -80°C freezer, it is useful to keep the working stock solution separated from the concentrated stock solution.
- Aliquots are thawed once from -20°C, when needed, and kept at 4°C for a period of up to one month.

The 2 mg/ml stock can be used to prepare the 100 µg/ml working stock, respecting the expiration date for it. Remove from the freezer and place on ice immediately.

[1]The 5 mM HCl is prepared using the commercially available HCl from Mallinckrodt. Cat No 2062. The 5 mM solution is prepared in a sterile container, in the fume hood and it is only used for preparing Insulin. The 5 mM HCl solution is prepared in a sterile deionized water, using a sterile container, in the laminar flow hood and it is only used for preparing the insulin.

[2] Should you touch the wall or neck of a container; the tip should be discarded. If a vial containing an aliquot might have become accidentally contaminated (e.g., if there is any doubt that the tip used was not properly handled), it should be discarded. The bottom line is, under suspicion of risk of contamination, better discard than regret!!

[3]The stock bottle of sterile deionized Milli-Q water used for the preparation of additives must NOT be used for any other purpose.

[4]Spray dry ice with 70% ethanol (to decrease the temperature of the ice) before placing the aliquots

Prolactin

Sigma catalog L-6520 with name "Luteotropic hormone"

- Prepare fresh 40 ml of 2.22 mg/ml solution of Sodium Bicarbonate ($NaCHO_3$)[1]. Weigh 88.67 mg of Sodium bicarbonate in a 20 ml sterile beaker. Cover the beaker immediately with the aluminum foil (the one used to sterilize the beaker). This step can be performed under nonsterile conditions.
- From here onwards, work must be performed in the laminar flow hood. Disinfect the beaker and any other material (e.g. ice-bucket) appropriately by wiping with a tissue paper sprayed with 70% ethanol, before introducing in the hood. Also, carefully follow all other rules for working inside the cell culture room. Place the prolactin 1000 I.U. bottle on ice as soon as it is brought in the hood.
- Before beginning, it is better to prepare the Eppendorf tubes needed for aliquoting. We usually UV sterilize the autoclaved 1.5 ml Eppendorf tubes used for this purpose overnight, by opening their caps, facing upward such that the surface of the tube is properly sterilized. You can prepare the labels on the Eppendorf tubes before they are UV sterilized and label as many tubes as you will need, from a stock of sterile Eppendorf tubes only used for preparing additives. The proper labelling should include the additive's code, concentration, expiration date and the initials of the person preparing the additive.
- Add 10 ml of cold sterile deionized Milli-Q water[2] to the sodium bicarbonate. When completely dissolved, transfer to an ice-cold, labeled 50 ml falcon tube. Add 40 ml of sterile deionized water to make a 2.22 mg/ml solution. Filter and transfer to another ice-cold 50 ml falcon tube, using a 60 ml syringe and a 0.22 μm pore size filter.
- Disinfect the bottle of prolactin thoroughly, especially the neck and top of the bottle. Do this by wiping it with a 70% ethanol-sprayed tissue paper, before and after removing the metal cap (there is a rubber stopper underneath). Avoid spraying the bottle directly. Leave rubber stopper lose and keep the bottle on ice.

- Add 10 ml of sterile 2.2 mg/ml Sodium bicarbonate solution to the 1000 I.U. of prolactin. Once fully dissolved (swirl the bottle) and place the solution on ice. Repeat this twice to make sure to remove all prolactin from the bottle. If easier to handle, transfer the solution to an ice-cold 50 ml falcon tube and keep on ice. Add the remaining solution to remove all the prolactin from the bottle. Transfer to the same falcon tube, kept on ice. Add the remaining 3.3 ml of sodium bicarbonate to the tube to make a 30.3 I.U./ml working solution (the total volume for solution must be 33.3 ml. Filter and transfer to another ice-cold 50 ml falcon tube, using a 60 ml syringe and a 0.22 μm pore size filter.
- Keeping the falcon tube on ice, make 1 ml aliquots. Prepare each aliquot separately. Use a new tip for each aliquot and avoid touching the walls of the Eppendorf tube[3]. Place each aliquot on ice, immediately after preparation.
- Fast freeze all aliquots by placing them on dry ice[4] for about 5-10 minutes. When completely frozen (solution is completely white) transfer to the appropriate freezer.

Storage and Usage:

- Some aliquots of the working stock are kept at -20°C for ready availability. The rest of the stock is kept at -80°C and transferred to -20°C when the -20°C stock runs out.
- Aliquots are thawed once from -20°C, when needed and kept at 4°C for a period of up to one month.

An alternative source is biological prolactin from Ovine (10 mg) available from the National Hormone and Peptide Program (Harbor-UCLA Medical Center)

[1]The sodium bicarbonate used, is cell culture tested from SIGMA, catalog number S-5761.

[2]The stock bottle of sterile deionized Milli-Q water used for the preparation of additives must NOT be used for any other purpose.

[3] Should you touch the wall or neck of a container; the tip should be discarded. If a vial containing an aliquot might have become accidentally contaminated (e.g., if there is any doubt that the tip used was not properly handled), it should be discarded. The bottom line is, under suspicion of risk of contamination, better discard than regret!!

[4]Spray dry ice with 70% ethanol (to decrease the temperature of the ice) before placing the aliquots.

Sodium Selenite

BD Biosciences, Selenous acid, sodium salt, catalog #354201

Preparation Procedure:

- Work must be performed under the laminar flow hood. Disinfect the Sodium Selenite (100 mg) bottle and any other material (e.g. ice-bucket) appropriately by wiping with a tissue paper sprayed with 70% ethanol, before introducing it in the hood. Also, carefully follow all other rules for working inside the cell culture room. Place the 100 mg Sodium selenite bottle on ice as soon as it is brought into the hood.
- Before beginning, it is better to prepare the Eppendorf tubes needed for aliquoting. We usually UV sterilize the autoclaved 1.5 ml Eppendorf tubes used for this purpose overnight, by opening their caps, facing upward such that the tube is properly sterilized. You can prepare the labels on the Eppendorf tubes before they are UV sterilized and label as many tubes as you will need, from a stock of sterile Eppendorf tubes only used for preparing additives. The proper labelling should include the additive's code, concentration, expiration date and the initials of the person who prepared the additive.
- Filter 15 ml of sterile deionized Milli-Q water[1] using a 10 ml syringe and a 0.22 µm pore size filter; transfer to an ice-cold 15 ml falcon tube. Place the tube on ice.
- Disinfect the 100 mg bottle of sodium selenite thoroughly, especially the neck and top of the bottle. Do this by wiping it with a 70% ethanol-sprayed tissue paper, before and after removing the metal cap (there is a rubber stopper underneath). Avoid spraying the bottle directly. Leave the rubber stopper lose and keep the bottle on ice.
- Dissolve the 100 mg of sodium selenite contained in the bottle, in 5 ml of prefiltered cold, sterile Milli-Q water to make a 20 mg/ml stock. When completely dissolved (swirl the bottle) and place on ice. If easier to handle, transfer the solution to an ice-cold 15 ml falcon tube and keep it on ice. Do not filter.
- Serially dilute the 20 mg/ml stock in the following manner:

- Dilute 25 µl of the 20 mg/ml stock in 1 ml of cold prefiltered sterile Milli-Q water to make a 500 µg/ml stock.
- Dilute 26 µl of the 20 mg/ml stock in 5 ml of cold prefiltered sterile Milli-Q water to make a 2.6 µg/ml working stock.
- Do not filter. Place tubes on ice right after use.

- Keeping the bottle/tube on ice, make 1 ml aliquots of the 20 mg/ml stock[2]; 50 µl aliquots of the 500 µg/ml stock[2] and 250 µl aliquots of the 2.6 µg/ml stock. Prepare each aliquot separately. Use a new tip for each aliquot and avoid touching the walls of the Eppendorf tube[3]. Place each aliquot on ice, immediately after preparation.
- Fast freeze all aliquots by placing them on dry ice[4] for about 5-10 minutes. When completely frozen (solution is completely white) transfer to the appropriate freezer. Note the number of aliquots made, concentration, expiration date etc. on the usage log for sodium selenite.

Storage and Usage:

- The 20 mg/ml and 500 µg/ml concentrated stocks are always kept at -80°C. Some aliquots of the 2.6 µg/ml working stock are kept at -20°C for ready availability. The rest of the working stock is kept at -80°C and transferred to -20 °C when the -20°C stock runs out.
- To avoid confusions in the -80 °C freezer, it is useful to keep the working stock separated from the concentrated stocks.
- Aliquots are thawed once from -20°C, when needed and kept at 4°C for a period of up to one week.
- Write down on the Eppendorf tube the date when an aliquot is thawed, for reference to determine the expiration date.

Important Note*: Sodium Selenite is oxygen-sensitive. For this reason, the tubes should not be left opened for long.*

[1]*The stock bottle of sterile deionized Milli-Q water used for the preparation of additives must NOT be used for any other purpose.*

[2]The 20 mg/ml and 500 µg/ml stocks can be used later to prepare a 2.6 µg/ml working stock. For this reason, it is useful to aliquot them, to avoid repeated freezing and thawing. When preparing a working stock, remove a tube from the freezer and place it on ice immediately. All tubes are kept on ice; once the preparation is done, fast freeze and transfer the tubes to the corresponding freezer.

[3] Should you touch the wall or neck of a container; the tip should be discarded. If a vial containing an aliquot might have become accidentally contaminated (e.g., if there is any doubt that the tip used was not properly handled), it should be discarded. The bottom line is, under suspicion of risk of contamination, better discard than regret!!

[4]Spray dry ice with 70% ethanol (to decrease the temperature of the ice) before placing the aliquots on dry ice.

Transferrin

Sigma, catalog #T-2252 (Apo-transferrin)

- Weigh 50 mg of Transferrin in a 20 ml sterile beaker. Cover the beaker immediately with the aluminum foil (the one used to sterilize the beaker). This step can be performed under nonsterile conditions.
- From here onwards, work must be performed under the laminar flow hood. Disinfect beaker and any other material (e.g. ice-bucket) appropriately by wiping with a tissue paper sprayed with 70% ethanol, before introducing it in the hood. Also, carefully follow all other rules for working inside the cell culture room.
- Before beginning, it is better to prepare the Eppendorf tubes needed for aliquoting. We usually UV sterilize the autoclaved 1.5 ml Eppendorf tubes used for this purpose overnight, by opening their caps, facing upward such that the surface of the tube is properly sterilized. You can prepare the labels on the Eppendorf tubes before they are UV sterilized and label as many tubes as you will need, from a stock of sterile Eppendorf tubes only used for preparing additives. The proper labelling should include the additive's code, concentration, expiration date and the initials of the person who prepared the additive.
- Add 2.5 ml of cold sterile deionized Mili-Q water[1] to make a 20 mg/ml stock. When completely dissolved (swirl beaker), place on ice. Filter and transfer to an ice-cold 15 ml falcon tube, using a 3 ml syringe and a 0.22 µm pore size filter.

- Keeping the tube on ice, make 250 µl aliquots of the 20 mg/ml stock. Prepare each aliquot separately. Use a new tip for each aliquot and avoid touching the walls of the Eppendorf tube[2]. Place each aliquot on ice, immediately after preparation.
- Fast freeze all aliquots by placing them on dry ice[3] for about 5-10 minutes. When completely frozen (solution is completely white) transfer to the appropriate freezer.

Storage and Usage:

- Some aliquots of the working stock are kept at -20°C for ready availability. The rest of the stock is kept at -80°C and transferred to -20°C when the -20°C stock runs out.
- Aliquots are thawed once from -20°C, when needed and kept at 4°C for a period of up to one month.

[1]The stock bottle of sterile deionized Mili-Q water used for the preparation of additives must NOT be used for any other purpose.

[2]*Should you touch the wall or neck of a container; the tip should be discarded. If a vial containing an aliquot might have become accidentally contaminated (e.g., if there is any doubt that the tip used was not properly handled), it should be discarded. The bottom line is, under suspicion of risk of contamination, better discard than regret!!*

[3]Spray dry ice with 70% ethanol (to decrease the temperature of the ice) before placing the aliquots.

Transforming Growth Factor beta

Thermo-Fisher, catalog PHG9204

Preparation Procedure:

- Before beginning, it is better to prepare the Eppendorf tubes needed for aliquoting. We usually UV sterilize the autoclaved 1.5 ml Eppendorf tubes used for this purpose overnight, by opening their caps, facing upward such that the entire surface of the tube is properly sterilized. You can prepare the labels on the Eppendorf tubes before they are UV sterilized and label as many tubes as you will need, from a stock of sterile Eppendorf tubes only used

for preparing additives. The proper labelling should include the additive's code, concentration, expiration date and the initials of the person preparing the additives.

- Weigh 20 mg of BSA in a sterile 20 ml beaker used only for cell culture. Immediately close the lid of the beaker with aluminum foil after adding the BSA.
- The bottle of TGF-β should be briefly centrifuged prior to opening. DO NOT VORTEX!
- Work must be performed under the laminar flow hood. Disinfect TGF-β (5 µg) bottle and any other material including the beaker and ice-bucket appropriately by wiping with a tissue paper sprayed with 70% ethanol, before introducing it in the hood. Also, carefully follow all other rules for working inside the cell culture room. Place the 5 µg TGF-β bottle on ice as soon as it is brought into the hood.
- Prepare 10 mM Citric Acid of pH 3.0 in Milli-Q water[1] and filter it using 0.22 µm pore size filter. (Citric Acid can be stored in the dark at Room Temperature for two years).
- Dissolve the weighed BSA in 20 ml of 1X PBS[2] to prepare 0.1 % w/v solution and transfer it to a 20 ml falcon tube.
- Add 33 µl of 10 mM Citric Acid solution (intermediate solution) to the tube containing 0.1% BSA in PBS, to obtain a concentration of 300 ng/ml of primary stock solution. This solution can be stored at 2°C to 8°C for up to one week.
- Aliquot the primary stock solution into 1 ml Eppendorf tubes with 500 µl in each. Ensure that the tip is changed for each Eppendorf tube[3].
- To prepare the working solution, take 500 µl of one primary stock solution and add this primary stock in 2 ml of 0.1% BSA PBS to make 2.5 ml of working stock solution at a concentration of 60 ng/ml.
- Aliquot 50 µl from the working stock solution in each Eppendorf tube and store the tubes at -20°C. Prepare each aliquot separately. Use a new tip for each aliquot and avoid touching the walls of the Eppendorf[2]. Place each aliquot on ice, immediately after its preparation.
- Fast freeze all aliquots by placing them on dry ice[3] for about 5-10 minutes. When completely frozen (solution is completely white) transfer to the appropriate freezer.

Storage and Usage:

1. Some aliquots of the working stock are kept at -20°C for ready availability. The rest of the stock is kept at -80°C and transferred to -20°C when the -20 °C stock runs out.

2. Aliquots are thawed once from -20°C, when needed and kept at 4°C for a period of up to one week.

Note:

[1]The stock bottle of sterile deionized Mili-Q water used for the preparation of additives must NOT be used for any other purpose.

[2]The bottle of sterile PBS used for the preparation of additives must NOT be used for any other purpose.

[3]Should you touch the wall or neck of a container; the tip should be discarded. If a vial containing an aliquot might have become accidentally contaminated (e.g., if there is any doubt that the tip used was not properly handled), it should be discarded. The bottom line is, under suspicion of risk of contamination, better discard than regret!!

Soybean trypsin inhibitor

Sigma, catalog #T-6522 type I-S

- Weigh 100 mg of SBTI in a 20 ml sterile beaker. Cover the beaker immediately with the aluminum foil (the one used to sterilize the beaker). This step can be performed under nonsterile conditions.
- From here onwards, work must be performed in the laminar flow hood. Disinfect the beaker and any other material (e.g. ice-bucket) appropriately by wiping with a tissue paper sprayed with 70% ethanol, before introducing it in the hood. Also, carefully follow all other rules for working inside the cell culture room.
- Before beginning, it is better to prepare the Eppendorf tubes needed for aliquoting. We usually UV sterilize the autoclaved 1.5 ml Eppendorf tubes used for this purpose overnight, by opening their caps, facing upward such that the entire surface of the tube is properly sterilized. You can prepare the labels on the Eppendorf tubes before they are UV sterilized and label as many tubes as you will need, from a stock of sterile Eppendorf tubes only used for preparing additives. The proper labelling should include the additive's code, concentration, expiration date and the initials of the person who prepared the additive.

- Add 10 ml of cold sterile deionized Milli-Q water[1] to make a 10 mg/ml stock. When completely dissolved (swirl beaker), place on ice. Filter and transfer to an ice-cold 15 ml falcon tube, using a 10 ml syringe and a 0.22 µm pore size filter.
- Keeping the tube on ice, make 500 µl aliquots of the 10 mg/ml stock. Prepare each aliquot separately. Use a new tip for each aliquot and avoid touching the walls of the Eppendorf tube[2]. Place each aliquot on ice, immediately after preparation.
- Fast freeze all aliquots by placing them on dry ice[3] for about 5-10 minutes. When completely frozen (solution is completely white) transfer to the appropriate freezer.

Storage and Usage:

- Some aliquots of the working stock are kept at -20°C for ready availability. The rest of the stock is kept at -80°C and transferred to -20°C when the -20°C stock runs out.
- Aliquots are thawed once from -20°C, when needed and kept at 4°C for a period of up to two weeks.

[1]The stock bottle of sterile deionized Milli-Q water used for the preparation of additives must NOT be used for any other purpose.

[2]Should you touch the wall or neck of a container; the tip should be discarded. If a vial containing an aliquot might have become accidentally contaminated (e.g., if there is any doubt that the tip used was not properly handled), it should be discarded. The bottom line is, under suspicion of risk of contamination, better discard than regret!!

[3]Spray dry ice with 70% ethanol (to decrease the temperature of the ice) before placing the aliquots.

COMMENTARY

Background Information

Historically, 3D cell culture started with floating type 1 collagen (a nontunable system usually purified from rat tail) (Emerman, 1977). With the discovery of the possibility of extracting the EHS matrix enriched with basement membrane components from rhabdomyosarcomas, 3D cell culture methods switched to the making of spheroids in EHS-derived gel, such as Matrigel™ for

the past three decades. However, physical considerations have reoriented 3D cell culture when it was reported that not only the chemical signals, but also the mechanical constraints from the ECM were paramount to best recapitulate cell behavior. For this reason, we have devoted the protocols described in this article to using possibilities offered by tunable collagen I that are essential, notably for the study of cancer (Fang, 2014). Another exciting development in 3D culture is the engineering of tissue-chips with which microenvironmental parameters can be exquisitely controlled. We have given an example of chip with the DOC with which we can achieve a reproducible curved geometry within the diameter of a terminal breast duct. There are also chips that make use of microfluidics to modify the tumor microenvironment (Chittiboyina, 2018) or study the interaction between cell types (Rothbauer, 2018). The ECM is still an essential part of these tissue-chips if the cells cannot make all the components themselves, as we showed with the use of laminin 111 to provide the necessary differentiation stimulus for the non-neoplastic cells.

Techniques that are optimal for 3D cell culture ought to consider chemical and physical parameters of the cells' microenvironment. Therefore, methods used to create tumor nodules via aggregation (e.g., hanging drop, certain hydrogels, reactors) are less powerful as they do not reproduce a cellular organization as *in vivo*. In addition, the use of serum free medium as we present it in these protocols, is essential to conduct reproducible experiments, especially those involving treatment with therapeutic drugs and other molecules.

Critical Parameters

The protocols used for 3D cell culture can only work well if the cells are properly handled via standard methods used for propagation of cells in 2D culture (i.e., cell 'passages'). We reported previously the importance of propagating cells from the same confluence and with a set number of cells seeded (Vidi, 2013). Indeed, cancer cell populations left in 2D culture for too long will become enriched with cells that are less aggressive. In contrast, non-neoplastic cells that are not given the time to settle in their medium (and are propagated too soon, prior to reaching the desired confluence) will usually be enriched with cells that have a lesser capability to differentiate. Phenotypic drift that might result from poor cell culture practice may not be seen until cells are in 3D culture, at which time it is usually too late to revert the phenotype to what it used to be.

Other factors that influence the protocols are the cell culture medium conditions. Unknown factors in the serum might protect the cells against a particular drug treatment or prevent the recapitulation of the phenotype normally observed *in vivo*. The use of well-chosen additives will provide reproducibility; however, specific attention needs to be given to their concentration, storage and shelf-life since departing away from the set conditions is likely to perturb the phenotype or even kill the cells.

Features of tissue differentiation are the main tools to confirm the validity of the model. They are usually based on immunostaining and help catch differentiation issues with the cell culture conditions or with the cells themselves. Each set of differentiation features for testing will depend on the type of cells and the expected phenotype (i.e., the phenotype that would represent a physiologically relevant situation). For instance, DCIS tumors are expected to have a measurable level of basal polarity as we show in Fig. 1.

Troubleshooting

If the desired phenotype is not achieved (e.g., lack of proper cellular organization, increase in cell death, abnormal functional parameters), troubleshooting should start with the preparation of the culture conditions for that experiment (medium, serum or additives) before venturing into cellular issues (e.g., mycoplasma contamination, phenotypic drift) and environmental issues (incubator, etc.). It is essential to keep a log of cell vials thawed and of the batches of medium, additives, serum and ECM that were bought to trace the issue back in time (Fig. 8). Since the culture without serum makes the cells particularly sensitive to any alteration of their environment, when all ‘in-house’ potential issues have been dismissed as the sources of the problem, it is critical to investigate potential issues with commercially available reagents and any change in their manufacture. The increased sensitivity of cells to their microenvironment is particularly noted in 3D culture. As an example, medium prepared with water contaminated with low concentrations of potential toxicants could lead to cell death in 3D culture only; whereas cells could survive in standard 2D culture.

Understanding Results

Results are typically those related to the analysis used with the cells and do not pertain to 3D culture per se, except with differentiation. Anticipated results regarding differentiation are signs

of organizational and functional mimicry of physiologically relevant tissues. Therefore, markers of differentiation typical of the tissue of interest should not only be expressed but also be localized properly within the tissue (e.g., lateroapical distribution of tight junction markers in the phenotypically normal epithelium; basal location of β4-integrin in DCIS). To validate the functional aspect of the culture, the activity of major pathways involved in the functions or behavior of the cells of interest should correlate with that observed *in vivo* (e.g., activation of a signaling pathway characteristic of a specific subtype of tumors, shut down of stress response pathways in aggressive tumors or activation of certain metalloproteinases in invasive cancers).

There will be unexpected results with 3D culture when certain techniques normally used in 2D culture and set up with 2D cultures are translated for 3D culture. For instance, washing steps for immunostaining in 3D culture should be longer than in 2D culture to reduce the nonspecific fluorescence background from the matrix. More subtly, there might be altered possibilities to extract and break materials from cells obtained from 3D culture, especially since the tissue structures are usually kept intact (e.g., no cell separation) before lysis. For instance, the DNA breakage for experiments like chromatin immunoprecipitation (ChIP) needs to be optimized in 3D culture compared to 2D culture for the same cell line in order to get the necessary small size of DNA pieces.

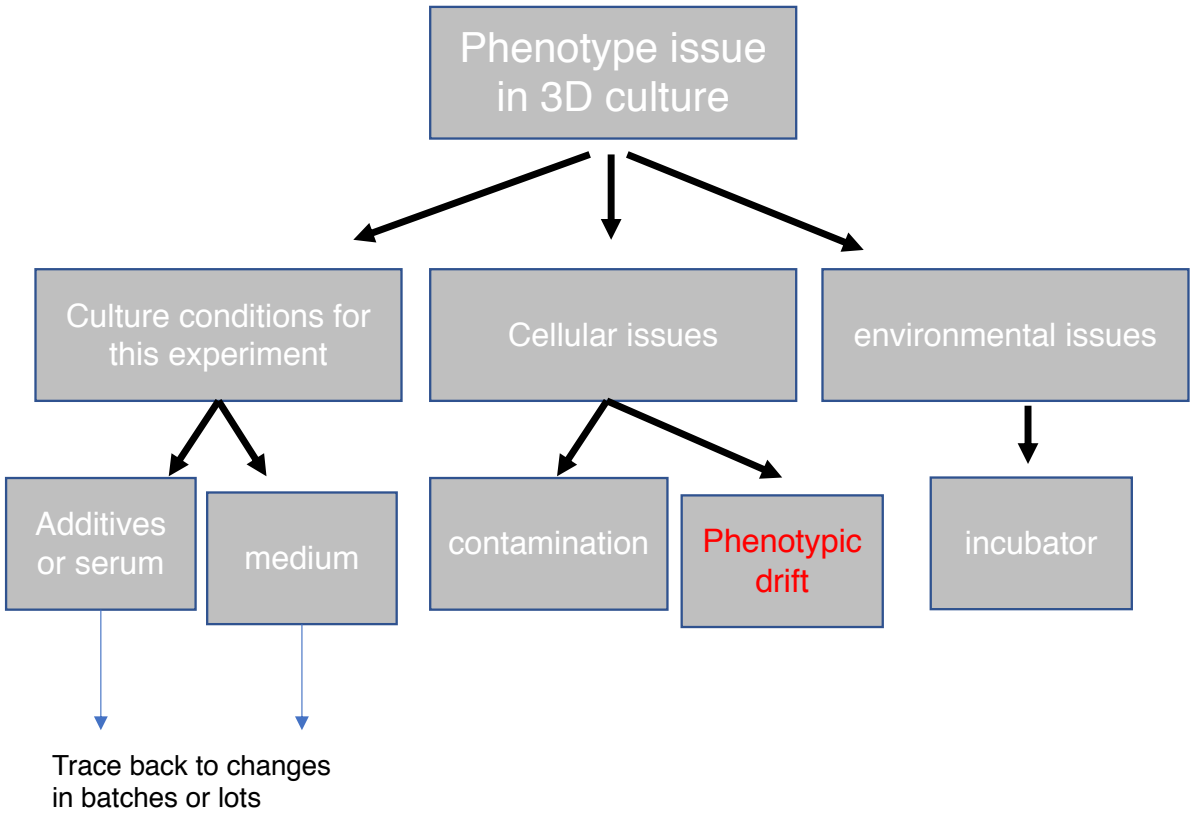

Fig 8. Schematic of troubleshooting steps if the phenotype is not achieved anymore in 3D cell culture. Note: The phenotypic drift is usually an irreversible issue due to mishandling of the cells in standard 2D culture (maintenance and propagation steps).

Time Considerations

The minimum amount of time necessary for 3D culture depends on the cell type used. Differentiation requires adequate signaling pathways and gene expression patterns and in many cases the presence of a certain architecture of the cell assemblies that occurs via the ordered division of cells. Five days might be enough for many tumors; however, these tumors will be of small sizes. We may wait 10 days with the breast cancer cells. Other models in which the cells proliferate very slowly, like certain glioblastomas may take two to three weeks to get tumors of acceptable sizes for experiments. With fibroblasts, the usual amount of time to achieve differentiation and resting (or nonactivated) phenotype is usually five days, but for the phenotypically normal differentiation of epithelial cells, the minimum period of culture is usually eight days. With cocultures, the amount of time needed to reach differentiation of all cells

involved might take longer depending on the approach used. Finally, it is important to realize that in contrast to 2D cultures in which cells might keep proliferating and start piling up, 3D cultures can be kept for a long time (over months if necessary) since once the tissues reach their differentiation state, they remain stable, unless stimulated. This type of culture permits chronic treatments to investigate pathways involved in cancer progression for instance.

ACKNOWLEDGEMENT

Part of the work presented with the monoculture of fibroblasts was supported by the Congressionally-Directed Medical Research Program/Breast Cancer Research Program (CDMRP/BCRP) (W81XWH-17-1-0250 to SL).

3.6 References

Amaro, A., Angelini, G., Mirisola, V., Isabella, A., Reverberi, D., Matis, S., Maffei, M., Giaretti W., Viale M., Gangemi R., Emionite L., Astigiano S., Cilli M., Bachmeier B.E., Killian P.H., Albini A., & Pfeffer, U. (2016). A highly invasive subpopulation of MDA-MB-231 breast cancer cells shows accelerated growth , differential chemoresistance , features of apocrine tumors and reduced tumorigenicity in vivo. *Oncotarget, 7,* 68803-68820. doi: 10.18632/oncotarget.11931

Bissell, M. J., Hall, H. G., & Parry, G. (1982). How does the extracellular matrix direct gene expression? *Journal of Theoretical Biology, 99,* 31–68. doi:10.1016/0022-5193(82)90388-5

Bonnans, C., Chou, J., & Werb, Z. (2014). Remodelling The Extracellular Matrix In Development And Disease. *Nature Reviews Molecular Cellular Biology, 15*, 786–801. https://doi.org/10.1038/nrm3904.

Briand P., Nielson K.V., Madsen M.W., & Peterson O.W. (1996). Trisomy 7p and malignant transformation of human breast epithelial cells following epidermal growth factor withdrawal. *Cancer Research, 56,* 2039-2044.doi: published May 1996

Briand, P., Petersen, O. W., & Van Deurs, B. (1987). A new diploid nontumorigenic human breast epithelial cell line isolated and propagated in chemically defined medium. *In vitro Cellular & Developmental Biology, 23,* 181-188. doi:10.1007/BF02623578

Chittiboyina, S., Rahimi, R., Atrian, F., Ochoa, M., Ziaie, B. & Lelièvre S.A. (2018). Gradient-on-a-Chip with Reactive Oxygen Species Reveals Thresholds in the Nucleus Response of Cancer Cells Depending on the Matrix Environment. *American Chemical Society, Biomaterials Science and Engineering 4,* 432-445. doi:10.1021/acsbiomaterials.7b00087

Cohen, N., Shani, O., Raz, Y., Sharon, Y., Hoffman, D., Abramovitz, L., & Erez, N. (2017). Fibroblasts drive an immunosuppressive and growth-promoting microenvironment in breast cancer via secretion of Chitinase 3-like 1. *Oncogene 36*, 4457–4468. doi.org:10.1038/onc.2017.65

Conlon G.A. & Murray G.I. (2018). Recent advances in understanding the roles of matrix metalloproteinases in tumour invasion and metastasis. *The Journal of Pathology*, .doi: 10.1002/path.5225

Emerman, J.T., & Pitelka, D.R. (1977). Maintenance and induction of morphological differentiation in dissociated mammary epithelium on floating collagen membranes. *Journal of Society for In Vitro Biology, 13,* 316-328

Fang M., Yuan J., Peng C., & Li Y. (2014). Collagen as a double-edged sword in tumor progression. *Tumor Biology,* 35, 2871-2882. doi: 10.1007/s13277-013-1511-7

Fullár, A., Dudás, J., Oláh, L., Hollósi, P., Papp, Z., Sobel, G., Karászi K, Paku S, Baghy K, Kovalszky, I. (2015). Remodeling of extracellular matrix by normal and tumor-associated fibroblasts promotes cervical cancer progression. *BMC Cancer*, 1–16. doi:10.1186/s12885-015-1272-3

Goers, L., Freemont, P., & Polizzi, K. M. (2014). Co-culture systems and technologies : taking synthetic biology to the next level. *Journal of the Royal Society, Interface, 11.* doi: 10.1098/rsif.2014.0065

Kular, J. K., Basu, S., & Sharma, R. I. (2014). The extracellular matrix : Structure , composition , age-related differences, tools for analysis and applications for tissue engineering. *Journal of Tissue Engineering, 5,* 1-17. doi:10.1177/2041731414557112

Lee, J., Kim, S., Khawar, I. A., Jeong, S., Chung, S., & Kuh, H. (2018). Microfluidic co-culture of pancreatic tumor spheroids with stellate cells as a novel 3D model for investigation of stroma-mediated cell motility and drug resistance. *Journal of Clinicial Cancer Research, 37,*. https://doi.org/10.1186/s13046-017-0654-6

Leight, J. L., Drain, A. P., & Weaver, V. M. (2016). Extracellular Matrix Remodeling and Stiffening Modulate Tumor Phenotype and Treatment Response. *Annual Review of Cancer Biology*, *1*, 313–334. https://doi.org/10.1146/annurev-cancerbio-050216-034431

Lelièvre S. A. and Chittiboyina S. (2018). Microphysiological systems to study microenvironment cell nucleus interaction: importance of tissue geometry and heterogeneity. *Microphysiological Systems,* doi: 10.21037/mps.2018.11.02

Lin S. & Gu L., (2015). Influence of Crosslink Density and Stiffness on Mechanical Properties of Type I Collagen Gel. *Materials, 8*, 551-560. doi:10.3390/ma8020551

Lopez JI., Kang I., You WK., McDonald DM., & Weaver VM (2011). In situ force mapping of mammary gland transformation. *Integrative Biology: quantitative biosciences from nano to macro, 3,* 910-921. doi: 10.1039/c1ib00043h.

Mi, S., Du, Z., Xu, Y., Wu, Z., Qian, X., Zhang, M. & Sun W. (2016). Microfluidic co-culture system for cancer migratory analysis and anti-metastatic drugs screening. *Nature: Scientific Reports*, **6**, 35544; doi: 10.1038/srep35544.

Northey, J. J., Przybyla, L., & Weaver, V. M. (2017). Tissue Force Programs Cell Fate and Tumor

Aggression. *Cancer Discovery, 7,* 1224–1237. doi: 10.1158/2159-8290.CD-16-0733

Paszek, M. J ., Zahir N., Johnson G. I., Lakins J.N., Rozenberg G.I., Gefen A., Reinhart-King C.A., Margulies, S. S, Dembo M., Boettiger, D., Hammer, D. A., & Weaver, V. M. (2005). Tensional homeostasis and the malignant phenotype. *Cancer Cell*, *8*, 241–254. doi:10.1016/j.ccr.2005.08.010

Plachot, C., Chaboub, L. S., Adissu, H. A., Wang, L., Urazaev, A., Sturgis, J., Asem E K., & Lelièvre, S. A. (2009). Factors necessary to produce basoapical polarity in human glandular epithelium formed in conventional and high-throughput three-dimensional culture : example of the breast epithelium. *BMC Biology,* 7. doi:10.1186/1741-7007-7-77

Rijal, G., & Li ,W. (2017). A versatile 3D tissue matrix scaffold system for tumor modeling and drug screening. *Science Advance, 3,* e1700764. doi:10.1126/sciadv.1700764

Rizki, A., Weaver, V. M., Lee, S., Rozenberg, G. I., Chin, K., Myers, C. A., Bascom J.L., Mott J.D., Semeiks J.R., Grate L.R., Mian I.S., Borowsky A.D., Jensen R.A., Idowu M.O., Chen F., Chen D.J., Peterson O.W., Grey J.W., & Bissell M.J. (2008). A Human Breast Model of Preinvasive to Invasive Transition. *Cancer Research 68*, 1378–1387. doi:10.1158/0008-5472.CAN-07-2225.

Rothbauer, M., Zirath, H., & Ertl, P. (2018). Recent advances in microfluidic technologies for cell-to-cell interaction studies. *Lab on a Chip*,18, 249–270. doi: 10.1039/c7lc00815e

Sampson, N., Koziel, R., Zenzmaier, C., Bubendorf, L., Plas, E., Jansen-Dürr, P., & Berger, P. (2011). ROS signaling by NOX4 drives fibroblast-to-myofibroblast differentiation in the diseased prostatic stroma. *Mol Endocrinology, 25*, 503-15. doi: 10.1210/me.2010-0340

Shay JW, Van Der Haegen BA, Ying Y, & Wright WE. (1993). The frequency of immortalization of human fibroblasts and mammary epithelial cells transfectedwith SV40 large T-antigen. *Exp Cell Res, 209,* 45-52. doi: 10.1006/excr.1993.1283.

Shay JW, Tomlinson G, Piatyszek MA, & Gollahon LS. (1995) Spontaneous in vitro immortalization of breast epithelial cells from a patient with Li-Fraumeni syndrome. *Molecular Cellular Biology, 15,* 425-432. doi: 10.1128/MCB.15.1.425

Spill, F., Reynolds D.S., Kamm R.D., & Zaman M.H. (2016). Impact of the Physical Microenvironment on Tumor Progression and Metastasis. *Current Opinion Biotechnology, 40,* 41-48. doi:10.1016/j.copbio.2016.02.007.

Subbaramaiah, K., Brown, K. A., Zahid, H., Balmus, G., Weiss, R. S., Herbert, B. S., & Dannenberg, A. J. (2016). Hsp90 and PKM2 Drive the Expression of Aromatase in Li-Fraumeni Syndrome Breast Adipose Stromal Cells. *The Journal of biological chemistry*, *291*, 16011-16023. doi: 10.1074/jbc.M115.698902

Theocharis, A. D., Skandalis, S. S., Gialeli, C., & Karamanos, N. K. (2016). Extracellular matrix structure. *Advanced Drug Delivery Reviews*, *97*, 4–27. doi:10.1016/j.addr.2015.11.001

Vidi, P.A., Bissell M.J., & Lelièvre S. A. (2013). Three-Dimensional Culture of Human Breast Epithelial Cells: The How and the Why. *Methods in Molecular Biology, 945,* 193–219. doi:10.1007/978-1-62703-125-7_13.

Vidi P.A., Maleki T., Ochoa M., Wang L., Clark S. M., Leary J. F. & Lelièvre S. A. (2014) *Lab on a chip,* 14. doi: 10.1039/c3lc50819f

KEY REFERENCE (optional)

INTERNET RESOURCES

The 3D Cell Culture (3D3C) facility at Purdue University is compiling short movies under NanoHub on certain aspects of the techniques that we have described in this protocol article. Visit https://nanohub.org/resources/25058/supportingdocs. These movies were made with the help of members from the Lelièvre laboratory and the Online Production Managing team of Joe Cychosz. Below we include specific short movies that illustrate steps of the methods that we have discussed in the text above.

Table 1 Stock, working and final concentrations of cell culture additives with their storage conditions.

Additive	Company	Initial stock concentration		Aliquot with working stock concentration		Final concentration
			Expiration at -80°C		Expiration at 4°C	In cell culture medium
Prolactin	Sigma L-6520	30.03 I.U./ml (1 mg/ml)	One year	1 mg/ml	one month	5 µg/ml
Insulin	SIGMA I-4011	2 mg/ml	six months	100 µg/ml	one month	250 ng/ml
β-estradiol	SIGMA E-2758	8 mg/ml (0.03 M stock)	one year	2.67×10^{-5} µg/ml	one month	2.67×10^{-8} µg/ml (or 0.1 nM)
Hydrocortisone	SIGMA H-0888	5 mg/ml (1.4×10^{-2} M)	one year	0.5 mg/ml	one month	0.5 µg/ml (or 1.4 µM)
Sodium selenite	BD-Biosciences 354201	20 mg/ml	three months	2.6 µg/ml	one week	2.6 ng/ml
Transferrin	SIGMA T-2252	20 mg/ml	three months	20 mg/ml	one month	10 µg/ml
Epidermal growth factor	Corning Life Sciences 354001	20 µg/ml	three months	20 µg/ml	one week	5 ng/ml
Fibroblast growth factor	ThermoFisher PHG0264	10 µg/ml	one year	10 µg/ml	one week	2.5 ng/ml
Transforming growth factor- β	ThermoFisher PHG9204	300 ng/ml	one year	60 ng/ml	one week	7.5 pg/ml
Soybean trypsin inhibitor	SIGMA, T-6522 type I-S	10 mg/ml	six months	10 mg/ml	two weeks	0.18 mg/ml

Table 2. Example of cell seeding depending on the culture mode. For 2D culture, cancer cell seeding for the indicated cell lines is usually 11,700 cells/cm^2 and non-neoplastic epithelial cell seeding is usually 23,300 cells/cm^2; for EHS gel drip culture, cancer cell seeding for the indicated cell lines is usually 17,400 cells/cm^2 and 34,700 cells/cm^2 for non-neoplastic epithelial cells on a gel coat of 42 µl/cm^2 and with 5% final EHS gel concentration in the cell culture medium; for collagen I embedded culture, cancer cell seeding for the indicated cell lines is usually 43,150 cells/cm^2, within 55 µl of gel/cm^2 on a thin gel coat of 14 µl/cm^2.

Culture container	Surface Area	T4-2; S2; MDA-MB-231 cells	H-14 medium	S1 cells
Standard 2D culture				
4-well plate/well	2.01 cm^2	23,500	300 µl	47,000
6-well plate/well	9.08 cm^2	106,000	1.2 ml	212,000
12-well plate/well	3.8 cm^2	44,500	500 µl	473,000
35 mm dish	9.62 cm^2	112,500	1.3 ml	660,000
60 mm dish	28.27 cm^2	330,000	3.8 ml	225,000
T-25 flask	25 cm^2	291,500	3 ml	583,000
T-75 flask	75 cm^2	875,000	10 ml	1,750,000
Embedded culture in collagen I				
4-well plate /well	2.01 cm^2	86,700	500 µl	
4-well slide/well	1.44 cm^2	62,100	500 µl	
35 mm dish	9.62 cm^2	415,100	1.5 ml	
60 mm dish	28.27 cm^2	1,220,000	4.5 ml	
Drip culture with EHS gel				
4-well slide/well	1.44 cm^2	25,000	400 µl (on 60 µl gel coat)	50,000
35 mm dish	9.62 cm^2	200,000	1.2 ml (on 500 µl gel coat)	400,000
60 mm dish	28.27 cm^2	600,000	3.8 ml (on 1.5 ml gel coat)	1,200,000

Table 2 References

1. Wang, M., et al., *Role of tumor microenvironment in tumorigenesis.* J Cancer, 2017. **8**(5): p. 761-773.
2. Tan, Y., et al., *Matrix softness regulates plasticity of tumour-repopulating cells via H3K9 demethylation and Sox2 expression.* Nat Commun, 2014. **5**: p. 4619.
3. Rowat, A.C., J. Lammerding, and J.H. Ipsen, *Mechanical properties of the cell nucleus and the effect of emerin deficiency.* Biophys J, 2006. **91**(12): p. 4649-64.
4. Madrazo, E., A.C. Conde, and J. Redondo-Munoz, *Inside the Cell: Integrins as New Governors of Nuclear Alterations?* Cancers (Basel), 2017. **9**(7).
5. Vidi, P.A., et al., *Disease-on-a-chip: mimicry of tumor growth in mammary ducts.* Lab Chip, 2014. **14**(1): p. 172-7.

3.7 Discussion and Conclusion

The acquisition by cancer cells of resistance to chemotherapy is an ongoing and unsolved obstacle in anticancer drug use and development. In order to address this problem, novel *in vitro* models are essential to study chemoresistance in a more physiological context. For example, matrix-based scaffolds led to the identification of signaling pathways associated with matrix rigidity as the key promoters of cancer cell resistance to chemotherapy (Castells, Thibault, Delord, & Couderc, 2012). During my thesis work I also identified that tumor geometry affects cancer cells' drug response and that a ductal-like geometry better illustrates the physiological response of cancer cells to chemotherapy. These results are in agreement with the fact that the physical aspects of the TME are highly associated with tumor aggressiveness and chemotherapeutic response (Senthebane et al., 2017).

In order to faithfully mimic the situations in which tumors are functioning, the role of phenotypic biomarkers as reporters of tumor behavior seems pivotal. My results demonstrated that nuclear morphometric features respond to matrix stiffness, geometry and chemotherapy. Specifically, features such as size and shape could predict the drug response in triple negative breast cancer cells cultured as a monolayer (2D culture). However, the role of nuclear morphometry in chemotherapeutic response in cells cultured in a collagen matrix was more complicated to grasp. Notably, it depended on initial tumor phenotype illustrated by the cell population status of chemosensitivity. Although changes in nuclear shape and size are associated with tumor phenotype, it appeared that other phenotypic alterations such as chromatin reorganization needed

to be incorporated in the study model to conclude that nuclear morphology could act as a reliable predictor of cancer cells behavior under chemotherapeutic treatment. A possible explanation for such apparent complexity is that matrix rigidity could affect an upstream controller of nuclear morphometry and chromatin organization based on the tumor ability to sense microenvironmental mechanical forces. To further unravel the relationship between microenvironmental physical stress, nuclear organization, and resistance to treatment, 3D culture models of breast tumors such as those presented in detail in the second part of this thesis were essential.

The mechanical signals from the microenvironment transfer through the cytoskeleton and reach the cell nucleus to induce changes in gene expression and epigenetic regulation. Microenvironmental effects were also observed at the phenotypic (architectural) level, as it was shown here and by others, via alterations of the nuclear morphology in cancer cells (Guilluy & Burridge, 2015; Imbalzano et al., 2013). However, it is still not clear how phenotypic changes at the level of the cell nucleus affect gene expression in malignant cells. The unique role of nuclear matrix proteins in maintaining nuclear structure and linking the cytoskeleton to the DNA make them good candidates to further explore the link between phenotypic changes and gene expression regulation.

Here, we have shown that NuMA, an abundant nuclear matrix protein, which closely interacts with chromatin, maintains nuclear morphometry. Similarly, nuclear lamin provides physical support for the nucleus and organizes the genome. Lamin proteins are also known as nuclear mechanosensors. Lamin scaffold is mainly linked to the heterochromatin at the periphery of the nucleus where it connects with the cytoskeleton via specific protein complexes located in nuclear envelope. In addition, NuMA is distributed throughout the nucleus and is interacting with euchromatin (Merdes & Cleveland, 1998). Hence, it seemed logical to further investigate the role of NuMA in nuclear mechanosensing. Indeed, our ATAC-seq results showed that NuMA was associated with open chromatin regions in a matrix stiffness-dependent manner, and chromatin immunoprecipitation results obtained by other laboratory members also support this possibility. In the future, novel therapeutic targets could emerge by focusing on nuclear matrix proteins, such as NuMA, that are responding to environmental changes by acting at the level of chromatin. Knowing the constant rate of matrix remodeling in cancer progression and the link it has with

chemoresistance, targeting the major nuclear mediators of the TME during drug response, seems essential.

3.8 References

Castells, M., Thibault, B., Delord, J.-P., & Couderc, B. (2012). Implication of Tumor Microenvironment in Chemoresistance: Tumor-Associated Stromal Cells Protect Tumor Cells from Cell Death. *International Journal of Molecular Sciences, 13*(8), 9545-9571. doi:10.3390/ijms13089545

Guilluy, C., & Burridge, K. (2015). Nuclear mechanotransduction: forcing the nucleus to respond. *Nucleus, 6*(1), 19-22. doi:10.1080/19491034.2014.1001705

Imbalzano, K. M., Cohet, N., Wu, Q., Underwood, J. M., Imbalzano, A. N., & Nickerson, J. A. (2013). Nuclear shape changes are induced by knockdown of the SWI/SNF ATPase BRG1 and are independent of cytoskeletal connections. *PLoS One, 8*(2), e55628. doi:10.1371/journal.pone.0055628

Merdes, A., & Cleveland, D. W. (1998). The role of NuMA in the interphase nucleus. *J Cell Sci, 111 (Pt 1)*, 71-79.

Senthebane, D. A., Rowe, A., Thomford, N. E., Shipanga, H., Munro, D., Mazeedi, M., . . . Dzobo, K. (2017). The Role of Tumor Microenvironment in Chemoresistance: To Survive, Keep Your Enemies Closer. *Int J Mol Sci, 18*(7). doi:10.3390/ijms18071586

APPENDIX A. A PHYSIOLOGICALLY RELEVANT *IN VITRO* CANCER MODEL FOR DRUG SCREENING

Farzaneh Atrian[1], [Manuel Ochoa, Christopher Duffy], and Sophie A. Lelièvre[1,2]

(1) Department of Basic Medical Sciences, Purdue University, West Lafayette, IN 47906-2026, USA

(2) Purdue Center for Cancer Research

3.9 Abstract

The superiority of 3D cell culture leading to the formation of tumor nodules compared to standard 2D culture is increasingly recognized for drug screening. Many carcinomas initiate in the context of a circular structure (e.g., a duct), within a monolayer of epithelial cells. Therefore, we have developed a "disease-on-a-chip" (DOC) system, in which breast tumors grow within a curved geometry, in the presence of non-neoplastic cells, like ductal carcinomas *in vivo*. DOC devices consist of microfabricated acrylic-based hemichannels coated with the basement membrane protein laminin-111 that promotes the differentiation of non-neoplastic mammary epithelial cells into a polarized monolayer. Tiny tumor nodules are deposited on the DOC and rapidly anchor to the hemichannel surface and grow. We have shown previously that the tumor nodules cultured in hemichannels display significantly different drug sensitivities compared to those cultured on a flat surface and that a major morphological difference between these culture conditions is the nuclear shape. Nuclear morphological analysis of the breast cancer cells in the curved geometry as well as hydrogel (HG) and hanging drop (HD) systems (with amorphous geometry) showed that only nodules in the curved set-up have nuclear shape (circularity) and size (area) similar to that of tumors *in vivo*. In addition, we compared the sensitivity of triple negative breast tumors to cisplatin, with proven efficacy in the clinics, and SAHA, an epigenetic drug that so far failed in breast cancer treatment. Our results suggest higher sensitivity to cisplatin and lower sensitivity to SAHA of breast cancer cells cultured in ductal-like geometry compared to the amorphous systems. We further tested the sensitivity of three different breast cancer subtypes (triple negative, HER2 positive and Luminal A) to a cytotoxic drug currently in clinical trial, ARQ-761 (beta-lapachone),

in the DOC, HG and HD. Our results indicate that in general, the tumor nodules showed highest resistance to beta-lapachone in DOC compared to other models. Overall, triple negative and HER2 positive breast cancer subtypes displayed the lowest and highest sensitivity to the drug, respectively. Results obtained with DOC system appear the closest to the outcome of phase I clinical trial showing that beta-lapachone has only modest efficacy for solid tumors.

3.10 Introduction

Carcinomas initiate in the context of a ductal structure, within a monolayer of epithelial cells, which likely influences the behavior of the malignant cells - in particular, their responses to therapeutics. Currently available 3D culture models are often categorized into nonmatrix and matrix-based cultures. The main focus of the current *in vitro* cancer models for drug screening is to develop spheroids while ignoring the fact that environmental cues are as important as cell-cell interactions during the chemotherapeutic response. For example, the hanging drop (HD) plate is a nonmatrix method used for creating tumor spheroids via self-aggregation of cancer cells, for which the spheroid sizes depend on the initial number of cells. However, this approach lacks the ECM surrounding tumors, and the high number of necrotic cells at the center of the nodules is not representative of the tumor organization of most solid cancers. Matrix-based cultures include any nodule formation using extracellular matrix components or synthetic hydrogel scaffolds. The matrix is allowing cell proliferation, nodule formation and even cell migration. Such cultures are considered more physiologically relevant, especially if the hydrogel scaffolds are of biological origin. Still, many scientists consider that they lack important features of the tissue architecture such as geometry and stromal cells components (Edmondson, Broglie, Adcock, & Yang, 2014).

The disease-on-a-chip (DOC) was developed as an *in vitro* platform in which tumor nodules develop in their original spherical geometry in the presence of phenotypically normal cells (Vidi et al., 2014); patent information: SA Lelièvre et al. “Disease-on-a-chip for detection and treatment of neoplasias of exocrine glands”. US 9969964B2 (“Technology”), May 15, 2018). Non-neoplastic mammary epithelial cells (HMT-3522 S1) cultured on laminin-111 coated hemichannels differentiate into a polarized monolayer. This polarization is key to glandular tissue homeostasis and may protect the resting normal epithelium against the effect of drugs. Previously, we demonstrated that cancer cells cultured on different geometries (curved vs. flat) have different nuclear circularity and susceptibility to anticancer drugs (Vidi et al., 2014). We also showed that

nuclear morphometry is a marker of cancer cell phenotype in 3D cell culture (Chittiboyina et al., 2017) and somewhat of an indicator of drug sensitivity depending on the type of tumors (Atrian, unpublished data)

Here, we compared the DOC system with other established 3D cell culture techniques for drug screening such as hydrogels and hanging drops to determine which system is closest to the *in vivo* context in terms of nuclear morphometry (notably size and shape). To further assess the responsiveness of drugs in the DOC, we also compared the sensitivity of triple negative breast tumors to cisplatin, currently used in breast cancer therapy (Silver et al., 2010), and SAHA (Eckschlager et al., 2017), an FDA approved drug for hematopoietic cancer with reported efficacy against breast cancer cells in 2D culture, and beta-lapachone, a drug currently under clinical trial for breast cancer treatment with possibly selective efficacy for certain tumor subtypes, in the different 3D cell culture systems. We also investigated the possibility to make the DOC a high-throughput screening platform.

3.11 Results

We have compared the size and circularity of the nuclei within tumors formed by breast cancer cell lines corresponding to different cancer subtypes (i.e., triple negative, luminal A and Luminal B) in the DOC as well as in currently advertised hydrogel (HG) and HD systems for drug screening. The latter two systems trigger nodule formation via the aggregation of cancer cells and/or are devoid of extracellular constraints (e.g., extracellular matrix, organ geometry) for their growth. Only nodules produced on the DOC have both nuclear area and circularity similar to those of real tumors of the same type, as shown by imageJ analysis of DAPI-staining nuclei (Figure 1. A-G).

In addition, to assess the sensitivity of tumors in the DOC model to drugs, we have compared their responsiveness to cisplatin, with proven efficacy against triple negative breast tumors in the clinics, and SAHA, an epigenetic drug that so far failed in breast cancer treatment. However, effects opposite to those documented *in vivo* for these two drugs have been reported in 2D culture of cells. We chose drug concentrations and treatment lengths similar to those used with demonstrated efficacy in 2D culture (Petrelli et al., 2014; Walters, Theriault, Holmes, Hortobagyi, & Esparza, 1992). Proliferation assessment with Ki67 immunostaining revealed by the HG system demonstrated significant sensitivity of triple negative tumors to SAHA. Whereas, cell death assessment with caspase 3 immunostaining showed that the HD system did not favor sensitivity to

cisplatin. Hence, only the DOC correctly informed on both the lack of sensitivity to SAHA and the strong sensitivity to cisplatin (Figure 1.H-I).

Figure 1. A and **B.** Nuclear area and circularity of T4-2 cells (triple-negative-TN) in the DOC, hanging drop and hydrogel, compared with triple-negative invasive ductal carcinoma (TN IDC) **C.** and **D.** Nuclear area and circularity of luminal A cells (T47D) using DOC, hanging drop and hydrogel systems compared with luminal A IDC **E.** From left to right, the IHC image is a representative of triple negative invasive ductal carcinoma (TN IDC), the next three images are from T4-2 nodules in a DOC culture, hanging drop culture and hydrogel culture. **F and G.** Nuclear area and circularity of luminal B cells (BT474) using DOC and hanging drop systems compared with luminal B IDC. **H.** means and standard deviations of the T4-2 cell death in control and cisplatin treated groups in different culture msystems. **I.** means and standard deviations of T4-2 cells proliferation in control and SAHA treated groups in different culture models. N=3 with 100 nuclei per replicate analyzed, scale bar 10 μm, $*P<0.05$.

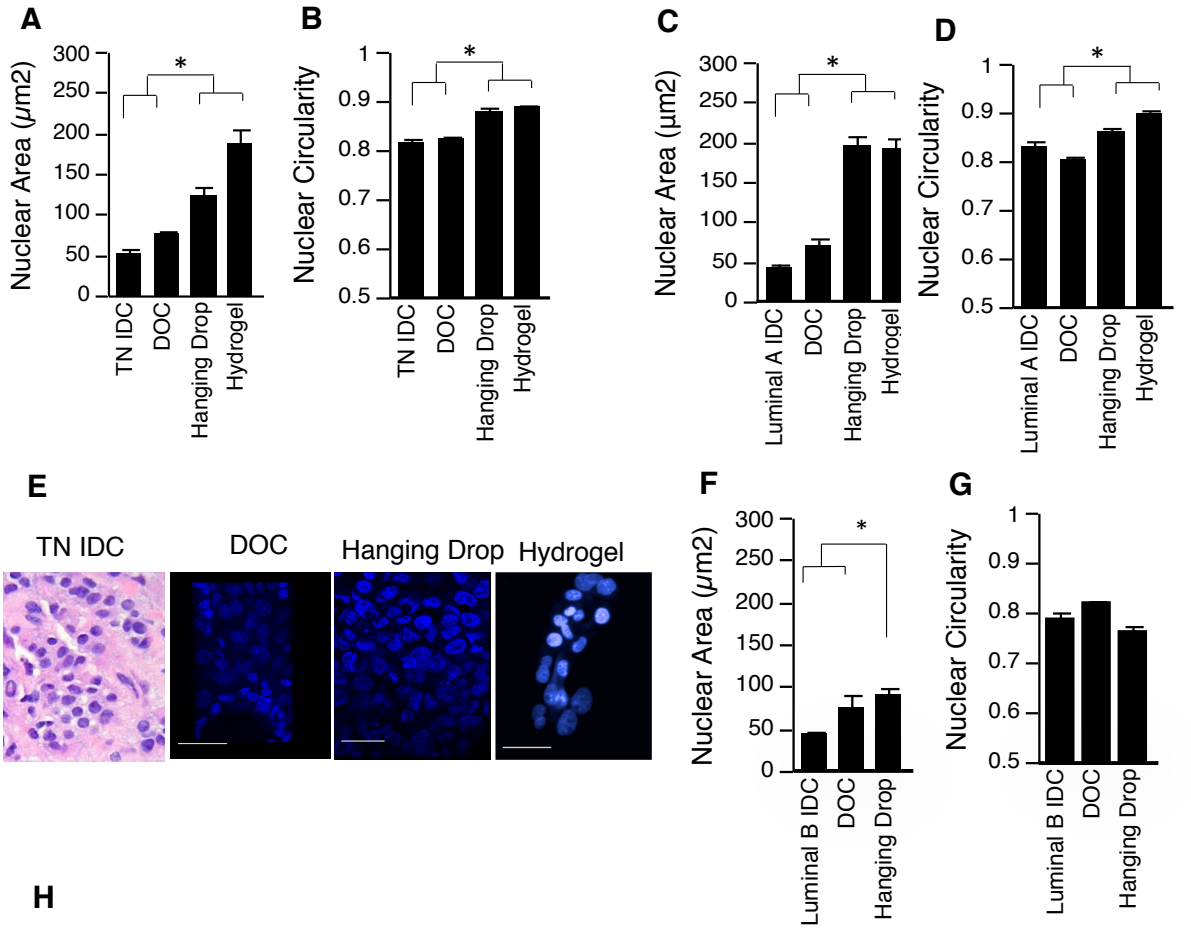

H

Culture models	Mean of cell death for control (%)	Standard Deviation-control	Mean of cell death for cisplatin treated (%)	Standard Deviation-cisplatin treated	P-value
DOC	9.6167	4.80850	41.2667	16.7077	0.0012
Hanging Drop	18.7033	8.74894	29.6667	10.2632	0.2319
Hydrogel	7.9000	2.15174	63.3333	8.6217	0.0004

I

Culture models	Mean of cell proliferation for control (%)	Standard Deviation-control	Mean of cell proliferation for SAHA treated (%)	Standard Deviation-SAHA treated	P-value
DOC	48.4000	11.1834	36.4500	10.1427	0.0812
Hanging Drop	28.9333	11.2024	12.6000	4.8867	0.0816
Hydrogel	55.0000	14.7309	10.3333	2.3094	0.0066

To further evaluate the DOC usefulness for anticancer drug screening we treated breast cancer cells with ARQ-761/beta lapachone in 2D culture as well as DOC, HD and HG systems. Beta lapachone (β-lap) is currently in two clinical trials, as a monotherapy for advanced solid tumors (such as lung, breast, pancreatic, colon cancers) and in combinational therapy with Gemcitabine/Nab-Paclitaxel for pancreatic cancer (Beg et al., 2017; Silvers et al., 2017). We selected cell lines from three subtypes of breast cancer and treated them with a range of concentration (2-8 μM) of β-lap for two hours, since this concentration range was previously shown to induce cytotoxicity in different breast cancer cells lines (including MCF-7, T47D and MDA-MB-468) (Pink et al., 2000). Based on the results from 2D culture and determination of LD50 (a drug dose which causes 50% cell death) (Figure 2. A), we identified MDA-MB-231 cells (triple negative) as resistant to β-lap, T47D cells (luminal A), as moderately sensitive to β-lap and HCC1954 (HER2-positive) as highly sensitive to β-lap as shown by staining for cisplatin and γ- H2AX. Tumor nodules formed by each cell lines were treated with the same range of β-lap concentrations in DOC as well as HD and HG (PuraMatrix) models. The duration of β-lap exposure for all the cell lines was similar (two hours); however, the culture times prior to treatment varied based on the time needed for tumor formation in the different culture models (the nodules preformed in the presence of Matrigel for three days, were cultured in DOC for two days. For HD, cancer cells were seeded in 20 μl drops of cell culture medium either on the inverted lid of the petri dish or in the HD plates for three days. For the HG, the cancer cells were mixed with the PuraMatrix hydrogel and cultured for four days to form the nodules). To measure the anticancer activity of β-lap treatment we used apoptosis (caspase 3) and DNA damage (γ-H2AX) markers as well as nuclear condensation based on cell nucleus staining with DAPI. For MDA-MB-231 the LD50 could not be estimated within the β-lap concentrations range (2-8 μM) for any of the culture systems (Figure 2. B). The observed LD50 for DOC and HG with higher drug concentrations in Figure 2. B was only extrapolated by the JMP statistical software and was not concluded from our results. However, the number of dead cells in HG increased with increasing concentrations of β-lap. This is in agreement with our previous data showing that cancer cells in the HG model are usually highly responsive to anticancer drugs. The T47D cells showed the highest sensitivity to β-lap in HG and HD (LD 50 of 3 and 5 μM respectively), while only with the highest dose of the drug (8 μM) the LD50 could be observed in the DOC model (Figure 2. C). The HCC1954 cells that are the most sensitive based on drug testing done in 2D

culture (Figure 2A) did not respond to the drug in the DOC model until the highest concentrations of β-lap in the range were reached.

These cells showed highest β-lap sensitivity in both HG and HD systems (Figure 2. D). Together, these data predicted that ARQ-761 (β-lap) might be very effective in luminal A tumors and HER2 positive tumors based on HG and HD systems, whereas the DOC indicated that for the drug to be effective higher concentrations needed to be reached. Regardless of the culture system triple negative tumors notoriously resistant to chemotherapy were also difficult to treat with β-lap. These assessments were performed blindly as the phase I clinical results, which currently shows low performance of β-lap in multiple types of solid tumors including lung, colorectal, pancreas, breast, etc., were not out yet at the time when our cell culture results were obtained. In fact, out of 32 evaluable patients, the best response was stable disease (n=12) and six had tumor shrinkage which shows that ARQ-761 has modest single-agent activity (Gerber et al., 2018). These data suggest that the DOC is the only 3D cell culture model out of the three systems tested to reveal the modest sensitivity level to β-lap.

The hemichannels of the DOC have been prepared in two different manners. Initially the hemichannel was in a square shape (Grafton, Wang, Vidi, Leary, & Lelievre, 2011) but the S1 cells were reproducing a curved channel by piling up in the corners. This configuration was not physiologically relevant and led us to laser-carve the hemichannels to obtain a smooth curvature (Vidi et al., 2014). To determine the importance of the initial geometry of the hemichannel for tumor phenotypes, tumor nodules were prepared using a Matrigel drip for three days and released from the gel to be placed in the DOC (with curved hemichannel) or the initial device with square hemichannels both covered with the monolayer of polarized non-neoplastic epithelial S1 cells. Tumor size, and nuclear area and circularity were significantly bigger in the square shape hemichannel compared with the current DOC model (Figure 3 A-D). Importantly, only in DOC hemichannels, did cancer cells show a significantly higher sensitivity to cisplatin for the triple negative T4-2 cells, compared with the control group (Figure 3. E). Therefore, the initial geometry of the DOC matters to conduct drug sensitivity experiments.

Figure 2. A. MDA-MB-231(triple negative), T47D (luminal A) and HCC1954 (HER2-positive) breast cancer cell lines were cultured (as a monolayer in 2D) for 48 h, then treated with 0, 0.5, 2, 4, 6, 8, 12, 14 μM of Beta-lapachone for two hours, following bya rest (beta-lapachone free medium) for 48 hours. After paraformaldehyde fixation the cells were immunostained for Caspase-3 (apoptosis marker), Gamma-H2AX (DNA damage marker) and the number of dead cells or cells with high number of Gamma-H2AX foci were visually scored using fluorescence microscopy. Shown are the curves representing beta lapachone dose responsve curves. **B.** MDA-MB-231(Triple Negative) **C.** T47D (Luminal A) **D.** HCC-1954 (HER2 positive) cells were cultured as nodules on the DOC for two days/ as suspension of cells in hanging drop (HD) for three days/ as a mixture with PuraMatrix hydrogel (HG) for four days. The cells in different cultures were then treated with 0, 0.5, 2, 4, 6, 8 μM of Beta-Lapachone for two hours and then left in culture for 48 hours in drug-free medium. The cells were immuonostained and analyzed for cell death as explained for 2D culture. N=4 with 50 nuclei scored per replicate.

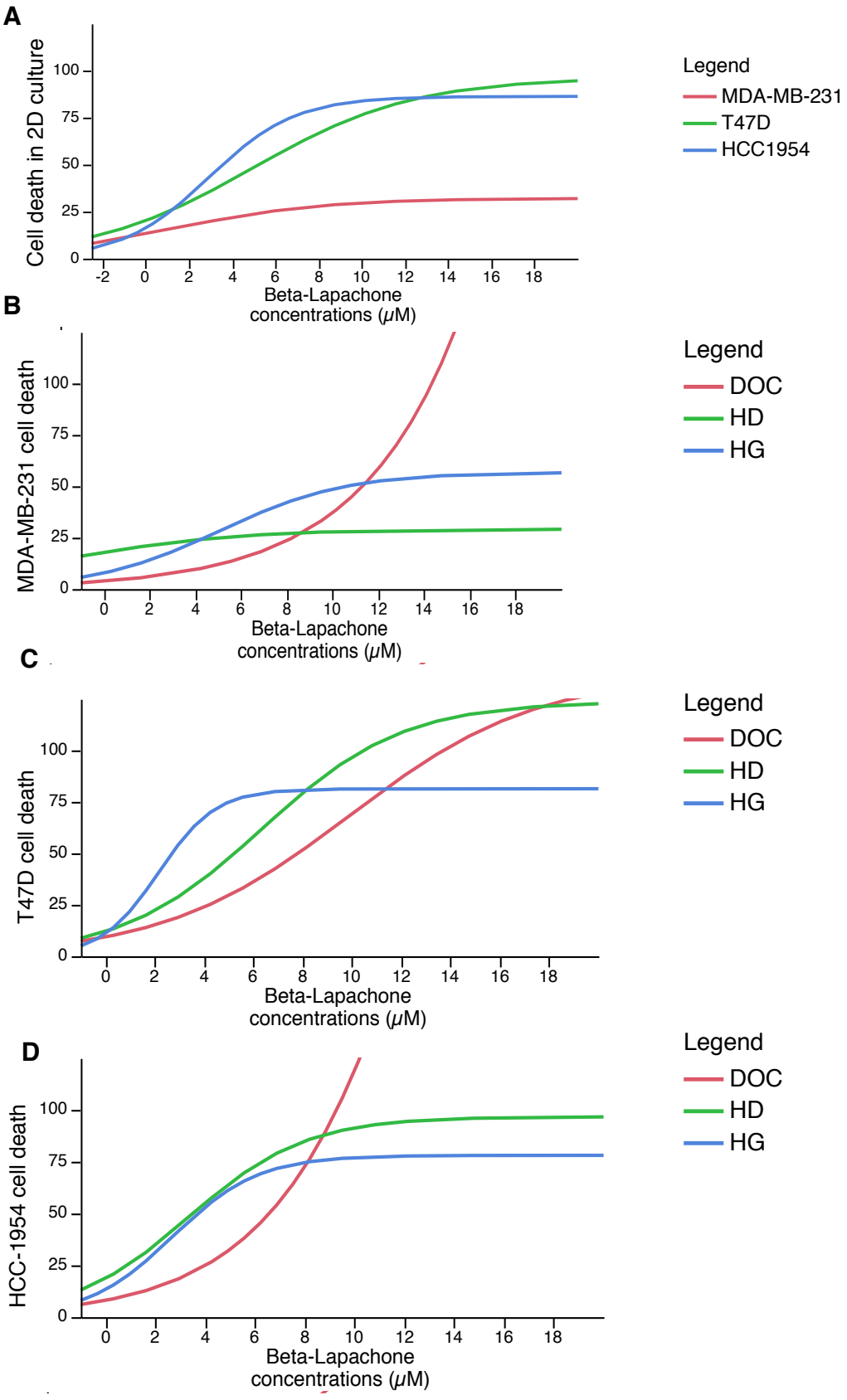
A
Cell death in 2D culture
100
75
50
25
0
-2 0 2 4 6 8 10 12 14 16 18
Beta-Lapachone concentrations (μM)
Legend
MDA-MB-231
T47D
HCC1954
B
MDA-MB-231 cell death
100
75
50
25
0
0 2 4 6 8 10 12 14 16 18
Beta-Lapachone concentrations (μM)
Legend
DOC
HD
HG
C
T47D cell death
100
75
50
25
0
0 2 4 6 8 10 12 14 16 18
Beta-Lapachone concentrations (μM)
Legend
DOC
HD
HG
D
HCC-1954 cell death
100
75
50
25
0
0 2 4 6 8 10 12 14 16 18
Beta-Lapachone concentrations (μM)
Legend
DOC
HD
HG

Improve the DOC system for high throughput drug screening

The data mentioned above suggest that microenvironmental geometry influences nuclear morphometry and the phenotypic response of cancer cells to antiproliferative drugs and that proper geometry is key to improving *in vitro* models for drug screening. However, fast handling of the experiments is an important factor in the drug screening process and the need to precoat the DOC with non-neoplastic cells for 10 days prior to drug testing, added to the requirement to preform tiny tumor (otherwise individual tumor cells would not form a tumor in the presence of the non-neoplastic cells), led us to explore ways to bypass the use of non-neoplastic cell coating. We chose a stearate-modified methyl cellulose, A3DH polymer from Akina, Inc. that can form a gel at biological temperatures (37°C) and has appropriate biocompatibility and physicomechanical properties for the formation of spheroids with tumors cells. A thin layer of 3DCM gel was spin-coated on top of the DOC hemichannels and tumors preformed in Matrigel were deposited on the DOC. The tumor nodules maintained their appearance on the 3DCM coated DOC (Figure 3. F), whereas, in the absence of epithelial cells tumor nodules fell apart and cells were spread out as a monolayer if only laminin coating was used (results not shown). Importantly, 3DCM gel-coated DOC, on which individual cancer cells were directly seeded, also permitted the formation of tumor nodules, further simplifying the cell culture process (Figure 3. G).

Figure 3. A. Tumors made by T4-2 cells were removed from Matrigel at day 3 and seeded in hemichannels with curved shape (DOC) or square shape. Tumor cells were stained with DAPI and DiI, then the sizes were analyzed using Imagej software. **B.** Image on the right and left panels are representing T4-nodule in a curved and square shape hemichannels respectively. The dashed line shows the area in which the tumors expand. The sizes of the channels are similar (however, the size might look bigger for the square shape channel compared to the DOC, this is due to the fact that the bottom area of the square shape channel is bigger (simply because of its geometry) in comparison with the curved hemichannel. The red staining is DiI (the tumor cells were stained with DiI before being seeded in thehemi channels). Nuclei were stained with DAPI (blue). **C and D.** Nuclear morphometry (area, circularity) analysis for triple negative breast cancer cells (T4-2) in DOC vs square shape channel. **E.** Graph showing the sensitivity of T4-2 cells to 50 μM of cisplatin in square shape hemichannel vs. DOC. Caspase 3 immunostaining was used to assess cell death. **F.** Previously formed T4-2 nodules cultured on the DOC devices with a thin layer of 3DCM hydrogel for 48 hr. The nodules were fixed and stained with DAPI **G.** T4-2 cells were cultured as single cells on the A3DH coated duct for 72 hours to allow tumor formation. The cells were then fixed with paraformaldehyde and stained with DAPI. N=3, 100 nuclei were scored per condition. Scale bar 20 μm, *P<0.05.

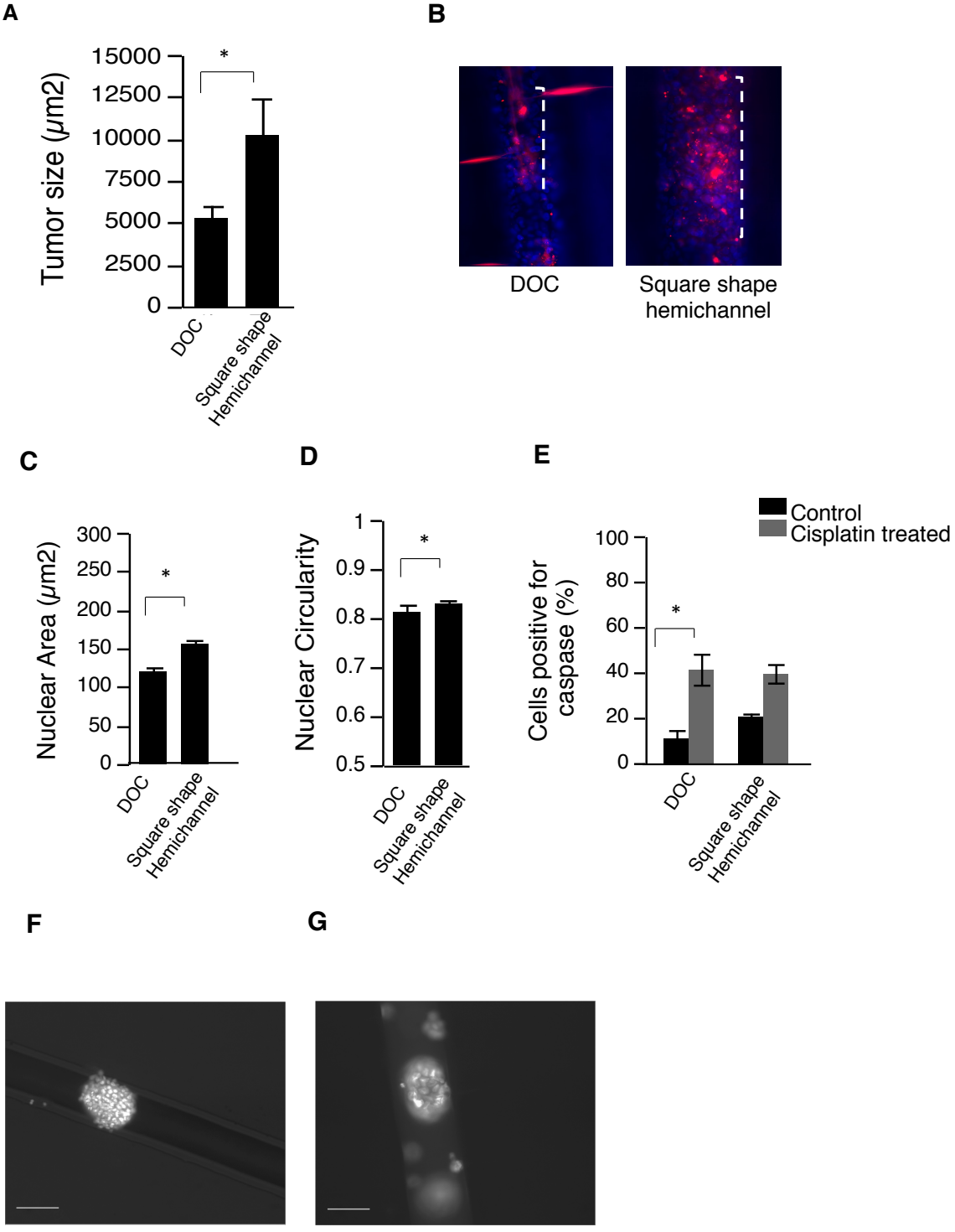
A
Tumor size (μm2)
15000
12500
10000
7500
5000
2500
0
*
DOC
Square shape Hemichannel
B
DOC
Square shape hemichannel
C
Nuclear Area (μm2)
300
250
200
150
100
50
0
*
DOC
Square shape Hemichannel
D
Nuclear Circularity
1
0.9
0.8
0.7
0.6
0.5
*
DOC
Square shape Hemichannel
E
Control
Cisplatin treated
Cells positive for caspase (%)
100
80
60
40
20
0
*
DOC
Square shape Hemichannel
F
G

3.12 Discussion

Well-defined three-dimensional (3D) *in vitro* cancer models that mimic the tumor architecture found *in vivo* and allow cell–cell and cell–matrix interactions have received increasing attention for a wide variety of prognostic and therapeutic applications. We have developed a physiologically relevant *in vitro* system, called Disease on-a-chip (DOC), for epithelial cancers, notably those developing within ducts (e.g., breast, prostate), that shows superiority compared to other classical models for drug screening. Compared to HD plates and PuraMatrix peptide HG that are commercially available and widely advertised for drug screening, the DOC was the only system to distinguish between the false positive/negative drug responses as observed *in vivo* compared to the other two systems. Moreover, only the DOC, but not the other two systems tested, induced a nuclear morphometry (area and circularity) of tumors formed *in vitro* that is not statistically different from real tumor samples of the same cancer types.

A few experiments are still ongoing to finish this manuscript. We anticipate that the DOC can be used for drug discovery to identify new targets by providing a physiologically relevant system to study pathways that control human cancer behavior and development. Indeed, the importance of 3D culture to modulate signaling pathways has been firmly established (F. Wang et al., 1998; Weaver et al., 1997) Further confirmation of the superiority of the DOC for drug testing and screening would make this system a filter to significantly reduce the number of drugs to be tested in current standard animal models, hence reducing the burden of drug research and development on animals and financially. Another important goal of this project is to optimize the DOC system at the clinical level for individualized therapy approach. Every patient has a unique set of molecular factors and genetic background, which influences their response to therapies (Ogino, Fuchs, & Giovannucci, 2012; Wheler, Lee, & Kurzrock, 2014). But even if the patient has the necessary molecular and genetic profile to withstand a given therapy based on optimal activation or metabolism of the therapeutic components, the efficacy of the treatment might be challenged at the tumor site, not by the genetic make-up of the cancer cells but by the tumor organization. Therefore, preclinical models that can test the drug sensitivity of patients' tumors in context are an absolute necessity. Although, patient derived xenograft (PDX) models maintain many features of the native tumor (e.g., metastatic potential, gene expression pattern) multiple limitations such as the use of immunocompromised rodent as hosts for human tumors and the replacement of human stroma with murine connective tissue (Kurdistani, 2014; Seligson et al., 2009) are

triggering a quest for dependable preclinical models. The translational power of the DOC would be to facilitate the comparison of efficacy of a panel of drugs or drug combinations for individual patients in the same test (as the DOC can be scaled up for high-throughput screening in 96-well plate; unpublished data), hence leading to faster and more accurate prognostic and consideration of therapeutic options and improvement of healthcare delivery.

3.13 Materials and Methods

Cell culture

Non-neoplastic S1 HMT-3522 breast epithelial cells (Briand et al., 1987) were seeded at 2.4 × 10^4 cells/cm^2 and cultured between passages 52 and 60 in H14 medium [Dulbecco's modified Eagle's medium (DMEM)/F12 (Invitrogen), supplemented with 5 µg/ml prolactin (Sigma-Aldrich), 250 ng/ml insulin (Sigma-Aldrich), 2.6 ng/ml sodium selenite (BD Biosciences), 2.67 x 10^{-8} µg/ml

β-estradiol (Sigma-Aldrich), 0.5 µg/ml hydrocortisone (Sigma-Aldrich), 10 µg/ml transferrin (Sigma-Aldrich) and 5 ng/ml Epidermal Growth Factor (EGF) (BD Biosciences)] as previously described. S1-derived malignant T4–2 HMT-3522 cells (Briand et al., 1987). MDA-MB-231, HCC1954, T47D and BT474 cells were obtained from American Tissue Culture Collection (ATCC, Manasas, VA) and seeded at 1.16 × 10^4 cells/cm^2 and cultured in H14 medium without EGF (Briand et al., 1987). Malignant cells were used after four to six days in 2D culture and after two to four days when tumor formation was the goal (Matrigel, DOC, hydrogel and hanging drop). For the drip method, cancer cells were seeded on a thin layer of EHS-derived hydrogel (Matrigel, BD Biosciences) in H14 that was supplemented with 5% Matrigel drip, as described previously (Plachot et al., 2009). The co-culture of different cancer nodules (that were prepared in Matrigel) with S1 cells on the DOC model was performed following published steps (Vidi et al., 2012). The 3D culture of cancer cells in PuraMatrix™ Peptide Hydrogel (Corning, Tewksbury, MA) was performed based on a previously published method (Abu-Yousif et al., 2009). The nodule formation of cancer cells in hanging drop was achieved by mixing a 20 µl aliquot of the cell culture medium with the desired number of cells (8000 cells for T4-2, T47D and HCC1954 and 4000 cells for MDA-MB-231), in a HD plates or on the inverted lid of the petri dish for two-three days. In drug treatment experiments, cells were incubated with 50 µM of

cisplatin (Sigma-Aldrich, St Louis, MO) for 24 hours, or 10 μM of SAHA (Sigma-Aldrich) for 24 hours followed by 24 hour in drug-free medium, or in 0, 0.5, 2, 4, 6, 8 μM of Beta-Lapachone (a gift from Dr. Boothman, University of Texas Southwestern Medical Center, Dallas, Texas) for two hours and then cultured in drug free medium for 48 hours (Silvers et al., 2017). For certain experiments, cancer cells were treated with diI (Thermo Fisher Scientific, Waltham, MA Cat #D-282; stock solution 1 mg/ml) a vital dye that is not toxic for the HMT3522 cells in 3D culture, for 30 minutes in the cell culture incubator at 37°C prior to cell seeding.

Fabrication of the DOC

Acrylic was used to prepare hemichannels of 100 μm in width to mimic the diameter of the terminal ducts in the breast (where tumors arise normally). The in-house preparation of these channels has been described previously (Vidi et al., 2014).

These chips were sterilized by ethylene oxide exposure in an Anprolene Sterilizer model AN74i (Andersen Products Inc.). Sterilization was performed in accordance with the manufacturer's instructions for a 24-hour sterilization cycle and ETO exposure confirmed by observing color-change on enclosed Anpro Dosimeter (Andersen Products Inc.). The sterilized products were aseptically handled and packaged in sterilized materials in a UV laminar flow hood (Labconco Purifier Class II biosafety cabinet, Model 36204-00) wiped down with 70% ethanol (Decon Laboratories) solution.

Antibodies

Caspase-3 (Cell Signaling Technologies, Boston, MA 1/300 dilution), γ- H2AX (Ser139; Millipore, clone JBW301, 3.3 μg/ml), Ki67 (Vector Laboratories, Inc., Burlingame, CA, 0.1 μg/ml)

Immunofluorescence staining of cell in cultures

Immunofluorescence labelling was performed as described previously (Plachot & Lelievre, 2004). Overnight incubation at 4°C with primary antibodies encompassed monoclonal antibodies for caspase-3, Ki67 and incubation for 50 minutes at room temperature with secondary antibodies including either 12.5 μg/ml fluorescein isothiocyanate (FITC)-conjugated donkey anti-rabbit IgG (Jackson Immunoresearch, West Grove, PA) or 6.7 μg/ml Alexa-Fluor 568-conjugated goat anti-

mouse IgG (InVitrogen Corporation). Nuclei were counterstained for DNA with 0.5 μg/ml DAPI. After removal of excess DAPI, samples were mounted with ProLong® Diamond antifade reagent.

Image acquisition and analysis

Immunofluorescence images were captured using Q-capture image acquisition software linked to a IX70 inverted fluorescence microscope (Olympus, Waltham, MA), with 20 x objective (NA = 0.5) and the images were processed using the image analysis software *ImageJ*.

Statistical analysis

Statistical analysis was performed using JMP® 13.2.0 software. Data are presented as means ± s.e.m. We used unpaired Student's *t*-test for comparison of two conditions, analysis of variance (ANOVA) with Tukey's HSD (Honest Significant Difference) test for comparison of more than two conditions. $P < 0.05$ was considered significant.

Based on JMP software manual guideline (SAS Institute Inc. 2012) sigmoid curves were generated to model dose response curve. The graphs were generated via Analyze>specialized Modeling>Fit Curve>Sigmoid Curves>Logistic Curves.

3.14 References

Abu-Yousif, A. O., Rizvi, I., Evans, C. L., Celli, J. P., & Hasan, T. (2009). PuraMatrix encapsulation of cancer cells. *J Vis Exp*(34). doi:10.3791/1692

Beg, M. S., Huang, X., Silvers, M. A., Gerber, D. E., Bolluyt, J., Sarode, V., . . . Boothman, D. A. (2017). Using a novel NQO1 bioactivatable drug, beta-lapachone (ARQ761), to enhance chemotherapeutic effects by metabolic modulation in pancreatic cancer. *J Surg Oncol, 116*(1), 83-88. doi:10.1002/jso.24624

Briand, P., Petersen, O. W., & Van Deurs, B. (1987). A new diploid nontumorigenic human breast epithelial cell line isolated and propagated in chemically defined medium. *In Vitro Cell Dev Biol, 23*(3), 181-188.

Chittiboyina, S., Rahimi, R., Atrian, F., Ochoa, M., Ziaie, B., & Lelièvre, S. A. (2017). Gradient-on-a-Chip with Reactive Oxygen Species Reveals Thresholds in the Nucleus Response of Cancer Cells Depending on the Matrix Environment. *ACS Biomaterials Science & Engineering, 4*(2), 432-445. doi:10.1021/acsbiomaterials.7b00087

Eckschlager, T., Plch, J., Stiborova, M., & Hrabeta, J. (2017). Histone Deacetylase Inhibitors as Anticancer Drugs. *Int J Mol Sci, 18*(7). doi:10.3390/ijms18071414

Edmondson, R., Broglie, J. J., Adcock, A. F., & Yang, L. (2014). Three-dimensional cell culture systems and their applications in drug discovery and cell-based biosensors. *Assay Drug Dev Technol, 12*(4), 207-218. doi:10.1089/adt.2014.573

Gerber, D. E., Beg, M. S., Fattah, F., Frankel, A. E., Fatunde, O., Arriaga, Y., . . . Boothman, D. A. (2018). Phase 1 study of ARQ 761, a beta-lapachone analogue that promotes NQO1-mediated programmed cancer cell necrosis. *Br J Cancer, 119*(8), 928-936. doi:10.1038/s41416-018-0278-4

Grafton, M. M., Wang, L., Vidi, P. A., Leary, J., & Lelievre, S. A. (2011). Breast on-a-chip: mimicry of the channeling system of the breast for development of theranostics. *Integr Biol (Camb), 3*(4), 451-459. doi:10.1039/c0ib00132e

Kurdistani, S. K. (2014). Chromatin: a capacitor of acetate for integrated regulation of gene expression and cell physiology. *Curr Opin Genet Dev, 26*, 53-58. doi:10.1016/j.gde.2014.06.002

Ogino, S., Fuchs, C. S., & Giovannucci, E. (2012). How many molecular subtypes? Implications of the unique tumor principle in personalized medicine. *Expert Rev Mol Diagn, 12*(6), 621-628. doi:10.1586/erm.12.46

Petrelli, F., Coinu, A., Borgonovo, K., Cabiddu, M., Ghilardi, M., Lonati, V., & Barni, S. (2014). The value of platinum agents as neoadjuvant chemotherapy in triple-negative breast cancers: a systematic review and meta-analysis. *Breast Cancer Res Treat, 144*(2), 223-232. doi:10.1007/s10549-014-2876-z

Pink, J. J., Planchon, S. M., Tagliarino, C., Varnes, M. E., Siegel, D., & Boothman, D. A. (2000). NAD(P)H:Quinone oxidoreductase activity is the principal determinant of beta-lapachone cytotoxicity. *J Biol Chem, 275*(8), 5416-5424.

Plachot, C., Chaboub, L. S., Adissu, H. A., Wang, L., Urazaev, A., Sturgis, J., . . . Lelievre, S. A. (2009). Factors necessary to produce basoapical polarity in human glandular epithelium formed in conventional and high-throughput three-dimensional culture: example of the breast epithelium. *BMC Biol, 7*, 77. doi:10.1186/1741-7007-7-77

Plachot, C., & Lelievre, S. A. (2004). DNA methylation control of tissue polarity and cellular differentiation in the mammary epithelium. *Exp Cell Res, 298*(1), 122-132. doi:10.1016/j.yexcr.2004.04.024

Seligson, D. B., Horvath, S., McBrian, M. A., Mah, V., Yu, H., Tze, S., . . . Kurdistani, S. K. (2009). Global levels of histone modifications predict prognosis in different cancers. *Am J Pathol, 174*(5), 1619-1628. doi:10.2353/ajpath.2009.080874

Silver, D. P., Richardson, A. L., Eklund, A. C., Wang, Z. C., Szallasi, Z., Li, Q., . . . Garber, J. E. (2010). Efficacy of neoadjuvant Cisplatin in triple-negative breast cancer. *J Clin Oncol, 28*(7), 1145-1153. doi:10.1200/JCO.2009.22.4725

Silvers, M. A., Deja, S., Singh, N., Egnatchik, R. A., Sudderth, J., Luo, X., . . . Merritt, M. E. (2017). The NQO1 bioactivatable drug, beta-lapachone, alters the redox state of NQO1+ pancreatic cancer cells, causing perturbation in central carbon metabolism. *J Biol Chem, 292*(44), 18203-18216. doi:10.1074/jbc.M117.813923

Vidi, P. A., Chandramouly, G., Gray, M., Wang, L., Liu, E., Kim, J. J., . . . Lelievre, S. A. (2012). Interconnected contribution of tissue morphogenesis and the nuclear protein NuMA to the DNA damage response. *J Cell Sci, 125*(Pt 2), 350-361. doi:10.1242/jcs.089177

Vidi, P. A., Maleki, T., Ochoa, M., Wang, L., Clark, S. M., Leary, J. F., & Lelievre, S. A. (2014). Disease-on-a-chip: mimicry of tumor growth in mammary ducts. *Lab Chip, 14*(1), 172-177. doi:10.1039/c3lc50819f

Walters, R. S., Theriault, R. L., Holmes, F. A., Hortobagyi, G. N., & Esparza, L. (1992). Phase II trial of fazarabine (ARA-AC, arabinosyl-5-azacytosine) in metastatic breast cancer. *Invest New Drugs, 10*(1), 43-44.

Wang, F., Weaver, V. M., Petersen, O. W., Larabell, C. A., Dedhar, S., Briand, P., . . . Bissell, M. J. (1998). Reciprocal interactions between beta1-integrin and epidermal growth factor receptor in three-dimensional basement membrane breast cultures: a different perspective in epithelial biology. *Proc Natl Acad Sci U S A, 95*(25), 14821-14826.

Weaver, V. M., Petersen, O. W., Wang, F., Larabell, C. A., Briand, P., Damsky, C., & Bissell, M. J. (1997). Reversion of the malignant phenotype of human breast cells in three-dimensional culture and in vivo by integrin blocking antibodies. *J Cell Biol, 137*(1), 231-245.

Wheler, J., Lee, J. J., & Kurzrock, R. (2014). Unique molecular landscapes in cancer: implications for individualized, curated drug combinations. *Cancer Res, 74*(24), 7181-7184. doi:10.1158/0008-5472.CAN-14-2329

SAS Institute Inc. 2012. JMP® 10 Modeling and Multivariate Methods. Cary, NC: SAS Institute Inc

APPENDIX B. MINING THE EPIGENETIC LANDSCAPE OF TISSUE POLARITY IN SEARCH OF NEW TARGETS FOR CANCER THERAPY

Special Report

For reprint orders, please contact: reprints@futuremedicine.com

Epigenomics

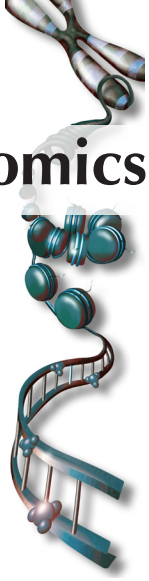

Mining the epigenetic landscape of tissue polarity in search of new targets for cancer therapy

Farzaneh Atrian[1] & Sophie A Lelièvre*,[1]

[1]Department of Basic Medical Sciences & Center for Cancer Research, Purdue University, 625 Harrison Street, Lynn Hall, West Lafayette, IN 47906, USA

*Author for correspondence:
Tel.: +1 765 496 7881;
Fax: +1 765 494 0781;
lelievre@purdue.edu

The epigenetic nature of cancer encourages the development of inhibitors of epigenetic pathways. Yet, the clinical use for solid tumors of approved epigenetic drugs is meager. We argue that this situation might improve upon understanding the coinfluence between epigenetic pathways and tissue architecture. We present emerging information on the epigenetic control of the polarity axis, a central feature of epithelial architecture created by the orderly distribution of multiprotein complexes at cell–cell and cell–extracellular matrix contacts and altered upon cancer onset (with apical polarity loss), invasive progression (with basolateral polarity loss) and metastatic development (with basoapical polarity imbalance). This information combined with the impact of polarity-related proteins on epigenetic mechanisms of cancer enables us to envision how to guide the choice of drugs specific for distinct epigenetic modifiers, in order to halt cancer development and counter the consequences of polarity alterations.

First draft submitted: 29 January 2015; Accepted for publication: 13 August 2015; Published online: 8 December 2015

Keywords: basoapical polarity • cancer • DNA methylation • epigenetic drug • epithelial-to-mesenchymal transition • EZH2 • histone modification • tissue architecture

An organ is defined by the exquisite arrangement of its cells into functional units; cancer is the negation of such arrangement. Examples of functional units made of epithelial cells encompass crypts, glandular structures, alveoli and ducts. For all epithelial units, the arrangement of cells follows a specific architectural plan dictated by cell–cell and cell–extracellular matrix (ECM) adhesion and communication complexes. The differential location of cell–cell and cell–ECM complexes participates in the formation of the polarity axis, which is the main feature of epithelial tissue architecture (Figure 1). It has been amply demonstrated that tissue architecture directs the cells' function and maintains homeostasis, including cell survival, proliferation and invasion capability [1]. Thus, unless tissue architecture is compromised, cancer can neither start, nor progress.

Epigenetic dysregulation, which affects the chemical modifications of DNA and histones controlling gene transcription and involves epigenetic enzymes and certain chromatin-associated proteins, is a major cause of carcinogenesis and cancer progression [2–5]. Less well known is the notion that epigenetic pathways are linked to tissue polarity (i.e., the presence of different multiprotein complexes along an axis going from the basal pole at cell–ECM contacts, via lateral cell–cell contacts and to the apical pole, against the lumen). A decade ago such a link was brought to light in a 3D cell culture model of phenotypically normal breast glandular differentiation via the demonstration that chemically induced DNA hypomethylation prevented the formation of the apical pole of the polarity axis, as defined by the presence of tight junctions against the lumen of glandular structures [6]. Moreover,

Future Medicine part of fsg

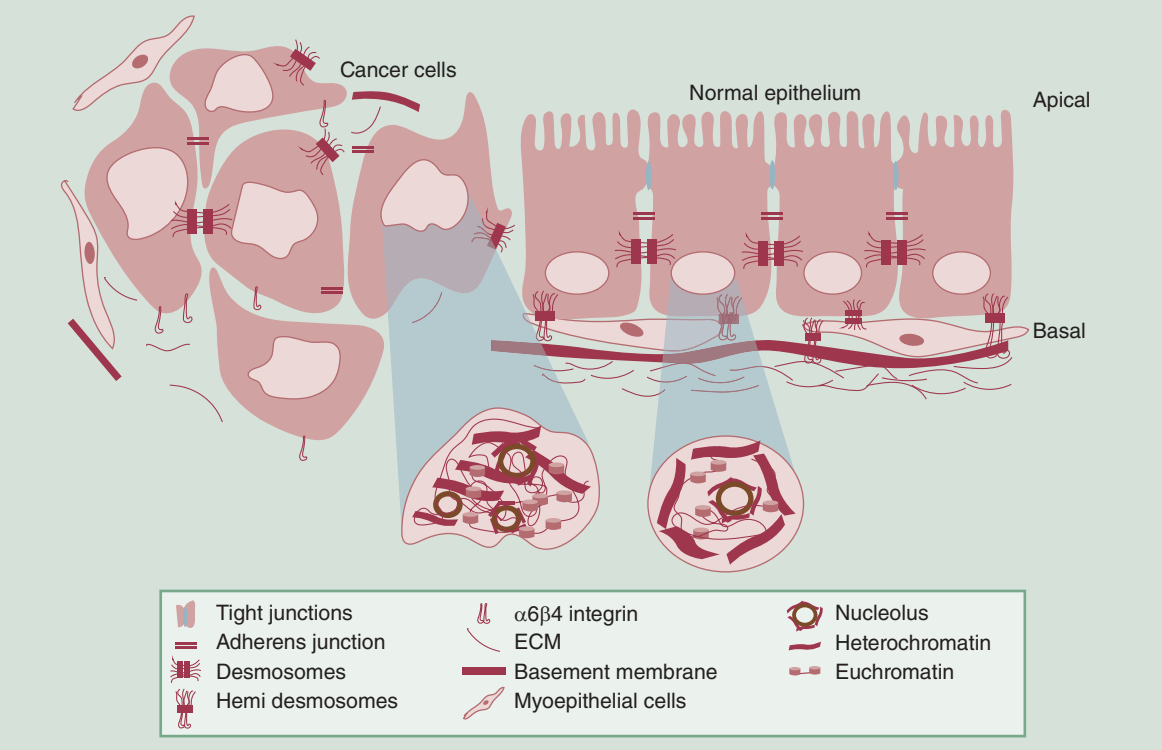

Figure 1. Normal breast epithelium and cancerous tissue differ in terms of architecture and nuclear organization.
Normal epithelial cells interact with each other and their extracellular environment via adhesion complexes (tight junctions, adherens junctions, desmosomes, hemidesmosomes [formed by β4-α6 integrin dimers]) that are differentially distributed on the apicolateral (at cell–cell contacts) and basal (against the basement membrane) sides of cells. This differential distribution can be used to identify, by immunostaining, specific changes in the polarity axis. These changes are used as readout for alterations such as apical polarity loss, basal polarity loss and epithelial–mesenchymal transition that accompany different stages of cancer development. The nuclear morphology is generally round or oval and heterochromatin domains are mainly at the nuclear periphery and perinucleolar area. In cancer cells adhesion complexes appear randomly localized and are often incomplete; the nuclear organization undergoes major alterations, such as increased size and convoluted morphology, as well as a redistribution of euchromatin and heterochromatin domains that illustrates the epigenetic remodeling in cancer development.
ECM: Extracellular matrix.

the establishment of the polarity axis appeared to be accompanied with a specific distribution of epigenetic marks of heterochromatin [7]. Since then, the increasing number of reports on the implication of polarity multiprotein complexes located at the cell membrane in downstream signaling related to transcription regulation has led to further evidence of a connection between tissue architecture and epigenome [1,8].

The role of epigenetic regulation in cancer is increasingly understood thanks to advances in the development of inhibitors specific for each type of enzyme responsible for distinct epigenetic modifications [9]. However, the potential for epigenetic pathways to provide effective targets in anticancer therapies is hampered by the lack of knowledge regarding how the cellular organization controlling the homeostasis of a particular tissue relates to epigenetic mechanisms. In this special report, using the epithelial polarity axis as main example, we present tissue architecture as a higher order of epigenetic control and discuss how understanding the relationship between epithelial polarity and epigenome might lead to more effective cancer therapies.

Tissue architecture, a progressive view of epigenetic regulation

Gradual alterations in the polarity axis illustrate major stages in cancer development, from tumor onset that requires loss of apical polarity (via the disruption of tight junctions), to invasion characterized by loss of basal polarity (via the disruption of hemidesmosomes) and metastasis associated with an overall imbalance in polarity, exemplified by epithelial–mesenchymal transition or EMT (via an impact on E-cadherin, β4-integrin, Crb, etc.). These stages are increasingly demonstrated to be associated with epigenetic modifications and, even, to be under epigenetic control. In the next paragraphs we illustrate the link between the

epigenome and cancer stages corresponding to specific alterations in the polarity axis. For each of these stages, as information is available, we present overall changes in epigenetic marks linked to alterations in polarity, before giving examples of indirect (e.g., via the control of epigenetic modifier compartmentalization and signal transduction) and direct impacts of polarity elements on epigenetic pathways. We also discuss the epigenetic regulation of polarity proteins involved in cancer onset and progression.

Loss of apical polarity is measured by the redistribution of apical polarity proteins away from the apical pole of luminal epithelial cells. This architectural alteration has been proposed as a necessary initial step in tumor onset since it allows cells to exit quiescence [10]. Moreover, apical polarity proteins like Scrib, Dlg and Lgl, have been shown to act as tumor suppressors [1,11–12]. An interesting attribute of apical polarity is to indirectly regulate epigenetic mechanisms via its propensity to trap proteins involved in gene transcription control. For instance, tight junction proteins ZO-1 and ZO-2 direct gene transcription by regulating the compartmentalization of transcription factor ZONAB. Once released from tight junctions, ZONAB promotes the transcription of genes involved in proliferation. ZONAB also influences the expression of histone 4 and high-mobility group HMG proteins involved in chromatin structure [13,14]. Transcription factor HuASH1, the human homolog of *Drosophila* protein ASH1, localizes both in the cell nucleus and within the apical polarity complex, at tight junctions; it functions as a histone methyltransferase specific for H3K4 (histone3 Lys4) and, as such, is associated with the transcribed regions of several highly active genes involved in cellular homeostasis [15,16]. Another example of indirect influence of apical polarity on epigenetic regulation is the promotion of MAPK pathway by the Par polarity complex that subsequently triggers the phosphorylation of histone 3 and HMG proteins [1,17–18].

A direct epigenetic influence of apical polarity proteins has been reported as well, although more research in this area is awaited. The polarity axis proteins ZO-1, ZO-2 and β-catenin are known to shuttle between cytoplasm and nucleus where they participate in the epigenetic regulation of gene transcription. For instance, β-catenin directly interacts with EZH2 of the polycomb group (PcG), resulting in the enhancement of gene transactivation by the Wnt signaling pathway [19]. The tumor suppressor APC, well known for its control of differentiation and polarity, regulates a DNA demethylase pathway. Hypomethylation of specific gene loci upon loss of APC contributes to an undifferentiated state of intestinal cells, which possibly underlies the mechanisms of colon cancer development [20]. Additional investigations are necessary to unravel the mechanisms by which apical polarity controls tumor onset. Encouragingly, studies in *Drosophila* have recently demonstrated the existence of enhancers that act as polarity-responsive elements and require both signaling (via JNK and aPKC) and epigenetic modulation by PcG for the activation of gene transcription leading to neoplastic growth [21].

Loss of basolateral polarity enables cancer progression to invasion and metastasis. The hemidesmosomes, formed by dimers of α6β4-integrins responsible for basal polarity, and adherens junctions, characterized by E-cadherin–β-catenin interactions, are essential for the control of these cancer stages [1,22–23]. E-cadherin is downregulated during the progression of certain tumors, leading to accumulation of β-catenin in the cell nucleus and dedifferentiation and invasiveness of carcinoma cells. As an example of epigenetic impact, once in the cell nucleus, β-catenin binds to the HMG type transcription factor LEF/TCF to activate Wnt responsive genes [24].

At this time a breadth of information on a link between epigenetic changes and polarity concerns EMT leading to cancer progression, including metastasis [25]. The mechanisms of EMT trigger a profound alteration of the polarity axis. Indeed, during EMT, E-cadherin as well as basal polarity α6β4-integrins and apical polarity proteins Lgl1, Scrib, Crb3 and Par3 are downregulated, whereas mesenchymal phenotype-specific proteins are transiently upregulated. The mesenchymal phenotype permits increased migratory and invasiveness capacity as well as higher resistance to apoptosis, hence facilitating cancer progression [26]. Importantly, upon TGFβ-induced EMT in the murine mammary gland the loss of expression of β4-integrin and E-cadherin has been associated with epigenetic modifications throughout the genome, including DNA methylation, a decrease in the amounts of histone 3 trimethylated on lysine 4 (H3K4me3) and histone 3 acetylated on lysine 9 (H3K9Ac), and an increase in the repressive histone modification histone 3 trimethylated on lysine 27 (H3K27me3) [27]. TGFβ-induced EMT in mouse hepatocytes also induced genome-wide reprogramming with a decrease in heterochromatin mark H3K9me2 and an increase in euchromatin mark H3K4me3 as well as transcriptional mark H3K36me3; yet, EMT occurred with no apparent change in DNA methylation pattern [28]. This example suggests that epigenetic modifications as common as DNA methylation in EMT are tissue dependent. How α6β4-integrins control gene expression by affecting the epigenetic environment at specific loci remains to be fully deciphered. The possibility that

they mainly target DNA methylation is strongly considered in light of the negative correlation between the methylation of *S100A4* gene promoter and the presence of this integrin dimer resulting in increased expression of the *S100A4* gene in melanoma cancer cells [29].

The impact of polarity alterations reported above on epigenetic marks, whether indirect or direct, ought to be further investigated in order to build a map of epigenetic changes and associated mechanisms under polarity control. However, there is another essential and obvious aspect of the relationship between polarity and epigenome that we wish to discuss as it relates to the epigenetic control of tissue polarity per se. Importantly, epigenetic silencing of polarity proteins involved in cancer progression has been reported. For instance, the large CpG island of the promoter of the gene coding for β4-integrin is methylated *de novo* upon TGFβ-mediated EMT, which results in the gene's downregulation [27]. The promoter of the gene coding for E-cadherin is shut down through the same mechanisms as β4-integrin. Notably, in a meta-analysis with patients' tissue samples, the methylation of E-cadherin gene has been shown to be associated with increased risk for lung cancer, especially in the Asian population [30]. Interestingly, during reversion of the EMT phenotype, the restoration of β4-integrin expression following TGFβ removal requires enrichment in histone modifications (H3K9Ac, H3K4me3) linked to gene activation at the promoter but not DNA demethylation [27]. Noticeably, Snail-induced EMT in Madin-Darby canine kidney (MDCK) epithelial cells is not associated with the methylation of the promoter of the gene coding for E-cadherin [31]. These findings confirm the importance of cell identity and context for DNA methylation events associated with EMT; they also suggest the great importance of plasticity for histone modifications during cancer progression.

Genes coding for several other polarity proteins have been reported to be epigenetically modified in cancer. Claudin 4 expression is often increased in ovarian cancers with its gene *CLDN4* hypomethylated and enriched with acetylated histone 3 [32]. Cell adhesion molecules (CADMs) that maintain cell polarity and tumor suppression have been found to be downregulated in clear renal cell carcinoma in part via DNA promoter hypermethylation [33]; the downregulation by promoter hypermethylation of CADM-2a seems particularly associated with prostate cancer [34]. The silencing of the gene coding for DACT1 involved in planar polarity, has been associated with promoter DNA hypermethylation in gastric cancer [35]. Promoter methylation of the gene coding for brush border protein MYO1A is present in colorectal tumors and low amounts of MYO1A are associated with tumor development and shorter patient survival [36]. Moreover, promoter methylation of the gene coding for MPP3 is associated with advanced stages of colorectal cancer [37]. The loss of the mesenchyme-specific transcription factor FOXF2 in triple negative breast cancer triggers EMT; FOXF2 disappearance has been associated with the methylation of CpG islands within its gene promoter [38].

In the literature the link between cancer and epigenetic changes is well-illustrated, as is the link between EMT and cancer. In the examples given above it appears that the relation between EMT and epigenetic changes is the most developed so far. Important proteins for EMT like β4-integrin are controlled by epigenetic pathways and some of these polarity proteins also trigger epigenetic changes. Therefore, we can safely consider that polarity loss illustrated by EMT is linked to epigenetic regulation. This assumption is strengthened by studies on signaling pathways that control EMT. Most of these pathways seem ultimately involved in the control of E-cadherin [39]. Moreover, the bivalent control of some of the chromatin domains within the E-cadherin promoter through repressive and active epigenetic regulations has been proposed to be the reason for the transient nature of EMT [40]. ZEB1 and ZEB2 are two important transcriptional repressors of genes coding for E-cadherin (*CDH1*) and polarity proteins Crb and Lgl (*CRB3* and *LGL2*). They are regulated by members of the miRNA 200 family, themselves under DNA methylation control. During metastasis and EMT–mesenchymal–epithelial transition (MET) switch the CpG islands of these miRs are finely tuned via reversible epigenetic mechanisms [41]. In turn, Crb, Lgl and E-cadherin participate in the regulation of the Hippo pathway that senses epithelial tissue architecture, especially polarity, and cell density [42–45]. The four members of the core Hippo signaling pathway, Mst 1–2, Lats1–2, MOBKL1A-B and Sav1/WW45, are themselves considered tumor suppressors [46–48]. Overall, the example of EMT-MET illustrates how the mutual influence of tissue polarity components and epigenetic pathways that enable phenotypic plasticity participates in the intricate regulation of cancer progression.

The epigenetic regulation that controls the maintenance of tissue organization and the epigenetic dysregulation consecutive to the loss of tissue architecture discussed in the previous paragraphs are accompanied with changes in chromatin structure. An example is for instance the involvement of HMG proteins that we illustrated earlier when discussing epigenetics and polarity proteins such as ZONAB, Par and β-catenin. HMG proteins are 'architectural transcription factors' that modify chromatin structure via binding to DNA and nucleosomes, and displacement of histones. The HMGA family in particular controls transcription and is involved in

Table 1. Examples of DNA methyltransferase inhibitors and histone acetyl transferase inhibitors for cancer therapy.

DNA and histone modifiers	Mechanism of action†	Clinical stage	Ref.
DNA methylation inhibitors			
Azacitidine (5-azacytine)	Pan-DNMT inhibition Cytosine analog	Approved for MDS Clinical trials‡ for AML, CML, MM, CMML, CLL, metastatic colorectal cancer, NSCLC	[55–58]
Decitabine (5-aza-2′-deoxycytidine)	Pan-DNMT inhibition Cytosine analog	Approved for MDS Clinical trials for AML, CML, CMML, ovarian cancer, metastases colorectal cancer	[56–57,59–60]
Genistein	Possibly via displacement of the SAM:SAH equilibrium	Clinical trials for prostate, breast, kidney, colorectal cancer, melanoma	[55,61–62]
MG98§; Zebularine, SGI-110 (decitabine prodrug), hydralazine		Clinical trials for MDS, AML, solid tumors	[55,63–64]
HDAC inhibitors			
Vorinostat (SAHA) [hydroxamic acid class]	Inhibitor of class I, (II), IV HDACs	Approved for CTCL; clinical trial‡ for breast cancer, pancreatic cancer, renal cell carcinoma, gastrointestinal cancer, glioblastoma, NSCLC	[65–69]
Romidepsin¶ (FK-228, depsipeptide) [cyclic peptide class]	Inhibitor of class I HDACs	Approved for CTCL and PTCL; clinical trials for prostate cancer, recurrent ovarian epithelial cancer, metastatic breast cancer, pancreatic cancer, NSCLC	[57,67,70]
Panobinostat# [hydroxamic acid class]	Inhibitor of class I, II, IV HDACs	Approved for MM; clinical trial for CTCL, CML, CMML, ALL, MDS, AML, HD, NHD, thyroid cancer, prostate cancer, breast cancer	[57,71]
Belinostat [hydroxamic acid class]	Inhibitor of class I, II, IV HDACs	Approved for relapsed or refractory PTCL; clinical trial for ALL, AML, MS, CML, ovarian cancer, solid tumors and several hematological malignancies	[70]
Pracinostat, abexinostat, resminostat, givinostat, dacinostat, CUDC-101. Mocetinostat, entinostat, valproic acid		Under clinical investigation	[70]

The table includes a list of epigenetic drugs that are currently US FDA approved (note: genistein and valproic acid have been approved for pharmacological treatment for a while, but their epigenetic impact was not known at the time of approval). Some examples of clinical trials are given, notably those with solid cancers (nonexhaustive list). For a recent list of DNMT inhibitors please refer to [55,56] and for a recent list of HDAC inhibitors please refer to [70].

†Only the mainstream mechanisms of action are indicated.

‡Clinical trials for the treatment of solid tumors usually include epigenetic drugs in combination with other anticancer drugs.

§An oligonucleotide antisense to DNMT1 denied US FDA approval due to high toxicity [55].

¶Romidepsin seems to have less activity in general for solid tumors than vorinostat.

#Accelerated approval (continued approval pending).

ALL: Acute lymphocytic leukemia; AML: Acute myeloid leukemia; CLL: Chronic lymphocytic leukemia; CML: Chronic myeloid leukemia; CMML: Chronic myelomonocytic leukemia; CTCL: Cutaneous T-cell lymphoma; DNMTi: DNA methyltransferase inhibitor; HD: Hodgkin Lymphoma; HDACi: Histone deacetylase inhibitor; MDS: Myelodysplastic syndrome; MM: Multiple myeloma; NHD: Non-Hodgkin Lymphoma; NSCLC: Nonsmall cell lung cancer; PTCL: Peripheral T-cell lymphoma; SAHA: Suberoylanilide hydroxamic acid.

EMT [49]. The relationship between chromatin structure and epigenetic mechanisms is well known [50] and is worth considering to improve the understanding of how epigenetic drugs might impact cell fate. Notably, chromatin structure controls further alteration of gene expression by epigenetic mechanisms, hence affecting how cells will respond to drugs that target epigenetic modifiers.

Epigenetic markers controlled by tissue architecture as potential targets for cancer therapy

The development of epigenetic drugs has been encouraged by the possibility of modifying gene transcription to tame cancer cells. Commonly used epigenetic drugs in therapies are mostly drugs with potentially broad impact on the epigenome (Table 1). These drugs belong

to two main categories, inhibitors of DNA methylation and inhibitors of histone deacetylation that might lead to activation of gene expression via chromatin remodeling. Drugs affecting DNA methylation are in majority inhibitors of DNA methyl transferases (DNMT), and inhibitors of histone deacetylation usually act on several members of the histone deacetylase (HDAC) family. However, a number of reports have revealed that certain HDAC inhibitors also have an effect on DNMT1 [51], which might partly explain differences in the efficacy of these drugs to reexpress genes important for the success of cancer therapies. The effect of HDAC inhibitors might encompass reduction in DNMT1 levels [52–54]. Noticeably, HDAC inhibitors and DNMT inhibitors seem to act differently to suppress DNMT1 function [51], which might contribute to observed synergistic effects when these inhibitors are combined.

The established clinical use of these epigenetic drugs has been limited mostly to hematopoietic malignancies and to a relatively small subset of responding patients [72,73]. Currently these drugs are considered inadequate for cancer treatment when used as single agents. In solid cancers, a number of Phase I and II clinical trials have been completed (Table 1) with some encouraging results warranting additional studies. Overall, epigenetic modifiers are tested for advanced stages of cancers (e.g., in breast cancers and nonsmall cell lung cancers). They have triggered the stabilization of the cancerous disease when used in combination regimens of two HDAC inhibitors or a combination of DNMT and HDAC inhibitors [65–66,74]. Interestingly, there is renewed interest in an old compound, the soy phytoestrogen genistein for its potential epigenetic impact. It is currently under clinical trial for breast and prostate cancers. Indeed, this drug has been found to reduce *GSTP1* promoter methylation in breast cancer cell lines and to decrease DNA methylation on *BRCA1, EPHB2* and *GSTP1* gene promoters in two prostate cell lines [61,62].

Although none of the US FDA approved epigenetic drugs have revolutionized the treatment of specific cancers, epigenetic therapy has led to a paradigm shift in anticancer treatment strategies. Indeed, these drugs ought to be utilized at a concentration that modifies gene transcription rather than a cytotoxic concentration, in order to enhance the efficacy of traditional cytotoxic drugs in combination therapy. Utilized in such a manner, epigenetic drugs have improved cancer management by increasing survival rate and reducing toxicity. They have also helped decrease resistance to usual chemotherapy regimens and sensitize cancers to multiprong therapy, including hormonal therapies and standard chemotherapy. Results from Phase I clinical trials have encouraged further investigation of epigenetic drugs such as valproic acid and vorinostat as sensitizers of radiotherapy [75,76]; however, more results are awaited to gain a clear understanding of the extent of possibilities to use epigenetic drugs in combination with radiotherapy [77]. A recognized power of epigenetic drugs is the (re-)sensitization of cancer cells to cytotoxic therapies via DNA methylation and/or histone modifications induced by these drugs that lead to the reexpression of tumor suppressors [78,79]. However, the administration of epigenetic drugs still needs to be optimized in order to readily improve cancer treatment [73,77].

Largely, epigenetic drugs have triggered a huge excitement in cancer chemotherapy; although there have been encouraging results in early phase clinical trials of combination regimens, there are currently no FDA approvals for use of HDAC and DNMT inhibitors in solid cancers. In light of the complexity of the epigenetic mechanisms involved in gene transcription control, a major road-block to effective applications of epigenetic therapy might be that currently approved epigenetic drugs lack specificity towards such epigenetic mechanisms [55–56,70].

The international Human Epigenome Consortium aims at mapping human epigenomes that correspond to specific cellular states in normal and diseased tissues. One of the envisioned outcomes is translation of discoveries to improve health, notably via therapy. Indeed, knowing the epigenetic map of each tissue to be treated and understanding differences between normal and cancer tissues, might help improve the use of epigenetic drugs. This endeavor is timely in light of the continuing development of very specific epigenetic drugs that target unique methylation pathways of histones for instance (Table 2), as well as the improved understanding of the relationship between tissue architecture, for example the polarity axis in epithelia, and epigenetic regulation that we discussed earlier. Treatments with mechanistically broad epigenetic modifiers typically result in a relatively small number of genes being affected within the whole genome [80], possibly because each particular cell status is accompanied with its own epigenomic pattern that either prevents or favors the response of given genes. Therefore, it is expected that epigenetic drugs restricted to a specific modifying enzyme would primarily also affect a small number of genes found to be controlled by the targeted epigenetic mechanism in a given cancer stage. We surmise that the use of targeted epigenetic drugs in cancer therapy would benefit from considering tissue architecture as a restoring force constraining epigenetic regulations in their normal state. We mean that, in light of the central role played by tis-

sue architecture in cell behavior, the epigenetic profile that maintains the normal tissue architecture ought to be known in order to identify epigenetic targets for cancer therapy. Each epigenetic pathway controlling a specific aspect of tissue architecture that participates in cancer onset and progression should be deciphered; moreover, the epigenetic consequences of alterations in tissue architecture ought to be understood as these pathways might also constitute targets for epigenetic therapy (Figure 2).

An interesting candidate for epigenetically targeted therapy is the EZH2 protein, the catalytic subunit of Polycomp Repressive Complex 2 (PRC2) that promotes trimethylation on H3K27. It was shown to be upregulated in multiple malignancies including those of prostate, breast, liver, ovary, stomach, brain, skin, kidney, lung, bladder, head and neck and has been associated with poor prognosis [89–91]. It is considered to possess oncogenic activity via its repression of tumor suppressor genes [92]. In breast cancer, the expression of EZH2 was identified to be increased up to 12 years before a tumor was clinically detectable [93]. Currently, there is substantial lack of information on modifications of phenotypes or key mechanisms underlying cancer onset that might result from the increase in EZH2. However, several reports demonstrate that this protein might play a key role in tissue architecture linked to cancer progression. EZH2 physically interacts with β-catenin, leading to its nuclear accumulation in mammary epithelial cells and the activation of Wnt/β-catenin signaling. EZH2 upregulation and colocalization with β-catenin in human epithelial intraductal hyperplasia is the earliest histologically identifiable precursor of breast carcinoma [94]. Moreover, EZH2 activity seems to be required for the repression of the E-cadherin gene *CDH1* by the EMT inducer and transcription factor Snail [95], and as mentioned earlier, downregulation of E-cadherin results in the accumulation of β-catenin in the cell nucleus. The epigenetic regulation of *SMAD4* loci by EZH2 has been proposed to participate in the control of EMT by TGF-β in ovarian cancer, and it has been suggested that EZH2 might be an interesting target to pursue in order to inhibit EMT [95]. Thus, EZH2 appears as an essential controller of a signaling pathway involved in polarity, and especially involved in EMT that might occur early on in the development of certain cancers. Targeting EZH2 might be an important avenue to consider for chemoprevention; as examples among others, initial studies on colorectal and prostate cancers with EZH2 inhibitors are encouraging [96,97]. The involvement of EZH2 in the regulation of stem cells thought to play an essential role in the renewal and expansion of epithelial architecture is another reason to consider this PcG protein as an interesting lead for epigenetically targeted therapy. EZH2 was shown to bind to the *NOTCH1* promoter in triple negative breast cancer cells. The resulting activation of NOTCH1 signaling expanded the stem cell pool, leading to accelerated breast cancer initiation and growth [98]. Noticeably, NOTCH1 has been linked to Scrib, a key player in the establishment of tissue polarity [1]. The epigenetic impact of PcG proteins has also been revealed in cervical cancer in which abnormal hypermethylation of genes controlled by such proteins has been measured in stem cells three years before the detection of neoplastic development [99].

The example of EMT is an illustration of how the use of epigenetic drugs might be optimized if taking into account tissue architecture. EZH2 seems to be implicated in changes necessary for EMT extremely early, possibly before tissue architecture is compromised. The powerful effect of EZH2 regulation on cell fate might be linked to the relationship between EZH2 product, H3K27me3, and higher order chromatin organizer CTCF that binds insulator DNA regions [100,101]. The increased presence of H3K27me3 might prevent the opening effect of CTCF on chromatin at individual loci and thus, consolidate EZH2-mediated silencing of genes important to control cancer onset and progression. Another possibility, since CTCF can also mediate PRC2-repressive higher order chromatin structure, is that CTCF reinforces EZH2 effect on gene silencing. When EZH2 is upregulated, there might be alterations already at the level of apical polarity as those can occur without any signs of active proliferation [10]. Acting directly on EZH2 early on might be sufficient to reorganize chromatin and thus, the transcriptional landscape by allowing the redistribution of CTCF, unless apical polarity loss has also modified the epigenetic landscape that would require additional epigenetic modifications. If the EMT process is engaged and there are already signs of basal polarity alterations, involving silencing of genes essential to establish EMT, like those coding for β4-integrin and claudin 4 that appear as early events in that process [27,102], other epigenetic drugs might be more effective. Since the expression of these two genes is controlled by DNA methylation and histone acetylation, either HDAC inhibitors alone or combined with DNMT inhibitors might be sufficient to stop cancer progression. When cancer progression is further advanced, in invasive tumors, the transient nature of epigenetic mechanisms associated with EMT might explain chemoresistance in cancer patients. The plethora of chromatin remodeling enzymes recruited at the *CDH1* gene promoter (e.g., LSD1, PRC2, G9a,

Table 2. Examples of histone methyltransferases and demethylases with their specific inhibitors.

Histone modifiers	Specific inhibitors	Cell lines/models	Ref.
Histone methyltransferase			
EZH2/PRC2 H3K27 methyltransferase H3K27→H3K27me1, me2, m3	GSK126/EPZ00568	DLBCL cell lines/ Lymphoma cells	[81,82]
G9a/GLP H3K9 methyltransferase H3K9→H3K9me1, me2	UNC0638/ BRD4770	MCF7, MDA-MB-231/ PANC-1	[83,84]
DOT1L H3K79 methyltransferase H3K79→H3K79me1	EPZ004777	Mouse MLL xenograft model	[85]
SU (VAR) 3-9 H3K9 methyltransferase H3K9→H3K9me1, me2	Chaetocin	SL-2 *Drosophila* tissue culture cells	[86]
Histone demethylases			
JMJC demethylases	N-octyl ester form of IOX	HeLa cells	[87]
LSD1 H3K4 demethylase (H3K4, H3k4me), H3K4me2, H3K4me→H3k4me, H3K4	Bizine (phenelzine analog)	LNCaP and H460	[88]

The cell lines and models in which the inhibitors have been tested are also indicated. DLBCL are diffuse large B-cell lymphoma cell lines, MCF7 and MDA-MB-231 are mammary epithelial cancer cell lines, PANC-1 is a pancreatic ductal carcinoma cell line, HeLa is a cervical cancer cell line, LNCaP is a prostate adenocarcinoma cell line and H460 is a nonsmall cell lung carcinoma cell line.

Suv39H1) [95] provides a means to promote and revert EMT by acting on E-Cadherin expression as needed. The combination of DNA methylation and H3K9 methylation via G9a and Suv39H1 [103] might permit effective silencing of key genes controlling EMT and might require to use combinations of DNMT inhibitors and inhibitors of H3K9 methylation. Therefore, specific epigenetic drugs effectively used based on the status of tissue polarity might improve the chances of successful treatments of epithelial cancers.

Conclusion

We have provided information that demonstrates the interactions between tissue polarity and epigenetic pathways in cancer onset and progression. The polarity axis is used here as main example of the tissue architecture representing the backbone of epithelial homeostasis. An approach to better target epigenetic drugs in cancer treatment is to use changes in tissue architecture as readout, for instance via the redistribution of polarity markers, to identify a meaningful epigenetic pathway that either controls a specific aspect of tissue architecture or is under the influence of a specific feature of tissue architecture, the alteration of which is known to promote cancer onset, invasion or metastasis. Importantly, it is likely that useful epigenetic information will be dependent on tissue types, hence requiring investigations with the proper tissue model to exquisitely link epigenetic mechanisms and specific architectural features. An illustration of tissue-dependent epigenetic state is DNA methylation. Many of the genes involved in polarity are silenced by DNA methylation. The genes implicated might be different depending on the tissue type (e.g., genes coding for CADM, MYO1A, MPP3, FOXF2), and some of these genes coding for proteins involved in polarity (e.g., E-cadherin) might not necessarily be methylated in processes like EMT depending on the cell type and possibly the circumstances of EMT induction. An interesting approach would be to assess whether tissues that differ for their methylation pattern associated with EMT also display differences in polarity alterations. Of particular interest also is the fact that in several examples, DNA hypermethylation of genes leading to EMT (e.g., β4-integrin) does not need to be necessarily reverted for the reexpression of the genes silenced, suggesting that emphasis on the development of epigenetic drugs targeting histone modifications is of great importance. Epigenetic drugs are being developed to treat cancer in general, but there is increasing evidence that epigenetic events are associated with defined steps in cancer onset and progression, like specific signaling pathways and the changes in polarity discussed in this special report. Future investigations should establish whether epigenetic drugs can alter tissue architecture in a targeted

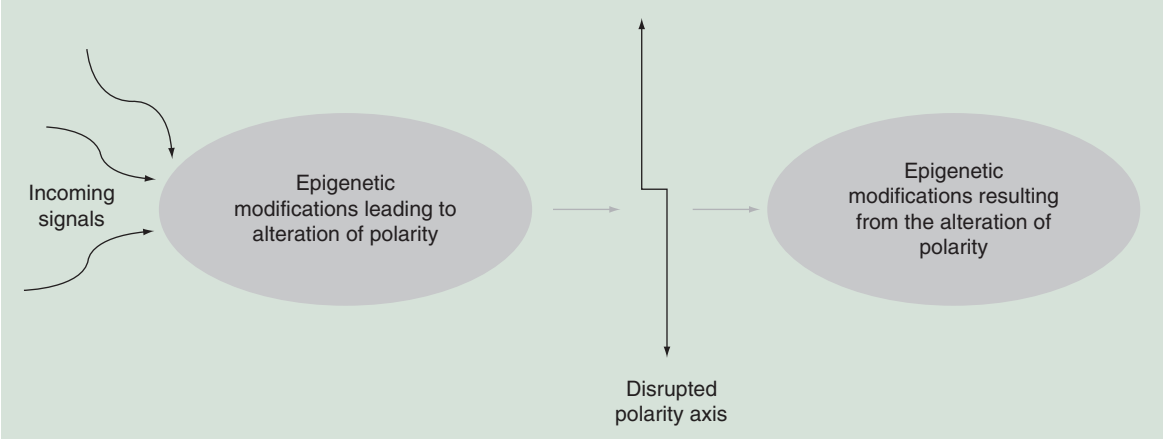

Figure 2. Understanding tissue polarity–epigenome relationship for improved use of epigenetic drugs. In order to identify epigenetic marks of interest to better target epigenetic drugs for cancer treatment, it is important to take into account modifications that occur upstream and downstream of alterations in the protein complexes controlling the polarity axis. Incoming signals into the cell nucleus might trigger epigenetic changes that would affect a component of the polarity axis and thus, disrupt specific aspects of polarity (left portion of the figure). In turn, the alteration of the polarity axis might have an impact on epigenetic pathways via signal transduction or the shuttling of proteins associated with polarity complexes to the cell nucleus (right portion of the drawing). The epigenetic marks directing the maintenance of polarity, and those modified following the loss of aspects of polarity associated with cancer development and progression should help determine the choice of epigenetic drugs based on their specificity for the enzymes controlling these epigenetic marks. These epigenetic drugs would either prevent or revert polarity alterations by acting on the epigenetic marks of interest. Whether or not the epigenetic landscape following therapy would be similar to that of the normal architecture remains to be determined.

manner. In such case these drugs might be used for prevention of the next step in cancer progression if the epigenetic pathway targeted is upstream of the architectural alteration; or they might be used for treatment if the epigenetic pathway targeted affects an important player of cancer progression downstream of the architectural alteration.

Future perspective

The future of epigenetic drugs will be increasingly promising as we gain more knowledge of the key players that generate epigenetic tissue maps such as architectural traits. Beyond the simple comparison of normal and cancer tissues, extended knowledge on the interaction between epigenome and environment (e.g., stress, pollutants, nutrition) will provide information on epigenetic marks relevant to a risk level for cancer onset and progression, and along with an extended knowledge of the interaction between epigenetic and genetic codes to control phenotypes, it will facilitate individualized interventions. Epigenetic marks should also constitute or lead to the identification of biomarkers that can predict and help monitor responses to epigenetics-based therapy in order

Executive summary

Tissue architecture, a progressive view of epigenetic regulation

- Essential architectural features of epithelia, mainly basoapical polarity, participate in key phases of cancer development, from onset, to invasion and metastasis.
- Certain aspects of polarity disruption are linked to the epigenetic dysregulation of the expression of components of multiprotein complexes that form the polarity axis.
- Multiprotein complexes that form the polarity axis are involved in the control of epigenetic mechanisms, via the presence of their components in the cell nucleus, and/or via their impact on signaling pathways influencing epigenetic mechanisms.

Epigenetic markers controlled by tissue architecture as potential targets for cancer therapy

- Broad-range epigenetic drugs currently approved for cancer chemotherapy are seldom used for the treatment of solid tumors.
- The emergence of epigenetic drugs that exquisitely target specific enzymes for epigenetic mechanisms might improve and expand treatment applications if these drugs are administered in order to modify epigenetic marks essential for cancer development and progression. One way of identifying these epigenetic marks is to focus on the aspect of tissue architecture that needs to be altered in order to allow cancer development and progression.

to devise more effective pharmacological as well as behavioral approaches to eradicate cancers.

Financial & competing interests disclosure

The authors acknowledge support from the NIH (CA171704 to SAL) and the Keck Foundation. The authors have no other relevant affiliations or financial involvement with any organization or entity with a financial interest in or financial conflict with the subject matter or materials discussed in the manuscript apart from those disclosed.

No writing assistance was utilized in the production of this manuscript.

References

Papers of special note have been highlighted as:
• of interest; •• of considerable interest

1 Lelièvre SA. Tissue polarity-dependent control of mammary epithelial homeostasis and cancer development: an epigenetic perspective. *J. Mammary Gland Biol. Neoplasia* 15(1), 49–63 (2010).

• **Sheds light on how apical polarity might control epigenetic mechanisms via indirect and direct effects in the cell nucleus. Presents a novel view of how tissue architecture connects with the cell nucleus.**

2 Baylin SB, Jones PA. A decade of exploring the cancer epigenome – biological and translational implications. *Nat. Rev. Cancer* 11(10), 726–734 (2011).

3 Timp W, Feinberg AP. Cancer as a dysregulated epigenome allowing cellular growth advantage at the expense of the host. *Nat. Rev. Cancer* 13(7), 497–510 (2013).

•• **The authors develop innovative concepts related to epigenetic control in normal and cancer contexts. In this comprehensive and provocative review of epigenetic regulation, emphasis is placed on the importance of epigenetic heterogeneity and the approach to detection and treatment based on epigenetics.**

4 Byler S, Goldgar S, Heerboth S *et al.* Genetic and epigenetic aspects of breast cancer progression and therapy. *Anticancer Res.* 34(3), 1071–1077 (2014).

5 Sarkar S, Horn G, Moulton K *et al.* Cancer development, progression, and therapy: an epigenetic overview. *Int. J. Mol. Sci.* 14(10), 21087–21113 (2013).

6 Plachot C, Lelièvre SA. DNA methylation control of tissue polarity and cellular differentiation in the mammary epithelium. *Exp. Cell Res.* 298(1), 122–132 (2004).

7 Abad PC, Lewis J, Mian IS *et al.* Numa influences higher order chromatin organization in human mammary epithelium. *Mol. Biol. Cell* 18(2), 348–361 (2007).

8 Bazzoun D, Lelièvre S, Talhouk R. Polarity proteins as regulators of cell junction complexes: implications for breast cancer. *Pharmacol. Ther.* 138(3), 418–427 (2013).

9 Dawson MA, Kouzarides T. Cancer epigenetics: from mechanism to therapy. *Cell* 150(1), 12–27 (2012).

10 Chandramouly G, Abad PC, Knowles DW, Lelièvre SA. The control of tissue architecture over nuclear organization is crucial for epithelial cell fate. *J. Cell Sci.* 120(Pt 9), 1596–1606 (2007).

11 Zhan L, Rosenberg A, Bergami KC *et al.* Deregulation of scribble promotes mammary tumorigenesis and reveals a role for cell polarity in carcinoma. *Cell* 135(5), 865–878 (2008).

12 Muthuswamy SK, Xue B. Cell polarity as a regulator of cancer cell behavior plasticity. *Annu. Rev. Cell Dev. Biol.* 28, 599–625 (2012).

13 Sourisseau T, Georgiadis A, Tsapara A *et al.* Regulation of PCNA and cyclin D1 expression and epithelial morphogenesis by the ZO-1-regulated transcription factor ZONAB/DBPA. *Mol. Cell Biol.* 26(6), 2387–2398 (2006).

14 Paris L, Tonutti L, Vannini C, Bazzoni G. Structural organization of the tight junctions. *Biochim. Biophys. Acta* 1778(3), 646–659 (2008).

15 Nakamura T, Blechman J, Tada S *et al.* HUASH1 protein, a putative transcription factor encoded by a human homologue of the drosophila *ash1* gene, localizes to both nuclei and cell–cell tight junctions. *Proc. Natl Acad. Sci. USA* 97(13), 7284–7289 (2000).

16 Gregory GD, Vakoc CR, Rozovskaia T *et al.* Mammalian ASH1L is a histone methyltransferase that occupies the transcribed region of active genes. *Mol. Cell Biol.* 27(24), 8466–8479 (2007).

17 Dunn KL, Espino PS, Drobic B, He S, Davie JR. The RAS-MAPK signal transduction pathway, cancer and chromatin remodeling. *Biochem. Cell Biol.* 83(1), 1–14 (2005).

18 Nolan ME, Aranda V, Lee S *et al.* The polarity protein PAR6 induces cell proliferation and is overexpressed in breast cancer. *Cancer Res.* 68(20), 8201–8209 (2008).

19 Shi B, Liang J, Yang X *et al.* Integration of estrogen and Wnt signaling circuits by the polycomb group protein EZH2 in breast cancer cells. *Mol. Cell Biol.* 27(14), 5105–5119 (2007).

20 Andersen A, Jones DA. APC and DNA demethylation in cell fate specification and intestinal cancer. *Adv. Exp. Med. Biol.* 754, 167–177 (2013).

21 Bunker BD, Nellimoottil TT, Boileau RM, Classen AK, Bilder D. The transcriptional response to tumorigenic polarity loss in drosophila. *eLife* doi:10.7554/eLife.03189 (2015) (Epub).

22 Weaver VM, Lelièvre S, Lakins JN *et al.* Beta4 integrin-dependent formation of polarized three-dimensional architecture confers resistance to apoptosis in normal and malignant mammary epithelium. *Cancer Cell* 2(3), 205–216 (2002).

23 Sehgal BU, Debiase PJ, Matzno S *et al.* Integrin beta4 regulates migratory behavior of keratinocytes by determining laminin-332 organization. *J. Biol. Chem.* 281(46), 35487–35498 (2006).

24 Huber O, Korn R, Mclaughlin J, Ohsugi M, Herrmann BG, Kemler R. Nuclear localization of beta-catenin by interaction with transcription factor lef-1. *Mech. Dev.* 59(1), 3–10 (1996).

25 Heerboth S, Housman G, Leary M *et al.* EMT and tumor metastasis. *Clin. Transl. Med.* 4, 6 (2015).

26 Kalluri R, Weinberg RA. The basics of epithelial-mesenchymal transition. *J. Clin. Invest.* 119(6), 1420–1428 (2009).

27 Yang X, Pursell B, Lu S, Chang TK, Mercurio AM. Regulation of beta 4-integrin expression by epigenetic modifications in the mammary gland and during the epithelial-to-mesenchymal transition. *J. Cell Sci.* 122(Pt 14), 2473–2480 (2009).

•• **Identification of complex epigenetic modifications involved in the regulation of the genes coding for β 4- integrin and E-cadherin.**

28 Mcdonald OG, Wu H, Timp W, Doi A, Feinberg AP. Genome-scale epigenetic reprogramming during epithelial-to-mesenchymal transition. *Nat. Struct. Mol. Biol.* 18(8), 867–874 (2011).

29 Chen M, Sinha M, Luxon BA, Bresnick AR, O'Connor KL. Integrin alpha6beta4 controls the expression of genes associated with cell motility, invasion, and metastasis, including s100a4/metastasin. *J. Biol. Chem.* 284(3), 1484–1494 (2009).

30 Liu ZL, Wang Q, Huang LN. E-cadherin gene methylation in lung cancer. *Tumour Biol.* 35(9), 9027–9033 (2014).

31 Ozawa M, Kobayashi W. Reversibility of the snail-induced epithelial-mesenchymal transition revealed by the CRE-LOXP system. *Biochem. Biophys. Res. Commun.* 458(3), 608–613 (2015).

32 Honda H, Pazin MJ, Ji H, Wernyj RP, Morin PJ. Crucial roles of sp1 and epigenetic modifications in the regulation of the cldn4 promoter in ovarian cancer cells. *J. Biol. Chem.* 281(30), 21433–21444 (2006).

33 He W, Li X, Xu S *et al.* Aberrant methylation and loss of *CADM2* tumor suppressor expression is associated with human renal cell carcinoma tumor progression. *Biochem. Biophys. Res. Commun.* 435(4), 526–532 (2013).

34 Chang G, Xu S, Dhir R *et al.* Hypoexpression and epigenetic regulation of candidate tumor suppressor gene *CADM-2* in human prostate cancer. *Clin. Cancer Res.* 16(22), 5390–5401 (2010).

35 Wang S, Kang W, Go MY *et al.* Dapper homolog 1 is a novel tumor suppressor in gastric cancer through inhibiting the nuclear factor-kappab signaling pathway. *Mol. Med.* 18, 1402–1411 (2012).

36 Mazzolini R, Dopeso H, Mateo-Lozano S *et al.* Brush border myosinia has tumor suppressor activity in the intestine. *Proc. Natl Acad. Sci. USA*109(5), 1530–1535 (2012).

37 Feng X, Chen K, Ye S *et al.* MPP3 inactivation by promoter CPG islands hypermethylation in colorectal carcinogenesis. *Cancer Biomark.* 11(2–3), 99–106 (2012).

38 Tian HP, Lun SM, Huang HJ *et al.* DNA methylation affects the sp1-regulated transcription of forkhead box f2 in breast cancer cells. *J. Biol. Chem.* (2015).

39 Moreno-Bueno G, Portillo F, Cano A. Transcriptional regulation of cell polarity in emt and cancer. *Oncogene* 27(55), 6958–6969 (2008).

40 Lamouille S, Xu J, Derynck R. Molecular mechanisms of epithelial-mesenchymal transition. *Nat. Rev. Mol. Cell. Biol.* 15(3), 178–196 (2014).

41 Davalos V, Moutinho C, Villanueva A *et al.* Dynamic epigenetic regulation of the microRNA-200 family mediates epithelial and mesenchymal transitions in human tumorigenesis. *Oncogene* 31(16), 2062–2074 (2012).

• **Demonstration of the epigenetic regulation of miR 200 family during EMT or MET phenotypes in tumor progression. Results include work with clinical samples.**

42 Chen CL, Gajewski KM, Hamaratoglu F *et al.* The apical-basal cell polarity determinant crumbs regulates hippo signaling in drosophila. *Proc. Natl Acad. Sci. USA* 107(36), 15810–15815 (2010).

43 Grzeschik NA, Parsons LM, Richardson HE. Lgl, the swh pathway and tumorigenesis: it's a matter of context & competition! *Cell Cycle* 9(16), 3202–3212 (2010).

44 Ling C, Zheng Y, Yin F *et al.* The apical transmembrane protein crumbs functions as a tumor suppressor that regulates hippo signaling by binding to expanded. *Proc. Natl Acad. Sci. USA* 107(23), 10532–10537 (2010).

45 Robinson BS, Huang J, Hong Y, Moberg KH. Crumbs regulates salvador/warts/hippo signaling in *Drosophila* via the ferm-domain protein expanded. *Curr. Biol.* 20(7), 582–590 (2010).

46 Pan D. The hippo signaling pathway in development and cancer. *Dev. Cell* 19(4), 491–505 (2010).

47 Martin-Belmonte F, Perez-Moreno M. Epithelial cell polarity, stem cells and cancer. *Nat. Rev. Cancer* 12(1), 23–38 (2012).

48 Ribeiro P, Holder M, Frith D, Snijders AP, Tapon N. Crumbs promotes expanded recognition and degradation by the scf(slimb/beta-trcp) ubiquitin ligase. *Proc. Natl Acad. Sci. USA* 111(19), e1980–e1989 (2014).

49 Ozturk N, Singh I, Mehta A, Braun T, Barreto G. Hmga proteins as modulators of chromatin structure during transcriptional activation. *Front. Cell. Dev. Biol.* 2, 5 (2014).

50 Tam WL, Weinberg RA. The epigenetics of epithelial–mesenchymal plasticity in cancer. *Nat. Med.* 19(11), 1438–1449 (2013).

51 Arzenani MK, Zade AE, Ming Y *et al.* Genomic DNA hypomethylation by histone deacetylase inhibition implicates dnmt1 nuclear dynamics. *Mol. Cell. Biol.* 31(19), 4119–4128 (2011).

52 Kishikawa S, Ugai H, Murata T, Yokoyama KK. Roles of histone acetylation in the dnmt1 gene expression. *Nucleic Acids Res. Suppl.* (2), 209–210 (2002).

53 You JS, Kang JK, Lee EK *et al.* Histone deacetylase inhibitor apicidin downregulates DNA methyltransferase 1 expression and induces repressive histone modifications via recruitment of corepressor complex to promoter region in human cervix cancer cells. *Oncogene* 27(10), 1376–1386 (2008).

54 Sarkar S, Abujamra AL, Loew JE, Forman LW, Perrine SP, Faller DV. Histone deacetylase inhibitors reverse cpg methylation by regulating dnmt1 through erk signaling. *Anticancer Res.* 31(9), 2723–2732 (2011).

55 Gros C, Fahy J, Halby L *et al.* DNA methylation inhibitors in cancer: recent and future approaches. *Biochimie* 94(11), 2280–2296 (2012).

56 Medina-Franco JL, Mendez-Lucio O, Duenas-Gonzalez A, Yoo J. Discovery and development of DNA methyltransferase inhibitors using *in silico* approaches. *Drug Discov. Today* 20(5), 569–577 (2015).

57 Seidel C, Florean C, Schnekenburger M, Dicato M, Diederich M. Chromatin-modifying agents in anti-cancer therapy. *Biochimie* 94(11), 2264–2279 (2012).

58 Kornblith AB, Herndon JE 2nd, Silverman LR *et al.* Impact of azacytidine on the quality of life of patients with myelodysplastic syndrome treated in a randomized Phase III trial: a cancer and leukemia group B study. *J. Clin. Oncol.* 20(10), 2441–2452 (2002).

59 Kantarjian H, Issa JP, Rosenfeld CS *et al.* Decitabine improves patient outcomes in myelodysplastic syndromes: results of a Phase III randomized study. *Cancer* 106(8), 1794–1803 (2006).

60 Hackanson B, Daskalakis M. Decitabine. *Recent Results Cancer Res.* 201, 269–297 (2014).

61 King-Batoon A, Leszczynska JM, Klein CB. Modulation of gene methylation by genistein or lycopene in breast cancer cells. *Environ. Mol. Mutagen.* 49(1), 36–45 (2008).

62 Adjakly M, Bosviel R, Rabiau N *et al.* DNA methylation and soy phytoestrogens: quantitative study in DU-145 and PC-3 human prostate cancer cell lines. *Epigenomics* 3(6), 795–803 (2011).

63 Klisovic RB, Stock W, Cataland S *et al.* A Phase I biological study of MG98, an oligodeoxynucleotide antisense to DNA methyltransferase 1, in patients with high-risk myelodysplasia and acute myeloid leukemia. *Clin. Cancer Res.* 14(8), 2444–2449 (2008).

64 Plummer R, Vidal L, Griffin M *et al.* Phase I study of MG98, an oligonucleotide antisense inhibitor of human DNA methyltransferase 1, given as a 7 day infusion in patients with advanced solid tumors. *Clin. Cancer Res.* 15(9), 3177–3183 (2009).

65 Luu TH, Morgan RJ, Leong L *et al.* A Phase II trial of vorinostat (suberoylanilide hydroxamic acid) in metastatic breast cancer: a California cancer consortium study. *Clin. Cancer Res.* 14(21), 7138–7142 (2008).

66 Vansteenkiste J, Van Cutsem E, Dumez H *et al.* Early Phase II trial of oral vorinostat in relapsed or refractory breast, colorectal, or non-small cell lung cancer. *Invest. New Drugs* 26(5), 483–488 (2008).

67 Wagner JM, Hackanson B, Lubbert M, Jung M. Histone deacetylase (HDAC) inhibitors in recent clinical trials for cancer therapy. *Clin. Epigenetics* 1(3–4), 117–136 (2010).

68 Zibelman M, Wong YN, Devarajan K *et al.* Phase I study of the MTOR inhibitor ridaforolimus and the hdac inhibitor vorinostat in advanced renal cell carcinoma and other solid tumors. *Invest. New Drugs* (2015).

69 Kelly WK, Marks P, Richon VM. CCR 20th anniversary commentary: vorinostat – gateway to epigenetic therapy. *Clin. Cancer Res.* 21(10), 2198–2200 (2015).

70 Mottamal M, Zheng S, Huang TL, Wang G. Histone deacetylase inhibitors in clinical studies as templates for new anticancer agents. *Molecules* 20(3), 3898–3941 (2015).

71 Giles F, Fischer T, Cortes J *et al.* A Phase I study of intravenous LBH589, a novel cinnamic hydroxamic acid analogue histone deacetylase inhibitor, in patients with refractory hematologic malignancies. *Clin. Cancer Res.* 12(15), 4628–4635 (2006).

72 Boumber Y, Issa JP. Epigenetics in cancer: what's the future? *Oncology (Williston Park)* 25(3), 220–226, 228 (2011).

73 Azad N, Zahnow CA, Rudin CM, Baylin SB. The future of epigenetic therapy in solid tumours – lessons from the past. *Nat. Rev. Clin. Oncol.* 10(5), 256–266 (2013).

• **Review on the importance of preclinical and clinical study designs to improve the epigenetic therapy of cancer.**

74 Thurn KT, Thomas S, Moore A, Munster PN. Rational therapeutic combinations with histone deacetylase inhibitors for the treatment of cancer. *Future Oncol.* 7(2), 263–283 (2011).

75 Barker CA, Bishop AJ, Chang M, Beal K, Chan TA. Valproic acid use during radiation therapy for glioblastoma associated with improved survival. *Int. J. Radiat. Oncol. Biol. Phys.* 86(3), 504–509 (2013).

76 Shi W, Lawrence YR, Choy H *et al.* Vorinostat as a radiosensitizer for brain metastasis: a Phase I clinical trial. *J. Neurooncol.* 118(2), 313–319 (2014).

77 Smits KM, Melotte V, Niessen HE *et al.* Epigenetics in radiotherapy: where are we heading? *Radiother. Oncol.* 111(2), 168–177 (2014).

78 Sarkar S, Goldgar S, Byler S, Rosenthal S, Heerboth S. Demethylation and re-expression of epigenetically silenced tumor suppressor genes: sensitization of cancer cells by combination therapy. *Epigenomics* 5(1), 87–94 (2013).

79 Oronsky BT, Oronsky AL, Lybeck M *et al.* Episensitization: defying time's arrow. *Front. Oncol.* 5, 134 (2015).

80 Menendez L, Walker D, Matyunina LV *et al.* Identification of candidate methylation-responsive genes in ovarian cancer. *Mol. Cancer* 6, 10 (2007).

81 Knutson SK, Wigle TJ, Warholic NM *et al.* A selective inhibitor of EZH2 blocks H3K27 methylation and kills mutant lymphoma cells. *Nat. Chem. Biol.* 8(11), 890–896 (2012).

82 Mccabe MT, Ott HM, Ganji G *et al.* EZH2 inhibition as a therapeutic strategy for lymphoma with EZH2-activating mutations. *Nature* 492(7427), 108–112 (2012).

83 Vedadi M, Barsyte-Lovejoy D, Liu F *et al.* A chemical probe selectively inhibits g9a and glp methyltransferase activity in cells. *Nat. Chem. Biol.* 7(8), 566–574 (2011).

84 Yuan Y, Wang Q, Paulk J *et al.* A small-molecule probe of the histone methyltransferase G9A induces cellular senescence in pancreatic adenocarcinoma. *ACS Chem. Biol.* 7(7), 1152–1157 (2012).

85 Daigle SR, Olhava EJ, Therkelsen CA *et al.* Selective killing of mixed lineage leukemia cells by a potent small-molecule DOT1L inhibitor. *Cancer Cell* 20(1), 53–65 (2011).

86 Greiner D, Bonaldi T, Eskeland R, Roemer E, Imhof A. Identification of a specific inhibitor of the histone methyltransferase SU(VAR)3–9. *Nat. Chem. Biol.* 1(3), 143–145 (2005).

87 Schiller R, Scozzafava G, Tumber A *et al.* A cell-permeable ester derivative of the JMJC histone demethylase inhibitor IOX1. *Chem. Med. Chem.* 9(3), 566–571 (2014).

88 Prusevich P, Kalin JH, Ming SA *et al.* A selective phenelzine analogue inhibitor of histone demethylase LSD1. *ACS Chem. Biol.* 9(6), 1284–1293 (2014).

89 Min J, Zaslavsky A, Fedele G *et al.* An oncogene-tumor suppressor cascade drives metastatic prostate cancer by coordinately activating ras and nuclear factor-kappab. *Nat. Med.* 16(3), 286–294 (2010).

90 Mccabe MT, Creasy CL. EZH2 as a potential target in cancer therapy. *Epigenomics* 6(3), 341–351 (2014).

91 Zhang J, Chen L, Han L *et al.* EZH2 is a negative prognostic factor and exhibits pro-oncogenic activity in glioblastoma. *Cancer lett.* 356(2 Pt B), 929–936 (2015).

92 Bracken AP, Pasini D, Capra M, Prosperini E, Colli E, Helin K. EZH2 is downstream of the PRB-E2F pathway, essential for proliferation and amplified in cancer. *EMBO. J.* 22(20), 5323–5335 (2003).

93 Ding L, Erdmann C, Chinnaiyan AM, Merajver SD, Kleer CG. Identification of EZH2 as a molecular marker for a precancerous state in morphologically normal breast tissues. *Cancer Res.* 66(8), 4095–4099 (2006).

94 Li X, Gonzalez ME, Toy K, Filzen T, Merajver SD, Kleer CG. Targeted overexpression of EZH2 in the mammary gland disrupts ductal morphogenesis and causes epithelial hyperplasia. *Am. J. Pathol.* 175(3), 1246–1254 (2009).

95 Lin Y, Dong C, Zhou BP. Epigenetic regulation of EMT: the snail story. *Curr. Pharm. Des.* 20(11), 1698–1705 (2014).

96 Maryan N, Statkiewicz M, Mikula M *et al.* Regulation of the expression of claudin 23 by the enhancer of zeste 2 polycomb group protein in colorectal cancer. *Mol. Med. Rep.* 12(1), 728–736 (2015).

97 Kirk JS, Schaarschuch K, Dalimov Z *et al.* TOP2A identifies and provides epigenetic rationale for novel combination therapeutic strategies for aggressive prostate cancer. *Oncotarget* 6(5), 3136–3146 (2015).

98 Gonzalez ME, Moore HM, Li X *et al.* EZH2 expands breast stem cells through activation of notch1 signaling. *Proc. Natl Acad. Sci. USA* 111(8), 3098–3103 (2014).

•• **The authors demonstrate a stimulating rather than repressive role for EZH2 and its involvement in *NOTCH1* mediated expansion of the stem cell pool and acceleration of breast cancer initiation and growth.**

99 Zhuang J, Jones A, Lee SH *et al.* The dynamics and prognostic potential of DNA methylation changes at stem cell gene loci in women's cancer. *PLoS Genet.* 8(2), e1002517 (2012).

100 Weth O, Paprotka C, Gunther K *et al.* CTCF induces histone variant incorporation, erases the h3k27me3 histone mark and opens chromatin. *Nucleic Acids Res.* 42(19), 11941–11951 (2014).

101 Xu M, Zhao GN, Lv X *et al.* CTCF controls HOXA cluster silencing and mediates PRC2-repressive higher-order chromatin structure in NT2/D1 cells. *Mol. Cell Biol.* 34(20), 3867–3879 (2014).

102 Lin X, Shang X, Manorek G, Howell SB. Regulation of the epithelial-mesenchymal transition by claudin-3 and claudin-4. *PLoS ONE* 8(6), e67496 (2013).

103 Hashimoto H, Vertino PM, Cheng X. Molecular coupling of DNA methylation and histone methylation. *Epigenomics* 2(5), 657–669 (2010).